WESTERN SYDNEY
UNIVERSITY

Numerical modelling of airflow dynamics and particle deposition in human lungs

Md. Mizanur Rahman
(B.Sc., M.Sc.)

A thesis submitted to fulfil the requirements of the degree
of
Doctor of Philosophy

School of Engineering, Design & Built Environment
Western Sydney University, Australia
2022

Dedication

I dedicate this thesis to my sweet and loving Father, the late Md. Hossain Ali, and my Mother, Mst Anwara Begum, whose affection, love, encouragement and prayers day and night have made me able to achieve success and honour.

Acknowledgements

I would like to convey my appreciation and greatest sense of obligation to my principal supervisor, Associate Professor Ming Zhao, for his exceptional guidance and continuous support during all stages of my research work. He helped me carry out my thesis work on this challenging topic. Also, he aided me with his patience, enthusiasm, constructive criticism and endless encouragement during the completion of the thesis. For me, he has been a continual source of motivation and inspiration. It is a pleasure for me to work with him and learn how to develop creative ideas.

I would like to express my gratitude to my co-supervisor, Associate Professor Kejun Dong and external co-supervisors Dr Suvash C. Saha and Dr Mohammad Saidul Islam from the University of Technology Sydney (UTS) for their encouragement and support throughout my candidature. I want to acknowledge their invaluable advice, inspiration and faith in my abilities. I want to give special thanks to Dr Mohammad Saidul Islam, who introduced me to the area of research in human lung modelling and provided me with a realistic lung model and HPC support.

I want to thank the Australian Government Research Training Program (RTP) and International Postgraduate Research Scholarship (IPRS). In addition, I would like to thank Western Sydney University (WSU) for access to the high-performance virtual machine (VM) that provided computational facilities.

Elite Editing provided copyediting and proofreading services according to the guidelines laid out in the university-endorsed national guidelines for editing research theses.

I am thankful to Mohammad Zohurul Islam, Dr Sheikh Imamul Hossain, Dr Adnan Munir, Mohammad Rashed Mia, Abdullah-Al-Mamoon and my other WSU and UTS friends for their encouragement.

Special thanks go to my family members, especially my mother, Mst. Anwara Begum, my sister Mst. Jesmin Ara Dristy, brother-in-law Md. Mamun-Or-Rashid and nephew Dihan Rashad for their immense care, unconditional love, support, inspiration and prayers, not only for this PhD journey but also for my whole life.

Last but not least, I would like to extend my deepest thanks to my wife, Tabassum Reya and my son Ehan Rahman for their endless support during this study. They give me strength and make my life full of joy. All of these factors have prompted me to devote and credit my thesis to them.

Statement of Authentication

The work presented in this thesis is, to the best of my knowledge and belief, original except as acknowledged in the text. I hereby declare that I have not submitted this material, either in full or in part, for a degree at this or any other institution.

…….

(Md. Mizanur Rahman)

Preface

This thesis consists of the peer-reviewed international journal and conference publications listed below, and is submitted for fulfilment of the degree of Doctor of Philosophy (PhD) at Western Sydney University, Australia. It describes the candidate's entire work during his study in the School of Engineering, Design and Built Environment at Western Sydney University under the principal supervision of Associate Professor Ming Zhao, co-supervision of Associate Professor Kejun Dong, and external co-supervision of Dr Suvash C. Saha and Dr Mohammad Saidul Islam from the University of Technology Sydney.

List of Publications

Refereed journal papers

1. Rahman, MM, Zhao, M, Islam, MS, Dong, K & Saha, SC 2021, 'Aerosol particle transport and deposition in upper and lower airways of infant, child and adult human lungs', *Atmosphere*, vol. 12, no.11, 1402. http://dx.doi.org/10.3390/atmos12111402
2. Rahman, MM, Zhao, M, Islam, MS, Dong, K & Saha, SC 2021, 'Aging effects on airflow distribution and micron-particle transport and deposition in a human lung using CFD-DPM approach', *Advanced Powder Technology*, vol. 32, no.10, pp. 3506–3516. http://dx.doi.org/10.1016/j.apt.2021.08.003
3. Rahman, MM, Zhao, M, Islam, MS, Dong, K & Saha, SC 2022, 'Nanoparticle transport and deposition in a heterogeneous human lung airway tree: An efficient one path model for CFD simulations', *European Journal of Pharmaceutical Sciences,* vol. 177, 106279. https://doi.org/10.1016/j.ejps.2022.106279
4. Rahman, MM, Zhao, M, Islam, MS, Dong, K & Saha, SC 2021, 'Numerical study of nanoscale and microscale particle transport in realistic lung models with and without stenosis', *International Journal of Multiphase Flow,* vol. 145, 103842. http://dx.doi.org/10.1016/j.ijmultiphaseflow.2021.103842
5. Rahman, MM, Zhao, M, Islam, MS, Dong, K & Saha, SC 2022, 'Numerical study of nano and micropollutant particle transport and deposition in realistic human lung airways', *Powder Technology,* vol.402, 117364. https://doi.org/10.1016/j.powtec.2022.117364

Refereed conference papers

1. Rahman, MM, Zhao, M, Islam, MS, Dong, K & Saha, SC 2019, 'Airflow dynamics and aerosol particle transport in a human lung', In *Proceedings of the 1st International Conference on Mechanical and Manufacturing Engineering Research and Practice*

(iCMMERP-2019), Sydney, Australia, 24–28 November 2019. http://icmmerp.net.au/Proceedings/2019/ProceedingsiCMMERP2019.pdf

2. Rahman, MM, Zhao, M, Islam, MS, Dong, K & Saha, SC 2020, 'Airflow dynamic and particle deposition in age-specific human lungs', In *Proceedings of the 22nd Australasian Fluid Mechanics Conference (AFMC2020)*, Brisbane, Australia, 7–10 December 2020. https://espace.library.uq.edu.au/view/UQ:6506e6f
3. Rahman, MM, Zhao, M, Islam, MS, Dong, K & Saha, SC 2021, 'The effects of physical activity on pollutant particle deposition in the realistic human lung airways', In *Proceedings of the 3rd International Symposium on Computational Particle Technology*, Suzhou and Melbourne, Australia 17–21 November 2021. https://www.monash.edu/simpascpthub-congress
4. Rahman, MM, Zhao, M, Islam, MS, Dong, K & Saha, SC 2021, 'The effects of density on particle deposition in the human respiratory tract', In *Proceedings of the Fifth Australasian Conference on Computational Mechanics (ACCM2021)*, Sydney, Australia, 13–15 December 2021. https://researchdirect.westernsydney.edu.au/islandora/object/uws:62044

Table of Contents

List of Figures

List of Tables

List of Abbreviations

CFD	Computational fluid dynamics
CT	Computerised tomography
CNG	Compressed natural gas
COPD	Chronic obstructive pulmonary disease
CSP	Cigarette smoke particles
DF	Deposition fraction
DPM	Discrete phase model
E–E	Euler–Euler
E–L	Euler–Lagrange
LES	Large eddy simulation
MRI	Magnetic resonance imaging
PLA	Polylactic acid
PM	Particulate matter
RANS	Reynolds-averaged Navier–Stokes
TD	Transport and deposition
3D	Three-dimensional

List of Symbols

p	Fluid pressure
T	Fluid temperature
D	Hydraulic diameter
S_t	Stokes number
u_i^p	Particle velocity
d_p	Particle diameter
u_i	Fluid velocity
F_{Di}	Drag force
F_{gi}	Gravitational force
F_{Bi}	Brownian force
F_{Li}	Saffman's lift force
C_D	Drag coefficient
u_0	Fluid inlet velocity
ρ	Air density
ρ_p	Particle density
μ	Molecular viscosity
Δt	Particle time step
G_i	Gaussian random number
S_0	Spectral intensity function
v	Kinematic viscosity
K_B	Boltzmann constant
C_c	Stokes–Cunningham correction factor
λ	Gas molecules' mean free path
d_{ij}	Deformation tensor
η_d	Deposition efficiency
Q_{in}	Flow rate
Re_P	Particle Reynolds number
U_τ	Friction velocity
τ_w	Wall shear stress
η_e	Escaping rate

Abstract

Airflow dynamics and inhaled aerosol particle transport in human lung airways are significant in terms of human health; the effectiveness of inhaled drug therapy; and the health risks caused by air pollution. Airflow and particle transport and deposition (TD) in human lungs are affected by various factors, including breathing pattern, lung geometry, particle properties, physical lung condition (stenosis airway/obstructions) and environmental conditions. The lung airway diameters and breathing capacity of human lungs normally increase with age until the age of 30. However, it has been shown that lung airway diameters reduce by around 10% every 10 years after the age of 50. However, age-specific particle TD in human lungs, particularly in aged people, is not well understood. This thesis discusses variation in the inhalation rate of air with age, which is important for determining particle deposition efficiency in lung airways. An efficient new cutting method was developed in this study to numerically examine the deposition of microscale aerosol particles in symmetric lung models over 14 generations (i.e. divisions of the trachea) in 50–70-year-old people. In the model, numerical simulation efficiency is increased dramatically by cutting the lung airways into many sections that can be simulated separately. The particle mass and flow rates satisfy continuity conditions at the interfaces between sections. This new cutting method overcomes the inability to simulate airflow and particle TD for many generations using a numerical method. The results indicate that microscale aerosol particle deposition increased when particle size or flow rate increased, because of strong impaction mechanisms. An increase in age caused more particles to deposit in the upper airway and fewer particles to enter the deeper airways.

It is evident that a complete understanding of nanoparticle TD in large-scale whole lung airway models is not possible in either experimental or numerical simulation because of the unavailable lung geometry. In this thesis, to further ensure the continuity of momentum, an efficient one-path numerical model is developed to simulate airflow and nanoparticle TD in

airway generations 0–11 (G0–G11), accounting for 93% of the whole airway length from G0 to terminal G23. The one-path model enables the simulation of particle TD in many generations of airways in a timely fashion. Because a continuous airway route is simulated, the conservation of all aspects of the flow and particles is ensured. It is found that particle deposition efficiency is 28.94%, or 5 nm, greater than 20 nm because of the higher dispersion capacity. The deposition efficiency at each generation decreases irrespective of the flow rate and particle size. The quantified deposition and escaping rates at G0–G11 provide valuable guidelines for drug delivery in human lungs.

Simplified symmetric lung models are also used because realistic lung models of many generations are not available. Fundamental mechanisms of particle TD including impaction, diffusion and sedimentation can be derived using symmetric lung models. Some available computerised tomography (CT) scanned models generally have a limited number of generations. These CT scans or digital reference-based models are useful for optimising a patient's drug delivery treatment for human lung airway problems such as stenosis, which is life threatening. However, studies of airflow and particle TD in lung models with stenosis are rare. This thesis examines the contribution of impaction and diffusion mechanisms to particle TD in realistic stenosis lung models. Three physical activities are considered: sleeping, resting and intense breathing, corresponding to inhalation flow rates of Q_{in} = 15, 30 and 60 L/min, respectively. It is found that the pressure drop in the stenosis model increases by 83% compared with the healthy model if the flow rate remains constant. The contribution of the diffusion mechanism significantly declines with an increase in either particle size or flow rate.

Inhalation of deposited particulate matter (PM) or pollutant particles is responsible for various lung diseases. However, a complete understanding of the TD of pollutant particles with various sizes and densities in lung airways remains elusive. This thesis thus evaluates PM deposition in a CT scan based on realistic lung airways from the mouth–throat to G3. Three

types of pollutant particle are considered (traffic, smoke and dust) with a wide range of sizes ranging from the nano- to microscale. The most important finding is that the effects of density on particle TD of nanoparticles are much weaker than for microparticles.

Keywords: Airflow Dynamics (AD), Stenosis Airway, Aerosol Particle Transport and Deposition (TD), Inhalation, Drug delivery, Aging Effect, Inhalation, Cutting Method, Airway Reduction, Lung Generations, Traffic Particle, Smoke Particle, Dust Particle, Human Lungs, Physical Activity, Deposition Mechanism, Heterogeneous Vasculature Tree, Truncated Path model, Boundary Condition.

Chapter 1: Introduction

Research into airflow dynamics and particle transport in human lungs is receiving considerable attention from many researchers because of its significance for human health. Drug delivery through inhalation of air into the human lung is important to prevent/cure respiratory diseases. Many researchers have investigated the process of particle transport and deposition (TD) in the respiratory airway through analytical as well as numerical methods, during the last century. Nowadays, numerical methods are used to model various biomechanical engineering problems, including particle flow in the respiratory system. The greatest challenge in numerical modelling of particle TD is the complexity of human lungs. Because the lung airway diameters can be reduced by around 10% for every 10 years after the age of 50 (Kim et al. 2017), understanding particle TD in the lung airways of various ages is important to prevent respiratory diseases in the human lung. In the current research, an advanced numerical model is developed for the first-ever approach to better prediction of particle TD in the terminal lung airways of large-scale lung models.

1.1 Background

Aerosol particle inhalation as a method of drug delivery is a modern technology for the management of lung diseases (Douafer et al. 2020) because it is cost effective and has fewer side effects than aggressive drugs (Tiwari et al. 2012). Drugs are inhaled into human lungs in the form of particles for the treatment of lung diseases in the respiratory tract (Kuzmov & Minko 2015). Nanotherapeutics, insulin delivery, pain management and cancer therapy have been common methods for the treatment of diseases of the respiratory tract in recent years (Kleinstreuer et al. 2008). The delivery of aerosol particles can be through the mouth–throat, nasal and pulmonary region as non-invasive alternative routes (Longest et al. 2011). The

delivery of a drug into a human lung can be achieved using standard devices such as nebulisers, metered-dose inhalers and dry-powder inhalers; the number of particles deposited in the human lung area is limited. The key goal of aerosol drug delivery is to maximise particle deposition in the human lung at the target position. Because the treatment of diseases is generally costly, effective targeted drug-aerosol delivery to a specific position in a human lung is important. Computational fluid dynamics (CFD) simulations offer an efficient way to study aerosol particle inhalation.

Studying particle inhalation in human lungs is also helpful for treating lung diseases like chronic obstructive pulmonary disease (COPD), lung cancer and asthma caused by air pollution (Kyung & Jeong 2020). Particulate matter **(**PM) is the sum of all solid and liquid particles suspended in air, many of which are hazardous (Yadav & Devi 2018). PM comes from different sources, including industrial pollutants, burning of vehicle fuels, coal combustion, drug delivery tools, pesticides and human activities (Davidson et al. 2005). Human lungs inhale a large number of particles daily. Some particles absorbed by epithelial cells may cause respiratory diseases (Hussain et al. 2012). Some like carcinoma and toxic particle may cause different health damages depending on their residence time in the lung. Both soluble and insoluble particles may be harmful in the deep airways, depending on their toxicity (Islam et al. 2017).

This thesis mainly focuses on developing numerical models and investigating the effectiveness of aerosol particle inhalation as drug delivery. Particle inhalation and deposition in human lungs is affected by the lung anatomy, breathing pattern and particle properties (Rissler et al. 2017). Therefore, airflow dynamics and inhaled aerosol particle transport in the lung airways are significant for human health; thus it is important to measure both the efficiency of inhaled drug therapy and the health implications of air pollution (Deng et al. 2018). Further, the lung airways become larger as people grow into adults, and the shape of the airway structure

and breathing habits change. Therefore, aging is an important factor in respiratory health. Hence, a comprehensive age-specified particle TD study is necessary to better predict drug delivery to the targeted position in a human lung.

1.2 Aim of the Research

This study aims to develop an advanced and efficient three-dimensional (3D) numerical model to analyse airflow characteristics and aerosol particle TD in human lungs. The model is used to analyse the contribution of fundamental impaction and diffusion mechanisms for nano- and microscale particle TD in age-specific terminal bronchiole airways. The outcomes of this study will help improve the effectiveness of delivery of drug aerosols into human lungs to treat obstructive lung diseases including asthma, lung cancer and COPD. In addition, the inhalation of different types of pollutant particles into human lungs is investigated further to understand the consequence of the pollution particle on lung health.

1.3 Research Objectives

The following objectives were achieved to meet the research aim:

1. Realistic mouth–throat and tracheobronchial lung airways were generated based on computerised tomography (CT) Scan DICOM images and used to analyse airflow dynamics and particle transport in real lungs, as well as the effects of stenosis.
2. A new cutting method was developed as an efficient numerical method to study the deposition of microscale aerosol particles in human lungs. The effects of particle size and inhalation flow rate on the deposition of microscale aerosols for a large-scale human lung model were investigated using this model.
3. Further, an efficient one-path numerical model was developed to enable simulation of the deposition of nanoparticle TD in many generations (i.e. divisions of the trachea).

Nanoparticle deposition in G0–G11 of a human lung, accounting for 93% of the whole airway length, was investigated using this model.

4. An age-specific lung model was generated for nanoparticle and microparticle TD in lung airways.
5. In addition, the deposition of pollutant (traffic, smoke and dust) particles with various sizes ranging from nano- to microscale TD in a CT scan based on realistic lung airways was investigated using CFD, to assess health risk.

When presenting each of the above achievements, the airflow, pressure and wall shear in human lung airways are discussed in detail, along with their association with deposition. Further, the distribution of deposited particles in various generations is calculated and the contributions of two fundamental mechanisms—impaction and diffusion—of particle TD in the human lung are quantified.

1.4 Significance, Scope and Innovation

It is important to measure the size and shape of aerosol particles transported in lung airways in regard to both the efficiency of inhaled drug therapy and the health implications of air pollution. This thesis presents a comprehensive and advanced computational analysis of particle TD in terminal airways. The study also develops a new framework to predict and analyse the realistic inhalation rate based on the aging effect (Chapter 3). The specific innovations of the thesis are described in the following sections.

1.4.1 Efficient Numerical Methods Developed

Until now, most studies of particle deposition in human lungs have considered only a limited number of generations, because realistic whole lungs are not available. The first-ever approach to the development of a new cutting method (Chapter 4), and the one-path model developed in this thesis (Chapter 5) can simulate micro- and nanoparticle TD in many generations of human lungs with affordable computational times. The research outcomes of

microparticle deposition in G0–G14 airways and nanoparticle deposition in G0–G11 airways provide a good understanding of particle TD over 90% of the lung airway length.

1.4.2 Realistic Lung Model Implemented

The developed CT scan-based mouth–throat and tracheobronchial stenosis and healthy lung airways model is important for identifying the pressure drop, wall shear effect and precise particle TD in the targeted area (Chapter 6). It was found that pressure drop in the stenosis model increased by 83% compared with the healthy model. Therefore, the findings of the present study will help improve drug delivery to targeted positions in a stenosis lung, and may provide guidelines for future studies applying biomedical engineering in lung modelling.

1.4.3 Contribution of Fundamental Deposition Mechanisms Quantified

The present study analysed the contribution of impaction and diffusion mechanisms to nano- and microscale aerosol and pollutant particle TD in a human lung (Chapters 6 & 7). A significant density effect based on the pollutant particle is observed during particle TD of nanoparticles that is much weaker than that of microparticles.

Further, up to the age of 30 years, human lung airway diameters and breathing capacity increase with age. However, it is evident that after the age of 50 years, lung airway diameters reduce by around 10% per decade. Therefore, this research developed a lung geometry that was dependent on age. Thus, the present findings regarding age-specified particle TD in human lungs may assist in medical therapy by individually simulating the distribution of drug aerosol for infants as well as aged people.

1.5 Research Methodology

This section briefly summarises the overall methodology; the methodology used for different numerical models is presented in individual chapters. In the numerical models developed in this thesis, airflow and particle transport are simulated using CFD. The governing equations for airflow are the Reynolds-averaged Navier–Stokes equations. They are solved via

the finite volume method using the Ansys Fluent 19.2 software with appropriate boundary conditions. In this method, the user develops an inlet velocity profile based on the aging effect that is used for advanced modelling. Simulation of airflow in large-scale human lungs is still impossible without any simplification or modification of the method. To enable the simulation of particle deposition in many generations of airways, two models were developed for this thesis: the cutting method for simulating microparticle deposition in Chapter 4; and the one-path method for simulating nanoparticle deposition in Chapter 5. The new cutting numerical method cuts the whole airflow route into a number of segments, and the airflow and particle TD within different segments are simulated separately. However, continuity of mass and momentum at the interfaces between segments is ensured. This new cutting method analyses microscale aerosol particle TD in human lung airways over 14 generations. In the efficient one-path numerical model, computational efficiency is increased significantly by choosing two representative bifurcations from each generation of airway along one route of the airway. The conservation of mass and particle number is ensured by setting appropriate boundary conditions. This new one-path model simulates the airflow and nanoparticle TD in airway G0–G11, which account for 93% of the whole airway length. The motion of particles in human lung airways is simulated by solving the particle motion equation, which considers the drag, diffusion, gravity and Saffman's lift forces. The contributions of various forces are quantified in Chapter 6. In addition to Ansys Fluent, the Tecplot software is used to visualise the deposition of particles in lung models.

Choosing a proper turbulence model is important for the accuracy of airflow simulation. Some researchers have used the standard k−ε turbulence model in their modelling (Ball et al. 2008; Stapleton et al. 2000). In this thesis, the realisable k-ε turbulence model is used to simulate turbulence because it performs better than the standard model under a variety of complex flow conditions, including rotating homogeneous shear flows; boundary-free shear

flows; channel and flat boundary layer flow with and without pressure gradients; and backwards-facing step flow (Shih et al. 1995). In addition, it has been demonstrated that the realisable k-ε model can accurately predict the flow of complicated lung geometries without the requirement for near-wall adjustment (Abolhassantash et al. 2020; Isa et al. 2014; Rahman et al. 2021).

1.6. Thesis Outline

The purpose of this research has been explained in **Chapter 1** (Introduction), which also provided a brief background to particle TD, including the role, causes and effects of aerosol particle deposition in human lung airways.

In **Chapter 2**, a comprehensive review of particle TD in a human lung airway is presented, including both numerical and experimental research. Chapter 2 begins with a brief overview of key concepts such as the respiratory system, with a focus on the development of lung models. In addition, the aging effect and pollutant particle properties are introduced, with a focus on health risk assessment.

Chapter 3 provides a detailed analysis of nanoparticle TD in the lungs of infants, children and adults. Human lung airway diameters and breathing capacity increase until the age of 30 years. Therefore, knowledge of inhalation airflow rates corresponding to different ages is important for determining particle deposition efficiency in the lung airways. This chapter has been published in a peer-reviewed journal (*Atmosphere*).[1]

Chapter 4 describes the age-specific particle TD in human lungs, particularly in aged people, as it is evident that lung airway diameters can reduce by around 10% every 10 years after the age of 50 years. A new cutting numerical method was developed to study the deposition of microscale aerosol particles in a symmetric lung model over 14 generations. In

[1]Rahman, MM, Zhao, M, Islam, MS, Dong, K & Saha, SC 2021, 'Aerosol particle transport and deposition in upper and lower airways of infant, child and adult human lungs', *Atmosphere*, vol. 12, no. 11, 1402. http://dx.doi.org/10.3390/atmos12111402

the model, airways were cut into several sections, and the particle mass and flow rates found to satisfy continuity conditions at the interfaces between sections, which was not true for the fluid momentum. This chapter has been published as an article in a peer-reviewed journal (*Advanced Powder Technology*).[2]

Chapter 5 explains a complete understanding of nanoparticle TD in large-scale lung airway models because of the lack of literature in either experimental or numerical studies in human lung airways. Therefore, an efficient one-path numerical model was developed to simulate airflow and nanoparticle TD in 0–G11 airways of the human lung, which account for 93% of the whole airway length from G0 to terminal G23. This chapter has been published in a peer-reviewed journal (*European Journal of Pharmaceutical Sciences)*.[3]

Chapter 6 describes the contribution of impaction and diffusion mechanisms for particle TD in CT scan-based stenosis lung models. First, the impaction term is included in the particle motion equation to achieve this. Second, the impaction, diffusion and Saffman's terms are considered to simulate both nano- and microparticle TD in human lung airways. The significant pressure drop in the stenosis model is greater than that in the healthy model. This chapter has been published in a peer-reviewed journal (*International Journal of Multiphase Flow*).[4]

Chapter 7 evaluates pollutant particle TD in a CT scan based on realistic lung airways responsible for lung diseases, to enable respiratory health risk assessment. The reported study also investigated TD of three types of pollutant particle—traffic, smoke and dust—of various

[2] Rahman, MM, Zhao, M, Islam, MS, Dong, K & Saha, SC 2021, 'Aging effects on airflow distribution and micron-particle transport and deposition in a human lung using CFD-DPM approach', *Advanced Powder Technology*, vol. 32, no. 10, pp. 3506–3516. http://dx.doi.org/10.1016/j.apt.2021.08.003

[3] Rahman, MM, Zhao, M, Islam, MS, Dong, K & Saha, SC 2022, 'Nanoparticle transport and deposition in a heterogeneous human lung airway tree: An efficient one path model for CFD simulations', *European Journal of Pharmaceutical Sciences,* vol. 177, 106279. https://doi.org/10.1016/j.ejps.2022.106279

[4]Rahman, MM, Zhao, M, Islam, MS, Dong, K & Saha, SC 2021, 'Numerical study of nanoscale and microscale particle transport in realistic lung models with and without stenosis', *International Journal of Multiphase Flow*, vol. 145, 103842. http://dx.doi.org/10.1016/j.ijmultiphaseflow.2021.103842

sizes ranging from nano- to microscale, in mouth–throat and tracheobronchial realistic human lung airways. A significant finding is that the effects of density on the particle TD of nanoparticles are much weaker than that for microparticles. This chapter has been published in a peer-reviewed journal (*Powder Technology*).[5]

Chapter 8 presents the conclusions and future study recommendations.

References

Abolhassantash, M, Tavakol, M, Abouali, O, Yaghoubi, M & Ahmadi, G 2020, 'Deposition fraction of ellipsoidal fibers in the human nasal cavity-Influence of non-creeping formulation of hydrodynamic forces and torques', *International Journal of Multiphase Flow*, vol. 126, 103238.

Ball, C, Uddin, M & Pollard, A 2008, 'High resolution turbulence modelling of airflow in an idealised human extra-thoracic airway', *Computers & Fluids*, vol. 37, no. 8, pp. 943-964.

Davidson, CI, Phalen, RF & Solomon, PA 2005, 'Airborne particulate matter and human health: a review', *Aerosol Science and Technology*, vol. 39, no. 8, pp. 737-749.

Deng, Q, Ou, C, Chen, J & Xiang, Y 2018, 'Particle deposition in tracheobronchial airways of an infant, child and adult', *Science of the Total Environment*, vol. 612, pp. 339-346.

Douafer, H, Andrieu, V & Brunel, JM 2020, 'Scope and limitations on aerosol drug delivery for the treatment of infectious respiratory diseases', *Journal of Controlled Release*, vol. 325, pp. 276-292.

Hussain, S, Laumbach, R, Coleman, J, Youseff, H, Kelly-McNeil, K, Ohman-Strickland, P et al. 2012, 'Controlled exposure to diesel exhaust causes increased nitrite in exhaled

[5] Rahman, MM, Zhao, M, Islam, MS, Dong, K & Saha, SC 2022, 'Numerical study of nano and micropollutant particle transport and deposition in realistic human lung airways', *Powder Technology*, vol. 402, 117364. https://doi.org/10.1016/j.powtec.2022.117364

breath condensate among subjects with asthma', *Journal of occupational and environmental medicine/American College of Occupational and Environmental Medicine*, vol. 54, no. 10, pp. 1186-1191.

Isa, NM, Ahmad Fara, ANK & Asmuin, NZ 2014, 'Investigation on the Turbulence Models Effect of a Coal Classifier by Using Computational Fluids Dynamics', In *Applied Mechanics and Materials*, vol. 465, pp. 617-621.

Islam, MS, Saha, SC, Sauret, E, Gemci, T, Yang, IA & Gu, Y 2017, 'Ultrafine particle transport and deposition in a large scale 17-generation lung model', *Journal of biomechanics*, vol. 64, pp. 16-25.

Kim, J, Heise, RL, Reynolds, AM & Pidaparti, RM 2017, 'Aging effects on airflow dynamics and lung function in human bronchioles', *PloS one*, vol. 12, no. 8, e0183654.

Kleinstreuer, C, Zhang, Z & Donohue, J 2008, 'Targeted drug-aerosol delivery in the human respiratory system', *Annu. Rev. Biomed. Eng.*, vol. 10, pp. 195-220.

Kuzmov, A & Minko, T 2015, 'Nanotechnology approaches for inhalation treatment of lung diseases', *Journal of controlled release*, vol. 219, pp. 500-518.

Kyung, SY & Jeong, SH 2020, 'Particulate-matter related respiratory diseases', *Tuberculosis and respiratory diseases*, vol. 83, no. 2, pp. 116-121.

Longest, PW, Tian, G & Hindle, M 2011, 'Improving the lung delivery of nasally administered aerosols during noninvasive ventilation—an application of enhanced condensational growth (ECG)', *Journal of aerosol medicine and pulmonary drug delivery*, vol. 24, no. 2, pp. 103-118.

Rahman, MM, Zhao, M, Islam, MS, Dong, K & Saha, SC 2021, 'Aging effects on airflow distribution and micron-particle transport and deposition in a human lung using CFD-DPM approach', *Advanced Powder Technology*, vol. 32, no.10, pp. 3506-3516.

Rissler, J, Gudmundsson, A, Nicklasson, H, Swietlicki, E, Wollmer, P & Löndahl, J 2017, 'Deposition efficiency of inhaled particles (15-5000 nm) related to breathing pattern and lung function: an experimental study in healthy children and adults', *Particle and fibre toxicology*, vol. 14, no. 1, pp. 1-12.

Shih, TH, Liou, WW, Shabbir, A, Yang, Z & Zhu, J 1995, 'A new k-ϵ eddy viscosity model for high reynolds number turbulent flows', *Computers and Fluids*, vol. 24, no. 3, pp. 227-238,

Stapleton, K-W, Guentsch, E, Hoskinson, M & Finlay, W 2000, 'On the suitability of k–ε turbulence modeling for aerosol deposition in the mouth and throat: a comparison with experiment', *Journal of aerosol science*, vol. 31, no. 6, pp. 739-749.

Tiwari, G, Tiwari, R, Sriwastawa, B, Bhati, L, Pandey, S, Pandey, P et al. 2012, 'Drug delivery systems: An updated review', *International journal of pharmaceutical investigation*, vol. 2, no. 1, pp. 2-11.

Yadav, IC & Devi, NL 2018, 'Biomass burning, regional air quality, and climate change', *Earth Systems and Environmental Sciences. Edition: Encyclopedia of Environmental Health. Elsevier. https://doi. org/10.1016/B978-0-12-409548-9.11022-X*.

Chapter 2: Literature Review

In this chapter, the overall biological aspects of the lung and the development of an anatomical lung model are summarised, and lung modelling and deposition mechanisms are discussed. In addition to the detailed literature review presented in this chapter, literature relevant to subsequent chapters is discussed.

2.1 Biological Aspects of the Lung

The human lung is part of the respiratory system consisting of two spongy organs (Gray & Goss 1878). These sponges situated on either side of the thorax are called the right and left lungs, respectively, and differ marginally in that the left and right lungs contain two and three lobes, respectively. Lung tissue is light, porous and highly elastic (Pasman et al., 2020). The lung structure includes three surfaces: coastal, mediastinal and diaphragmatic.

The human respiratory system (Figure 2.1) is divided into the upper and lower respiratory tract. The mouth–throat, nasal cavity and pharynx form the upper respiratory tract, while the larynx, trachea and bronchial tree form the lower respiratory tract (Ionescu 2013).

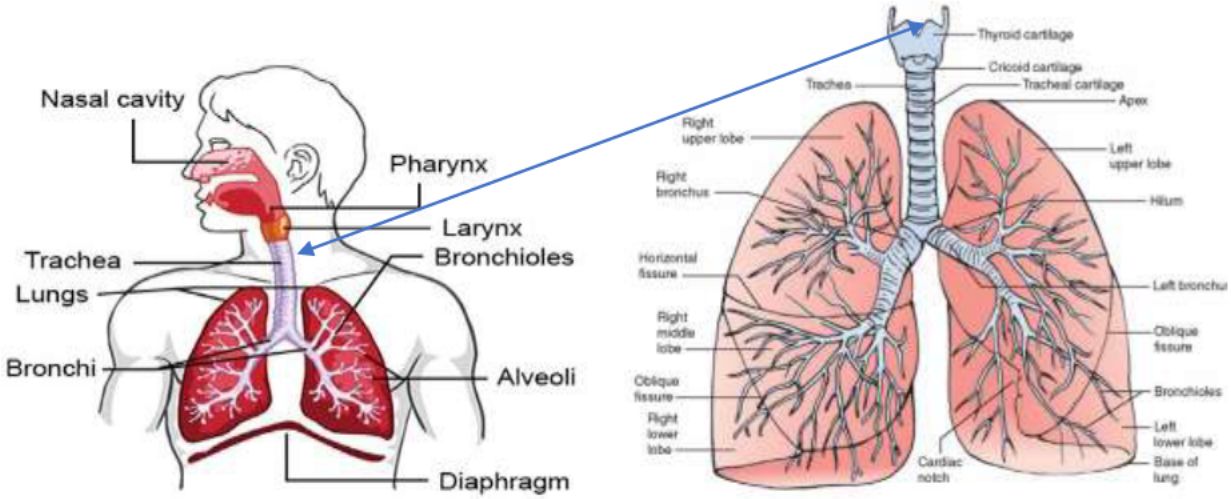

Figure 2.1. Human respiratory system (https://www.chestandallergyclinic.com/).

Chapter 2: Literature Review

The air coming from the outer environment passes through the larynx and the trachea wall (Ćurić et al. 2022; Tu et al. 2013). Two bronchi are divided by the trachea wall, and each consists of two smaller branches called bronchial tubes (Pump 1964). All the bronchial tubes are connected to the pathways of the alveoli. In this way, oxygen (O_2) passes through alveoli into capillaries. Gas exchange occurs at the alveoli region where O_2 diffuses across the cell membrane and is transferred into blood cells, and carbon dioxide (CO_2) is removed from the blood and travels to the alveoli region during exhalation (Figure 2.2).

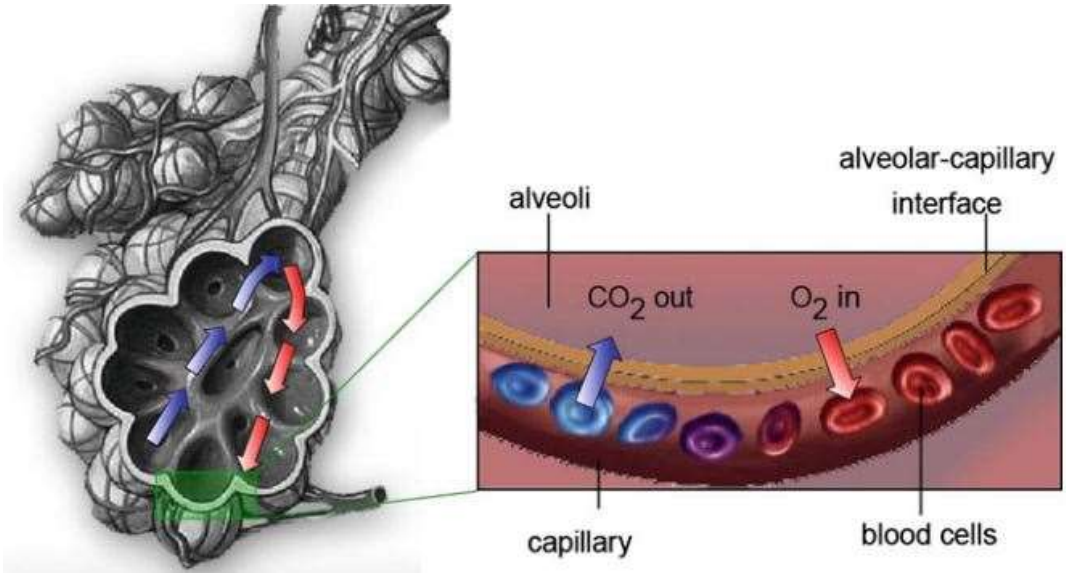

Figure 2.2. Oxygen and carbon dioxide gas exchange at the alveolar–capillary interface (https://socratic.org/questions/alveoli-in-the-lungs-greatly-increase-what).

There are two liquid surface layers (gel and sol) in the human lung (Figure 2.3). The sol layer, also called the periciliary layer, contains cilia, which are microscopic, hair-like organelles (Button et al. 2012). The gel layer, also called the luminal mucus layer, is very sticky and viscoelastic (Lai et al. 2009). The very sticky mucus surface layer traps inhaled aerosol particles (Duncan et al. 2016). The mucus contains water, ions and numerous kinds of anti-microbial and anti-oxidant macromolecules that protect the lung (Lillehoj & Kim 2002). Mucin is a lubricant protein produced by epithelial tissue and is an essential element of mucus.

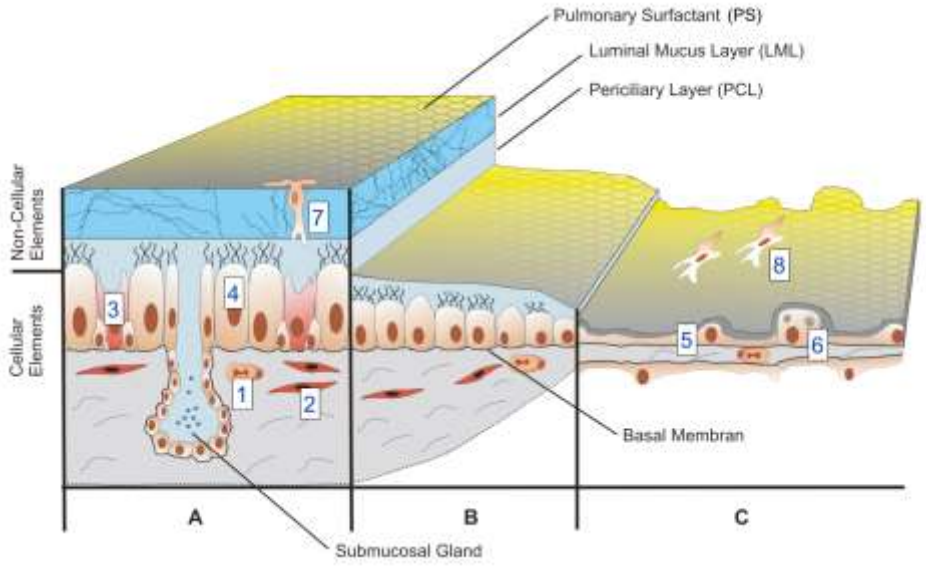

Figure 2.3. Lung morphology showing pulmonary surfactant, luminal mucus layer and periciliary layer: (A) trachea and bronchus, (B) bronchioles, and (C) alveoli (Ruge 2012).

Foreign particle deposition and clearance in the lung is affected by the viscoelastic mucus (Marttin et al, 1998). The viscosity of mucus is around 1,000–10,000 times more than water viscosity because of its low shear rate (Lai et al. 2007). The thickness of the mucus layer in the respiratory system varies between individuals, but in general lies in the range of 5–10 µm (Widdicombe 1997). However, in some disease conditions, such as cystic fibrosis, the mucus layer is increased in thickness up to 55 µm (Lee et al. 2011). The mucus layer serves an important function in particle deposition in human lung airways (Knowles & Boucher 2002).

2.1.1 Anatomy of the Lung Airway Tracheobronchial Tree

Each division of the trachea is called a generation. A lung includes many airway cell generations. The tracheobronchial tree has two types of airway: conducting (trachea, bronchi and bronchioles) and acinus (respiratory bronchioles, alveolar ducts and alveolar sacs) airways (Figure 2.4). The first generation (G0) is the trachea, which is a vertical duct ring structure. Bifurcation begins from the trachea, and the left and right main bronchi follow the trachea in

the same direction. Each bronchus is further divided into small bronchioles called lobar (Sarkar et al. 2015). The upper bronchial tract includes G1–G16, and the alveoli region includes G17–G23. Given these 23 generations, the number of branches in the lung is 2^{23} = 8,388,608 (Soong et al. 1979).

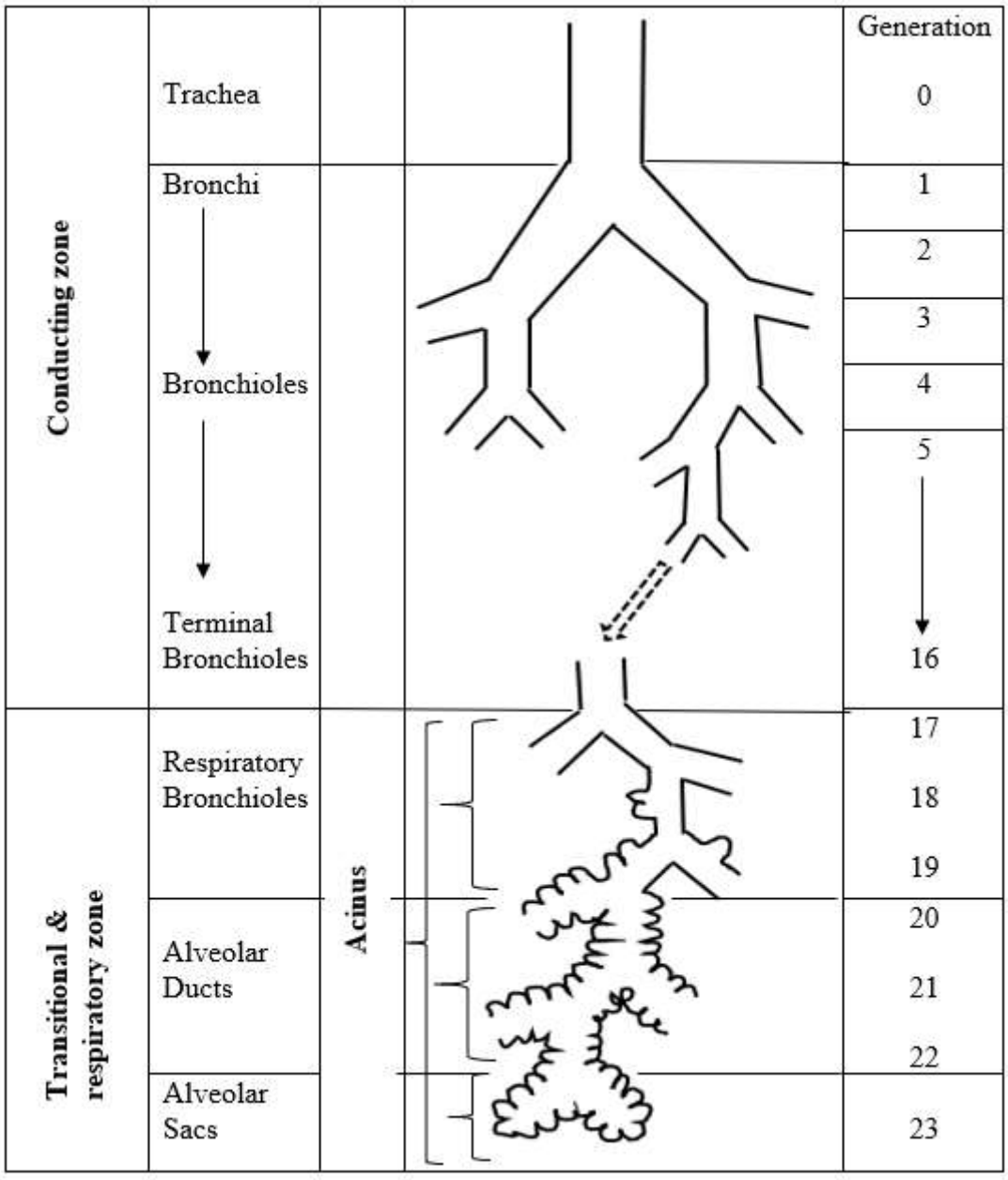

Figure 2.4. Airway generations in the human adult lung (redrawn from Weibel et al. 1963).

2.2 Inhaled Microparticles and Nanoparticles as Drug Delivery

Drug delivery in the lung by aerosol inhalation is a procedure used to treat respiratory disorders in lung airways. The inhalation of aerosols allows direct delivery of high drug concentrations for selective treatment of the lungs (Anderson et al. 2022; Darquenne 2012). Particles with sizes of one to several micrometres are usually referred to as 'microparticles' in drug delivery applications (Kuzmov & Minko 2015; Shi et al. 2021). Microparticles in the range of 1–1,000 µm can be used in a drug delivery system (Lengyel et al. 2019). Different types of spherical and non-spherical microparticle are considered for drug delivery (Figure 2.5).

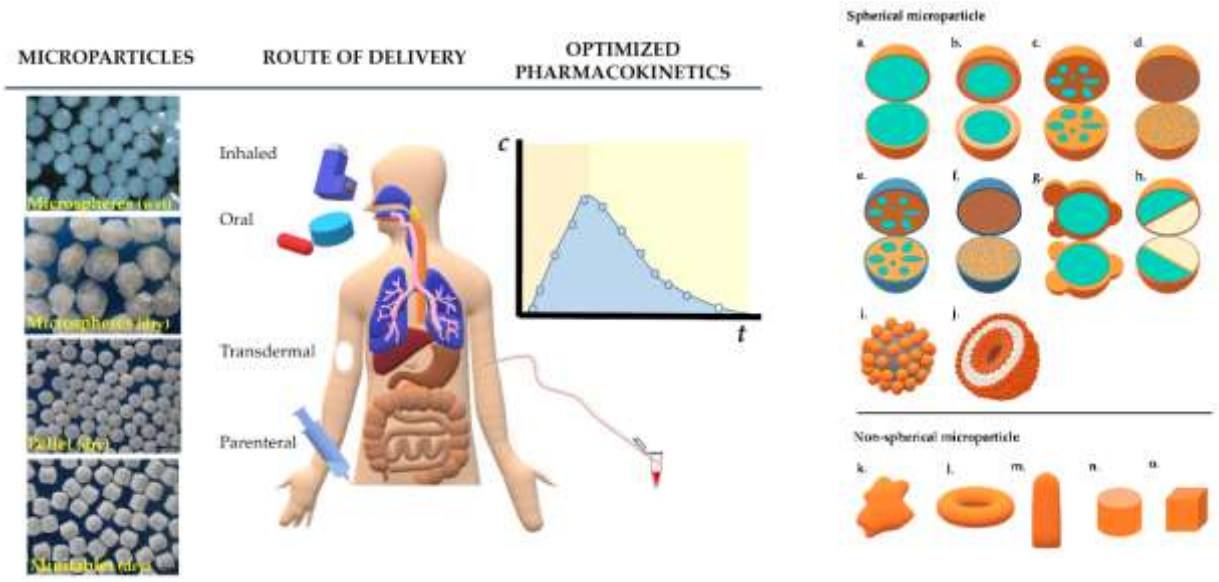

(a) (b)

Figure 2.5. Diagram showing (a) inhaled microparticles in a human lung and (b) different types of microparticle structure (Lengyel et al., 2019)

Lipid-based nanoparticles (particle size ~100 nm) are important for drug delivery in the pharmaceutical industry. Different types of lipid nanoparticle can be used in the respiratory system to help overcome biological barriers (Rajabi & Mousa 2016). Figure 2.6 shows examples of organic (micelles, liposomes, nanogels and dendrimers) and inorganic (gold

nanoparticles, iron oxide nanomaterials, quantum dots and paramagnetic lanthanide ions) nanoparticles. The size of pharmaceutical nanoparticles is determined by their ingredients and physical contents. For example, polylactic acid (PLA) is a biodegradable polymer used as a potential carrier, in nanoparticles typically in the range of 50–500 nm.

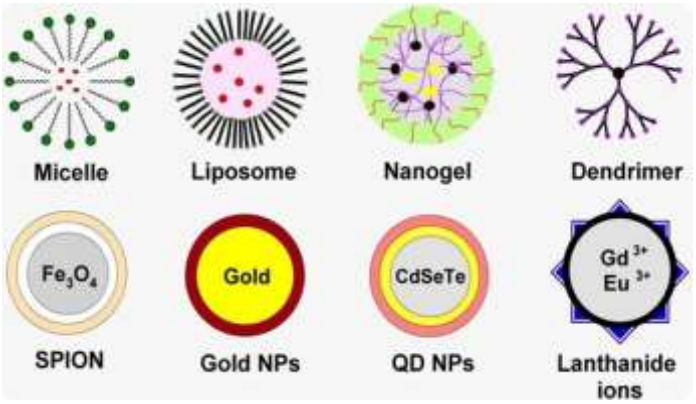

Figure 2.6. Different types of nanoparticle (Rajabi & Mousa 2016).

Nanoparticles (d_p<100 nm) arise from different sources, such as the nucleation, combustion and nanomaterial industries (Borm et al. 2006). It is difficult to refine and expand existing deposition models because of the size range of available particles. Inhaled nanoparticles are essential for drug delivery in the human lung airway. Nano (ultrafine) particle transport in the deep lung airway is becoming the most popular way to treat lung diseases. Nanomedicines are made by encapsulating or adsorbing the drug onto the surface of nanoparticles (Figure 2.7).

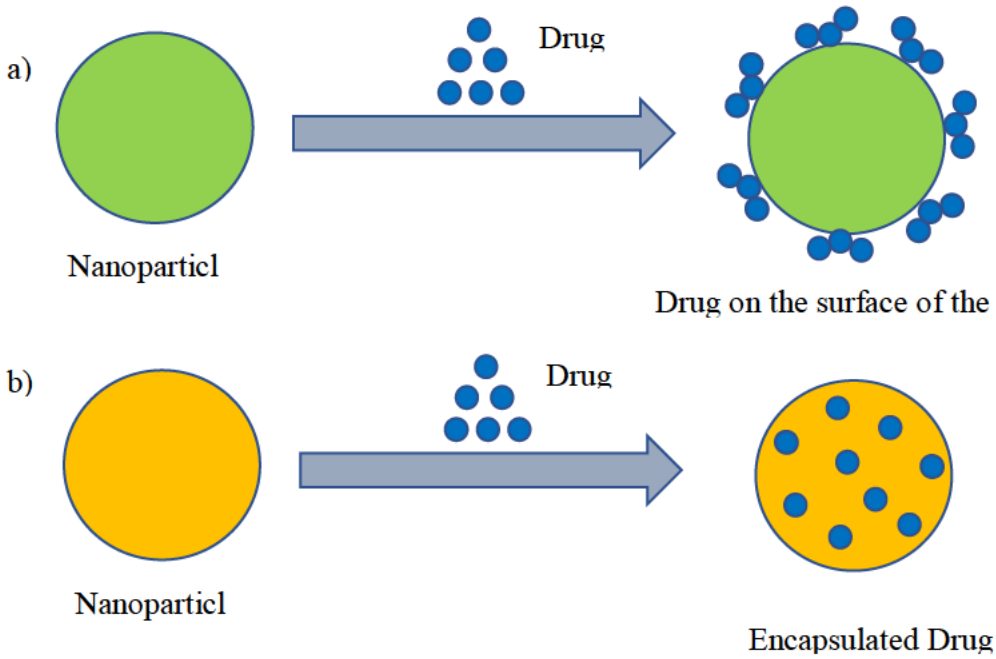

Figure 2.7. Drugs can be associated with nanoparticles via (a) surface modification or (b) coating (reproduced from Wanigasekara & Witharana 2016).

2.3 Lung Anatomical Model

A lung anatomical model is a lung structure used to represent the lung morphology in the respiratory system. The development of idealised/non-realistic and realistic lung geometries is important for the study of airflow and particle TD in human lungs.

2.3.1 Ideal/Non-realistic Lung Model Development

The lung is an integrated structure including three zones (trachea, bronchioles and alveoli) and a number of airway generations. Each generation has its own distinct shape, surface properties and length. The airflow in the inner surface of a lung was first investigated by Hales (1731) in a calf lung. Studies have been conducted to determine lung volume and airway flow resistance (Cushley et al. 2004; Wiggs et al. 1990). Weibel et al. (1963) developed a symmetric lung model with an equal diameter for each branch and a circular pipe shape. Symmetric lung models have mainly been used to study fundamental mechanisms of airflow and particle TD in human lungs, though they are very different from realistic lungs. A more realistic branching

lung model was introduced by Horsfield et al. (1971), who considered young males and mentioned that lung airway branching is not identical. Yeh et al. (1976) introduced a more realistic anatomical lung model based on a human cast. The branching in the model is asymmetric. Subsequently, a five-lobe branching lung model based on a rubber cast rat model has developed by Yeh and Schum (1980). This model represents the exact position of the lung in the respiratory system (Figure 2.1) All the idealised lung models mentioned above are very different from a realistic lung model and do not consider the surface roughness effect, which is very important in natural lung. In CT scan images, the lung model has a rough surface, which is important for determining precise particle deposition in the human lung. Geometrically, real lungs are much more complex than idealised lung models and it is thus desirable to use realistic lung models to study airflow and particle TD in human lungs.

2.3.2 Realistic Lung Model Development

Various software including DOCTOR (Rahimi-Gorji et al. 2016) and AMIR (Islam et al. 2017; Vranicar et al. 2008) has been used to develop 3D realistic anatomical models. Both CT scans and magnetic resonance imaging (MRI) can be used to develop realistic lung geometry (Corcoran & Chigier 2002; Zhou & Cheng 2005). Sauret et al. (1999) were the first to use CT scan data from human lungs to calculate the dimension and length of the airways. However, chest movement during heart beats makes it difficult to develop high-resolution CT images for constructing lung models. Therefore, lung casts scanned by CT, and resultant digital models, can be used in the development of numerical models. 3D lung geometries have been developed using various image processing techniques, such as CT scan DICOM (Sharma & Jindal 2011) and MRI (Vallières et al. 2015). Sauret et al. (2002) developed a realistic lung model up to G9 based on low-resolution CT scan data. Moreover, a 3D realistic lung model up to G17 was introduced by Islam et al. (2018a). These studies described airflow dynamics and

particle deposition in deep lung airways. However, most researchers have studied only a limited number of generations of realistic lung airways.

2.4 Particle Deposition Mechanisms in the Human Lung

Understanding the mechanisms of deposition of inhaled particles in human lungs is challenging because of the complex structure of the lung (Kumar et al. 2009; Soni & Aliabadi 2013; Weibel 1963). Nowadays, CFD is used to analyse the deposition efficiency of particles in human lungs. Deposition mechanisms are now known to include gravitational sedimentation, Brownian diffusion, interception, inertial impaction and electrostatic force (Choi & Kim 2007; Hofmann 2011). However, which mechanism plays a more important role than others depends on lung geometry, physical properties of particles and breathing patterns. Interception deposition occurs when particles travel close to the surfaces of lung airways (Inthavong 2020). Because of their size and shape, fibre particles are generally deposited via an interception mechanism. Such particles can follow the path of the airflow and travel into the deep lung airways.

Deposition efficiency refers to the percentage of particle absorption in human lung airways. A particle's shape (Kasper 1982) and size (Hofmann 2011) affect deposition efficiency. Large-diameter particles (≥5 μm) are deposited via the inertial impaction mechanism (Hofmann 2011). CT-based realistic lung geometry presents a complex shape and uneven surface. Impaction occurs on an uneven surface and in the cardinal angles of realistic lungs, mostly in upper generation airways. Small particles usually follow the fluid streamline; however, large particles (d_p≥5 μm) cannot follow a curved flow path because of inertia. As a result, they hit the tracheal walls at significant speed and are deposited there. Particles larger than 5 μm are deposited in the oropharynx, while particles smaller than 1 μm are deposited in the alveoli and peripheral airways (Everard 2001). Aarnes et al. (2019) reported that deposition efficiency increases with the increase in particle diameter.

The sedimentation deposition mechanism occurs because of the effect of gravitational force. Particles can be deposited under gravitational force in horizontal airways. The sedimentation deposition mechanism is the only mechanism that enables deposition for particles larger than 0.2 µm, and it mainly occurs in lower generation airways (peripheral and alveoli airways), where the airflow velocity is relatively low (Heyder et al. 1986).

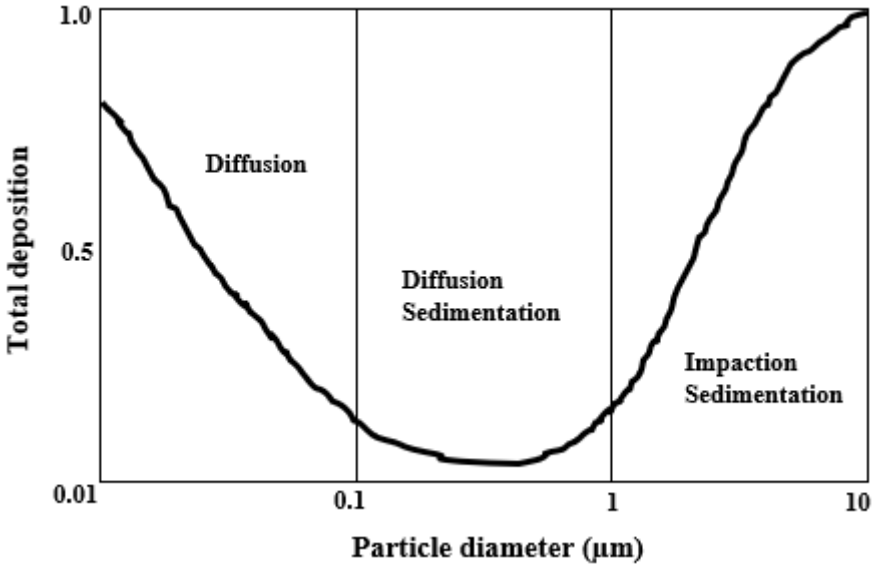

Figure 2.8. Particle deposition mechanism curve (redrawn from Heyder 2004).

Diffusion is another important deposition mechanism; it relies on Brownian motion, which is defined as the random motion caused by collision of gas molecules (Brush 1968). Therefore, the Brownian diffusion mechanism is important for nanoparticles (Rahman et al. 2021c). However, this diffusion mechanism is also important in the upper airways for nanoscale particles. Nanoparticles are mainly deposited through Brownian diffusion, and deposition efficiency via this mechanism increases with the reduction in particle size (Xi & Longest 2008).

The deposition efficiency due to the inertial impaction and diffusion mechanisms is lowest for particles sizes of 0.1–1 µm (Figure 2.8) (Bennett et al. 2007; Longest & Vinchurkar 2007). Density also affects the deposition of particles; large, high-density particles do not enter the deep airways. However, large, low-density particles can pass through the upper airways and

become deposited in the deep airways of the pulmonary region through the sedimentation process (Deng et al. 2019). The breathing pattern also affects particle deposition efficiency in the lung: rapid breathing increases impaction deposition (Rahimi-Gorji et al. 2016). Conversely, the contribution of the sedimentation and Brownian diffusion mechanisms increases with slow breathing (during sleep or rest) because of long residence time (Hofmann 2011).

Nanoparticles deposited in the airways are considerably more distributed than are microparticles (Rahman et al. 2021c) because the motion of particles in the crossflow direction during the diffusion process is observed not to be affected by the geometry and alignment of the airway. Particles can travel in the crossflow direction and reach the inner airway wall through diffusion in a vertical straight airway. For nanoscale particles, diffusion is a prominent deposition mechanism (Champion et al. 2007), whereas microparticles do not travel in the crossflow direction and thus diffusion is much weaker than impaction for these particles.

2.5 Numerical Modelling of Particle Transport and Deposition in the Human Lung

Which mechanisms are important in the numerical study of particle TD in human lungs depends on particle properties, lung geometry and breathing patterns (Hussain et al. 2011; Rahman et al. 2021c). The literature review revealed that microparticles are deposited in the upper airways via the inertial impaction mechanism. Nanoparticles are deposited in deep airways such as the alveolar region through diffusion and gravitational sedimentation. Important studies on particle TD in human lungs, covering different ages and using different models for different airways generations, are summarised in Table 2.1. Numerical methods for simulating particle TD for different sized particles are reviewed in detail in the following sections.

Table 2.1 Literature review on particle TD

Author	Anatomy	Particle type	Model	Particle deposition	Aging effect	Generation
Xu & Yu 1986	Non-realistic	Microparticles 0.01≤dp≤10 µm	Theoretical	Yes	Yes 0.5, 2, 8 & 30 yrs	G0–G23
Asgharian et al. 2004	Non-realistic	Microparticles 0.01, 1 & 10 µm	Multiple-path particle	Yes	Yes 3 & 23 mths; 8, 14 & 21 yrs	G0–G23
Kim et al. 2017	Non-realistic	No	Ansys Fluent	No	Yes 50, 60, 70 &80 yrs	G1–G23
Deng et al. 2018	Non-realistic	Microparticles 1≤dp≤10 µm	Ansys Fluent	Yes	Yes 7 mths; 4 & 20 yrs	G3–G6 G9–G12
Patterson et al. 2014	Non-realistic	Nanoparticles 10–100 nm	Multiple-path particle dosimetry	Yes	Yes 8, 9, 14 & 18 yrs	G0–G14
Rahman et al. 2021a	Non-realistic	Nanoparticles 5≤dp≤500 nm	Laminar	Yes	Yes 9 mths; 6 & 30 yrs	G0–G3 G12–G1
Rahman et al. 2021b	Non-realistic	Microparticles 5≤dp≤20 µm	Realisable k-ε turbulence	Yes	Yes 50, 60 & 70 yrs	G0–G14
Rahimi-Gorji et al. 2016	CT-realistic	Microparticles 1≤dp≤10 µm	k-ω turbulence	Yes	No	G0–G6
Chen et al. 2012	Idealised	Microparticles 10 µm	CFD-DEM	Yes	No	G3–G5
Kleinstreuer et al. 2008b	Non-realistic	Nanoparticles 20 nm≤dp≤3 µm	Laminar	Yes	No	G0–G6
Stapleton et al. 2000	CT-realistic	Polydisperse 1.65 & 4.8 µm	k-ε turbulence	Yes	No	Mouth–throat
Van de Moortele et al. 2018	CT-realistic	-	In vivo, in vitro	Yes	No	G0–G7
Keith Walters et al. 2014	CT-realistic	-	Laminar	Yes	No	G0–G15
Zhang et al. 2009	Non-realistic	Microparticles 1≤dp≤10 µm	Low Reynolds number k-ω turbulence	Yes	No	G0–G16
Islam et al. 2018b	CT-realistic	Polydisperse 1≤dp≤10 µm	k-ε turbulence	Yes	No	G0–G16
Dong et al. 2021	CT-realistic	Nanoparticles 3–100 nm	KG model	Yes	No	G0–G3

2.5.1 Numerical Modelling of Microparticle Transport and Deposition

The TD of microparticles in the range of 1–10 μm in the tracheobronchial airways had been studied using symmetric (Kim & Iglesias, 1989; Rahimi-Gorji et al., 2016) and asymmetric (Islam et al. 2019) anatomical models to understand the characteristics of airflow and particle deposition efficiency. Comer et al. (1999) developed a double-bifurcation lung geometry based on Weibel's model. They presented a comprehensive comparison of their findings with those of other numerical studies using a double-bifurcation non-realistic lung model. Kleinstreuer et al. (2008) investigated the airflow characteristics and TD of microparticles and nanoparticles in a triple-bifurcation symmetric model. In addition to the impaction mechanism for microparticle deposition, the Stokes–Einstein diffusion equation was used to simulate nanoparticle deposition. The results showed that microparticles are deposited at the cardinal angle because of the strong inertial impaction mechanism. Zhang et al. (2008) studied laminar-to-turbulent flows of a 16-generation triple-bifurcation non-realistic lung model using the low Reynolds number k–ω model. Subsequently, Islam et al. (2017) studied aerosol particle transport in lung models up to G17 using a large eddy simulation (LES) model. Their study proved additional evidence that the inertial impaction mechanism leads to particle deposition in the upper airways. Moreover, Pourmehran et al. (2016) conducted CFD simulations of a realistic lung model to identify particle deposition in tracheobronchial airways. Aerosol microparticle TD was found to be significant in the upper tracheobronchial lung airways.

A lung can be damaged in any lobar position in the upper, middle or deep airways (Subramaniam et al. 2003). Cancer occurs more often in the right than left lung (Parkash 1977). To treat diseases, small drug particles must travel to those damaged areas. Asgharian et al. (2004) used a multiple-path theoretical model to study age-specified particle deposition in a

five-lobe geometry. The study concluded that age does not affect the total deposition efficiency in the tracheobronchial region, but does affect deposition in the terminal airways.

Some particle TD research has been conducted using realistic lung models, but only over a small number of generations. Pourmehran et al. (2016) conducted CFD simulations of a realistic lung model from G0 to G6 and found most microparticles were deposited in the upper tracheobronchial lung airways. Asgari et al. (2021) investigated the deposition of aerosol particles in a realistic lung model from mouth to G6 under particular temperature and humidity conditions. They found that aerosol evolution happens mostly in the upper airway segments over relatively short timeframes.

2.5.2 Numerical Modelling of Nano (Ultrafine) Particle Transport and Deposition

Nanoparticles deposit in human lungs via the diffusion mechanism (Inthavong et al. 2011; Saha et al. 2018; Wang & Fan 2014; Zhang & Kleinstreuer 2004). Studies have shown that the deposition efficiency for nanoparticles in the deep airways is higher than that for microparticles. Cheng et al. (1996) conducted an experimental study of nanoparticle deposition in the nasal and oral airways, finding that the highest percentage of particles is deposited in the bifurcation area. Balásházy and Hofmann (1995) studied the deposition of 10-nm diameter particles in G3 and G4 of the Weibel model (Weibel et al. 1963) through numerical simulations, and discussed the association between deposition efficiency, and flow rate and particle size. Moskal and Gradoń (2002) numerically simulated the deposition of 10- and 100-nm-diameter particles in the first two bifurcations of a symmetric lung model. The study analysed details of the flow pattern and particle deposition at hot spots. Asgharian and Anjilvel (1994) simulated the TD of 100-nm particles in G16 and G17 of the Weibel model (Weibel et al. 1963), and monitored the trajectories of individual particles in the lung airways. Hofmann et al. (2003) simulated the TD of nanoparticles ranging from 1 to 500 nm in G3 and G4 under three flow rates. They found that more small nanoparticles are deposited in the lung airways than are large

nanoparticles. Zhang et al. (2008) studied airflow dynamics and nanoparticle ($1 \leq d_p \leq 100$ nm) deposition in a 16-generation symmetric model under two flow rates (15 & 30 L/min). Zhang and Kleinstreuer (2004) recommended that turbulence be modelled in numerical simulations if the flow rate (Q_{in}) is high (≥30 L/min).

Particle TD in realistic lung models is more complex than in symmetric lung models (Huang et al. 2021). Russo et al. (2018) used a G0–G3 realistic lung model of a patient to perform CFD simulations of magnetic nanoparticle drug delivery. They found that despite the high intensity of the magnetic field, only a small proportion of the particles entered the pulmonary airways. Through CFD simulations, Rahman et al. (2021c) studied nanoparticle TD from mouth to G3 airways. The results showed that over 90% of 5-nm particles pass through G3 and enter the deeper lung airways. Dong et al. (2021) also studied nanoparticle TD in realistic human airways up to G3, with similar conclusions. Brownian diffusion is the most common particle deposition mechanism for particles smaller than 10 nm. However, when particle size is greater than 100 nm, deposition efficiency decreases.

2.5.3 Numerical Modelling of Polydisperse Particle Deposition

Polydisperse particles are mixed particles of different sizes, which are very common in real life. Most studies have focused on the deposition of monodisperse particles with uniform size in vivo, in silico and in vitro. The deposition of polydisperse particles and its efficiency in the respiratory tract has been investigated in a very limited number of studies (Islam et al. 2018b; Montoya et al. 2004). The deposition of polydisperse particles in the lung airways is essential for the treatment of lung diseases (Dockery et al. 1993).

Rosati et al. (2003) studied the TD of polydisperse and monodisperse particles in packed beds. The results indicated that monodisperse particles have less deposition than polydisperse particles. Islam et al. (2018b) investigated the deposition of polydisperse particles in up to 17 generations of lung airways through LES. It was found that smaller size particles are deposited

in the lower airways, and larger size particles are deposited in the upper airways. Through CFD, Islam et al. (2021) investigated polydisperse aerosol particle deposition in the upper airways, up to G5. The analysis indicated that reducing the diameter of the lung airway had a considerable effect on particle deposition.

2.6 Age-related Particle Deposition Modelling

People of different ages may suffer from lung diseases such as pneumonia, COPD and asthma. Because lung volume and breathing capacity reduce as age increases, age-specific modelling of aerosol particle TD in the human lung is essential for the treatment of diseases in the respiratory tract. Research outcomes based on young patients do not apply to older people (Hogg et al. 1970). It has been reported that airborne particles deposit more easily in the lungs of school-aged people than adults because their lungs are smaller (Hruba et al. 2001; Roemer et al. 2000). However, most lung geometries available to study particle TD were created based on adults (Landahl 1950); the literature on particle TD in children and elderly people is limited.

Deng et al. (2018) studied particle deposition for three age groups: infant, child and adult. Their study emphasised that it is crucial to develop particle deposition as targeted drug delivery for elderly people. Xu and Yu (1986) developed a theoretical model for predicting deposition of inhaled aerosol in the respiratory tract of newborn babies and adults. Particles with different spherical microparticles ($0.01 \leq dp \leq 10$ μm) and four ages of people (0.5, 2, 8, & 30 years) were considered during the simulation. The results showed that the total deposition in the mouth–throat region of children is higher than in adults. However, total deposition in the tracheobronchial and alveolar regions of children can be either smaller or larger than in adults, depending on the size of the particles.

Kim et al. (2017) studied the effect of age on airflow dynamics and lung function mechanisms in Weibel's symmetric lung models up to G23. Their work was mainly focused on middle-aged to elderly people (50, 60, 70 & 80 years). Only the effects of age on airflow

characteristics in G10–G23 were studied; deposition of particles was not included. The results showed a 38% vacuum pressure reduction in the lung airways for 80-year-olds compared with 50-year-olds.

Asgharian et al. (2004) studied the effect of age on particle deposition in a multi-path symmetric branching lung model and calculated the lobe-specific deposition fraction in different regions and airway generations. They considered impaction, sedimentation and diffusion deposition mechanisms during the simulation. The deposition efficiencies of a five-lobe (right upper, right middle, right lower, left upper & left lower) lung model at five different ages (3 months, 23 months, 8 years, 14 years & 21 years) were compared. The results showed that deposition efficiency in the tracheobronchial region is similar at different ages. However, age significantly affects deposition in the alveolar region.

Deng et al. (2018) studied age effects on the TD of micron-sized particles ($1 \leq dp \leq 10$ μm) in a symmetric tracheobronchial lung airway model at three ages (7-month infant, 4-year old child and 20-year old adult) using Ansys Fluent software. Inertial impaction and gravitational sedimentation deposition mechanisms were considered to calculate deposition efficiency. Particle deposition was calculated for two groups of airway generation: upper (G3–G6) and lower (G9–G12). The results showed that the deposition efficiency in infants and children is higher than in adults in the tracheobronchial region. However, deposition efficiency in the lower airways is higher in adults than in children.

Patterson et al. (2014) studied particle deposition in the respiratory tract in school-aged children by considering flow rates in different microenvironments, such as the residential home, classroom, school bus and outdoor air. They developed a multiple-path particle dosimetry model to calculate the deposition fraction in the head, tracheobronchial and pulmonary region. Nanoparticles (10–100 nm) and four different school ages (8, 9, 14, and 18 years) were

considered in numerical simulations. The results indicated that total lung deposition efficiency in the pulmonary region is higher in younger children than in adults.

In summary, deposition efficiency in children is higher than in adults in the tracheobronchial region (Deng et al. 2018; Liu et al. 2012; Xu & Yu 1986). However, in the pulmonary and alveolar region, the deposition fraction varies with age (Asgharian et al. 2004; Patterson et al. 2014). CFD simulation has become more and more attractive in recent years because it provides clear mechanisms to explain local particle deposition patterns (Farghadan et al. 2020; Kleinstreuer et al. 2008a).

Asgharian et al. (2004) studied age-specified particle deposition using a five-lobe geometry in a non-realistic lung model. Stenosis of tracheal airways is caused by air pollution and breathing impairment (Brouns et al. 2007). Therefore, studying lobe-specific particle deposition and stenosis airways is important. In addition, it was evident from the literature review that particle TD in realistic lung models in regard to age has not been well studied. The current study aims to address this scholarly gap by investigating age-specified particle deposition in a realistic and non-realistic lung model and the effects on this of stenosis.

2.7 Particulate Matter or Pollutant Particle Transport and Deposition Modelling

Large numbers of pollutant particles are nowadays a major concern for public health, particularly for anyone with pulmonary lung diseases. PM of various sizes and from various sources absorbed into human lungs has an effect on respiratory health (Gautam et al. 2018; Valavanidis et al. 2008). PM is a complex combination of solid and liquid particles suspended in the air, and can move with wind across long distances (Gupta et al. 2006). Hazardous PM harms human health when it is breathed into the lungs and then circulated via the bloodstream (Fiordelisi et al. 2017; Mabahwi et al. 2014). Respiratory diseases such as asthma, lung cancer and COPD can all be caused by particles absorbed by epithelial cells (Chellappan et al. 2020;

Silva et al. 2015). Air pollution causes 3.1 million premature deaths and 3.2% of global disability-adjusted life each year, according to the Global Burden of Disease Study (Babatola 2018; Olaniyan et al. 2015). The ambient PM was ranked sixth out of 79 risk variables in the global burden of human diseases since 1990 (Feigin et al. 2016).

Pollutant-related particles emitted from different sources have different diameters (de Fatima Andrade et al. 2017). The most ultrafine traffic particles are produced by diesel and compressed natural gas (CNG) engines (Hammond et al. 2007). The majority of diesel particles are between 1 nm and 1 µm in size (de Sarabia et al. 2003). Diesel particles have a huge surface area, which permits them to absorb a variety of hazardous (Zhao & Castranova 2011). Coughing, itchy or burning eyes and neuropsychiatric symptoms such as headache, vomiting, nausea, difficult breathing, chest tightness and wheezing can all be caused by diesel particle exposure (Oravisjärvi et al. 2011). Because of their ability to enter deep lungs and lung cell membranes (Schraufnagel 2020), fine particles may constitute a substantial hazard to humans, affecting the entire organ system, including the brain (Guerrera et al. 2021; Oberdörster et al. 2005). It has been proven that fine particles are more dangerous than larger particles (Souza et al. 2021). However, studies have also demonstrated that the health effects of large pollutant particles are substantially more harmful than, or at least as strong as, those of small pollutants (Brunekreef & Forsberg 2005; Kelly & Fussell 2015). The morbidity and mortality caused by large/coarse pollution particles (2.5–10 µm) created by crustal materials are unknown (Diao et al. 2019; Pui et al. 2014).

Further, biomass burning creates a considerable quantity of PM dangerous to human health, an may include bushfire smoke and smoke from organised burns (Stefanidou et al. 2008; Yadav & Devi 2018). These small particles can travel throughout the distal lobes of the lungs, producing chronic cardiovascular diseases. Long-term exposure to fine particles has been linked to an increased risk of death. Further, cigarette smoke particles (CSP) cause serious

injury to the human lung (Ghio et al. 2022). Tobacco use releases 5.2 million tonnes of methane and 2.6 million tonnes of CO_2 annually into the atmosphere (Buchanan & Honey 1994; Paul et al. 2021). In cigarettes and other tobacco products, almost 7,000 substances have been discovered, 250 of which are dangerous to individuals and 70 of which are carcinogenic to humans (Dusautoir et al. 2021). This is because of the induction of epithelial cell mutagenesis, which results in cancers being physiologically produced. Smoking remains a major cause of death and disability across the world (Zaher et al. 2004).

After being inhaled, coarse dust particles (>10 μm) usually lodge in the upper respiratory tract. Toxic dust particles can end up anywhere in the respiratory system, presenting a health risk. A dust particle (<10 μm) can remain suspended in the atmosphere for weeks and then enter the deep lung airways (Brauer 2000). Finer dust particles (≤4 μm) can be inhaled and eventually deposit in the pulmonary alveoli, causing chronic lung disease. Particles appear to be absorbed quickly and deposited in the alveolar area of the lungs (Bakand et al. 2012). Several factors affect the deposition of inhaled particles in human lungs, including exposure concentration and particle characteristics such as size, density and shape, as well as individual breathing patterns (Braakhuis et al. 2014). This thesis has comprehensively analysed pollutant particle TD and found that the effects of density of nanoparticles are much weaker than those for microparticles.

2.8 Summary and Implications

A full understanding of particle TD in a 3D anatomical lung model is important for drug delivery in the respiratory tract, to advance treatment of lung diseases (Kuzmov & Minko 2015). The mouth–throat and nasal pathways have been used as non-invasive alternative routes for drug delivery in the respiratory system. Nebulisers, dry-powder inhalers and metered-dose inhalers are considered standard delivery devices (Hess 2008). However, all available devices are nondirectional and costly, and a very small proportion of aerosol particles is deposited in

the deep lung area. A numerical model of aerosol drug delivery is important to maximise particle deposition, reduce costs and minimise side effects of aggressive medicine.

Most numerical lung models are based on idealised or non-realistic lung models. Simulating TD of particles in realistic lung models is necessary to accurately predict deposition into the respiratory tract (Asgharian et al. 2006; Islam et al. 2017). Lung models such as in silico, in vitro and vivo models (Barnes 1995; Cabal et al. 2016; Göttlich et al. 2016) represent microparticle transport in the upper airways with limited branches, which is very different from real lung branches. The development of a lung model is essential for particle TD in terminal airways. Ultrafine particle simulation is important for therapeutic targeted drug delivery in the deep airways. It is also important to study the TD of PM air pollution, which causes a range of lung diseases including asthma, chronic bronchitis and lung cancer (Thurston & Lippmann 2015). Polydisperse particles are non-uniform and are thus applicable in the pharmaceutical industry. Several researchers have studied polydisperse particle deposition in human lung airways (Islam et al. 2018b; Martonen & Katz 1993).

Moreover, age-specific lung morphology is important for aerosol particle deposition in the realistic lung. Lung airway dimensions change with age (Reid 1977), and it has been shown that around 3.2 million people globally die before maturity each year, and 3.1% of people are disabled according to a 2010 report on global burden in health (Lim et al. 2012). Immature people (children) are more affected than adults by ambient PM air pollution because of their physical structure. Symmetric and planner lung airway models have been used because of the lack of high-resolution CT images for age-specific realistic lung geometry (Islam et al. 2021; Rahman et al. 2021a). Therefore, understanding of particle deposition in the realistic lung for people of every age is necessary for therapeutic drug delivery in the respiratory tract.

References

Aarnes, JR, Haugen, NE & Andersson, HI 2019, 'Inertial particle impaction on a cylinder in turbulent cross-flow at modest Reynolds numbers', International Journal of Multiphase Flow, vol. 111, pp. 53-61.

Anderson, S, Atkins, P, Bäckman, P, Cipolla, D, Clark, A, Daviskas, E et al. 2022, 'Inhaled Medicines: Past, Present, and Future', Pharmacological reviews, vol. 74, no. 1, pp. 48-118.

Asgari, M, Lucci, F & Kuczaj, AK 2021, 'Multispecies aerosol evolution and deposition in a human respiratory tract cast model', Journal of Aerosol Science, vol. 153, 105720.

Asgharian, B & Anjilvel, S 1994, 'A Monte Carlo calculation of the deposition efficiency of inhaled particles in lower airways', Journal of Aerosol Science, vol. 25, no. 4, pp. 711-721.

Asgharian, B, Menache, M & Miller, F 2004, 'Modeling age-related particle deposition in humans', Journal of aerosol medicine, vol. 17, no. 3, pp. 213-224.

Asgharian, B, Price, O & Hofmann, W 2006, 'Prediction of particle deposition in the human lung using realistic models of lung ventilation', Journal of Aerosol Science, vol. 37, no. 10, pp. 1209-1221.

Babatola, SS 2018, 'Global burden of diseases attributable to air pollution', Journal of public health in Africa, vol. 9, no. 3, pp. 162-166.

Bakand, S, Hayes, A & Dechsakulthorn, F 2012, 'Nanoparticles: a review of particle toxicology following inhalation exposure', Inhalation Toxicology, vol. 24, no. 2, pp. 125-135.

Balásházy, I & Hofmann, W 1995, 'Deposition of aerosols in asymmetric airway bifurcations', Journal of Aerosol Science, vol. 26, no. 2, pp. 273-292.

Barnes, S 1995, 'Effect of genistein on in vitro and in vivo models of cancer', The Journal of nutrition, vol. 125, no. suppl_3, pp. 777S-83S.

Bennett, WD, Zeman, KL & Jarabek, AM 2007, 'Nasal contribution to breathing and fine particle deposition in children versus adults', Journal of Toxicology and Environmental Health, Part A, vol. 71, no. 3, pp. 227-237.

Borm, PJ, Robbins, D, Haubold, S, Kuhlbusch, T, Fissan, H, Donaldson, K et al. 2006, 'The potential risks of nanomaterials: a review carried out for ECETOC', Particle and fibre toxicology, vol. 3, no. 1, pp. 1-35.

Braakhuis, HM, Park, MV, Gosens, I, De Jong, WH & Cassee, FR 2014, 'Physicochemical characteristics of nanomaterials that affect pulmonary inflammation', Particle and fibre toxicology, vol. 11, no. 1, pp. 1-25.

Brauer, AC, Michael 2000, 'Ambient atmospheric particles in the airways of human lungs', Ultrastructural pathology, vol. 24, no. 6, pp. 353-361.

Brouns, M, Jayaraju, ST, Lacor, C, De Mey, J, Noppen, M, Vincken, W et al. 2007, 'Tracheal stenosis: a flow dynamics study', Journal of Applied Physiology, vol. 102, no. 3, pp. 1178-1184.

Brunekreef, B & Forsberg, B 2005, 'Epidemiological evidence of effects of coarse airborne particles on health', European Respiratory Journal, vol. 26, no. 2, pp. 309-318.

Brush, SG 1968, 'A history of random processes: I. Brownian movement from Brown to Perrin', Archive for history of exact sciences, vol. 5, no. 1, pp. 1-36.

Buchanan, AH & Honey, BG 1994, 'Energy and carbon dioxide implications of building construction', Energy and Buildings, vol. 20, no. 3, pp. 205-217.

Button, B, Cai, L-H, Ehre, C, Kesimer, M, Hill, DB, Sheehan, JK et al. 2012, 'A periciliary brush promotes the lung health by separating the mucus layer from airway epithelia', Science, vol. 337, no. 6097, pp. 937-941.

Cabal, A, Mehta, K, Guo, P & Przekwas, A 2016, 'In‐silico lung modeling platform for inhaled drug delivery', Proceedings Drug Delivery to the Lungs, vol. 27, pp. 82-86.

Champion, JA, Katare, YK & Mitragotri, S 2007, 'Particle shape: a new design parameter for micro-and nanoscale drug delivery carriers', Journal of controlled release, vol. 121, no. 1-2, pp. 3-9.

Chellappan, DK, Yee, LW, Xuan, KY, Kunalan, K, Rou, LC, Jean, LS et al. 2020, 'Targeting neutrophils using novel drug delivery systems in chronic respiratory diseases', Drug development research, vol. 81, no. 4, pp. 419-436.

Chen, X, Zhong, W, Zhou, X, Jin, B & Sun, B 2012, 'CFD–DEM simulation of particle transport and deposition in pulmonary airway', Powder technology, vol. 228, pp. 309-318.

Cheng, K-H, Cheng, Y-S, Yeh, H-C, Guilmette, RA, Simpson, SQ, Yang, Y-H et al. 1996, 'In vivo measurements of nasal airway dimensions and ultrafine aerosol deposition in the human nasal and oral airways', Journal of Aerosol Science, vol. 27, no. 5, pp. 785-801.

Choi, J-I & Kim, CS 2007, 'Mathematical analysis of particle deposition in human lungs: an improved single path transport model', Inhalation Toxicology, vol. 19, no. 11, pp. 925-939.

Comer, J, Kleinstreuer, C, Hyun, S & Kim, C 1999, 'Aerosol transport and deposition in sequentially bifurcating airways', J. Biomech. Eng., vol. 122, no. 2, pp. 152-158.

Corcoran, T & Chigier, N 2002, 'Inertial deposition effects: a study of aerosol mechanics in the trachea using laser Doppler velocimetry and fluorescent dye', J. Biomech. Eng., vol. 124, no. 6, pp. 629-637.

Ćurić, M, Zafirovski, O & Spiridonov, V 2022, 'The Basic Medicine of the Human Anatomy', in Essentials of Medical Meteorology, Springer, pp. 17-37.

Cushley, MJ, Tattersfield, AE & Holgate, ST 2004, 'Inhaled adenosine and guanosine on airway resistance in normal and asthmatic subjects', British journal of clinical pharmacology, vol. 58, no. 7, pp. 161-165.

Darquenne, C 2012, 'Aerosol deposition in health and disease', J Aerosol Med Pulm Drug Deliv, vol. 25, no. 3, pp. 140-147.

de Fatima Andrade, M, Kumar, P, de Freitas, ED, Ynoue, RY, Martins, J, Martins, LD et al. 2017, 'Air quality in the megacity of São Paulo: Evolution over the last 30 years and future perspectives', Atmospheric environment, vol. 159, pp. 66-82.

de Sarabia, ER-F, Elvira-Segura, L, Gonzalez-Gomez, I, Rodrıguez-Maroto, J, Munoz-Bueno, R & Dorronsoro-Areal, J 2003, 'Investigation of the influence of humidity on the ultrasonic agglomeration of submicron particles in diesel exhausts', Ultrasonics, vol. 41, no. 4, pp. 277-281.

Deng, Q, Deng, L, Miao, Y, Guo, X & Li, Y 2019, 'Particle deposition in the human lung: health implications of particulate matter from different sources', Environmental research, vol. 169, pp. 237-245.

Deng, Q, Ou, C, Chen, J & Xiang, Y 2018, 'Particle deposition in tracheobronchial airways of an infant, child and adult', Science of the Total Environment, vol. 612, pp. 339-346.

Diao, M, Holloway, T, Choi, S, O'Neill, SM, Al-Hamdan, MZ, Van Donkelaar, A et al. 2019, 'Methods, availability, and applications of PM2. 5 exposure estimates derived from ground measurements, satellite, and atmospheric models', Journal of the Air & Waste Management Association, vol. 69, no. 12, pp. 1391-1414.

Dockery, DW, Pope, CA, Xu, X, Spengler, JD, Ware, JH, Fay, ME et al. 1993, 'An association between air pollution and mortality in six US cities', New England journal of medicine, vol. 329, no. 24, pp. 1753-1759.

Dong, J, Li, J, Tian, L & Tu, J 2021, 'Transport and deposition of ultrafine particles in the upper tracheobronchial tree: a comparative study between approximate and realistic respiratory tract models', Computer Methods in Biomechanics and Biomedical Engineering, vol. 24, no. 10, pp. 1125-1135.

Duncan, GA, Jung, J, Hanes, J & Suk, JS 2016, 'The mucus barrier to inhaled gene therapy', Molecular Therapy, vol. 24, no. 12, pp. 2043-2053.

Dusautoir, R, Zarcone, G, Verriele, M, Garçon, G, Fronval, I, Beauval, N et al. 2021, 'Comparison of the chemical composition of aerosols from heated tobacco products, electronic cigarettes and tobacco cigarettes and their toxic impacts on the human bronchial epithelial BEAS-2B cells', Journal of hazardous materials, vol. 401, 123417.

Everard, M 2001, 'Guidelines for devices and choices', Journal of aerosol medicine, vol. 14, no. 1, Supplement 1, pp. 59-64.

Farghadan, A, Poorbahrami, K, Jalal, S, Oakes, JM, Coletti, F & Arzani, A 2020, 'Particle transport and deposition correlation with near-wall flow characteristic under inspiratory airflow in lung airways', Computers in biology and medicine, vol. 120, 103703.

Feigin, VL, Roth, GA, Naghavi, M, Parmar, P, Krishnamurthi, R, Chugh, S et al. 2016, 'Global burden of stroke and risk factors in 188 countries, during 1990–2013: a systematic analysis for the Global Burden of Disease Study 2013', The Lancet Neurology, vol. 15, no. 9, pp. 913-924.

Fiordelisi, A, Piscitelli, P, Trimarco, B, Coscioni, E, Iaccarino, G & Sorriento, D 2017, 'The mechanisms of air pollution and particulate matter in cardiovascular diseases', Heart failure reviews, vol. 22, no. 3, pp. 337-347.

Gautam, S, Patra, AK, Sahu, SP & Hitch, M 2018, 'Particulate matter pollution in opencast coal mining areas: a threat to human health and environment', International Journal of Mining, Reclamation and Environment, vol. 32, no. 2, pp. 75-92.

Ghio, AJ, Pavlisko, EN, Roggli, VL, Todd, NW & Sangani, RG 2022, 'Cigarette smoke particle-induced lung injury and iron homeostasis', International Journal of Chronic Obstructive Pulmonary Disease, vol. 17, pp. 117-140.

Göttlich, C, Müller, LC, Kunz, M, Schmitt, F, Walles, H, Walles, T et al. 2016, 'A combined 3D tissue engineered in vitro/in silico lung tumor model for predicting drug effectiveness in specific mutational backgrounds', JoVE (Journal of Visualized Experiments), no. 110, 53885.

Gray, H & Goss, CM 1878, Anatomy of the human body, vol. 8, Lea & Febiger.

Guerrera, MC, Aragona, M, Porcino, C, Fazio, F, Laurà, R, Levanti, M et al. 2021, 'Micro and nano plastics distribution in fish as model organisms: histopathology, blood response and bioaccumulation in different organs', Applied Sciences, vol. 11, no. 13, 5768.

Gupta, P, Christopher, SA, Wang, J, Gehrig, R, Lee, Y & Kumar, N 2006, 'Satellite remote sensing of particulate matter and air quality assessment over global cities', Atmospheric environment, vol. 40, no. 30, pp. 5880-5892.

Hales, S 1731, 'Vegetable Staticks: Analysis of the Air', Biodiversity Heritage Library: Washington, DC, USA, vol. 1.

Hammond, D, Jones, S & Lalor, M 2007, 'In-vehicle measurement of ultrafine particles on compressed natural gas, conventional diesel, and oxidation-catalyst diesel heavy-duty transit buses', Environmental monitoring and assessment, vol. 125, no. 1, pp. 239-246.

Hess, DR 2008, 'Aerosol delivery devices in the treatment of asthma', Respiratory care, vol. 53, no. 6, pp. 699-725.

Heyder, J 2004, 'Deposition of inhaled particles in the human respiratory tract and consequences for regional targeting in respiratory drug delivery', Proceedings of the American Thoracic Society, vol. 1, no. 4, pp. 315-320.

Heyder, J, Gebhart, J, Rudolf, G, Schiller, CF & Stahlhofen, W 1986, 'Deposition of particles in the human respiratory tract in the size range 0.005–15 μm', Journal of Aerosol Science, vol. 17, no. 5, pp. 811-825.

Hofmann, W 2011, 'Modelling inhaled particle deposition in the human lung—A review', Journal of Aerosol Science, vol. 42, no. 10, pp. 693-724.

Hofmann, W, Golser, R & Balashazy, I 2003, 'Inspiratory deposition efficiency of ultrafine particles in a human airway bifurcation model', Aerosol Science & Technology, vol. 37, no. 12, pp. 988-994.

Hogg, J, Williams, J, Richardson, J, Macklem, P & Thurlbeck, W 1970, 'Age as a factor in the distribution of lower-airway conductance and in the pathologic anatomy of obstructive lung disease', New England journal of medicine, vol. 282, no. 23, pp. 1283-1287.

Horsfield, K, Dart, G, Olson, DE, Filley, GF & Cumming, G 1971, 'Models of the human bronchial tree', Journal of Applied Physiology, vol. 31, no. 2, pp. 207-217.

Hruba, F, Fabianova, E, Koppova, K & Vandenberg, JJ 2001, 'Childhood respiratory symptoms, hospital admissions, and long-term exposure to airborne particulate matter', Journal of Exposure Science & Environmental Epidemiology, vol. 11, no. 1, pp. 33-40.

Huang, F, Zhu, Q, Zhou, X, Gou, D, Yu, J, Li, R et al. 2021, 'Role of CFD based in silico modelling in establishing an in vitro-in vivo correlation of aerosol deposition in the respiratory tract', Advanced Drug Delivery Reviews, vol. 170, pp. 369-385.

Hussain, M, Madl, P & Khan, A 2011, 'Lung deposition predictions of airborne particles and the emergence of contemporary diseases, Part-I', Health, vol. 2, no. 2, pp. 51-59.

Inthavong, K 2020, 'From indoor exposure to inhaled particle deposition: A multiphase journey of inhaled particles', Experimental and Computational Multiphase Flow, vol. 2, no. 2, pp. 59-78.

Inthavong, K, Zhang, K & Tu, J 2011, 'Numerical modelling of nanoparticle deposition in the nasal cavity and the tracheobronchial airway', Computer Methods in Biomechanics and Biomedical Engineering, vol. 14, no. 7, pp. 633-643.

Ionescu, CM 2013, 'The human respiratory system', in The Human Respiratory System, Springer, pp. 13-22.

Islam, MS, Saha, SC, Young, PM 2018a, 'Aerosol Particle Transport and Deposition in a CT-Based Lung Airway for Helium-Oxygen Mixture', *In Proceedings of the 21st Australasian Fluid Mechanics Conference,* AFMC, December 10-13.

Islam, MS, Larpruenrudee, P, Hossain, SI, Rahimi-Gorji, M, Gu, Y, Saha, SC et al. 2021, 'Polydisperse aerosol transport and deposition in upper airways of age-specific lung', International Journal of Environmental Research and Public Health, vol. 18, no. 12, 6239.

Islam, MS, Saha, SC, Gemci, T, Yang, IA, Sauret, E & Gu, Y 2018b, 'Polydisperse microparticle transport and deposition to the terminal bronchioles in a heterogeneous vasculature tree', Scientific Reports, vol. 8, no. 1, pp. 1-9.

Islam, MS, Saha, SC, Gemci, T, Yang, IA, Sauret, E, Ristovski, Z et al. 2019, 'Euler-Lagrange prediction of diesel-exhaust polydisperse particle transport and deposition in lung: anatomy and turbulence effects', Scientific Reports, vol. 9, no. 1, pp. 1-16.

Islam, MS, Saha, SC, Sauret, E, Gemci, T & Gu, Y 2017, 'Pulmonary aerosol transport and deposition analysis in upper 17 generations of the human respiratory tract', Journal of Aerosol Science, vol. 108, pp. 29-43.

Kasper, G 1982, 'Dynamics and measurement of smokes. I Size characterization of nonspherical particles', Aerosol Science and Technology, vol. 1, no. 2, pp. 187-199.

Keith Walters, D, Burgreen, GW, Hester, RL, Thompson, DS, Lavallee, DM, Pruett, WA et al. 2014, 'Cyclic Breathing Simulations in Large-Scale Models of the Lung Airway From the Oronasal Opening to the Terminal Bronchioles', Journal of Fluids Engineering, vol. 136, no. 10, pp. 1-10.

Kelly, FJ & Fussell, JC 2015, 'Air pollution and public health: emerging hazards and improved understanding of risk', Environmental geochemistry and health, vol. 37, no. 4, pp. 631-649.

Kim, CS & Iglesias, AJ 1989, 'Deposition of inhaled particles in bifurcating airway models: I. Inspiratory deposition', Journal of aerosol medicine, vol. 2, no. 1, pp. 1-14.

Kim, J, Heise, RL, Reynolds, AM & Pidaparti, RM 2017, 'Aging effects on airflow dynamics and lung function in human bronchioles', PloS one, vol. 12, no. 8, 0183654.

Kleinstreuer, C, Zhang, Z & Donohue, J 2008a, 'Targeted drug-aerosol delivery in the human respiratory system', Annual Review of Biomedical Engineering, vol. 10, pp. 195-220.

Kleinstreuer, C, Zhang, Z & Li, Z 2008b, 'Modeling airflow and particle transport/deposition in pulmonary airways', Respiratory Physiology & Neurobiology, vol. 163, no. 1-3, pp. 128-138.

Knowles, MR & Boucher, RC 2002, 'Mucus clearance as a primary innate defense mechanism for mammalian airways', The Journal of clinical investigation, vol. 109, no. 5, pp. 571-577.

Kumar, H, Tawhai, MH, Hoffman, EA & Lin, C-L 2009, 'The effects of geometry on airflow in the acinar region of the human lung', Journal of Biomechanics, vol. 42, no. 11, pp. 1635-1642.

Kuzmov, A & Minko, T 2015, 'Nanotechnology approaches for inhalation treatment of lung diseases', Journal of controlled release, vol. 219, pp. 500-518.

Lai, SK, O'Hanlon, DE, Harrold, S, Man, ST, Wang, Y-Y, Cone, R et al. 2007, 'Rapid transport of large polymeric nanoparticles in fresh undiluted human mucus', Proceedings of the National Academy of Sciences, vol. 104, no. 5, pp. 1482-1487.

Lai, SK, Wang, Y-Y & Hanes, J 2009, 'Mucus-penetrating nanoparticles for drug and gene delivery to mucosal tissues', Advanced Drug Delivery Reviews, vol. 61, no. 2, pp. 158-171.

Landahl, H 1950, 'On the removal of air-borne droplets by the human respiratory tract: I. The lung', The bulletin of mathematical biophysics, vol. 12, no. 1, pp. 43-56.

Lee, SH, Shim, JK, Kim, JM, Choi, H-K & Jeon, CO 2011, 'Henriciella litoralis sp. nov., isolated from a tidal flat, transfer of Maribaculum marinum Lai et al. 2009 to the genus Henriciella as Henriciella aquimarina nom. nov. and emended description of the genus Henriciella', International journal of systematic and evolutionary microbiology, vol. 61, no. 4, pp. 722-727.

Lengyel, M, Kállai-Szabó, N, Antal, V, Laki, AJ & Antal, I 2019, 'Microparticles, Microspheres, and Microcapsules for Advanced Drug Delivery', Scientia Pharmaceutica, vol. 87, no. 3, 20.

Lillehoj, EP & Kim, KC 2002, 'Airway mucus: its components and function', Archives of pharmacal research, vol. 25, no. 6, pp. 770-780.

Lim, SS, Vos, T, Flaxman, AD, Danaei, G, Shibuya, K, Adair-Rohani, H et al. 2012, 'A comparative risk assessment of burden of disease and injury attributable to 67 risk factors and risk factor clusters in 21 regions, 1990–2010: a systematic analysis for the Global Burden of Disease Study 2010', The lancet, vol. 380, no. 9859, pp. 2224-2260.

Liu, Z, Li, A, Xu, X & Gao, R 2012, 'Computational fluid dynamics simulation of airflow patterns and particle deposition characteristics in children upper respiratory tracts', Engineering Applications of Computational Fluid Mechanics, vol. 6, no. 4, pp. 556-571.

Longest, PW & Vinchurkar, S 2007, 'Validating CFD predictions of respiratory aerosol deposition: effects of upstream transition and turbulence', Journal of biomechanics, vol. 40, no. 2, pp. 305-316.

Mabahwi, NAB, Leh, OLH & Omar, D 2014, 'Human health and wellbeing: Human health effect of air pollution', Procedia-Social and Behavioral Sciences, vol. 153, pp. 221-229.

Martonen, T & Katz, I 1993, 'Deposition patterns of polydisperse aerosols within human lungs', Journal of aerosol medicine, vol. 6, no. 4, pp. 251-274.

Marttin, E, Schipper, NG, Verhoef, JC & Merkus, FW 1998, 'Nasal mucociliary clearance as a factor in nasal drug delivery', Advanced Drug Delivery Reviews, vol. 29, no. 1-2, pp. 13-38.

Montoya, L, Lawrence, J, Murthy, GK, Sarnat, J, Godleski, J & Koutrakis, P 2004, 'Continuous measurements of ambient particle deposition in human subjects', Aerosol Science and Technology, vol. 38, no. 10, pp. 980-990.

Moskal, A & Gradoń, L 2002, 'Temporary and spatial deposition of aerosol particles in the upper human airways during breathing cycle', Journal of Aerosol Science, vol. 33, no. 11, pp. 1525-1539.

Oberdörster, G, Maynard, A, Donaldson, K, Castranova, V, Fitzpatrick, J, Ausman, K et al. 2005, 'Principles for characterizing the potential human health effects from exposure to nanomaterials: elements of a screening strategy', Particle and fibre toxicology, vol. 2, no. 1, pp. 1-35.

Olaniyan, T, Dalvie, M & Jeebhay, M 2015, 'Ambient air pollution and childhood asthma: a review of South African epidemiological studies: allergies in the workplace', Current Allergy & Clinical Immunology, vol. 28, no. 2, pp. 122-127.

Oravisjärvi, K, Pietikäinen, M, Ruuskanen, J, Rautio, A, Voutilainen, A & Keiski, RL 2011, 'Effects of physical activity on the deposition of traffic-related particles into the human lungs in silico', Science of the Total Environment, vol. 409, no. 21, pp. 4511-4518.

Parkash, O 1977, 'Lung cancer', Respiration, vol. 34, no. 5, pp. 295-304.

Pasman, T, Baptista, D, van Riet, S, Truckenmüller, RK, Hiemstra, PS, Rottier, RJ et al. 2020, 'Development of porous and flexible PTMC membranes for in vitro organ models fabricated by evaporation-induced phase separation', Membranes, vol. 10, no. 11, 330.

Patterson, RF, Zhang, Q, Zheng, M & Zhu, Y 2014, 'Particle deposition in respiratory tracts of school-aged children', Aerosol Air Qual. Res, vol. 14, pp. 64-73.

Paul, AR, Khan, F, Jain, A & Saha, SC 2021, 'Deposition of smoke particles in human airways with realistic waveform', Atmosphere, vol. 12, no. 7, 912.

Pourmehran, O, Gorji, TB & Gorji-Bandpy, M 2016, 'Magnetic drug targeting through a realistic model of human tracheobronchial airways using computational fluid and particle dynamics', Biomechanics and Modeling in Mechanobiology, vol. 15, no. 5, pp. 1355-1374.

Pui, DY, Chen, S-C & Zuo, Z 2014, 'PM2. 5 in China: Measurements, sources, visibility and health effects, and mitigation', Particuology, vol. 13, pp. 1-26.

Pump, K 1964, 'The morphology of the finer branches of the bronchial tree of the human lung', Diseases of the Chest, vol. 46, no. 4, pp. 379-398.

Rahimi-Gorji, M, Gorji, TB & Gorji-Bandpy, M 2016, 'Details of regional particle deposition and airflow structures in a realistic model of human tracheobronchial airways: two-phase flow simulation', Computers in biology and medicine, vol. 74, pp. 1-17.

Rahman, MM, Zhao, M, Islam, MS, Dong, K & Saha, SC 2021a, 'Aerosol Particle Transport and Deposition in Upper and Lower Airways of Infant, Child and Adult Human Lungs', Atmosphere, vol. 12, no. 11, 1402.

Rahman, MM, Zhao, M, Islam, MS, Dong, K & Saha, SC 2021b, 'Aging effects on airflow distribution and micron-particle transport and deposition in a human lung using CFD-DPM approach', Advanced Powder Technology, vol. 32, no. 10, pp. 3506-3516.

Rahman, MM, Zhao, M, Islam, MS, Dong, K & Saha, SC 2021c, 'Numerical study of nanoscale and microscale particle transport in realistic lung models with and without stenosis', International Journal of Multiphase Flow, vol. 145, 103842.

Rajabi, M & A Mousa, S 2016, 'Lipid nanoparticles and their application in nanomedicine', Current pharmaceutical biotechnology, vol. 17, no. 8, pp. 662-672.

Reid, L 1977, '1976 Edward BD Neuhauser lecture: the lung: growth and remodeling in health and disease', American Journal of Roentgenology, vol. 129, no. 5, pp. 777-788.

Roemer, W, Hoek, G, Brunekreef, B, Clench-Aas, J, Forsberg, B, Pekkanen, J et al. 2000, 'PM10 elemental composition and acute respiratory health effects in European children (PEACE project). Pollution Effects on Asthmatic Children in Europe', European Respiratory Journal, vol. 15, no. 3, pp. 553-559.

Rosati, JA, Leith, D & Kim, CS 2003, 'Monodisperse and polydisperse aerosol deposition in a packed bed', Aerosol Science & Technology, vol. 37, no. 6, pp. 528-535.

Ruge, CA 2012, 'Bio-nano interactions in the peripheral lungs: role of pulmonary surfactant components in alveolar macrophage clearance of nanoparticles', pp. 1-129.

Russo, F, Boghi, A & Gori, F 2018, 'Numerical simulation of magnetic nano drug targeting in patient-specific lower respiratory tract', Journal of Magnetism and Magnetic Materials, vol. 451, pp. 554-564.

Saha, S, Islam, MS & Luo, Z 2018, 'Ultrafine Particle Transport and Deposition in the Upper Airways of a CT-Based Realistic Lung', In *Proceedings of the 21st Australasian Fluid Mechanics Conference, AFMC*.

Sarkar, M, Madabhavi, I, Niranjan, N & Dogra, M 2015, 'Auscultation of the respiratory system', Annals of thoracic medicine, vol. 10, no. 3, 158.

Sauret, V, Goatman, K, Fleming, J & Bailey, A 1999, 'Semi-automated tabulation of the 3D topology and morphology of branching networks using CT: application to the airway tree', Physics in Medicine & Biology, vol. 44, no. 7, 1625.

Sauret, V, Halson, P, Brown, I, Fleming, J & Bailey, A 2002, 'Study of the three‐dimensional geometry of the central conducting airways in man using computed tomographic (CT) images', Journal of anatomy, vol. 200, no. 2, pp. 123-134.

Schraufnagel, DE 2020, 'The health effects of ultrafine particles', Experimental & molecular medicine, vol. 52, no. 3, pp. 311-317.

Sharma, D & Jindal, G 2011, 'Computer aided diagnosis system for detection of lungcancer in CT scan images', International Journal of Computer and Electrical Engineering, vol. 3, no. 5, 714.

Shi, W, Ching, YC & Chuah, CH 2021, 'Preparation of aerogel beads and microspheres based on chitosan and cellulose for drug delivery: A review', International journal of biological macromolecules, vol. 170, pp. 751-767.

Silva, R, Oyarzún, M & Olloquequi, J 2015, 'Pathogenic mechanisms in chronic obstructive pulmonary disease due to biomass smoke exposure', Archivos de Bronconeumología (English Edition), vol. 51, no. 6, pp. 285-292.

Soni, B & Aliabadi, S 2013, 'Large-scale CFD simulations of airflow and particle deposition in lung airway', Computers & Fluids, vol. 88, pp. 804-812.

Soong, T, Nicolaides, P, Yu, C & Soong, S 1979, 'A statistical description of the human tracheobronchial tree geometry', Respiration physiology, vol. 37, no. 2, pp. 161-172.

Souza, IdC, Morozesk, M, Mansano, AS, Mendes, VA, Azevedo, VC, Matsumoto, ST et al. 2021, 'Atmospheric particulate matter from an industrial area as a source of metal nanoparticle contamination in aquatic ecosystems', Science of the Total Environment, vol. 753, 141976.

Stapleton, K-W, Guentsch, E, Hoskinson, M & Finlay, W 2000, 'On the suitability of k–ε turbulence modeling for aerosol deposition in the mouth and throat: a comparison with experiment', Journal of aerosol science, vol. 31, no. 6, pp. 739-749.

Stefanidou, M, Athanaselis, S & Spiliopoulou, C 2008, 'Health impacts of fire smoke inhalation', Inhalation Toxicology, vol. 20, no. 8, pp. 761-766.

Subramaniam, RP, Asgharian, B, Freijer, JI, Miller, FJ & Anjilvel, S 2003, 'Analysis of lobar differences in particle deposition in the human lung', Inhalation toxicology, vol. 15, no. 1, pp. 1-21.

Thurston, G & Lippmann, M 2015, 'Ambient particulate matter air pollution and cardiopulmonary diseases', Thieme Medical Publishers, vol. 36, no. 03, pp. 422-432.

Tu, J, Inthavong, K & Ahmadi, G 2013, 'The human respiratory system', in Computational fluid and particle dynamics in the human respiratory system, Springer, pp. 19-44.

Valavanidis, A, Fiotakis, K & Vlachogianni, T 2008, 'Airborne particulate matter and human health: toxicological assessment and importance of size and composition of particles for oxidative damage and carcinogenic mechanisms', Journal of Environmental Science and Health, Part C, vol. 26, no. 4, pp. 339-362.

Vallières, M, Freeman, CR, Skamene, SR & El Naqa, I 2015, 'A radiomics model from joint FDG-PET and MRI texture features for the prediction of lung metastases in soft-tissue sarcomas of the extremities', Physics in Medicine & Biology, vol. 60, no. 14, 5471.

Van de Moortele, T, Wendt, CH & Coletti, F 2018, 'Morphological and functional properties of the conducting human airways investigated by in vivo computed tomography and in vitro MRI', Journal of Applied Physiology, vol. 124, no. 2, pp. 400-413.

Vranicar, M, Gregory, W, Douglas, WI, Di Sessa, P & Di Sessa, TG 2008, 'The use of stereolithographic hand held models for evaluation of congenital anomalies of the great arteries', Studies in health technology and informatics, vol. 132, 538.

Wang, J & Fan, Y 2014, 'Lung injury induced by TiO2 nanoparticles depends on their structural features: size, shape, crystal phases, and surface coating', International journal of molecular sciences, vol. 15, no. 12, pp. 22258-22278.

Wanigasekara, J & Witharana, C 2016, 'Applications of nanotechnology in drug delivery and design-an insight', Current Trends in Biotechnology and Pharmacy, vol. 10, no. 1, pp. 78-91.

Weibel, ER 1963, 'Geometric and dimensional airway models of conductive, transitory and respiratory zones of the human lung', in Morphometry of the human lung, Springer, pp. 136-142.

Weibel, ER, Cournand, AF & Richards, DW 1963, Morphometry of the human lung, vol. 1, Springer.

Widdicombe, J 1997, 'Airway liquid: a barrier to drug diffusion?', European Respiratory Journal, vol. 10, no. 10, pp. 2194-2197.

Wiggs, B, Moreno, R, Hogg, J, Hilliam, C & Pare, P 1990, 'A model of the mechanics of airway narrowing', Journal of Applied Physiology, vol. 69, no. 3, pp. 849-860.

Xi, J & Longest, PW 2008, 'Numerical predictions of submicrometer aerosol deposition in the nasal cavity using a novel drift flux approach', International Journal of Heat and Mass Transfer, vol. 51, no. 23-24, pp. 5562-5577.

Xu, G & Yu, C 1986, 'Effects of age on deposition of inhaled aerosols in the human lung', Aerosol science and technology, vol. 5, no. 3, pp. 349-357.

Yadav, IC & Devi, NL 2018, 'Biomass burning, regional air quality, and climate change', Earth Systems and Environmental Sciences. Edition: Encyclopedia of Environmental Health. Elsevier. https://doi. org/10.1016/B978-0-12-409548-9.11022-X.

Yeh, H-C, Raabe, O, Schum, G & Phalen, R 1976, 'Tracheobronchial geometry: human, dog, rat, hamester', Lovelace Foundation for Medical Education and Research, Report number LF-53.

Yeh, H-C & Schum, G 1980, 'Models of human lung airways and their application to inhaled particle deposition', Bulletin of mathematical biology, vol. 42, no. 3, pp. 461-480.

Zaher, C, Halbert, R, Dubois, R, George, D & Nonikov, D 2004, 'Smoking-related diseases: the importance of COPD', The international journal of tuberculosis and lung disease, vol. 8, no. 12, pp. 1423-1428.

Zhang, Z & Kleinstreuer, C 2004, 'Airflow structures and nano-particle deposition in a human upper airway model', Journal of computational physics, vol. 198, no. 1, pp. 178-210.

Zhang, Z, Kleinstreuer, C & Kim, CS 2008, 'Airflow and nanoparticle deposition in a 16-generation tracheobronchial airway model', Annals of Biomedical Engineering, vol. 36, no. 12, pp. 2095-2110.

Zhang, Z, Kleinstreuer, C & Kim, CS 2009, 'Comparison of analytical and CFD models with regard to micron particle deposition in a human 16-generation tracheobronchial airway model', Journal of aerosol science, vol. 40, no. 1, pp. 16-28.

Zhao, J & Castranova, V 2011, 'Toxicology of nanomaterials used in nanomedicine', Journal of Toxicology and Environmental Health, Part B, vol. 14, no. 8, pp. 593-632.

Zhou, Y & Cheng, Y-S 2005, 'Particle deposition in a cast of human tracheobronchial airways', Aerosol science and technology, vol. 39, no. 6, pp. 492-500.

Chapter 3: Aerosol Particle Transport and Deposition in Upper and Lower Airways of Infant, Child and Adult Human Lungs

This chapter presents a final accepted version paper published in 2021, Atmosphere, 12 (11), 1402. The first page of the published paper was shown at the beginning of the chapter, followed by the accepted version.

Chapter 3: Aerosol Particle Transport and Deposition in Upper and Lower Airways of Infant, Child and Adult Human Lungs

atmosphere

MDPI

Article

Aerosol Particle Transport and Deposition in Upper and Lower Airways of Infant, Child and Adult Human Lungs

Md. M. Rahman [1,2,*], Ming Zhao [1,*], Mohammad S. Islam [3], Kejun Dong [4] and Suvash C. Saha [3]

1 School of Engineering, Design and Built Environment, Western Sydney University, Penrith, NSW 2751, Australia
2 Department of Mathematics, Faculty of Science, Islamic University, Kushtia 7003, Bangladesh
3 School of Mechanical and Mechatronic Engineering, University of Technology Sydney, Ultimo, NSW 2007, Australia; mohammadsaidul.islam@uts.edu.au (M.S.I.); Suvash.Saha@uts.edu.au (S.C.S.)
4 Center for Infrastructure Engineering, Western Sydney University, Penrith, NSW 2751, Australia; Kejun.Dong@westernsydney.edu.au
* Correspondence: 19615253@student.westernsydney.edu.au (M.M.R.); M.Zhao@westernsydney.edu.au (M.Z.)

Abstract: Understanding transportation and deposition (TD) of aerosol particles in the human respiratory system can help clinical treatment of lung diseases using medicines. The lung airway diameters and the breathing capacity of human lungs normally increase with age until the age of 30. Many studies have analyzed the particle TD in the human lung airways. However, the knowledge of the nanoparticle TD in airways of infants and children with varying inhalation flow rates is still limited in the literature. This study investigates nanoparticle (5 nm $\leq d_P \leq$ 500 nm) TD in the lungs of infants, children, and adults. The inhalation air flow rates corresponding to three ages are considered as Q_{in} = 3.22 L/min (infant), 8.09 L/min (Child), and Q_{in} = 14 L/min (adult). It is found that less particles are deposited in upper lung airways (G0–G3) than in lower airways (G12–G15) in the lungs of all the three age groups. The results suggest that the particle deposition efficiency in lung airways increases with the decrease of particle size due to the Brownian diffusion mechanism. About 3% of 500 nm particles are deposited in airways G12–G15 for the three age groups. As the particle size is decreased to 5 nm, the deposition rate in G12–G15 is increased to over 95%. The present findings can help medical therapy by individually simulating the distribution of drug-aerosol for the patient-specific lung.

Keywords: particle transport and deposition (TD); airway reduction; drug-aerosol delivery; aging effect; lung generations; diffusion mechanism

Citation: Rahman, M.M.; Zhao, M.; Islam, M.S.; Dong, K.; Saha, S.C. Aerosol Particle Transport and Deposition in Upper and Lower Airways of Infant, Child and Adult Human Lungs. *Atmosphere* **2021**, *12*, 1402. https://doi.org/10.3390/atmos12111402

Academic Editor: Deborah Traversi

Received: 28 September 2021
Accepted: 22 October 2021
Published: 26 October 2021

1. Introduction

Inhalation of aerosol particles is employed directly as a drug delivery method for the treatment of lung diseases [1,2]. However, the effectiveness of particle deposition as a drug delivery depends on particle size, shape, and breathing capacity [3]. Therefore, a detailed understanding of particle deposition in the human lung airways is important for human health to measure both the efficiency of inhaled drug therapy and the health implications of air pollution.

Many researchers have studied nanoparticles deposition in human lung models to investigate the diffusion mechanism [4–8]. The results revealed that the percentage of nanoparticles deposited in the deep airways was greater than microparticles. Cheng, et al. [9] found significant amount of particles are deposited in bifurcation areas by conducting experiments of nanoparticle deposition in the nasal and oral airways. Balásházy and Hofmann [10] studied numerically the deposition of 10-nm diameter particles in the third and fourth generation of human lungs based on the Weibel model [11]. They found significant effects of flow rate and particles size on the deposition efficiency. The whole human respiratory system is made up of 23 generations (the number of divisions of

Aerosol Particle Transport and Deposition in Upper and Lower Airways of Infant, Child and Adult Human Lungs

Md. M. Rahman [1*, 2], Ming Zhao [1,*], Mohammad S. Islam [3], Kejun Dong [4], and Suvash C. Saha [3]

[1] School of *Engineering*, Design and Built Environment, Western Sydney University, Penrith, NSW 2751, Australia.

[2] Department of Mathematics, Faculty of Science, Islamic University, Kushtia-7003, Bangladesh.

[3] School of Mechanical and Mechatronic Engineering, University of Technology Sydney, Ultimo, NSW 2007, Australia; mohammadsaidul.islam@uts.edu.au (M.S. I); suvash.saha@uts.edu.au (S.C.S);

[4] Center for Infrastructure Engineering, Western Sydney University, Penrith, NSW 2751, Australia; kejun.dong@westernsydney.edu.au

***Correspondence:** 19615253@student.westernsydney.edu.au (M.M.R); M.Zhao@westernsydney.edu.au (M.Z)

3.1 Abstract

Understanding transportation and deposition (TD) of aerosol particles in the human respiratory system can help clinical treatment of lung diseases using medicines. The lung airway diameters and the breathing capacity of human lungs normally increase with age until the age of 30. Many studies have analyzed the particle TD in the human lung airways. However, the knowledge of the nanoparticle TD in airways of infants and children with varying inhalation flow rates is still limited in the literature. This study investigates nanoparticle ($5\ \text{nm} \le d_p \le 500$ nm) TD in the lungs of infants, children, and adults. The inhalation air flow rates corresponding to three ages are considered as $Q_{in} = 3.22\ \text{L/min}$ (infant), $8.09\ \text{L/min}$ (Child), and $Q_{in} = 14\ \text{L/min}$ (adult). It is found that less particles are deposited in upper lung airways (G0–G3) than in lower airways (G12–G15) in the lungs of all the three age groups. The results suggest that the particle deposition efficiency in lung airways increases with the decrease of particle size due to the Brownian diffusion mechanism. About 3% of 500 nm particles are deposited in airways G12–G15 for the three age groups. As the particle size is decreased to 5 nm, the

deposition rate in G12–G15 is increased to over 95%. The present findings can help medical therapy by individually simulating the distribution of drug-aerosol for the patient-specific lung.

Keywords: particle transport and deposition (TD); airway reduction; drug-aerosol delivery; aging effect; lung generations; diffusion mechanism.

3.2 Introduction

Inhalation of aerosol particles is employed directly as a drug delivery method for the treatment of lung diseases (Pulivendala et al. 2020, Sorino et al. 2020). However, the effectiveness of particle deposition as a drug delivery depends on particle size, shape, and breathing capacity (Matera et al. 2021). Therefore, a detailed understanding of particle deposition in the human lung airways is important for human health to measure both the efficiency of inhaled drug therapy and the health implications of air pollution.

Many researchers have studied nanoparticles deposition in human lung models to investigate the diffusion mechanism (Zhang and Kleinstreuer 2004, Inthavong et al. 2011, Wang and Fan 2014, Saha et al. 2018, Islam et al. 2021). The results revealed that the percentage of nanoparticles deposited in the deep airways was greater than microparticles. Cheng et al. (1997) found significant amount of particles are deposited in bifurcation areas by conducting experiments of nanoparticle deposition in the nasal and oral airways. Balásházy and Hofmann (1995) studied numerically the deposition of 10-nm diameter particles in the third and fourth generation of human lungs based on the Weibel model (Weibel et al. 1963). They found significant effects of flow rate and particles size on the deposition efficiency. The whole human respiratory system is made up of 23 generations (the number of divisions of bronchioles is called generation) of airway branches (G0–G23). Moskal and Gradoń (2002) conducted numerical simulations of the TD of 10 nm and 100 nm particles in the first two bifurcations of

a symmetric lung model. The study explained the flow pattern and particle deposition through flow visualizations. The numerical study of the particle TD in the third and fourth generation conducted by Hofmann et al. (2003) demonstrated that in the range of 1 nm $\leq d_p \leq$ 500 nm, more small size nanoparticles is deposited in the lung airways than large size nanoparticles. CFD simulations of a realistic lung model from generations G0 to G6 were performed by Pourmehran et al. (2016). Using Large Eddy Simulations (LES), Islam et al. (2017) simulated nanoparticle transport in lung models of up to 17 generations and discussed the total deposition efficiency of particles across the 17 generations. Asgari et al. (2021) investigated aerosol microparticle deposition in a realistic lung model of generations mouth to sixth generations (G6). The results showed that aerosol deposition happens mainly in the upper lung airway.

The lung airways get larger as people grow to adult, and the shape of alveoli changes (Ménache et al. 2008). During postnatal growth, tidal and residual volumes, respiration rate, and respiratory compliance rise, but respiratory resistance decreases (Veneroni et al. 2020). This is due to the fact that infants and children have immature and growing lung systems, higher physical activity levels, and lower body weight than adults (Anderko et al. 2020, Kim, Prunicki et al. 2020). The airway structure and breathing habits of children are different from adults (Vriesman et al. 2020). When it comes to aerosol inhalation treatment, infants and children constitute a distinct demographic of patients (Schechter 2007). Xu and Yu (1986) established a theoretical model for predicting inhaled aerosol TD in the respiratory tracts of children to adults and found that children had a higher deposition efficiency in the upper airway region than adults.

Most medications were developed and approved based on adult trials. There is relatively little information on the acceptability of different dose forms based on a children. As a result, it is important to understand and improve particle TD in infants' and children's lungs.

Lung airway branching pattern is different irrespective of age and sex. The lack of high-resolution CT images also makes the geometry generation process complicated. As a result, it is nearly impossible to generate an age-specific realistic lung model with consistent similar branching patterns. Therefore, the age-specific micro-particles deposition into the idealized lung airways model has been studied through CFD simulation (Deng, Ou et al. 2018, Rahman, Zhao et al. 2021).

3.3 Lung Model

3.3.1 Lung Geometry

According to the age categories used by the World Health Organization (Knoppert et al. 2007, Kwok and Chan 2014), we consider 9-month, 6-year, and 30-year-old people as infants, children, and adults, respectively. Weibel et al. (1963) developed planar and symmetric lung models of adult people. However, the lung airway branching patterns for different ages of people are different. Therefore, Xu and Yu (1986) developed mathematical description of symmetric lung airways structure for different ages people. We have calculated the details of the lung airways diameter and length for infants, children, and adults (in Table 3.1) based on the mathematical description (Xu and Yu 1986). The right-hand side of Figure 3.1 shows three-dimensional (3D) lung models for upper (G0–G3) and lower generation (G12–G15) that are constructed using SolidWorks software. The detailed geometric parameters of infant, child, and adult lung airways are listed in Table 3.1.

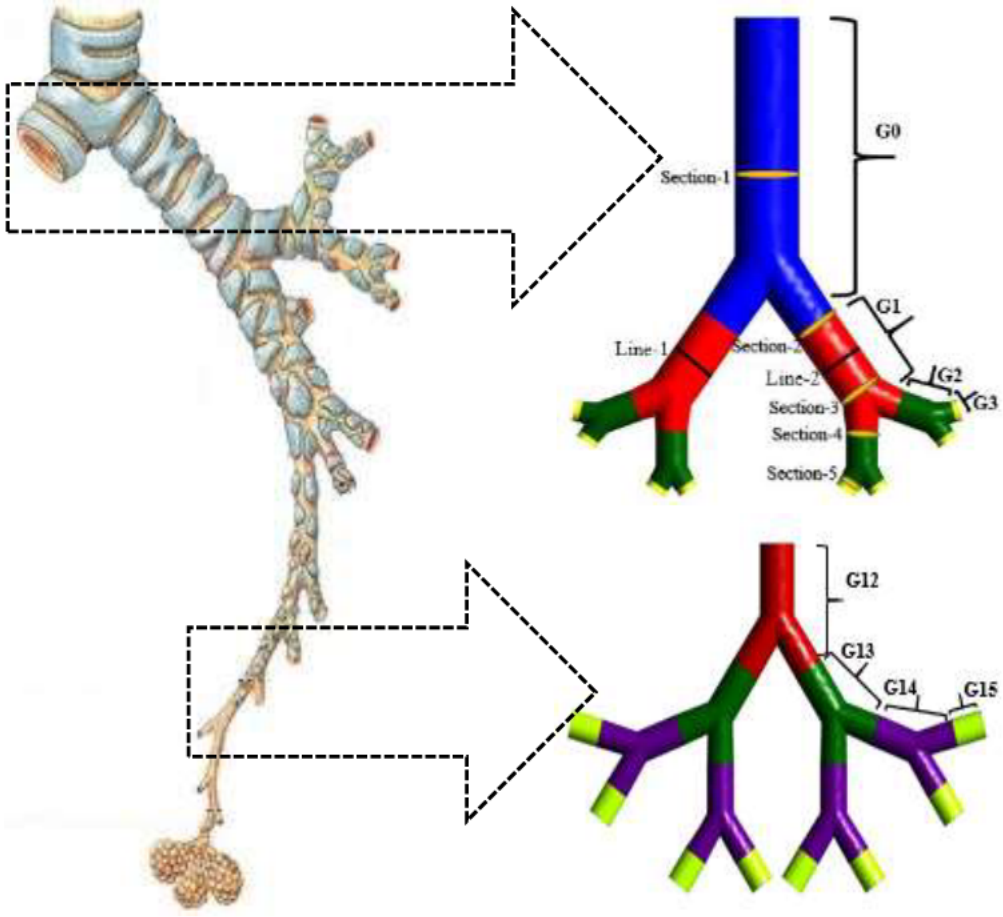

Figure 3.1. Symmetric models (Weibel et al. 1963) (right) were used in this study to represent the human respiratory system provided by Zhang, Xiang et al. (2020) (Permission has been taken to use the left Figure 3.1). The details of the geometric parameters of the lung airways are presented in Table 3.1.

Table 3.1 The parameters of symmetric lung airways (Xu and Yu 1986)

Generation (G)	Diameter (cm)	Length (cm)	Diameter (cm)	Length (cm)	Diameter (cm)	Length (cm)
Upper airways (G0–G3)	9 month old infant		6 year old child		30 year old adult	
0	0.615	4.630	0.985	7.934	1.665	12.286
1	0.491	1.712	0.842	2.822	1.219	4.284
2	0.333	0.761	0.572	1.307	0.829	1.896
3	0.227	0.307	0.387	0.525	0.559	0.759
Lower airways (G12–G15)						
12	0.041	0.143	0.067	0.233	0.095	0.330
13	0.036	0.121	0.058	0.193	0.082	0.271
14	0.031	0.097	0.052	0.161	0.074	0.231
15	0.028	0.087	0.046	0.142	0.066	0.201

3.3.2 Mesh Generation

High resolution mesh in the lung airways has been developed and shown in Figure 3.2a. In addition, Ten-layer smooth inflation is implemented near the wall to accurately predict the wall boundary flow inside the lung airway, as illustrated in Figure 3.2b.

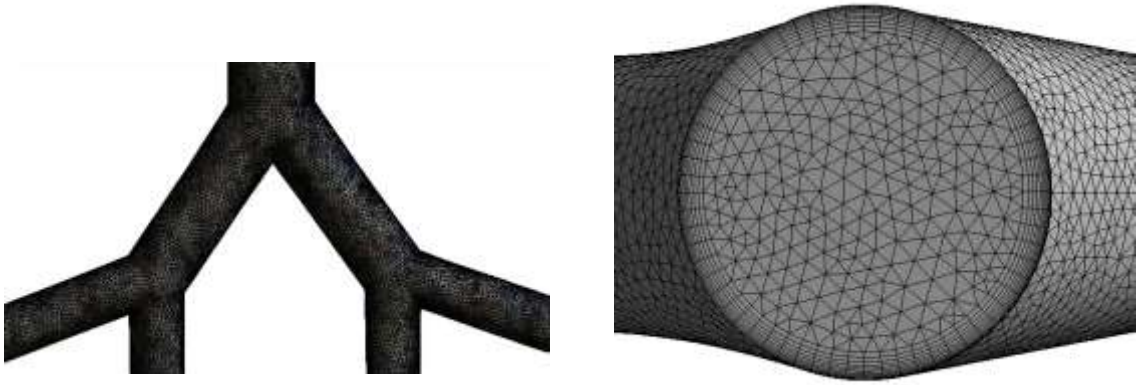

Figure 3.2. An overview mesh generation for symmetric lung model. (a) The mesh resolution of lung airway and (b) the refined inflation mesh near the airway wall.

3.4 Numerical Method

3.4.1 Airflow Model

The airflow in airways is solved using the software ANSYS FLUENT. The maximum Reynolds numbers based on the airway diameter at G0 are 800, 1253, and 1281 for 9-month,

6-year, and 30-year ages, respectively. The flow for such small Reynolds numbers was assumed steady and laminar. The governing equations for solving the flow is the 3D Navier-Stokes equations:

$$\frac{\partial}{\partial x_i}(\rho u_i) = 0 \tag{3.1}$$

$$\frac{\partial}{\partial x_j}(\rho u_i u_j) = -\frac{\partial p}{\partial x_i} + \frac{\partial}{\partial x_j}\left[\mu\left(\frac{\partial u_i}{\partial x_j} + \frac{\partial u_j}{\partial x_i}\right)\right] \tag{3.2}$$

where x_i (i = 1, 2 and 3) are the Cartesian coordinates, u_i is the fluid velocity in the x_i-direction, μ is the molecular viscosity, ρ is the air density, and p is the pressure.

The Navier-Stokes equations are solved using the second-order upwind momentum SIMPLE scheme and the pressure-velocity coupling method. A constant inhalation flow rate can be calculated by (Deng et al. 2018):

$$Q_{in} = 2 f_b V_t \tag{3.3}$$

where V_t is the tidal volume, which is defined as the amount of air that flows in and out of the lungs during each respiratory cycle, and f_b is the breathing frequency. Table 3.2 lists the flow parameters used in this study. The velocity inlet and pressure outlet boundary conditions are considered at the lung model's inlet and outlet, respectively (Gu et al. 2019, Islam et al. 2019, Ghosh et al. 2020, Rahman et al. 2020, Singh et al. 2020). The airway wall was considered to be stationary, and a non-slip boundary condition is used on the wall surface (Hendryx et al. 2020, Islam et al. 2020, Islam et al. 2021). The inhaled air flow rate is considered evenly distributed among all the 2^n bifurcations of generation G-n. As a result, the inlet air flow rate of each inlet of G-n is $Q_e^n = Q_{in}/2^n$, where Q_{in} is the inlet flow rate at G0. Therefore, the inlet velocity of each inlet boundary of G-n is calculated by:

$$u = Q_e^n / A_n \tag{3.4}$$

where A_n is the cross-sectional area of the inlet.

Table 3.2. Breathing parameter as a function of age based on the human activity (Hofmann 1982)

	Breathing Frequencies f_b (min^{-1})	Tidal Volume V_t (mL)	Inhalation Flow Rate Q_{in} (L/min)	Flow Velocity (m/s)	
				Upper Airways (G0–G3)	Lower Airways (G12–G15)
Infant	33.82	47.68	3.22	1.806	0.098
Child	19.34	209.44	8.09	1.766	0.093
Adult	13.98	500	14	1.071	0.080

3.4.2 Particle Transport Model

The present particle TD model is a one-way coupling model that considers particle movement in airflow but ignores particle effects on the airflow (Inthavong et al. 2011). Initially, the airflow field is simulated to obtain the converged flow solution. Then the particles are injected at the inlet surface into the lung model. The discrete phase model (DPM) model based on the Lagrangian approach is used in this study to model the motion of particles. The equation of motion of each particle is expressed as (Inthavong et al. 2011):

$$\frac{du_i^p}{dt} = F_{Di} + F_{gi} + F_{Bi} + F_{Li} \tag{3.5}$$

where u_i^p is particle velocity in the x_i-direction, F_{Di}, F_{gi}, F_{Bi} and F_{Li} are the drag force, gravitational force, Brownian force, and Saffman's lift force per unit mass. The gravitational force is calculated by

$$F_{gi} = \left(\frac{\rho_p - \rho}{\rho}\right) g_i \tag{3.6}$$

where g_i is the gravitational acceleration and ρ_p is the density of particles. The drag force is calculated by

$$F_{Di} = \frac{18\mu}{\rho_p d_p^2} C_D \frac{Re_P}{24} (u_i - u_i^p) \tag{3.7}$$

where the particle Reynolds number $\mathrm{Re_p} = \rho \mathrm{d_p} \left| \mathrm{u_i^p} - \mathrm{u_i} \right| / \mu$ and the drag coefficient $\mathrm{C_D}$ for the spherical particles is calculated by (Morsi and Alexander 1972) $\mathrm{C_D} = \mathrm{a_1} + \frac{\mathrm{a_2}}{\mathrm{Re_P}} + \frac{\mathrm{a_3}}{\mathrm{Re_P}^2}$ for $0 < \mathrm{Re_p} < 10$. The Brownian force due to Brownian motion of the fluid is defined as

$$\mathrm{F_{Bi}} = \mathrm{G_i} \sqrt{\frac{\pi \mathrm{S_0}}{\Delta \mathrm{t}}} \tag{3.8}$$

where, $\mathrm{G_i}$ is zero mean, unit-variance independent Gaussian random number, $\Delta \mathrm{t}$ is the particle time step, and $\mathrm{S_0}$ is the spectral intensity function which is related to the diffusion coefficient by:

$$\mathrm{S_0} = \frac{216 \nu \mathrm{k_B T}}{\pi^2 \rho_\mathrm{p} \mathrm{d_p^2} \left(\frac{\rho_\mathrm{p}}{\rho}\right)^2 \mathrm{C_c}} \tag{3.9}$$

where, $\mathrm{T} = 300\mathrm{K}$ is the absolute fluid temperature, $\mathrm{K_B} = 1.380649 \times 10^{-23}\ \mathrm{J/K}$ is the Boltzmann constant, ν is the kinematic viscosity, and the Stokes-Cunningham slip correction coefficient $\mathrm{C_c}$ is defined as

$$\mathrm{C_c} = 1 + \frac{2\lambda}{d_\mathrm{p}} \left(1.257 + 0.4 \mathrm{e}^{-\left(\frac{1.1 d_\mathrm{p}}{2\lambda}\right)}\right) \tag{3.10}$$

where, $\lambda = 65\ \mathrm{nm}$ is the mean free path of the gas molecules. The Saffman's lift force is calculated by:

$$\mathrm{F_{Li}} = \frac{2\mathrm{K} \nu^{\frac{1}{2}} \rho \mathrm{d_{ij}}}{\rho_\mathrm{p} \mathrm{d_p} (\mathrm{d_{lk}} \mathrm{d_{kl}})^{\frac{1}{4}}} (\mathrm{u_j} - \mathrm{u_j^p}) \tag{3.11}$$

where, $\mathrm{K} = 2.594$ is the constant coefficient of Saffman's lift force and $\mathrm{d_{ij}} = (\mathrm{u_{i,j}} - \mathrm{u_{j,i}})/2$ is the deformation tensor.

In the simulations, 64,400 spherical particles with a uniform diameter and a density of 1100 kg/m^3 were injected randomly at the inlet surface at one time (Islam et al. 2020, Rahman et al. 2021). A 'trap' boundary condition is considered in the lung airways wall, and an escape condition is considered at all outputs for particle deposition (Rahman et al. 2019, Zhang et al. 2020). Due to the trap situation, the coefficient of restitution is zero. Hence no bounce occurs

when the particles meet the lung airways surface. As a result, the particles are trapped on the surface and remain there. Finally, the Tecplot software is used to visualize the deposition of particles in the lungs.

3.4.3 Deposition Efficiency Calculation

The deposition efficiency of the n-th generation, denoted by η, is the percentages of the particles absorbed (trapped) in this generation of airways relative to the particles released at the inlet surface, given by:

$$\eta = \frac{\text{Number of particles are trapped in a lung airway}}{\text{Total number of particles released at the lung inlet}}$$

3.5 Grid Independence Study and Model Validation

3.5.1 Grid Dependency Test

Six meshes are used in the grid independency test, namely 64423 (Mesh-1), 116058 (Mesh-2), 192466 (Mesh-3), 290185 (Mesh-4), 364259 (Mesh-5), and 468164 (Mesh-6). The smallest grid size of the densest mesh is 0.79 mm adjacent to the wall, and the mesh size is proportional to the number of elements. The average velocity magnitude and the total pressure are shown in Figure 3.3 (the different lines and sections of the lung are defined in Figure 3.1). It was found that both velocity and pressure change with the increase of the grid number from 64423 to 468164. Due to the increased grid number, the velocity distribution trends are almost identical. The velocity difference between mesh-5 and mesh-6, especially, is 0.012%. The average velocity and total pressure converge at a mesh of 364,259 elements (Mesh-5), which is used to perform all the numerical calculations.

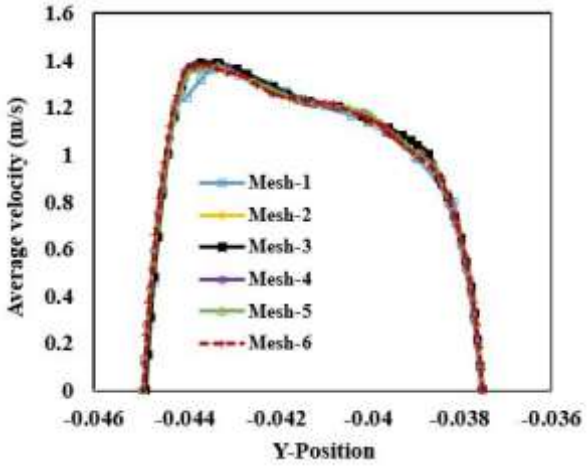

(a)

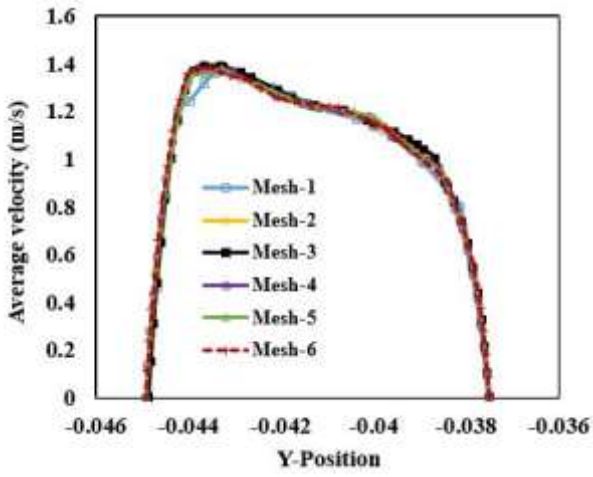

(b)

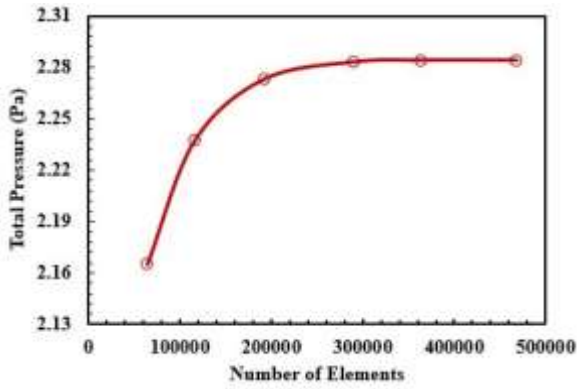

(c)

Figure 3.3. (a) Grid refinement/mesh-independent test for (a) velocity distribution as functions of grid number (average velocity calculated at the selected line-1 in Figure 3.1), (b) velocity distribution as functions of grid number (average velocity calculated at the selected line-2 in Figure 3.1), and (c) total pressure as functions of grid number at the flow rate 14 L/min (Total pressure calculated at the selected section-4 in Figure 3.1) for G0–G3 model for 30 year age.

3.5.2 Model Validation

To validate the numerical method, Figure 3.4 a,b show the CFD results of particle deposition efficiency as a function of particle diameter for three Reynolds numbers (Re = 200,

500, and 1000) in the first and second bifurcation areas for G3–G5 model, respectively. The deposition efficiency rate decreases exponentially with the increase of the particle diameter. The variation trend of the deposition efficiency with d_p agrees with those in other numerical studies (Zhang and Kleinstreuer 2004) and experimental data (Kim 2002), demonstrating that the present model is accurate to calculate the particle TD in the tracheobronchial airways of a lung.

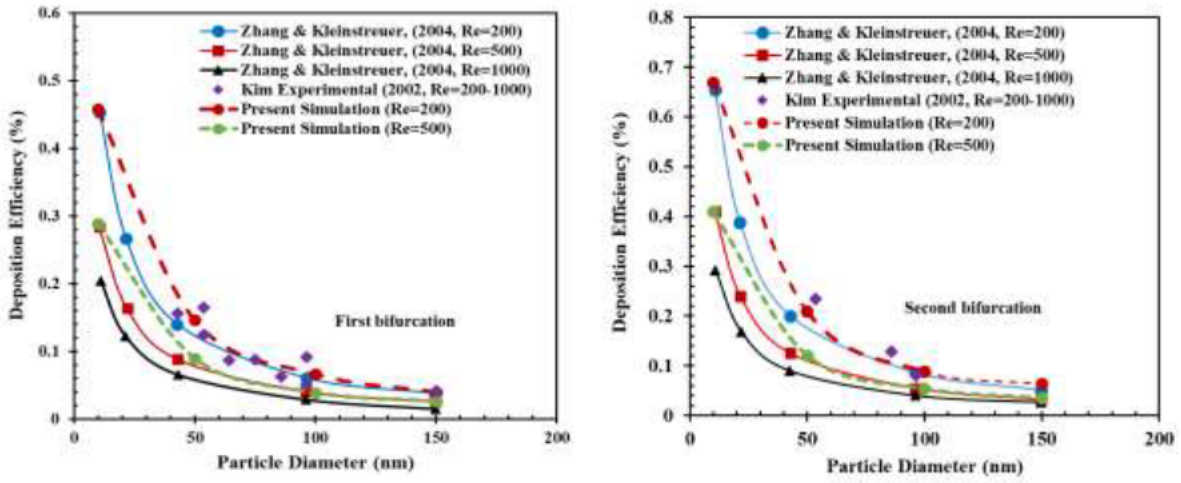

(a) (b)

Figure 3.4. Comparison between present simulation results at the generation G3–G5 model and results from literature (Kim 2002, Zhang and Kleinstreuer 2004) (a) for the first bifurcation area; and (b) for the second bifurcation area.

3.6 Results and Discussion

3.6.1 Airflow Characteristics

In this study, constant velocities at the inlets of the models of G0–G3 and G12–G15 are given based on Table 3.2. In many studies, the airflow velocity was considered to be constant (Kleinstreuer et al. 2008, Chen et al. 2018, Islam et al. 2021).

Figure 3.5 shows the velocity contours on the symmetric plane and five cross-sections for generation G0–G3 of infants to adults. The five sections (AA′, BB′, CC′, DD′, and EE′) are indicated on the symmetric plane. The velocity distribution in section-1 for three ages people is uniform at the central part. After the air enters the deep lung, the velocity distribution in the rest of the section (Section-2, Section-3, Section-4, and Section-5) is very non-uniform, as seen in Figure 3.5. The maximum velocity is observed for 9 months lung model since the lung airways diameter decreases compared to the 30-years age model. There is a qualitatively similar fluctuation in velocity inside the generation G0–G3 compared to the lower generation (G12–G15). According to our observations, lung airway flow rate influences patterns of velocity magnitude.

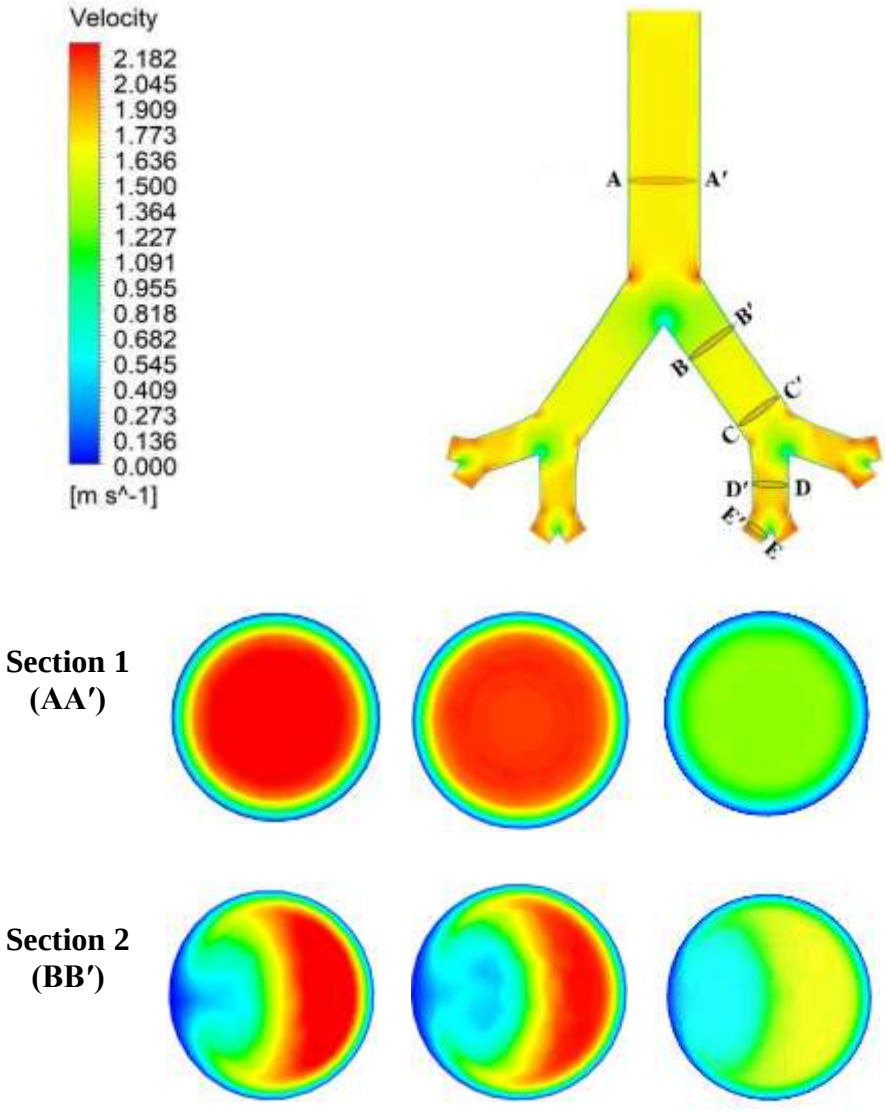

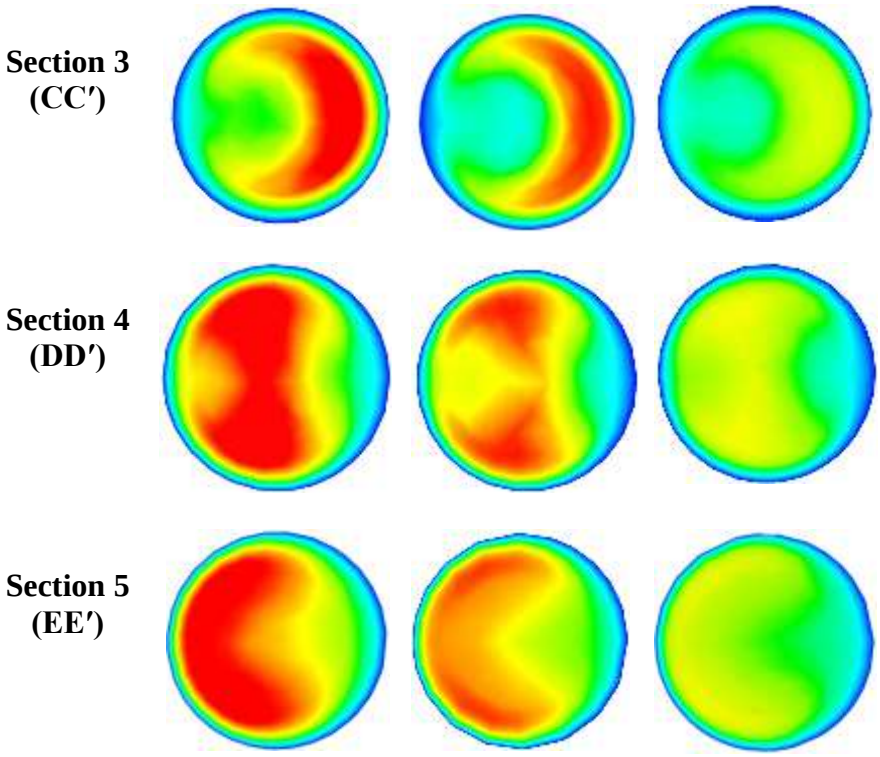

Figure 3.5. Velocity contours at upper airways generation (G0–G3) defined in the above Figure 3.1: (a) 9 months, velocity = 1.806 m/s, (b) 6 years age, velocity = 1.766 m/s, and (c) 30 years age, velocity = 1.071 m/s.

3.6.2 Wall Shear Stress

Figure 3.6 quantitatively shows the average wall shear stress along with the inner wall lung upper airways generation (G0–G3) on five sectional planes indicated in Figure 3.1. Since flow resistance occurs at complicated lung geometry, the wall shear stress varies considerably with each lung airway generation. With a contact inhaled air flow rate, the wall shear stress decrease with the increase in age.

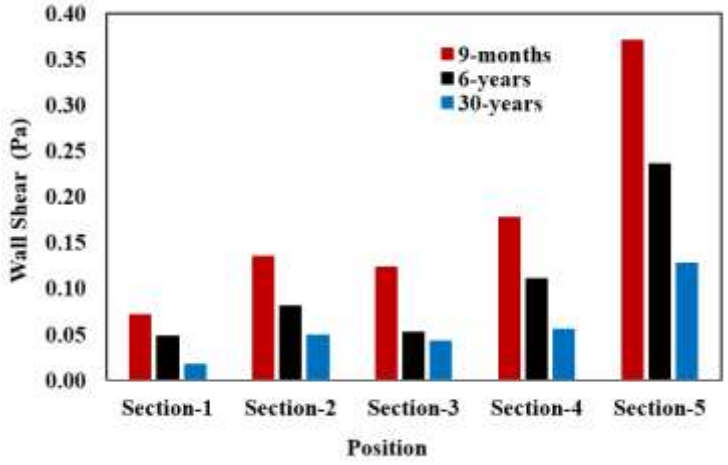

Figure 3.6. Averaged wall shear stress at a different section of the lung defined in Figure 3.1 for infant, child and adult ages.

Figure 3.7 depicts the average static pressures in the generation G0–G3 lung airways at various locations. For people of all ages, the highest pressure is shown in Section-1 (Figure 3.7). In addition to the reduction in velocity illustrated in Figure 3.5, the pressure progressively lowers when airflow enters the deep lung. Due to friction from the inner wall of the airways, the flow energy decreases when the airflow enters the deep lung. The high velocity at the nine-months-old lung shown in Figure 3.7 requires high pressure at the inlet to drive the flow. As a result, 56.35% pressure rise in the lung airways of 9-month-olds compared to 30-year-olds shown in Figure 3.7. Hence, inhaling air into the lung for a 9-month-old is more complex than for a 30-year-old. The pressure at section 5 is significantly lower than at section 1, owing to a drop in the volume flow rate. As a result of the decrease in velocity, the low-pressure drop-in section 5 was formed.

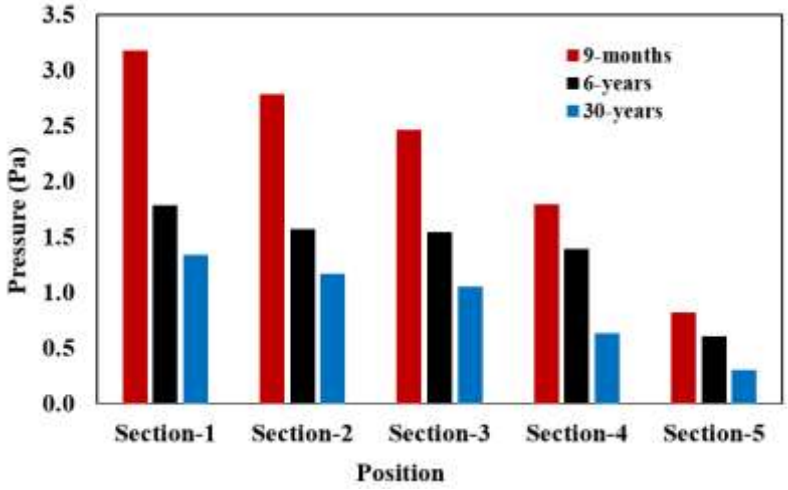

Figure 3.7. Pressure at a different section of the lung defined in Figure 3.1 for infant, child, and adult ages.

3.6.3 Particle Deposition

Figure 3.8 shows the effects of age on the particle deposition efficiency in G0–G3 and G12–G15 models. The deposition efficiency of 5-nm particles is much higher than those of the other three-particle diameters. The particle deposition efficiency decreases with the increase of the particle size due to the weakening of the diffusion mechanism (Dong et al. 2019). As seen in Table 3.2, the flow velocity at G12–G15 is reduced significantly compared with G0–G3. Since the diffusion mechanism is strong when the flow velocity is low (Dang Khoa et al. 2020), the deposition efficiency of G12–G15 is 30% higher than that of G0–G3 (Figure 3.8). Hence, the particles deposition efficiency is found to increase slightly with the increase of age. 2.13% more particles were deposited in the 30-years-old lungs compared to the 9-months-old.

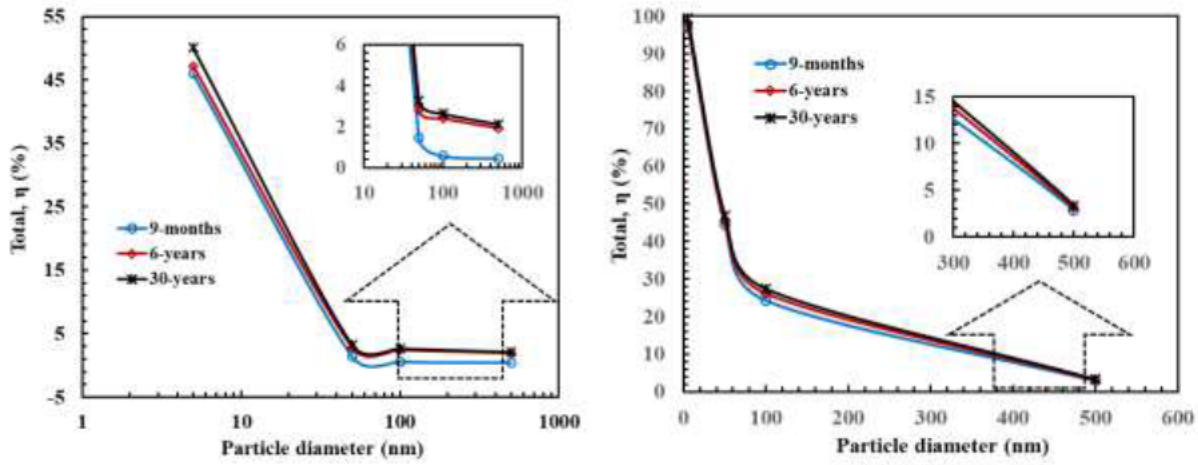

Figure 3.8. Particle deposition efficiencies of the lung are defined in Figure 3.1. (a) Upper airways (G0–G3) and (b) lower airways (G12–G15).

Figure 3.9 shows the visualization of the particle distribution of different sized particles at generation G12–G15 of 30-year age. The calculated total particle deposition efficiencies of G12–G15 are 99.42%, 46.80%, 27.45%, and 3.33% for 5 nm, 50 nm, 100 nm, and 500 nm particles, respectively. It can be found that 5 nm particles are more evenly distributed in each lung airways generation compared to the larger particles (500 nm). Hence, 500 nm size particle is observed to have less deposition than smaller diameters since the diffusion mechanism weakens with the increase of particle diameter. The Brownian diffusion mechanism results in more particles being deposited due to the low airflow velocity (Zhang and Kleinstreuer 2004, Islam et al. 2017).

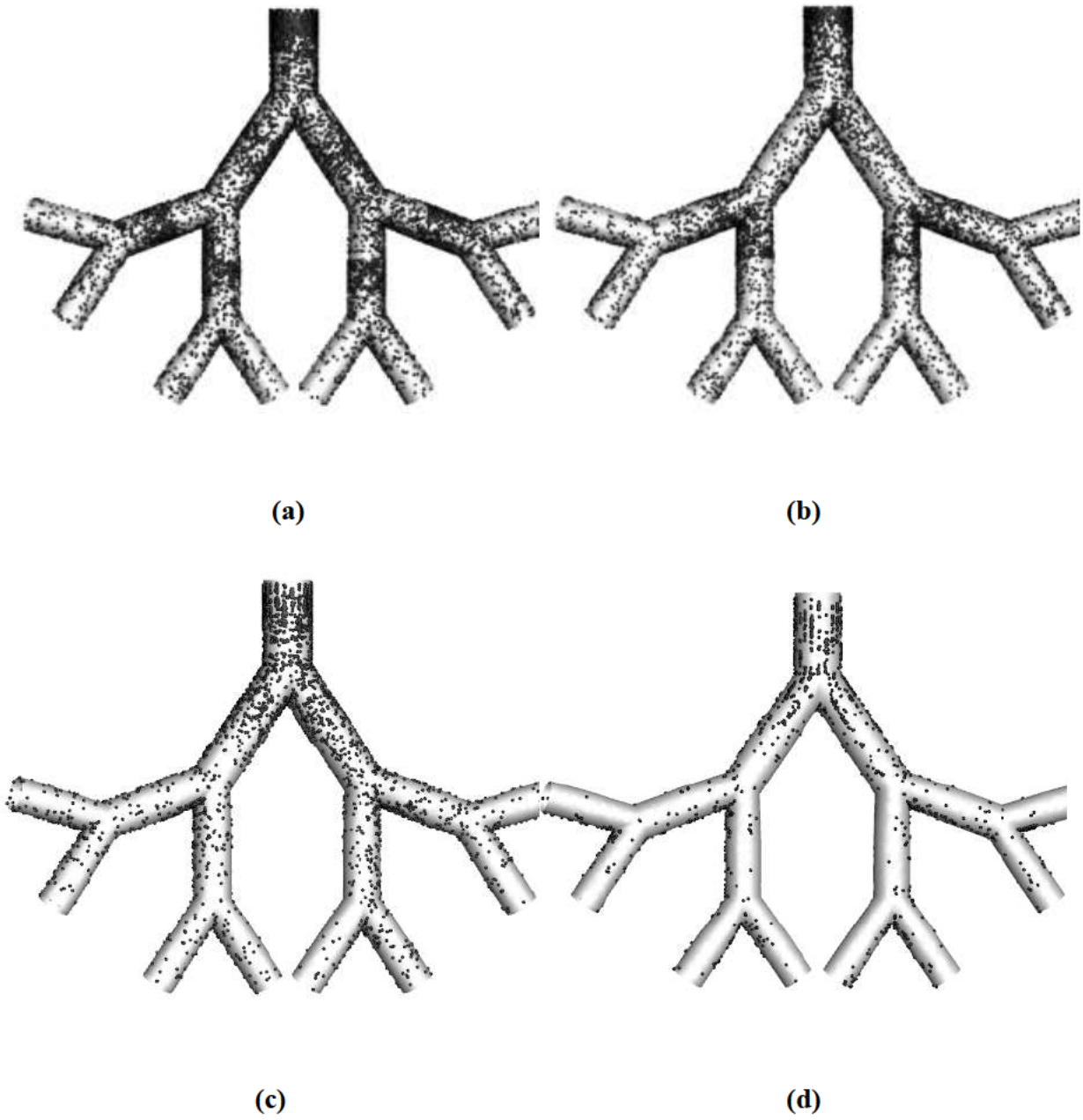

Figure 3.9. Visualization of particle deposition for the 30 years age for generation G12–G15 of the lung defined in Figure 3.1. (a) $d_p = 5$ nm, (b) $d_p = 50$ nm, (c) $d_p = 100$ nm, and (d) $d_p = 500$ nm at a flow rate of 14 L/min.

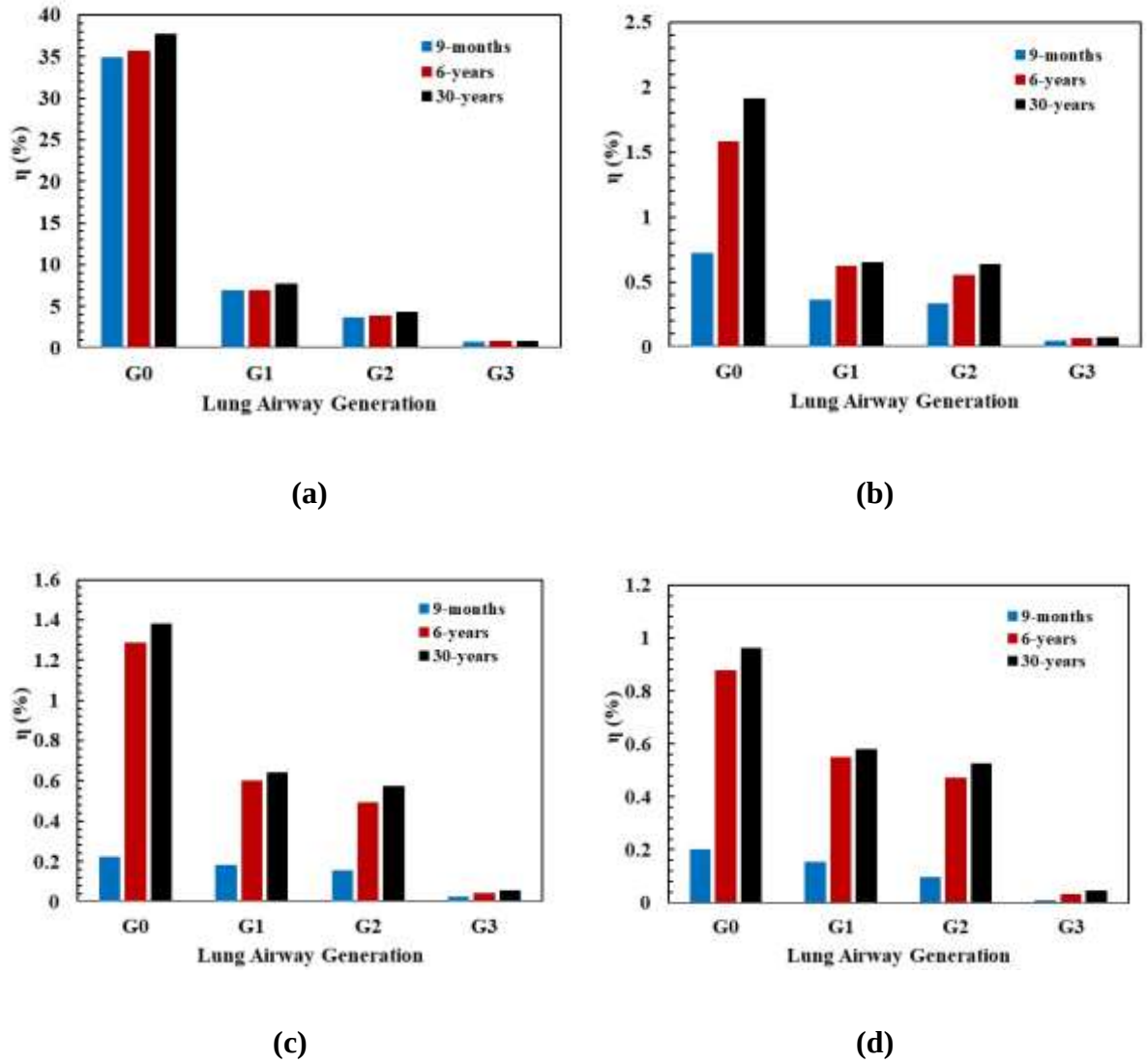

Figure 3.10. Different size particle deposition efficiencies at upper airways generation (G0–G3) of the lung are defined in Figure 3.1. (a) $d_p = 5$ nm, (b) $d_p = 50$ nm, (c) $d_p = 100$ nm, and (d) $d_p = 500$ nm.

How the ages and particle size affect deposition rates at individual generations in the upper lung airways (G0–G3) can be examined by the bar charts shown in Figure 3.10. The locations of different generations are defined in Figure 3.1. Most of the particles are deposited at generation G0 for all the studied ages and particle diameters. Around 34.88%, 35.67%, and 37.72% of 5 nm particles are deposited at generation G0 for 9-month, 6-years and 30-years of age, respectively (Figure 3.10 a). For the three ages, the lowest deposition efficiency occurs at

the largest particle size of 500 nm and it decreases with the increase of generation number. Figure 3.4 demonstrates that the deposition efficiency in generations G3–G5 increases with the reduction of either the Reynolds number or flow velocity. The decrease of the flow velocity decreases with age results in an increase in deposition efficiency in G0–G3 in Figure 3.10.

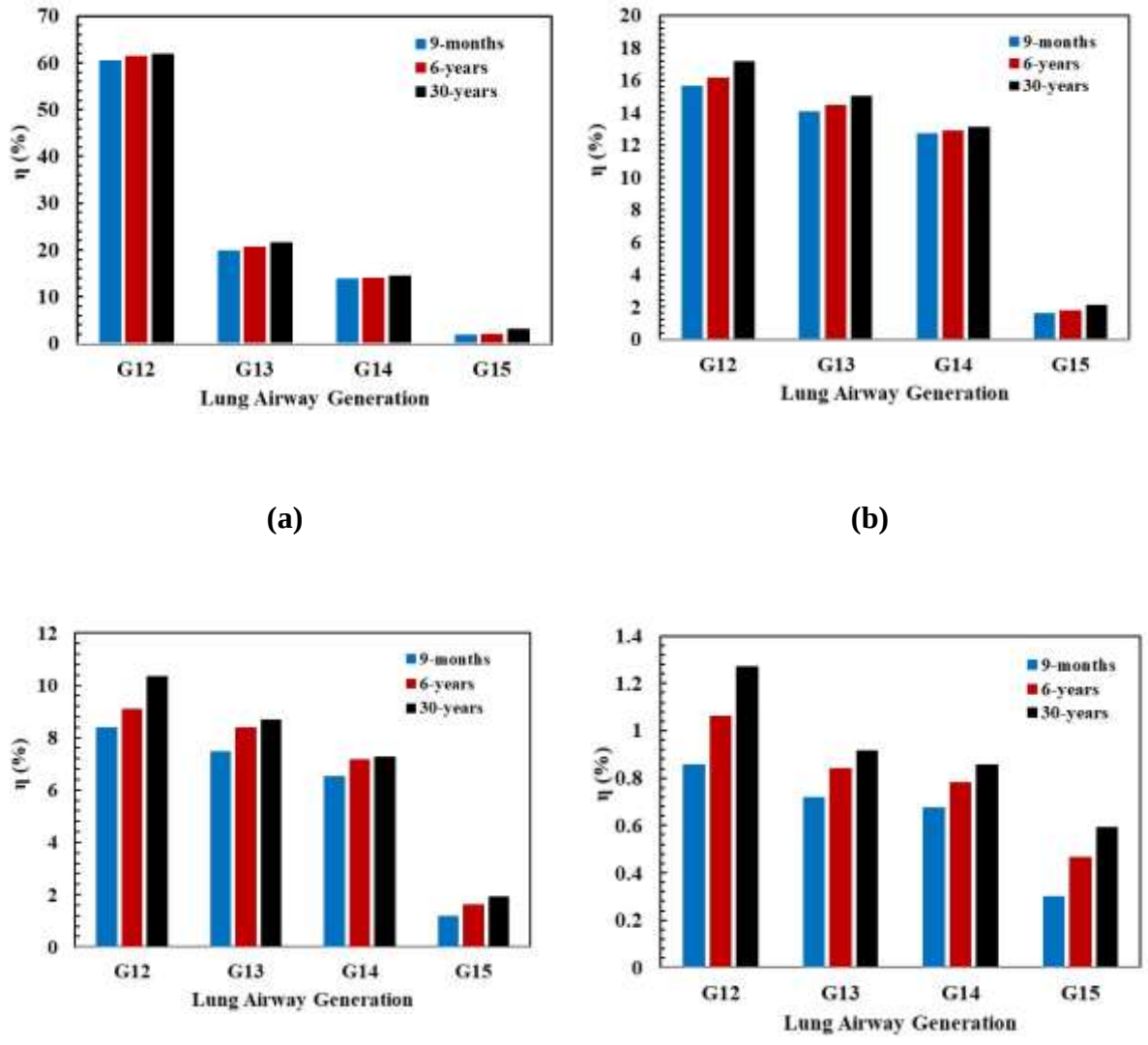

Figure 3.11. Different size particle deposition efficiencies at lower airways generation (G12–G15) of the lung are defined in Figure 3.1. (a) $d_p = 5$ nm, (b) $d_p = 50$ nm, (c) $d_p = 100$ nm, and (d) $d_p = 500$ nm.

Figure 3.11 shows the deposition efficiency at individual generations in the lower lung airways (G12–G15) for the three ages. The effect of age on the deposition efficiency of G12–G15 is the same as that for G0–G3. At nine-months of age, the deposition efficiencies of lower generations (G15) are smaller compared to the adult age. The deposition efficiency in G12–G15 for all the diameters was considerably reduced compared to that in G0–G3. At 9-month age, 15.61%, 14.05%, 12.71%, and 1.57% of 50 nm particles are deposited at the generation G12, G13, G14, and G15, respectively (Figure 3.11b). It is also observed that 8.02% at G12, 7.54% at G13, 6.37% at G14, and 1.16% at G15, more particles were deposited of 100 nm compared to 500 nm for six-year-olds (Figure 3.11 c,d). The particles deposition efficiency decreases with increases the particles size (Figure 3.11a).

Numerical calculations were conducted based on age-specific lung models in the upper and lower airways. The flow characteristics and pressures differ due to age-related differences in lung geometries that have varied diameters. Due to lung aging and flow rate, the diameter reduction influenced the velocity magnitude for infant to adult ages. Hence, the present study has several contributions: (1) we have considered the three age groups (infant, child, and adult) to identify the effects of age on particle TD; (2) we consider the nanoparticle TD through diffusion mechanism both in upper (G0–G3) and lower (G12–G15) airways; (3) we consider the different airflow velocity in different airway generations.

3.7 Limitations of the Study

There are some limitations in this study that should be addressed in future studies. Firstly, only an inhalation flow condition was considered in the simulation of particle TD. Secondly, deformation of the lung wall was not considered in this study. Thirdly, we have used symmetric and planner lung airways models due to the lack of high-resolution CT images for age-specific realistic lung geometry. However, despite the constraints of lung geometry used in this study, our current investigation of airflow characteristics and particle deposition patterns

can accurately predict (Kleinstreuer, Zhang et al. 2008, Ou, Jian et al. 2020). Thus, the results of this work could improve a basic understanding of airflow properties and nanoparticle TD in the human lung airways related to lung ageing.

3.8 Conclusions

We investigated nanoparticle TD in the upper (G0–G3) and lower (G12–G15) airways of the infant to adult ages. The variation of the airway geometry and the flow velocity with age has been considered. The deposition efficiency of particles is found to be significantly affected by lung airways reduction. The effects of age and particle diameter on the airflow and particle TD are summarized as follows.

- The average wall shear stress is decreased with an increase of age. The pressure of generation G0 to G3 of a 9-month-old lung is 56.35% higher than the 30-year-old lung due to the inhalation flow rate.
- 30% more particles are deposited in the lower airways (G12–G15) than in the upper airways (G0–G3).
- 60.32%, 61.31%, and 61.75% 5-nm particles are deposited in the generation G12 for 9-month, 6-year, and 30-year ages, respectively, which indicates that the number of particle deposition increases with increased age.
- A high percentage of the 5-nm particles (over 95%) entering G12 can be deposited in the deep lung airways (G12–G15). As the particle size is increased to 500 nm, only 3% of the particles are deposited in the G12–G15 lung airways. The above finding indicates that particles must have a small diameter to increase the deposition in the deep lung airways.
- The numerical study showed that deposition efficiency is significantly affected by lung airways reduction. Most of the particles are deposited in the 30-year-old lung than 9-month-old lung in the lower generations compared to the upper generation. Therefore,

our results further investigate that correctly choosing particles size as targeted drug-aerosol delivery size based on age.

Author Contributions: Conceptualization, Md. M Rahman; Formal analysis, Md. M Rahman; Investigation, Md. M Rahman and Ming Zhao; Methodology, Md. M Rahman and Ming Zhao; Software, Md. M Rahman and Mohammad S. Islam; Supervision, Ming Zhao, Mohammad S. Islam, Kejun Dong and Suvash C Saha; Validation, Md. M Rahman; Visualization, Ming Zhao; Writing – original draft, Md. M Rahman; Writing – review & editing, Ming Zhao, Mohammad S. Islam, Kejun Dong and Suvash C Saha.

Funding: This research received no external funding

Institutional Review Board Statement: Not applicable

Informed Consent Statement: Informed consent was obtained from all subjects involved in the study.

Acknowledgments: Mr. Rahman would like to thank the support of International Post-graduate Research Scholarship (IPRS) through Australian Government Research Training Program. The authors also acknowledge that the WSU High-Performance VM machine provided the computational facilities.

Conflicts of Interest: The authors state no conflicts of interest.

References

Anderko, L, Chalupka, S, Du, M & Hauptman, M 2020, 'Climate changes reproductive and children's health: a review of risks, exposures, and impacts', *Pediatric research*, vol. 87, no. 2, pp. 414-419.

Asgari, M, Lucci, F & Kuczaj, AK 2021, 'Multispecies aerosol evolution and deposition in a human respiratory tract cast model', *Journal of Aerosol Science*, vol. 153, 105720.

Balásházy, I & Hofmann, W 1995, 'Deposition of aerosols in asymmetric airway bifurcations', *Journal of Aerosol Science*, vol. 26, no. 2, pp. 273-292.

Chen, X, Feng, Y, Zhong, W, Sun, B & Tao, F 2018, 'Numerical investigation of particle deposition in a triple bifurcation airway due to gravitational sedimentation and inertial impaction', *Powder Technology*, vol. 323, pp. 284-293.

Cheng, K-H, Cheng, Y-S, Yeh, H-C & Swift, D 1997, 'Measurements of airway dimensions and calculation of mass transfer characteristics of the human oral passage', *Journal of biomechanical engineering*, Vol. 119, No.4, pp.476-482.

Dang Khoa, N, Phuong, NL & Ito, K 2020, 'Numerical modeling of nanoparticle deposition in realistic monkey airway and human airway models: a comparative study', *Inhalation Toxicology*, vol. 32, no. 7, pp. 311-325.

Deng, Q, Ou, C, Chen, J & Xiang, Y 2018, 'Particle deposition in tracheobronchial airways of an infant, child and adult', *Science of the Total Environment*, vol. 612, pp. 339-346.

Dong, J, Shang, Y, Tian, L, Inthavong, K, Qiu, D & Tu, J 2019, 'Ultrafine particle deposition in a realistic human airway at multiple inhalation scenarios', *International journal for numerical methods in biomedical engineering*, vol. 35, no. 7, 3215.

Ghosh, A, Islam, MS & Saha, SC 2020, 'Targeted drug delivery of magnetic nano-particle in the specific lung region', *Computation*, vol. 8, no. 1, 10.

Gu, Q, Qi, S, Yue, Y, Shen, J, Zhang, B, Sun, W et al. 2019, 'Structural and functional alterations of the tracheobronchial tree after left upper pulmonary lobectomy for lung cancer', *Biomedical engineering online*, vol. 18, no. 1, pp. 1-18.

Hendryx, M, Islam, MS, Dong, G-H & Paul, G 2020, 'Air pollution emissions 2008–2018 from australian coal mining: implications for public and occupational health', *International Journal of Environmental Research and Public Health*, vol. 17, no. 5, 1570.

Hofmann, W 1982, 'Mathematical model for the postnatal growth of the human lung', *Respiration physiology*, vol. 49, no. 1, pp. 115-129.

Hofmann, W, Golser, R & Balashazy, I 2003, 'Inspiratory deposition efficiency of ultrafine particles in a human airway bifurcation model', *Aerosol Science & Technology*, vol. 37, no. 12, pp. 988-994.

Inthavong, K, Zhang, K & Tu, J 2011, 'Numerical modelling of nanoparticle deposition in the nasal cavity and the tracheobronchial airway', *Computer Methods in Biomechanics and Biomedical Engineering*, vol. 14, no. 7, pp. 633-643.

Islam, MS, Gu, Y, Farkas, A, Paul, G & Saha, SC 2020, 'Helium–oxygen mixture model for particle transport in CT-based upper airways', *International Journal of Environmental Research and Public Health*, vol. 17, no. 10, 3574.

Islam, MS, Larpruenrudee, P, Hossain, SI, Rahimi-Gorji, M, Gu, Y, Saha, SC et al. 2021, 'Polydisperse Aerosol Transport and Deposition in Upper Airways of Age-Specific Lung', *International Journal of Environmental Research and Public Health*, vol. 18, no. 12, 6239.

Islam, MS, Larpruenrudee, P, Paul, AR, Paul, G, Gemci, T, Gu, Y et al. 2021, 'SARS CoV-2 aerosol: How far it can travel to the lower airways?', *Physics of Fluids*, vol. 33, no. 6, 061903.

Islam, MS, Larpruenrudee, P, Saha, SC, Pourmehran, O, Paul, AR, Gemci, T et al. 2021, 'How severe acute respiratory syndrome coronavirus-2 aerosol propagates through the age-specific upper airways', *Physics of Fluids*, vol. 33, no. 8, 081911.

Islam, MS, Saha, SC, Sauret, E, Gemci, T, Yang, IA & Gu, Y 2017, 'Ultrafine particle transport and deposition in a large scale 17-generation lung model', *Journal of biomechanics*, vol. 64, pp. 16-25.

Islam, MS, Saha, SC, Sauret, E, Ong, H, Young, P & Gu, Y 2019, 'Euler–Lagrange approach to investigate respiratory anatomical shape effects on aerosol particle transport and deposition', *Toxicology Research and Application*, vol. 3, 2397847319894675.

Kim, C 2002, *Ultrafine particle deposition in a double bifurcation tube with human G3–G5 airway geometry*, US EPA, Internal Report.

Kim, JB, Prunicki, M, Haddad, F, Dant, C, Sampath, V, Patel, R et al. 2020, 'Cumulative lifetime burden of cardiovascular disease from early exposure to air pollution', *Journal of the American Heart Association*, vol. 9, no. 6, 014944.

Kleinstreuer, C, Zhang, Z & Li, Z 2008, 'Modeling airflow and particle transport/deposition in pulmonary airways', *Respiratory physiology & neurobiology*, vol. 163, no. 1-3, pp. 128-38.

Knoppert, D, Reed, M, Benavides, S, Totton, J, Hoff, D, Moffett, B et al. 2007, 'Paediatric age categories to be used in differentiating between listing on a model essential medicines list for children', *Word Health Organization position paper*, vol. 1, no. 5.

Kwok, PCL & Chan, H-K 2014, 'Delivery of inhalation drugs to children for asthma and other respiratory diseases', *Advanced Drug Delivery Reviews*, vol. 73, pp. 83-88.

Matera, MG, Calzetta, L, Ora, J, Rogliani, P & Cazzola, M 2021, 'Pharmacokinetic/pharmacodynamic approaches to drug delivery design for inhalation drugs', *Expert Opinion on Drug Delivery*, pp. 1-16.

Ménache, M, Hofmann, W, Ashgarian, B & Miller, F 2008, 'Airway geometry models of children's lungs for use in dosimetry modeling', *Inhalation Toxicology*, vol. 20, no. 2, pp. 101-126.

Morsi, S & Alexander, A 1972, 'An investigation of particle trajectories in two-phase flow systems', *Journal of Fluid mechanics*, vol. 55, no. 2, pp. 193-208.

Moskal, A & Gradoń, L 2002, 'Temporary and spatial deposition of aerosol particles in the upper human airways during breathing cycle', *Journal of Aerosol Science*, vol. 33, no. 11, pp. 1525-1539.

Ou, C, Jian, H & Deng, Q 2020, 'Particle Deposition in Human Lung Airways: Effects of Airflow, Particle Size, and Mechanisms', *Aerosol and Air Quality Research*, vol. 20, no. 12, pp. 2846-2858.

Pourmehran, O, Gorji, TB & Gorji-Bandpy, M 2016, 'Magnetic drug targeting through a realistic model of human tracheobronchial airways using computational fluid and particle dynamics', *Biomechanics and modeling in mechanobiology*, vol. 15, no. 5, pp. 1355-1374.

Pulivendala, G, Bale, S & Godugu, C 2020, 'Inhalation of sustained release microparticles for the targeted treatment of respiratory diseases', *Drug delivery and translational research*, vol. 10, no. 2, pp. 339-353.

Rahman, MM, Zhao, M, Islam, MS, Dong, K & Saha, SC 2019, 'Airflow dynamics and aerosol particle transport in a human lung', In *Proceedings of the 1st International Conference on Mechanical and Manufacturing Engineering Research and Practice (iCMMERP),* Sydney, Australia, November 24-28.

Rahman, MM, Zhao, M, Islam, MS, Dong, K & Saha, SC 2020, 'Airflow dynamic and particle deposition in age-specific human lungs', In *Proceedings of the 22nd Australasian Fluid Mechanics Conference (AFMC2020),* Brisbane, Australia, December 7-10.

Rahman, MM, Zhao, M, Islam, MS, Dong, K & Saha, SC 2021a, 'Aging effects on airflow distribution and micron-particle transport and deposition in a human lung using CFD-DPM approach', *Advanced Powder Technology*, vol. 32, pp. 3506-3516.

Rahman, MM, Zhao, M, Islam, MS, Dong, K & Saha, SC 2021b, 'Numerical study of nanoscale and microscale particle transport in realistic lung models with and without stenosis', *International Journal of Multiphase Flow*, Vol. 145, 103842.

Saha, S, Islam, MS & Luo, Z 2018, 'Ultrafine particle transport and deposition in the upper airways of a CT-based realistic lung', In *Proceedings of the 21st Australasian Fluid Mechanics Conference*, AFMC.

Schechter, MS 2007, 'Airway clearance applications in infants and children', *Respiratory care*, vol. 52, no. 10, pp. 1382-1391.

Singh, P, Raghav, V, Padhmashali, V, Paul, G, Islam, MS & Saha, SC 2020, 'Airflow and particle transport prediction through stenosis airways', *International Journal of Environmental Research and Public Health*, vol. 17, no. 3, 1119.

Sorino, C, Negri, S, Spanevello, A, Visca, D & Scichilone, N 2020, 'Inhalation therapy devices for the treatment of obstructive lung diseases: the history of inhalers towards the ideal inhaler', *European journal of internal medicine*, vol. 75, pp. 15-18.

Veneroni, C, Mercadante, D, Lavizzari, A, Colnaghi, M, Mosca, F & Dellacà, RL 2020, 'Changes in respiratory mechanics at birth in preterm infants: A pilot study', *Pediatric pulmonology*, vol. 55, no. 7, pp. 1640-1645.

Vriesman, MH, Koppen, IJ, Camilleri, M, Di Lorenzo, C & Benninga, MA 2020, 'Management of functional constipation in children and adults', *Nature Reviews Gastroenterology & Hepatology*, vol. 17, no. 1, pp. 21-39.

Wang, J & Fan, Y 2014, 'Lung injury induced by TiO2 nanoparticles depends on their structural features: size, shape, crystal phases, and surface coating', *International journal of molecular sciences*, vol. 15, no. 12, pp. 22258-22278.

Weibel, ER, Cournand, AF & Richards, DW 1963, *Morphometry of the human lung*, vol. 1, Springer.

Xu, G & Yu, C 1986, 'Effects of age on deposition of inhaled aerosols in the human lung', *Aerosol Science and Technology*, vol. 5, no. 3, pp. 349-357.

Zhang, W, Xiang, Y, Lu, C, Ou, C & Deng, Q 2020, 'Numerical modeling of particle deposition in the conducting airways of asthmatic children', *Medical engineering & physics*, vol. 76, pp. 40-46.

Zhang, Z & Kleinstreuer, C 2004, 'Airflow structures and nano-particle deposition in a human upper airway model', *Journal of computational physics*, vol. 198, no. 1, pp. 178-210.

Chapter 4: Aging Effects on Airflow Distribution and Micron-Particle Transport and Deposition in a Human Lung Using CFD-DPM Approach

This chapter presents a final accepted version paper published in 2021, Advanced Powder Technology, 32, 3506-3516. The first page of the published paper was shown at the beginning of the chapter, followed by the accepted version.

Chapter 4: Aging Effects on Airflow Distribution and Micron-Particle Transport and Deposition in a Human Lung Using CFD-DPM Approach

Advanced Powder Technology 32 (2021) 3506–3516

Contents lists available at ScienceDirect

Advanced Powder Technology

journal homepage: www.elsevier.com/locate/apt

Original Research Paper

Aging effects on airflow distribution and micron-particle transport and deposition in a human lung using CFD-DPM approach

Md.M. Rahman [a,b], Ming Zhao [a,*], Mohammad S. Islam [c], Kejun Dong [d], Suvash C. Saha [c]

[a] School of Computing, Engineering, and Mathematics, Western Sydney University, Penrith, NSW 2751, Australia
[b] Department of Mathematics, Faculty of Science, Islamic University, Kushtia 7300, Bangladesh
[c] School of Mechanical and Mechatronic Engineering, University of Technology Sydney, Ultimo, NSW 2007, Australia
[d] Center for Infrastructure Engineering, Western Sydney University, 2751 Penrith, NSW, Australia

ARTICLE INFO

Article history:
Received 19 May 2021
Received in revised form 7 July 2021
Accepted 2 August 2021
Available online 12 August 2021

Keywords:
Aging effect
Airflow
Aerosol particle transport and deposition (TD)
Lung
Inhalation
Drug delivery
Cutting method

ABSTRACT

Understanding the transportation and deposition (TD) of inhaled aerosol particles in human lung airways is important for health risk assessment and therapeutic efficiency of targeted drug delivery. The particle TD into a human lung depends on lung anatomy, breathing pattern, as well as particle properties. The breathing capacity and lung airway diameters can be reduced by about 10% every 10 years after the age of 50. However, the age-specific particle TD in human lungs, particularly in the aged, has not been well understood in literature. This study investigates the particle TD in the lungs of people aged 50–70 years, using computational fluid dynamics (CFD). A new cutting method that splits the lung model into different sections has been developed as a feasible CFD method to simulate the particle TD in G0 to G14 lung airways. The inhalation of micron scale particles with three diameters (5 μm, 10 μm and 20 μm) and a constant air flow rate in inhalation is considered. It is found that different sized particles are deposited in different generation airways. Nearly 100% of 20 μm particles are deposited in the upper lung airways (G0-G5) and no particles pass through G7. Particles can go into deeper airways as their diameter decreases. When the particle size is decreased to 5 μm, over 48% of particles can pass through G14 and enter the deeper lung airways. An increase in age causes more particles to deposit in the upper airway and fewer particles to enter the deeper airways.

1. Introduction

Aerosol particle inhalation is commonly used as a drug delivery method to treat human lung diseases [1,2]. Hence, the study of particle transportation and deposition (TD) in human lung airways is important, to ensure the effectiveness of drugs delivered through aerosol particle inhalation [3–5]. It is also important for reducing the effects of inhaled pollutant in the air on human health [6,7].

Particle TD into non-realistic tracheobronchial lung airways has been studied extensively to analyse the airflow dynamics and particle TD in lung airways [8,9]. Comer, et al. [10] developed a double bifurcation lung geometry based on Weibel's model [11], simulated airflow and TD in G3-G5 of this model numerically, and made a comprehensive comparison of their results with other numerical studies. Kleinstreuer et al. (2008) investigated airflow characteristics and particle TD of microparticles in a symmetric, triple bifurcation model of generations G0-G3. The results showed that the microparticles are mostly deposited at the carinal angles due to their strong inertial impaction mechanism. Zhang, et al. [12] studied the micro- and nano-size particle TD in a non-realistic, triple bifurcation model of generations G0-G3 using the Low-Reynolds-number (LRN) k–ω model. The nanoparticles were found to be more uniformly deposited in the airways than microparticles. Moreover, Islam, et al. [13] simulated aerosol particle transport in lung models using Large Eddy Simulations (LES) for up to 17 generations. The study shows that the majority of particles are deposited in the upper airways through an inertial impaction mechanism. However, they only discussed the total deposition efficiency of particles of all the 17 generations but not the deposition efficiency of each individual generation. Ahookhosh, et al. [14] conducted a detailed analysis of the evolution of various views of respiratory airway modelling throughout the years. This review study is helpful in understanding the limitations of lung anatomy and

* Corresponding author.
E-mail addresses: 19615253@student.westernsydney.edu.au (M.M. Rahman), M.Zhao@westernsydney.edu.au (M. Zhao), mohammadsaidul.islam@uts.edu.au (M.S. Islam), kejun.dong@westernsydney.edu.au (K. Dong), suvash.saha@uts.edu.au (S.C. Saha).

https://doi.org/10.1016/j.apt.2021.08.003
0921-8831/

Aging effects on airflow distribution and micron-particle transport and deposition in a human lung using CFD-DPM approach

Md. M. Rahman [1, 2], Ming Zhao [1, *], Mohammad S. Islam [3], Kejun Dong [4], and Suvash C. Saha [3]

[1] School of *Engineering*, Design and Built Environment, Western Sydney University, Penrith, NSW 2751, Australia; 19615253@student.westernsydney.edu.au.

[2] Department of Mathematics, Faculty of Science, Islamic University, Kushtia-7003, Bangladesh.

[3] School of Mechanical and Mechatronic Engineering, University of Technology Sydney, Ultimo, NSW 2007, Australia; mohammadsaidul.islam@uts.edu.au (M.S. I); suvash.saha@uts.edu.au (S.C.S);

[4] Center for Infrastructure Engineering, Western Sydney University, Penrith, NSW 2751, Australia; kejun.dong@westernsydney.edu.au

***Correspondence author: m.zhao@westernsydney.edu.au**

4.1 Abstract

Understanding the transportation and deposition (TD) of inhaled aerosol particles in human lung airways is important for health risk assessment and therapeutic efficiency of targeted drug delivery. The particle TD into a human lung depends on lung anatomy,-breathing pattern, as well as particle properties. The breathing capacity and lung airway diameters can be reduced by about 10% every 10 years after the age of 50. However, the age-specific particle TD in human lungs, particularly in the aged, has not been well understood in literature. This study investigates the particle TD in the lungs of people aged 50-70 years, using computational fluid dynamics (CFD). A new cutting method that splits the lung model into different sections has been developed as a feasible CFD method to simulate the particle TD in G0 to G14 lung airways. The inhalation of micron scale particles with three diameters (5 μm, 10 μm and 20 μm) and a constant air flow rate in inhalation is considered. It is found that different sized particles are deposited in different generation airways. Nearly 100% of 20 μm particles are deposited in the upper lung airways (G0-G5) and no particles pass through G7. Particles can go into deeper airways as their diameter decreases. When the particle size is decreased to 5 μm, over 48% of

particles can pass through G14 and enter the deeper lung airways. An increase in age causes more particles to deposit in the upper airway and fewer particles to enter the deeper airways.

Keywords: Aging effect, Airflow, Aerosol particle transport and deposition (TD), Lung, Inhalation, Drug delivery, Cutting method.

4.2 Introduction

Aerosol particle inhalation is commonly used as a drug delivery method to treat human lung diseases (Kuzmov and Minko 2015, Pulivendala et al. 2020). Hence, the study of particle transportation and deposition (TD) in human lung airways is important, to ensure the effectiveness of drugs delivered through aerosol particle inhalation (Ikegami et al. 2000, Gradon and Sosnowski 2014, Paul and Lau 2020). It is also important for reducing the effects of inhaled pollutant in the air on human health (Davidson, Phalen et al. 2005, Nieder, Benbi et al. 2018).

Particle TD into non-realistic tracheobronchial lung airways has been studied extensively to analyse the airflow dynamics and particle TD in lung airways (Li et al. 2007, Islam et al. 2019). Comer et al. (1999) developed a double bifurcation lung geometry based on Weibel's model (Weibel 1963), simulated airflow and TD in G3-G5 of this model numerically, and made a comprehensive comparison of their results with other numerical studies. Kleinstreuer et al. (2008) investigated airflow characteristics and particle TD of microparticles in a symmetric, triple bifurcation model of generations G0-G3. The results showed that the microparticles are mostly deposited at the carinal angles due to their strong inertial impaction mechanism. Zhang et al. (2005) studied the micro- and nano-size particle TD in a non-realistic, triple bifurcation model of generations G0-G3 using the Low-Reynolds-number (LRN) k–ω model. The nanoparticles were found to be more uniformly deposited in the airways than microparticles. Moreover, Islam et al. (2017) simulated aerosol particle transport in lung models

using Large Eddy Simulations (LES) for up to 17 generations. The study shows that the majority of particles are deposited in the upper airways through an inertial impaction mechanism. However, they only discussed the total deposition efficiency of particles of all the 17 generations but not the deposition efficiency of each individual generation. Ahookhosh, Pourmehran et al. (2020) conducted a detailed analysis of the evolution of various views of respiratory airway modelling throughout the years. This review study is helpful in understanding the limitations of lung anatomy and drug distribution in the lungs. CFD has proved to be an efficient and accurate method for predicting the local particles deposition efficiency in the lung airways (Kleinstreuer et al. 2008, Zhang et al. 2009, Myojo et al. 2010, Khorasanizade et al. 2011, Kadota et al. 2020, Ou et al. 2020). Deposition efficiency is defined as the percentage of aerosol particles absorbed in the human lung airways.

Some research on particle TD in realistic lung models has been conducted but mainly for small number of generations. Pourmehran et al. (2016) conducted CFD simulations of a realistic lung model of generations G0 to G6. The microparticles were found to be mostly deposited in the upper tracheobronchial lung airways. Recently, Asgari et al. (2021) studied the aerosol particles deposition in a realistic lung model of generations mouth to six (G6) based on the temperature and humidity conditions. The results showed that at very short timescales, aerosol evolution occurs mostly in the upper airway segments.

The earliest lung geometries created for simulating airflow in human lungs are mainly for adults (Landahl 1950). The aerosol particle TD varies with age significantly, especially during the childhood/teenage stage and shrinks in older age. Xu and Yu (1986) conducted a theoretical calculation of the PD of aerosol particles with diameters in the range between 0.01μm and 10 μm in the respiratory tracts of ages ranging from newborn babies to adults. It was found that the deposition efficiency in the mouth-throat section of children is higher than the adults. However, in the pulmonary and alveolar section, the opposite results were found

(Asgharian et al. 2004). Patterson et al. (2014)) studied nanoparticle deposition in the respiratory tract of school-aged subjects (8- to 18-year-olds). The results proved that the total particle deposition efficiency in the pulmonary section of children is higher than that of older people. The airborne particles deposit more easily for the school-aged people than adults because their lungs are smaller in size (Roemer et al. 2000, Hruba, Fabianova et al. 2001). Moreover, Deng et al. (2018) studied the age-specific (7-month old infant, 4-year old child and 20-year old adult) particle deposition in generation G3-G6 and G9-G12 lung airways through CFD simulations. The results further proved that the deposition efficiency of microparticles for children is higher than for adults in the tracheobronchial section. Compared to those conducted for younger people, few studies have investigated the airflow dynamics and particle TD in lung models for the aged. The lung volume and breathing capacity of old people reduce with increased age (Niewoehner and Kleinerman 1974). Kim et al. (2017) analysed the airflow dynamics in the lungs of aged people and found that the pressure drop in the lung airways of 80-year-olds decreases by 38% compared to 50-year-olds. However, they did not study the particle TD in the lungs of aged people.

Because most people suffering from lung diseases are older, and the drug was usually prescribed for older people, it is important to improve the understanding of particle TD in their lungs. In addition, most studies of airflow and particle TD in the lungs considered a limited number (three or four) of generations. Airflow and particle TD in a whole lung using CFD has never been studied, due to consuming and unaffordable computing time.

In this paper, we employed an efficient cutting method to enable the CFD simulations to simulate airflow and particle TD in generations G0 to G14. This study does not investigate generations after G14 because the airway flow rate is very low after G14, and as a result, the inertial impaction deposition mechanism does not work properly (Koullapis et al. 2016). The cutting method divides generations G0 to G14 into five sections, and each section includes three

generations. The continuity of the airflow mass and the particle numbers is ensured at the boundaries of these sections. The details of the cutting method will be presented in section 3. The aim of this study is to understand the effects of particle size and age on the airflow and TD of particles in micrometer scales in human lungs. We consider the same inhaled air flow rate for all the ages, but varying airway diameters with age.

4.3 Lung Model

Three-dimensional (3D) lung models with symmetric and planner lung airways from generation G0 to G14 are constructed based on the geometry proposed by Xu and Yu (1986). We used simplified lung models because geometries of realistic lung models with all the generations from G0 to G14 are not available and simulating complicated G0-G14 generation realistic lung model requires unaffordable computational time. To understand fundamental mechanisms of particle TD in a lung model with many generations with affordable time, we used an efficient cutting method and simplified lung model. The solution of the present study will provide good understanding how particle TD is affected by the particle size and age, though quantitatively have difference from the realistic lung. Many researchers have studied human lungs in people aged up to 30 years (Asgharian et al. 2004, Xi et al. 2012). The lung geometries for older people are not straightforwardly available but can be generated based on the conclusions made in previous studies. The lung airway diameters of adults change little between those aged 30 and 50 years (Hofmann 1982). Therefore, we have assumed that a 50-year-old lung is the same as a 30-year-old lung. The 3D bifurcation symmetric lung airways of a 50-year old of up to generation G14 are generated by SolidWorks using the geometric parameters given by Xu and Yu (1986) and presented in Figure 4.1. The triple-bifurcation lung geometries of 60-year and 70-year old lungs (G0-G3, G3-G6, G6-G9, G9-G12, G12-G15) are generated by reducing airway diameter of each generation by 10% after every 10-year age (Niewoehner and Kleinerman 1974, Kim et al. 2017). Furthermore, the size of the alveolar sacs grows with age

(Turner et al. 1968). Because tissue parameter and lung morphology of the human lung have changed due to the ageing. Between the ages of 50 and 80, lung tissue becomes around 7% stiffer (Lai-Fook and Hyatt 2000). Lung compliance is a volumetric number that is dependent on lung size and represents the lung's elastic property. Compliance is described as the ability of the lung tissue to absorb the same applied force, which is usually caused by a change in pressure. In general, as people get older, they become more compliant (Wahba 1983). Lung compliance is an extrinsic parameter that rises as the size of the alveolar sacs grows. Low-compliance lungs are stiff lungs that require a lot more pressure to obtain the same capacity. To affect the capacity of the lungs, a stiff lung would require a larger than typical shift in pleural pressure, making breathing more difficult. As a result, we looked at lung compliance in order to determine elastic characteristics as people age. The details of the geometric parameters of the lung airways are listed in Table 4.1.

Table 4.1. Geometric parameters of lung airways generated use the method by Xu and Yu (1986)

Generation (G)	Diameter (cm)			Length (cm)
	50 year old	60 year old	70 year old	50-70 years
0	1.665	1.499	1.332	12.286
1	1.220	1.098	0.976	4.284
2	0.830	0.747	0.664	1.896
3	0.560	0.504	0.448	0.759
4	0.450	0.405	0.360	1.268
5	0.350	0.315	0.280	1.071
6	0.280	0.252	0.224	0.901
7	0.230	0.207	0.184	0.759
8	0.186	0.167	0.149	0.639
9	0.154	0.139	0.123	0.538
10	0.130	0.117	0.104	0.460
11	0.109	0.098	0.087	0.390

12	0.095	0.086	0.076	0.330
13	0.082	0.074	0.066	0.271
14	0.074	0.067	0.059	0.231
15	0.066	0.059	0.053	0.202

As shown in Figure 4.1, generation G0 has one bifurcation and the number of bifurcations of the *n*-th generation is 2^n. Simulating the airflow of all the generations from G0 to G14 using CFD without any simplification would mean unaffordable computing time. To enable CFD to simulate airflow in all the generations in affordable time, we cut the lung model into five sections: G0-G3, G3-G6, G6-G9, G9-G12, G12-G15, and their geometries are shown in Figure 4.1. The airflow and particle of each section is simulated separately, considering the continuity of air mass and particle mass at the interfaces between generations.

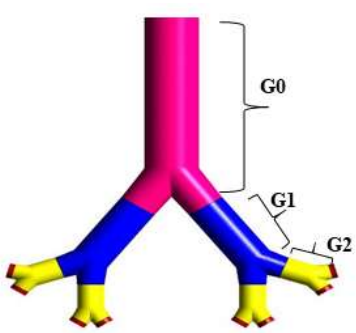

(a) Generations G0-G3

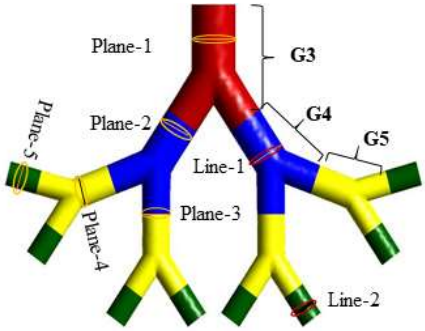

(b) Generations G3-G6

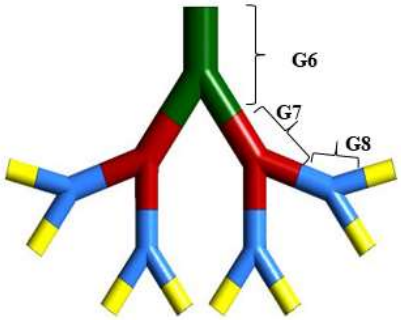

(c) Generations G6-G9

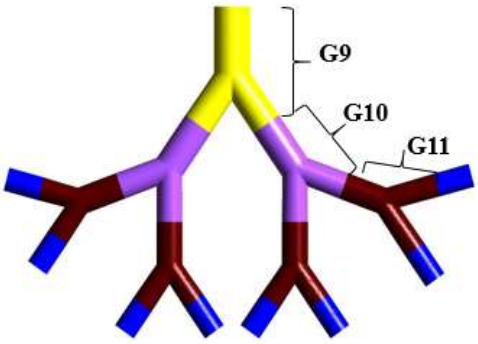

(d) Generations G9-G12

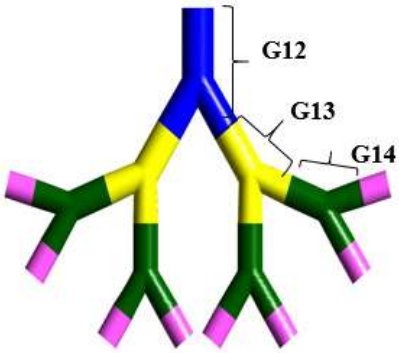

(e) Generations G12-G15

Figure 4.1. Tracheobronchial triple bifurcation lung airways model (G0-G14) for the 50-year-old lung

4.4 Numerical Method

4.4.1 Airflow Model

The airflow in lung airways is solved using software ANSYS FLUENT. The governing equations for airflow are the Reynolds-averaged Navier-Stokes (RANS) equations:

$$\frac{\partial \rho}{\partial t} + \frac{\partial}{\partial x_i}(\rho \vec{u}_i) = 0 \tag{4.1}$$

$$\frac{\partial}{\partial t}(\rho \vec{u}_i) + \frac{\partial}{\partial x_j}\left(\rho \vec{u}_i \vec{u}_j\right) = -\frac{\partial p}{\partial x_i} + \frac{\partial}{\partial x_j}\left[\mu\left(\frac{\partial \vec{u}_i}{\partial x_j} + \frac{\partial \vec{u}_j}{\partial x_i}\right)\right] + \frac{\partial}{\partial x_j}(-\rho\overline{u_i' u_j'}) \tag{4.2}$$

where $\vec{u}$ is the fluid velocity, μ is the molecular viscosity, ρ is the fluid density, p is the air pressure. The term $\rho\overline{u_i' u_j'}$ is the Reynolds stresses related to the turbulence model. The turbulence is simulated by the realisable k-ε turbulence model, which was proved to perform better than the standard k-ε model in various flow conditions including: rotating homogeneous shear flows; boundary-free shear flows; channel and flat boundary layer flows with and without pressure gradients; and backward facing step flows (Shih et al. 1995). The realisable k-ε model was proved to be able to accurately predict the mean flow rate of complex lung geometries (Tian et al. 2007, Ball et al. 2008, Isa et al. 2014, Srivastav et al. 2019).

The second-order upwind and the pressure-velocity coupling scheme are used to solve the RANS equations. The velocity inlet and the pressure outlet boundary conditions have been given in the triple bifurcation symmetric lung airway model. In the simulation of each section in Figure 4.1, the velocity at the inlet boundary is given and zero gauged pressure condition is considered at the exits (Freitas and Schröder 2008, Luo and Liu 2008, Islam et al. 2020). The effects of unsteady inhalation profile in unsteady flow on particle TD were studied in some studies (Ahookhosh et al. 2019, Kadota et al. 2020). However, a constant velocity is given at the inlet boundary of each section instead of an unsteady inhalation profile in order to testify the effectiveness of the current cutting method without the influence of the velocity variation.

The airway wall was considered stationary, and the wall surfaces of airways was treated as no-slip walls (Rahimi-Gorji et al. 2016, Farghadan et al. 2020, Rahman et al. 2020).

If the inhaled air flow rate is considered to be evenly distributed among all the 2^n bifurcations of generation G-n, the inlet air flow rate of each bifurcation of G-n is $Q_e^n = Q/2^n$, where Q is the inlet flow rate at G0. Therefore, the inlet velocity of each section starting from G-n is calculated by:

$$u = Q_e^n / A_n \tag{4.3}$$

where A_n is the cross-sectional area of the inlet.

4.4.2 Particle Transport and Deposition Model

The current model is a one-way coupling model that consider the particle transportation in air flow without considering the effect of the particles on the airflow. When the volume concentration of the particles is greater than 15%, two-way models that considers particle–particle interaction are required. However, the volume concentration is much less than 15% in all the drug delivery applications (Islam et al. 2019). To simulate transportation of dilute, suspended particles in the human lung, collision-free condition can be implemented, or particle–particle interaction can be ignored (Tsuji 2007). Most of the published literature did not consider particle-particle interaction because direct particle-particle interactions can be ignored if the particle suspension entering the tracheobronchial airway is dilute (Islam, Saha et al. 2019). In this paper, the interaction of the continuous and discrete phases has been accomplished by the Discrete Phase Model *(*DPM) model.

The Lagrangian approach is applied to determine the particle TD in human lung airways. The force balance equation of each individual particle is represented as:

$$\frac{d\vec{u}_p}{dt} = F_D\left(\vec{u} - \vec{u}_p\right) + \frac{\vec{g}}{\rho_p}\left(\rho_p - \rho\right) \tag{4.4}$$

where $\vec{u}$ and $\vec{u}_p$ are the fluid and particle velocities, respectively, $\vec{g}$ is the gravitational acceleration, ρ_P is the particle density, which is 1100 kg/m^3 (Moskal and Sosnowski 2009,

Islam et al. 2020). $F_D\left(\vec{u}-\vec{u}_p\right)$ is the drag force per unit particle mass, and the coefficient F_D is calculated by:

$$F_D = \frac{18\mu}{\rho_p d_p^2} C_D \frac{Re_P}{24} \tag{4.5}$$

where C_D is the drag coefficient calculated by (Morsi and Alexander 1972):

$$C_D = a_1 + \frac{a_2}{Re_P} + \frac{a_3}{{Re_P}^2} \tag{4.6}$$

The particle Reynolds number ($\mathrm{Re_P}$) is defined as:

$$Re_P = \rho d_P \left|\vec{u}_p - \vec{u}\right|/\mu. \tag{4.7}$$

and a_1, a_2, a_3 are functions of the Reynolds number Re_P given by:

$$\mathrm{a_1, a_2, a_3} = \begin{cases} 0, & 24, & 0 & 0 < R_e < 0.1 \\ 3.690, & 22.73, & 0.0903 & 0.1 < R_e < 1 \\ 1.222, & 29.17, & 3.89 & 1 < R_e < 10 \\ 0.617, & 46.50, & -116.67 & 10 < R_e < 100 \\ 0.364, & 98.33, & -2778 & 100 < R_e < 1000 \\ 0.357, & 148.62, & -47500 & 1000 < R_e < 5000 \\ 0.46, & -490.546, & 578700 & 5000 < R_e < 10000 \\ 0.519, & -1662.5, & 5416700 & R_e > 10000 \end{cases}$$

The maximum Reynolds numbers based on the airway diameter at G0 are 5480, 6052 and 6855 for 50-,60- and 70-year ages, respectively. For particle deposition purposes, a trap condition is considered on the lung airways wall and an escape condition is considered at all outlets (Islam et al. 2018, Zhang et al. 2020). Specifically, if a particle collides with the inner wall of an airway, it will be trapped by the wall surface (i.e. the coefficient of restitution is zero).

4.4.3 Deposition Efficiency calculation

The local deposition efficiency of the *n*-th generation is defined as the percentages of the particles absorbed (trapped) in this generation of airways out of the particles released at the inlet boundary of each section, and it is represented by $\eta_{L,n}$, where the subscript n stands for *n*-th generation. In the simulations, 79800 spherical particles with a uniform diameter were

injected randomly from the inlet surface at one time at the inlet of each section. The deposited particle numbers are then converted by the local deposition efficiency using Eq. (4.8).

$$\eta_{L,n} = \frac{\text{Number of particles are trapped in a lung airways}}{\text{Total number of particles released at the inlet of this section}} \tag{4.8}$$

In a lung, G0-G14 are divided into five sections, and the number of particles at the inlet boundary of each section is smaller than the previous section because of the absorption of particles in the previous section. As a result, the global deposition efficiency (η_n) of the *n*-th section is calculated by:

$$\eta_n = \eta_{L,n} \times (1 - \sum_{i=1}^{K} \eta_i) \tag{4.9}$$

where K stands for the number of generations in all the previous sections. The percentage of particles that escape from all the outlets of each generation and enter the deeper lung is defined as particle escaping rate. The formula for calculating the particle escaping rate of generation *n* (α_n) is:

$$\alpha_n = 1 - \sum_{i=1}^{n} \eta_i \tag{4.10}$$

4.5 Grid Dependency Study and Model Validation

4.5.1 Grid Dependency Test

The grid dependency test is performed by conducting numerical simulations of G3-G6 at $d_p = 10\ \mu m$ using six meshes with the same mesh structure but different mesh densities. The smallest grid sizes next to the wall of Mesh 1 and Mesh 6 are 0.8 mm and 0.235 mm, respectively. The node numbers of Meshes 1 to 6 range from 172726 to 865461. Figure 4.2 (b) shows the mesh near one bifurcation of generation G4. Ten-layers of smooth inflation are implemented near the wall to accurately predict the wall boundary flow inside the lung airway, as seen in Figure 4.2 (a). The mesh structure of all other generations is similar to that shown in Figure 4.2.

Figure 4.2. Computational mesh for the section of G4 (a) Refined inflation mesh near the airway wall (b) The mesh resolution on the airway wall.

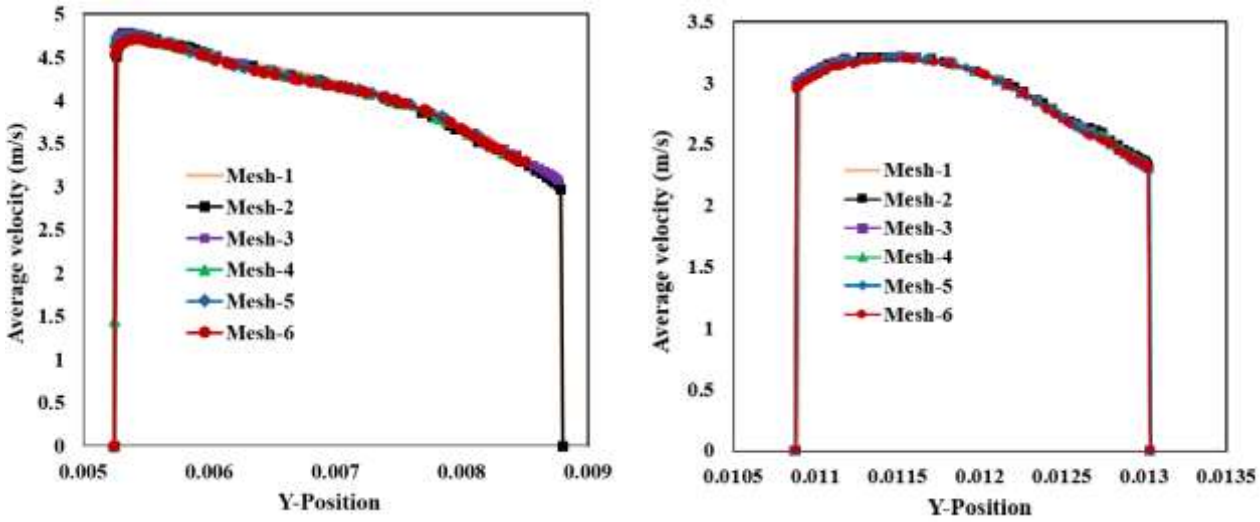

(a) (b)

Figure 4.3. Velocity distributions along the two lines indicated in Figure 4.(b) from six meshes for G3-G6 model, 50-year of age, particle diameter of $d_p = 10\ \mu m$ and inlet flow rate of 60 l/min. (a) Line-1 (b) Line-2.

The velocity distributions along two lines indicated in Figure 4.1 (b) calculated from the six meshes are shown in Figure 4.3. The velocity distribution of all the meshes follow the same

trend and very small differences can be observed between different meshes. Particularly, the maximum velocity difference between Mesh 5 and Mesh 6 is 0.0174%.

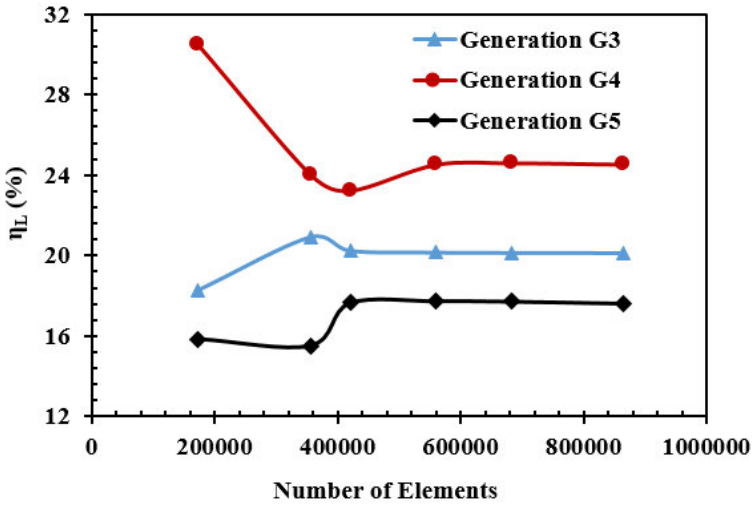

Figure 4.4. Comparison of local deposition efficiency as functions of the grid number for G3-G6 of the 50-year age model, particle diameter of $d_p = 10\ \mu m$ and inlet flow rate of $60\ l/\text{min}$.

The variations of the local deposition efficiency with the element numbers of the mesh are presented in Figure 4.4. The local deposition efficiencies nearly remain unchanged as the mesh density is higher than Mesh-4 with about 0.56 million elements. In the rest of the paper, we used the density of Mesh-5 with 0.68 million elements to do all the numerical simulations.

4.5.2 Model Validation

The present CFD method is validated against available published data of airflow and particle TD in G3-G5 at Re=1000 and 2000 (Kim and Fisher 1999, Chen et al. 2012, Feng and Kleinstreuer 2014). The inhalation flow rates $3.87\ l/\text{min}$ $(Re = 1000)$ and $7.78\ l/\text{min}$ $(Re = 2000)$are calculated based on the inlet diameter of G3. Simulations are conducted for particle diameters of dp=1µm, 3µm, 5µm, 6µm, 7µm, 8µm and 10µm. Figure 4.5 (a) and (b) shows the comparison of the total deposition efficiency of G3 and G4 against the Stokes number, respectively. The Stokes number is defined as:

$$\mathrm{St} = \frac{\rho_p d_p^2 u}{18\mu D}$$

where D represents the hydraulic diameter, which is the same as the inlet diameter of G3; u is the flow velocity at the inlet of G3. The one-way and two-way coupling models result in similar results in Figure 4.5, because the concentration of particles in the air in drug delivery is so small that the airflow is not affected by the particle motion. It can be found that the deposition efficiency increases with the increase of the Stokes number. The variation trend of the deposition efficiency with the Stokes number is in good agreement with other numerical results and the experimental data, demonstrating that the present model is accurate to calculate the particle TD in the tracheobronchial airways of a lung. In Figure 4.5, the deposition efficiencies of Re=1000 and 2000 do not differ from each other, indicating the deposition efficiency is mainly controlled by St.

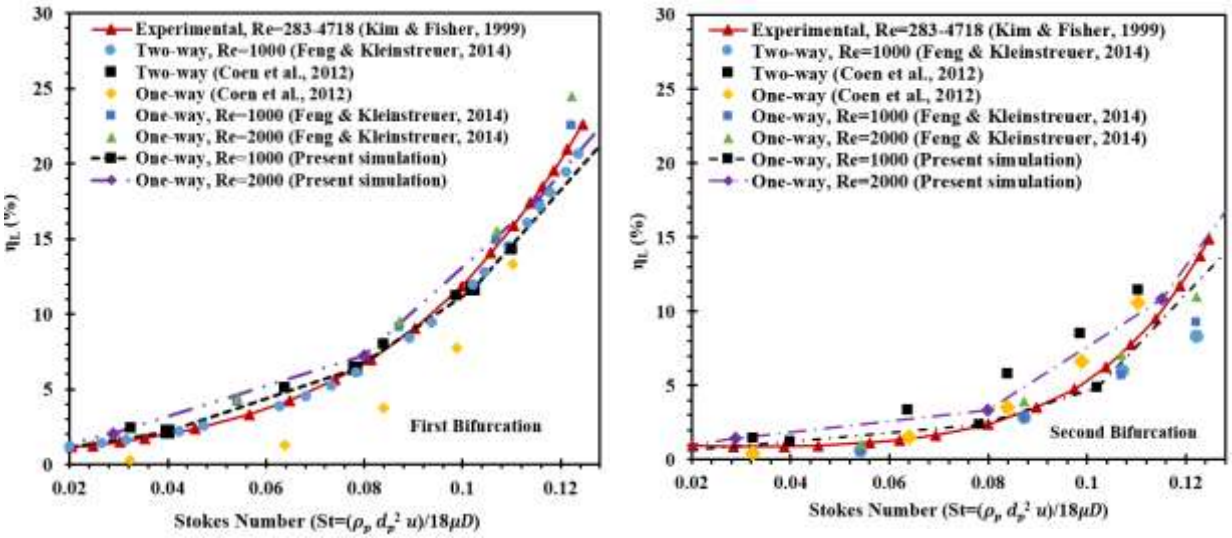

(a) (b)

Figure 4.5. Comparison between present simulation results of deposition efficiency of G3-G5 and results from literature (Kim and Fisher 1999, Chen et al. 2012, Feng and Kleinstreuer 2014): (a) Generation G3; (b) Generation G4.

4.6 Results and Discussion

In the present study, the inhalation flow airflow rate of $Q = 60$ l/min at G0 (Hickey et al. 1996, Kleinstreuer and Zhang 2003) is considered for different ages and the inlet velocities of the five sections and three ages are listed in Table 4.2**.** However, the inhalation velocity profile affects the calculation of particle deposition in human lung airways**.** Kadota, Inoue et al. (2020) studied the constant and inhalation flow pattern to calculate particles deposition in a realistic human airway. The results showed that vortex generation employing an inhalation flow pattern aided particle deposition in the airways. Ahookhosh et al. (2019) investigated an experimental for particles deposition in a realistic lung model of generations mouth to four (G4) considering three constant flow rates. The results showed that the deposition density increased with an increased flow rate. The inhalation route (mouth and nasal) has influence particle deposition in upper and tracheobronchial lung airways (Lizal et al. 2020). However, the results showed that the inhaling route had no effect on the distribution of deposited particles downstream of the trachea.

Hence, the inlet velocity changes with changes in the lung geometry for different ages of people. Aging has been associated with progressive decline in lung function and depends on the breathing parameters such as tidal volume and breathing frequency. The breathing frequency for 50-year, 60-year, and 70-year are 13.65(min^{-1}), 13.19(min^{-1}), and 12.92 (min^{-1}) respectively. Moreover, the tidal volumes are 500 ml, 403 ml and 179 ml for 50-year, 60-year, and 70-year respectively (Hofmann 1982).

Table 4.2. Inlet airflow velocities for the five sets of models

Generations	50-Years	60-Years	70-Years
G0-G3	4.591	5.667	7.173
G3-G6	5.079	6.271	7.937
G6-G9	2.536	3.131	3.963
G9-G12	1.048	1.295	1.639
G12-G15	0.344	0.425	0.538

4.6.1 Airflow Characteristics

The air density and viscosity are 1.225 kg/m^3 and 1.79×10^{-5} kg/m·s respectively. Simulations are conducted for three particle diameters of d_p=5 μm, 10 μm and 20 μm and three ages in Table 4.2. Figure 4.6 shows the airflow velocity contours on the symmetric plane within the lung generations G3-G6 of the three ages. The variation of velocity inside other sections are qualitatively similar to that of section G3-G6. The velocity decreases as air goes into the deep lung because the total cross-sectional area increases. For a constant flow rate, the 70-year-old lung model in Figure 4.6 has the maximum velocity because it has the smallest lung diameter. The velocity varies significantly in each bifurcation area in the lung airways. After the air passes through the splitting point of each bifurcation, the velocity increases locally as the result of the streamline contraction. The local increase of the velocity and the sudden change of the velocity direction at the bifurcation point enhances the potential of particle deposition due to impaction mechanism.

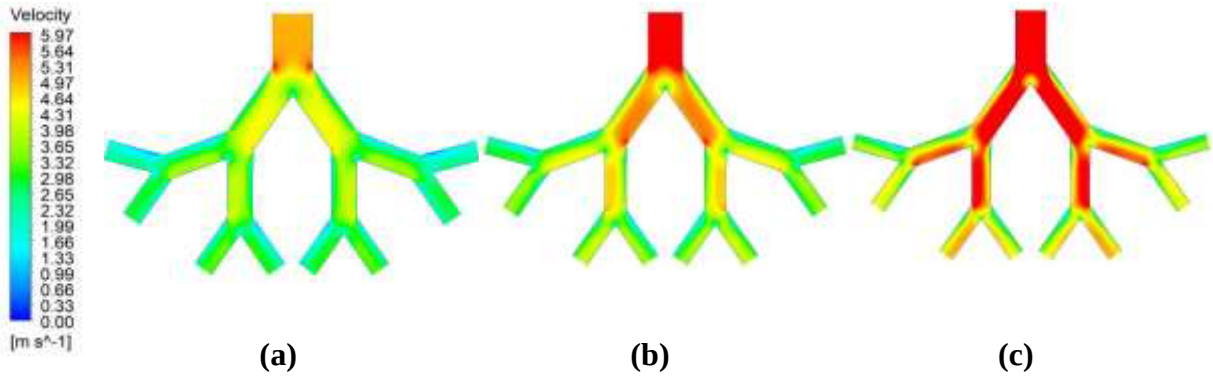

Figure 4.6. Airflow velocity contours for generation G3-G6 at a flow rate of 60 l/min. (a) 50-years-old (b) 60-years-old, and (c) 70-years-old model.

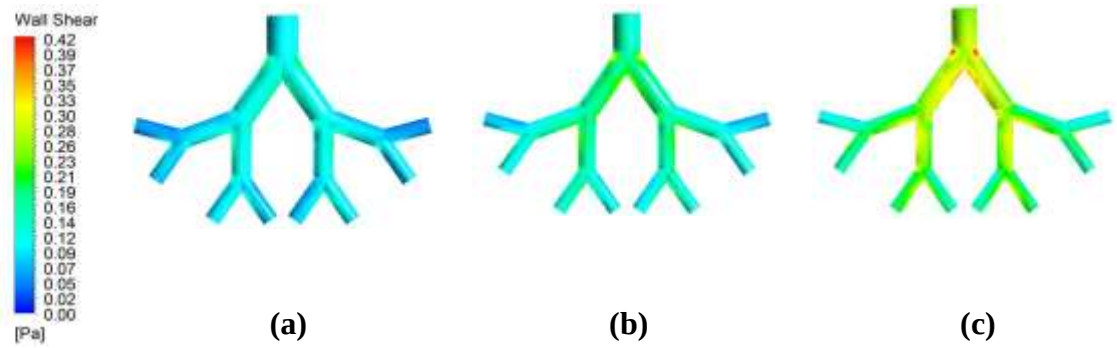

Figure 4.7. Wall shear stress for generations G3-G6. (a) 50-years-old (b) 60-years-old, and (c) 70-years-old models.

Figure 4.7 shows the distributions of airflow-induced wall shear stress along the inner wall of G3-G6 lung airways for the three ages. The localised velocity increase at the splitting point of each generation shown in Figure 4.6 leads to the local increase in the wall shear. The motion of the fluid and particles near the wall can be understood by observing the wall shear stress, which is proportional to the velocity in the boundary layer flow next to the wall. The wall shear stress changes significantly in each lung airway generation because the flow resistance happens at complex lung geometry. At each sharp edge, the wall shear stress is increased significantly because of the flow contraction. The maximum wall shear stress occurs in the splitting point of each bifurcation. Figure 4.8 quantitatively shows the maximum area-weighted average wall shear stress on five sectional planes indicated in Figure 4.1(b). With a contact inhaled air flow rate, the wall shear stress increases with the increase in age, as shown in Figure 4.8.

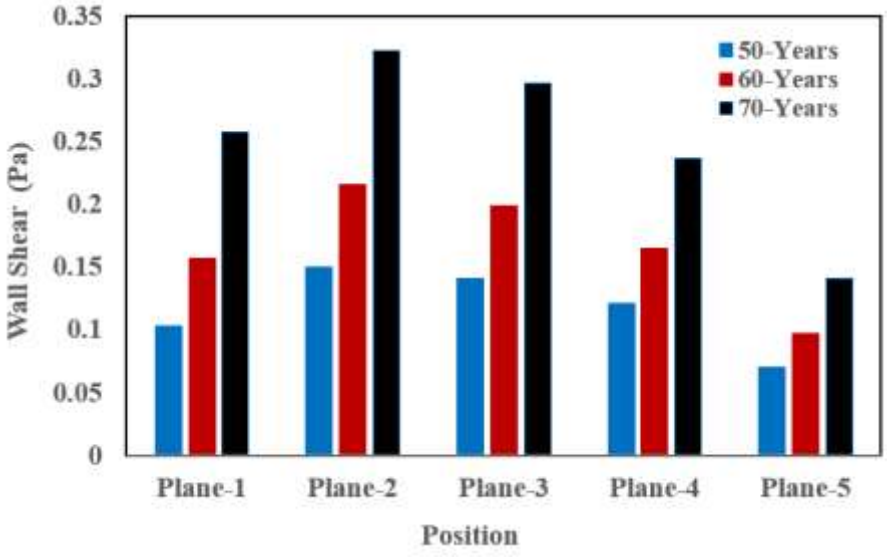

Figure 4.8. Area-weighted average wall shear stress at different planes of the three ages' lung models for generation G3-G6 at a flow rate of 60 l/min; see Figure 4.1(b) for plane numbers.

The maximum area-weighted average static pressures at different positions in the section G3-G6 lung airways are shown in Figure 4.9. The maximum pressure is observed at plane-1 (Fig.-1b) for all ages. In addition to the decrease in velocity as shown in Figure 4.6, the pressure also decreases gradually when the airflow goes into the deep lung. The flow energy reduces as the airflow goes into deep lung because of the friction from the inner wall of the airways. The high velocity at 70-year-old lung shown in Figure 4.6 requires high pressure at the inlet to drive the flow. Figure 4.9 shows a 72.38% pressure increase for 70-year-old people compared to the 50-year-old in the lung airways. Therefore, breathing air into the lung for a 70-year-old is more complicated than for a 50-year-old. A significant pressure at Plane 5 is decreased compared with that at plane 1, mainly because of the volume flow rate decrease. Hence, the decrease in velocity led to the low-pressure drop-in plane 5.

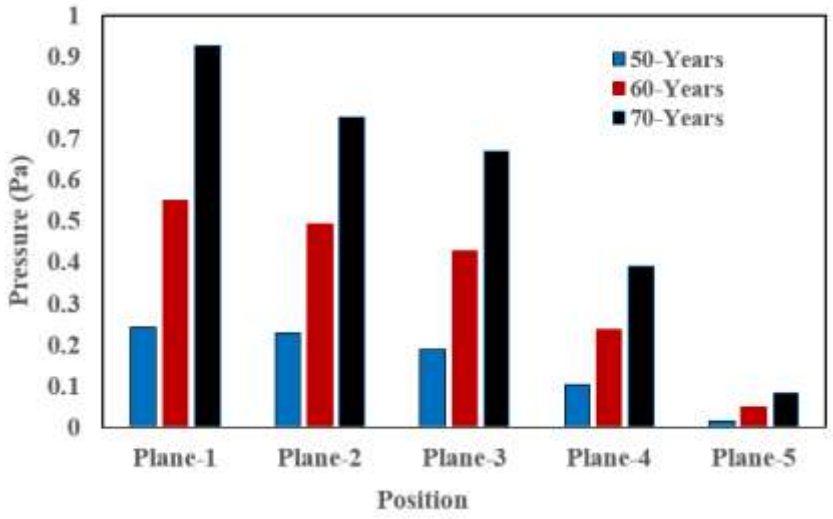

Figure 4.9. Pressure at different planes of 50-70-year-old ages' model for generations G3-G6 at a flow rate of 60 $l/\min$; see Figure 4.1(b) for plane numbers.

4.6.2 Particle Deposition

Figure 4.10 shows the visualisation of local particle distribution of different sized particles at generation G3-G6 of 50-year age. The calculated local total particle deposition efficiencies of G3-G6 are 90.83%, 62.93% and 10.45% for of 20 µm, of 10 µm and 5 µm particles, respectively. The 5-µm particles have much smaller deposition efficiency than 20 µm particles at Generation G3-G6, because the impaction mechanism becomes weak as particle diameter decreases. Moreover, the 5-µm particles are more evenly distributed in each bifurcation lung area compared to the larger particles. When particle size is small, the inertia mechanism becomes weak. When the flow direction changes, small particles can change direction and follow the flow easily and as a result, they can spread, and deposition occurs at different areas. When the particle size is large, the inertia effect makes particles hit the wall at the first and second bifurcations. Even if the flow direction bends, large particles change their direction slowly and do not follow the flow direction easily. This reduces the chance of large particle deposition in other places.

(a) d_s=5 µm (b) d_s=10 µm (c) d_s=20 µm

Figure 4.10. Local Particle Deposition for the 50 years age for generation G3-G6 (a) 5 µm particles, (b) 10 µm particles, and (c) 20 µm particles at flow rate of 60 l/min

Figure 4.11 shows the effects of the age on the global particle deposition efficiency in lung airway generations G0-G14. When the particle size is 5 µm, more particles can go deeper into the lung and the deposition efficiency in upper lung airways reduces significantly, compared with 10 µm and 20 µm. Around 0.61%, 0.28% and 0.11% of 5 µm particles are deposited at the generation G14 for 70-years, 60-years and 50-years of age, respectively (Figure 4.11a). The maximum deposition efficiency of 10 µm particles is found at generation G4, G2 and G2 for the 50-, 60- and 70-year ages, respectively. With a constant inhaled flow rate, the decrease in the diameter of the G0 lung airway (as the result of aging) causes an increase in the velocity and higher Stokes number. It has been reported that the higher Stokes number causes higher deposition efficiency in the upper generations, as shown in Figure 4.5. As the age increases, the increase of the flow velocity causes large deposition efficiency at early generations. In a younger age, the deposition efficiencies of early generations are small, allowing more particles to pass upper generations and deposit in the deeper lung. Unlike 20 µm particles that are all trapped before G8, very small amount of 10 µm particles (0.09% for a 50-year-old) can reach G14.

The position of the maximum deposition efficiency is found to move towards the deep lung as the particle diameter decreases. The maximum deposition rate of 20 µm particles occurs at G0 and the majority of the 20 µm particles are deposited in the upper lung airways up to G4 because of the strong impaction mechanism at large particles. No 20 µm particles can pass through G8, resulting in zero deposition efficiency in all the generations after G8, as shown in Figure 4.11 (c). More 20 µm particles are deposited at G0 than all other generations for all the three ages in Figure 4.11 (c). The deposition efficiency of 20 µm particles in G0 for 70-years, 60-years, and 50-years of age people, are 50.83%, 38.62%, and 29.69%, respectively. The deposition efficiency increases in upper generations and decreases in lower generations with the increase in age. All the 20 µm particles are deposited between G0 to G8 generations for those of 50-70 years old, leaving no deposition after G9 (Figure 4.11c). The deposition efficiency in the deeper lung airways for a 5 µm particle is better than 10 µm and 20 µm. Hence, the results suggest that the capacity for particle absorption in the deep lung airway generation (G14) for 50-year-olds is better than 70-year-olds.

The escaping rate from generations G0-G14 for 50-, 60- and 70-year ages are represented in Figure 4.12. The escape rate at G14 are the percentage of particles that can pass G14 and enter generations after G15. The effects of the age and particle size on the escaping rate is opposite to their effects on the deposition rate. An increase in the deposition rate makes the escaping rate decrease with the increase in age (Figure 4.12a). The escaping rates at G14 of 20-µm particles are zero for all the ages. Only 0.64%, 0.09% of 20-µm particles pass G6 and go into the deeper lung for 50-years, 60-years age lung models, respectively. The 20-µm particles cannot pass G5 of a 70-years age lung because all particles are deposited in the upper lung airways.

The escaping rates of 5-µm particles at every generation is significantly increased compared with 20-µm. Percentages of 66.65%, 53.51%, and 39.59% of 5-µm particles can pass

G14 and go into the deeper lung airways for 50-year, 60-year, and 70-year-olds, respectively (Figure 4.12(a)). The escaping rates of 10-µm particles at G14 of all the three ages are not zero but much smaller than those of 5-µm particles (Figure 4.12b); 3.12% of 10-µm particles pass G14 and enter G15 for the 50-year age, while only 0.12% of particles can enter G15 for the 70-year age.

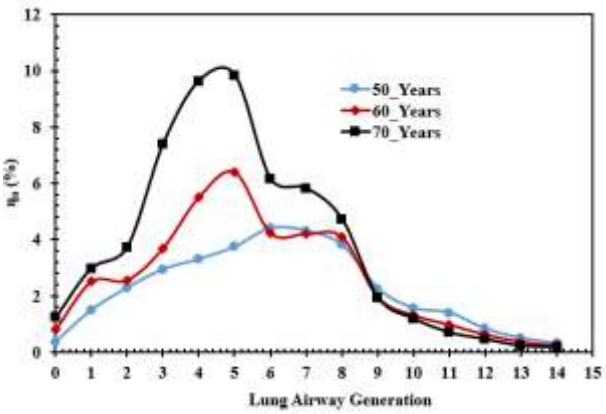

(a) 5 µm particles

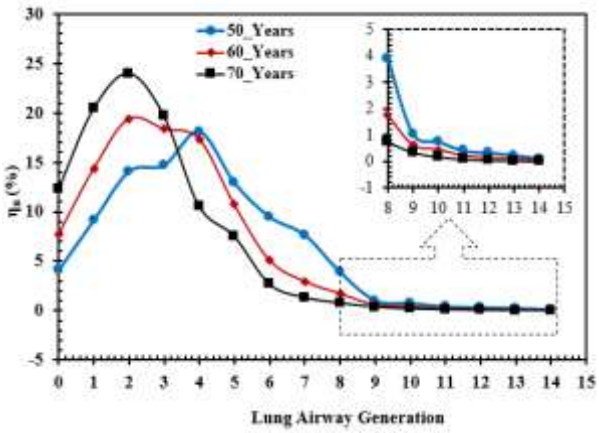

(b) 10 µm particles

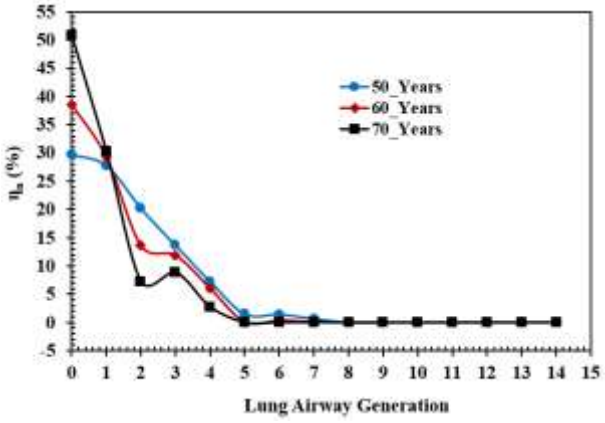

(c) 20 µm particles

Figure 4.11. Effects of age on the global particle deposition efficiency in airway lung generation G0-G14 for: (a) 5 µm particles, (b) 10 µm particles, and (c) 20 µm particles.

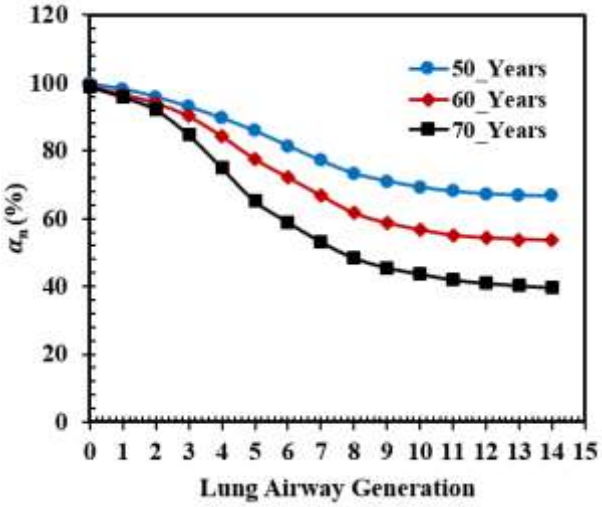

(a) 5 µm particles

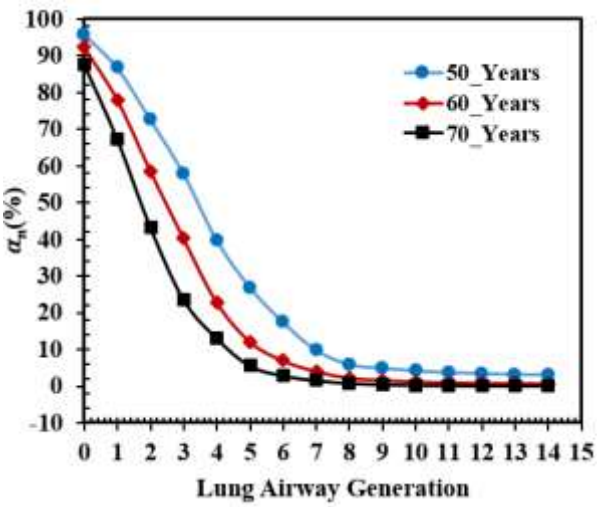

(b) 10 µm particles

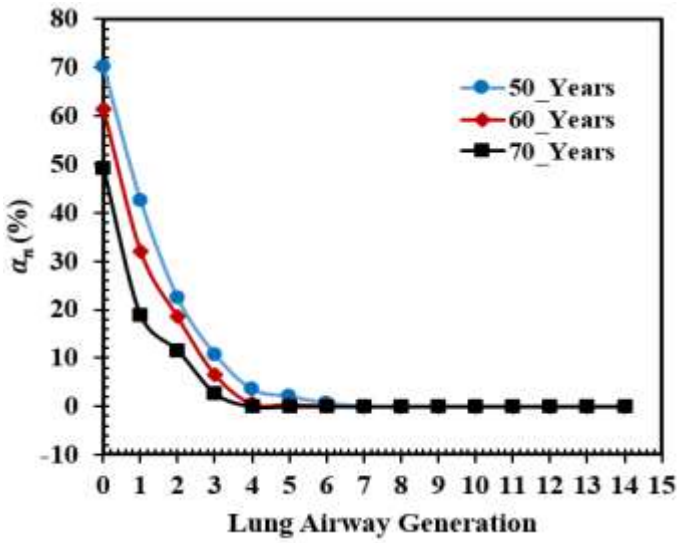

(c) 20 µm particles

Figure 4.12. Particle escaping through rate (α_n) for ages 50-70 years at a flow rate of 60 l/min: (a) 5 µm particles, (b) 10 µm particles, and (c) 20 µm particles.

4.7 Conclusions

The microparticles TD in the Tracheobronchial lung airway generations G0-G14 for 50-, 60- and 70-year-old lung models are investigated numerically. We have developed a cutting

method to enable the airflow and particle TD in generations from G0 to G14 of a lung to be simulated using computational fluid dynamics. The effects of age and particle diameter on the airflow and particle TD are discussed in detail and the conclusions are summarised as follows.

- The airflow velocity in the airways increased with increase of age due to the reduction of airway diameters. The local increase in wall shear stress is observed in each bifurcation lung airway because the flow resistance happens in that area. If the gauged pressure is zero at the exit at G15, the pressure in the lung airways increases with the increase of age. The pressure of G3 to G6 of a 70-year-old lung is 27.62% higher than that of a 50-year-old lung.
- Different sized particles are deposited in different positions of the lung. For a 50-year-old lung, 5-μm, 10-μm and 20-μm particles are mostly deposited in G6, G5 and G0, respectively. However, as the age increases to that of a 70-year-old, the maximum deposition rates of 5-μm, 10-μm and 20-μm particles occur at G5, G2 and G0, respectively.
- When the particle size is 20 μm, a high percentage of the particles (over 85%) are deposited in the upper lung airways (G0-G4). As the particle size is decreased to 5 μm, 52% of the particles are deposited in the lung airways, allowing over 48% of particles to enter the deep lung after G14. The above finding indicates that particles must have a small diameter to treat diseases in the deep lung.
- The numerical study showed that deposition efficiency is affected by ages. Most of the particles are deposited in 70-year-olds rather than 50-year-olds in the upper generations. The capacity for the particles to escape each generation decreases with the increase of age. The results suggest that to increase the number of particles deposited into deep lung airways, the particle size needs to be reduced. Therefore, our results indicate that the

particles as targeted drug delivery should be provided based on the appropriate age (Labiris and Dolovich 2003, Newman 2017).

There are some limitations in this study that should be addressed in future studies. First, only an inhalation condition was considered in the simulation of particle TD. We will consider the inhalation as well as the exhalation process for both deposition and clearance of particles in the forthcoming studies. Second, we considered the micron-size ($5\mu m \leq d_p \leq 20\ \mu m$) particle deposition in the G0-G14. The PD of nanoparticle in airways is mainly governed by the Brownian diffusion mechanism. We will investigate nanoscale particles in future studies. Third, we considered symmetric and planner lung airways, instead of real lungs due to unavailability of the lung geometry. Nonetheless, the symmetric and planner lung airways model can predict the particle deposition pattern correctly (Kleinstreuer et al. 2008, Deng et al. 2019). Even considering the above limitations, the airflow characteristic and particle deposition pattern in our present study are valid, based on the published literature.

Conflicts of Interest

The authors state no conflict of interest.

Acknowledgement

The authors would like to acknowledge the computing facility at WSU.

References

Ahookhosh, K, Pourmehran, O, Aminfar, H, Mohammadpourfard, M, Sarafraz, MM & Hamishehkar, H 2020, 'Development of human respiratory airway models: A review', *European Journal of Pharmaceutical Sciences*, vol. 145, 105233.

Ahookhosh, K, Yaqoubi, S, Mohammadpourfard, M, Hamishehkar, H & Aminfar, H 2019, 'Experimental investigation of aerosol deposition through a realistic respiratory airway replica: an evaluation for MDI and DPI performance', *International journal of pharmaceutics*, vol. 566, pp. 157-172.

Asgari, M, Lucci, F & Kuczaj, AK 2021, 'Multispecies aerosol evolution and deposition in a human respiratory tract cast model', *Journal of Aerosol Science*, vol. 153, 105720.

Asgharian, B, Menache, M & Miller, F 2004, 'Modeling age-related particle deposition in humans', *Journal of aerosol medicine*, vol. 17, no. 3, pp. 213-224.

Ball, C, Uddin, M & Pollard, A 2008, 'High resolution turbulence modelling of airflow in an idealised human extra-thoracic airway', *Computers & Fluids*, vol. 37, no. 8, pp. 943-964.

Chen, X, Zhong, W, Zhou, X, Jin, B & Sun, B 2012, 'CFD–DEM simulation of particle transport and deposition in pulmonary airway', *Powder technology*, vol. 228, pp. 309-318.

Comer, J, Kleinstreuer, C, Hyun, S & Kim, C 1999, 'Aerosol transport and deposition in sequentially bifurcating airways', *J. Biomech. Eng.*, vol. 122, no. 2, pp. 152-158.

Davidson, CI, Phalen, RF & Solomon, PA 2005, 'Airborne particulate matter and human health: a review', *Aerosol Science and Technology*, vol. 39, no. 8, pp. 737-749.

Deng, Q, Ou, C, Chen, J & Xiang, Y 2018, 'Particle deposition in tracheobronchial airways of an infant, child and adult', *Science of the Total Environment*, vol. 612, pp. 339-346.

Deng, Q, Ou, C, Shen, Y-M, Xiang, Y, Miao, Y & Li, Y 2019, 'Health effects of physical activity as predicted by particle deposition in the human respiratory tract', *Science of the Total Environment*, vol. 657, pp. 819-826.

Farghadan, A, Poorbahrami, K, Jalal, S, Oakes, JM, Coletti, F & Arzani, A 2020, 'Particle transport and deposition correlation with near-wall flow characteristic under inspiratory airflow in lung airways', *Computers in biology and medicine*, vol. 120, 103703.

Feng, Y & Kleinstreuer, C 2014, 'Micron-particle transport, interactions and deposition in triple lung-airway bifurcations using a novel modeling approach', *Journal of Aerosol Science*, vol. 71, pp. 1-15.

Freitas, RK & Schröder, W 2008, 'Numerical investigation of the three-dimensional flow in a human lung model', *Journal of biomechanics*, vol. 41, no. 11, pp. 2446-2457.

Gradon, L & Sosnowski, TR 2014, 'Formation of particles for dry powder inhalers', *Advanced Powder Technology*, vol. 25, no. 1, pp. 43-55.

Hickey, AJ, Martonen, TB & Yang, Y 1996, 'Theoretical relationship of lung deposition to the fine particle fraction of inhalation aerosols', *Pharmaceutica Acta Helvetiae*, vol. 71, no. 3, pp. 185-190.

Hofmann, W 1982, 'Mathematical model for the postnatal growth of the human lung', *Respiration physiology*, vol. 49, no. 1, pp. 115-129.

Hruba, F, Fabianova, E, Koppova, K & Vandenberg, JJ 2001, 'Childhood respiratory symptoms, hospital admissions, and long-term exposure to airborne particulate matter', *Journal of Exposure Science & Environmental Epidemiology*, vol. 11, no. 1, pp. 33-40.

Ikegami, K, Kawashima, Y, Takeuchi, H, Yamamoto, H, Momose, D-I, Saito, N et al. 2000, 'In vitro inhalation behavior of spherically agglomerated steroid particles with carrier lactose', *Advanced Powder Technology*, vol. 11, no. 3, pp. 323-332.

Isa, NM, Ahmad Fara, ANK & Asmuin, NZ 2014, 'Investigation on the Turbulence Models Effect of a Coal Classifier by Using Computational Fluids Dynamics', *Trans Tech Publ*, vol. 465, pp. 617-621.

Islam, MS, Gu, Y, Farkas, A, Paul, G & Saha, SC 2020, 'Helium–Oxygen Mixture Model for Particle Transport in CT-Based Upper Airways', *International Journal of Environmental Research and Public Health*, vol. 17, no. 10, 3574.

Islam, MS, Paul, G, Ong, HX, Young, PM, Gu, Y & Saha, SC 2020, 'A review of respiratory anatomical development, air flow characterization and particle deposition', *International Journal of Environmental Research and Public Health*, vol. 17, no. 2, 380.

Islam, MS, Saha, SC, Gemci, T, Yang, IA, Sauret, E & Gu, Y 2018, 'Polydisperse microparticle transport and deposition to the terminal bronchioles in a heterogeneous vasculature tree', *Scientific reports*, vol. 8, no. 1, pp. 1-9.

Islam, MS, Saha, SC, Gemci, T, Yang, IA, Sauret, E, Ristovski, Z et al. 2019, 'Euler-Lagrange prediction of diesel-exhaust polydisperse particle transport and deposition in lung: anatomy and turbulence effects', *Scientific Reports*, vol. 9, no. 1, pp. 1-16.

Islam, MS, Saha, SC, Sauret, E, Gemci, T & Gu, Y 2017, 'Pulmonary aerosol transport and deposition analysis in upper 17 generations of the human respiratory tract', *Journal of Aerosol Science*, vol. 108, pp. 29-43.

Islam, MS, Saha, SC, Sauret, E, Ong, H, Young, P & Gu, Y 2019, 'Euler–Lagrange approach to investigate respiratory anatomical shape effects on aerosol particle transport and deposition', *Toxicology Research and Application*, vol. 3, 2397847319894675.

Kadota, K, Inoue, N, Matsunaga, Y, Takemiya, T, Kubo, K, Imano, H et al. 2020, 'Numerical simulations of particle behaviour in a realistic human airway model with varying inhalation patterns', *Journal of Pharmacy and Pharmacology*, vol. 72, no. 1, pp. 17-28.

Kadota, K, Sosnowski, TR, Tobita, S, Tachibana, I, Tse, JY, Uchiyama, H et al. 2020, 'A particle technology approach toward designing dry-powder inhaler formulations for personalized medicine in respiratory diseases', *Advanced Powder Technology*, vol. 31, no. 1, pp. 219-226.

Khorasanizade, S, Shams, M & Mansoori, B 2011, 'Calculation of aerosol deposition in human lung airways using Horsfield geometric model', *Advanced Powder Technology*, vol. 22, no. 6, pp. 695-705.

Kim, CS & Fisher, DM 1999, 'Deposition characteristics of aerosol particles in sequentially bifurcating airway models', *Aerosol Science & Technology*, vol. 31, no. 2-3, pp. 198-220.

Kim, J, Heise, RL, Reynolds, AM & Pidaparti, RM 2017, 'Aging effects on airflow dynamics and lung function in human bronchioles', *PloS one*, vol. 12, no. 8, e0183654.

Kleinstreuer, C & Zhang, Z 2003, 'Laminar-to-turbulent fluid-particle flows in a human airway model', *International Journal of Multiphase Flow*, vol. 29, no. 2, pp. 271-289.

Kleinstreuer, C, Zhang, Z & Donohue, J 2008, 'Targeted drug-aerosol delivery in the human respiratory system', *Annu. Rev. Biomed. Eng.*, vol. 10, pp. 195-220.

Kleinstreuer, C, Zhang, Z & Li, Z 2008, 'Modeling airflow and particle transport/deposition in pulmonary airways', *Respiratory physiology & neurobiology*, vol. 163, no. 1-3, pp. 128-138.

Koullapis, P, Kassinos, SC, Bivolarova, MP & Melikov, AK 2016, 'Particle deposition in a realistic geometry of the human conducting airways: Effects of inlet velocity profile, inhalation flowrate and electrostatic charge', *Journal of biomechanics*, vol. 49, no. 11, pp. 2201-2212.

Kuzmov, A & Minko, T 2015, 'Nanotechnology approaches for inhalation treatment of lung diseases', *Journal of controlled release*, vol. 219, pp. 500-518.

Labiris, N & Dolovich, M 2003, 'Pulmonary drug delivery. Part I: physiological factors affecting therapeutic effectiveness of aerosolized medications', *British journal of clinical pharmacology*, vol. 56, no. 6, pp. 588-599.

Lai-Fook, SJ & Hyatt, RE 2000, 'Effects of age on elastic moduli of human lungs', *Journal of Applied Physiology*, vol. 89, no. 1, pp. 163-168.

Landahl, H 1950, 'On the removal of air-borne droplets by the human respiratory tract: I. The lung', *The bulletin of mathematical biophysics*, vol. 12, no. 1, pp. 43-56.

Li, Z, Kleinstreuer, C & Zhang, Z 2007, 'Particle deposition in the human tracheobronchial airways due to transient inspiratory flow patterns', *Journal of Aerosol Science*, vol. 38, no. 6, pp. 625-644.

Lizal, F, Elcner, J, Jedelsky, J, Maly, M, Jicha, M, Farkas, Á et al. 2020, 'The effect of oral and nasal breathing on the deposition of inhaled particles in upper and tracheobronchial airways', *Journal of Aerosol Science*, vol. 150, 105649.

Luo, H & Liu, Y 2008, 'Modeling the bifurcating flow in a CT-scanned human lung airway', *Journal of biomechanics*, vol. 41, no. 12, pp. 2681-2688.

Morsi, S & Alexander, A 1972, 'An investigation of particle trajectories in two-phase flow systems', *Journal of Fluid mechanics*, vol. 55, no. 2, pp. 193-208.

Moskal, A & Sosnowski, TR 2009, 'Dynamics of aerosol pulse in a simplified mouth-throat geometry and its significance for inhalation drug delivery', *Chemical Engineering and Processing*, vol. 30, pp. 545-558.

Myojo, T, Ogami, A, Oyabu, T, Morimoto, Y, Hirohashi, M, Murakami, M et al. 2010, 'Risk assessment of airborne fine particles and nanoparticles', *Advanced Powder Technology*, vol. 21, no. 5, pp. 507-512.

Newman, SP 2017, 'Drug delivery to the lungs: challenges and opportunities', *Therapeutic delivery*, vol. 8, no. 8, pp. 647-661.

Nieder, R, Benbi, DK & Reichl, FX 2018, 'Soil-Borne Gases and Their Influence on Environment and Human Health', in *Soil Components and Human Health*, Springer, pp. 179-221.

Niewoehner, DE & Kleinerman, J 1974, 'Morphologic basis of pulmonary resistance in the human lung and effects of aging', *Journal of Applied Physiology*, vol. 36, no. 4, pp. 412-418.

Ou, C, Jian, H & Deng, Q 2020, 'Particle Deposition in Human Lung Airways: Effects of Airflow, Particle Size, and Mechanisms', *Aerosol and Air Quality Research*, vol. 20, no. 12, pp.2846-2858.

Patterson, RF, Zhang, Q, Zheng, M & Zhu, Y 2014, 'Particle deposition in respiratory tracts of school-aged children', *Aerosol Air Qual. Res*, vol. 14, pp. 64-73.

Paul, M & Lau, R 2020, 'Potentials and challenges of Levodopa particle formulation for treatment of Parkinson's disease through intranasal and pulmonary delivery', *Advanced Powder Technology*, vol. 31, no. 6, pp. 2357-2365.

Pourmehran, O, Gorji, TB & Gorji-Bandpy, M 2016, 'Magnetic drug targeting through a realistic model of human tracheobronchial airways using computational fluid and particle dynamics', *Biomechanics and Modeling in Mechanobiology*, vol. 15, no. 5, pp. 1355-1374.

Pulivendala, G, Bale, S & Godugu, C 2020, 'Inhalation of sustained release microparticles for the targeted treatment of respiratory diseases', *Drug delivery and translational research*, vol. 10, no. 2, pp. 339-353.

Rahimi-Gorji, M, Gorji, TB & Gorji-Bandpy, M 2016, 'Details of regional particle deposition and airflow structures in a realistic model of human tracheobronchial airways: two-phase flow simulation', *Computers in biology and medicine*, vol. 74, pp. 1-17.

Rahman, MM, Zhao, M, Islam, MS, Dong, K & Saha, SC 2020, 'Airflow dynamic and particle deposition in age-specific human lungs', In *Proceedings of the 22nd Australasian Fluid Mechanics Conference (AFMC2020)*, Brisbane, Australia, December 7-10.

Roemer, W, Hoek, G, Brunekreef, B, Clench-Aas, J, Forsberg, B, Pekkanen, J et al. 2000, 'PM10 elemental composition and acute respiratory health effects in European children (PEACE project). Pollution Effects on Asthmatic Children in Europe', *European Respiratory Journal*, vol. 15, no. 3, pp. 553-559.

Shih, TH, Liou, WW, Shabbir, A, Yang, Z & Zhu, J 1995, 'A new k-ϵ eddy viscosity model for high reynolds number turbulent flows', *Computers and Fluids*, vol. 24, no. 3, pp. 227-238.

Srivastav, VK, Paul, AR & Jain, A 2019, 'Capturing the wall turbulence in CFD simulation of human respiratory tract', *Mathematics and Computers in Simulation*, vol. 160, pp. 23-38.

Tian, Z, Tu, J & Yeoh, G 2007, 'CFD studies of indoor airflow and contaminant particle transportation', *Particulate Science and Technology*, vol. 25, no. 6, pp. 555-570.

Tsuji, Y 2007, 'Multi-scale modeling of dense phase gas–particle flow', *Chemical engineering science*, vol. 62, no. 13, pp. 3410-3418.

Turner, JM, Mead, J & Wohl, ME 1968, 'Elasticity of human lungs in relation to age', *Journal of Applied Physiology*, vol. 25, no. 6, pp. 664-671.

Wahba, W 1983, 'Influence of aging on lung function-clinical significance of changes from age twenty', *Anesthesia & Analgesia*, vol. 62, no. 8, pp. 764-776.

Weibel, ER 1963, 'Geometric and dimensional airway models of conductive, transitory and respiratory zones of the human lung', in *Morphometry of the human lung*, Springer, pp. 136-142.

Xi, J, Berlinski, A, Zhou, Y, Greenberg, B & Ou, X 2012, 'Breathing resistance and ultrafine particle deposition in nasal–laryngeal airways of a newborn, an infant, a child, and an adult', *Annals of Biomedical Engineering*, vol. 40, no. 12, pp. 2579-2595.

Xu, G & Yu, C 1986, 'Effects of age on deposition of inhaled aerosols in the human lung', *Aerosol science and technology*, vol. 5, no. 3, pp. 349-357.

Zhang, W, Xiang, Y, Lu, C, Ou, C & Deng, Q 2020, 'Numerical modeling of particle deposition in the conducting airways of asthmatic children', *Medical engineering & physics*, vol. 76, pp. 40-46.

Zhang, Z, Kleinstreuer, C, Donohue, JF & Kim, C 2005, 'Comparison of micro-and nano-size particle depositions in a human upper airway model', *Journal of Aerosol Science*, vol. 36, no. 2, pp. 211-233.

Zhang, Z, Kleinstreuer, C & Kim, CS 2009, 'Comparison of analytical and CFD models with regard to micron particle deposition in a human 16-generation tracheobronchial airway model', *Journal of Aerosol Science,* vol. 40, no. 1, pp. 16-28.

Chapter 5: Nanoparticle Transport and Deposition in a Heterogeneous Human Lung Airway Tree: An Efficient One Path Model for CFD Simulations

This chapter presents a final accepted version paper published in 2022, European Journal of Pharmaceutical Sciences, 177, 106279. The first page of the published paper was shown at the beginning of the chapter, followed by the accepted version.

Chapter 5 Nanoparticle Transport and Deposition in a Heterogeneous Human Lung Airway Tree: An Efficient One Path Model for CFD Simulations

European Journal of Pharmaceutical Sciences 177 (2022) 106279

Contents lists available at ScienceDirect

European Journal of Pharmaceutical Sciences

journal homepage: www.elsevier.com/locate/ejps

Nanoparticle transport and deposition in a heterogeneous human lung airway tree: An efficient one path model for CFD simulations

Md.M. Rahman [a,b], Ming Zhao [a,*], Mohammad S. Islam [c], Kejun Dong [a], Suvash C. Saha [c]

[a] School of Engineering, Design and Built Environment, Western Sydney University, Penrith, NSW 2751, Australia
[b] Department of Mathematics, Faculty of Science, Islamic University, Kushtia 7003, Bangladesh
[c] School of Mechanical and Mechatronic Engineering, University of Technology Sydney, Ultimo, NSW 2007, Australia

ARTICLE INFO

Keywords:
Airflow dynamics (AD)
Heterogeneous vasculature tree
Particle transport and deposition (TD)
Cutting/truncated path model
Drug delivery
Boundary condition

ABSTRACT

Understanding nano-particle inhalation in human lung airways helps targeted drug delivery for treating lung diseases. A wide range of numerical models have been developed to analyse nano-particle transport and deposition (TD) in different parts of airways. However, a precise understanding of nano-particle TD in large-scale airways is still unavailable in the literature. This study developed an efficient one-path numerical model for simulating nano-particle TD in large-scale lung airway models. This first-ever one-path numerical approach simulates airflow and nano-particle TD in generations 0–11 of the human lung, accounting for 93% of the whole airway length. The one-path model enables the simulation of particle TD in many generations of airways with an affordable time. The particle TD of 5 nm, 10 nm and 20 nm particles is simulated at inhalation flow rates for two different physical activities: resting and moderate activity. It is found that particle deposition efficiency of 5 nm particles is 28.94% higher than 20 nm particles because of the higher dispersion capacity. It is further proved that the diffusion mechanism dominates the particle TD in generations 0–11. The deposition efficiency decreases with the increase of generation number irrespective of the flow rate and particle size. The effects of the particle size and flow rate on the escaping rate of each generation are opposite to the corresponding effects on the deposition rate. The quantified deposition and escaping rates at generations 0–11 provide valuable guidelines for drug delivery in human lungs.

1. Introduction

Nanoparticles have been successfully used as multipurpose carrier frameworks for the therapeutic delivery of drugs for treating respiratory illnesses such as lung cancer, cystic fibrosis, and asthma (Sung et al., 2007; Willis et al., 2012). Targeted distribution of drugs reduces the overall dose and the number of adverse effects associated with high levels of systemic drug treatment (Azarmi et al., 2008). As a result, the study of particle transportation and deposition (TD) in human pulmonary airways is essential to the effectiveness of drugs delivered by the aerosol inhalation (Koullapis et al., 2018; Mangal et al., 2017; Nahar et al., 2013; Valiulin et al., 2021).

For the treatment of respiratory illnesses, many nanomedicines and drug delivery systems have been developed. Intravenous injection and inhalational delivery are the most popular methods to deliver therapeutic or diagnostic materials to the lungs (Babu et al., 2013; Lee et al., 2015; Scherließ et al., 2022). Significant research has been done on nanoparticle transport during inhalational delivery (Azarmi et al., 2008; Ruge et al., 2013). However, little investigation has been done on nanoparticle transport in the pulmonary circulation (Sohrabi et al., 2017). Thus, developing an efficient technique for evaluating nanoparticle delivery in human lungs is essential. To achieve this, a detailed investigation of nanoparticle TD in a human lung model, taking into consideration as many as the lung airways as possible, is necessary.

The factors influencing drug carrier distribution in a heterogeneous vasculature tree include particle size, particle density, inhalation flow conditions, and lung geometry (Kim and Iglesias, 1989). Nanoparticles are solid colloidal particles made up of macromolecular material with diameters ranging from 1 to 1000 nm (Kaur et al., 2008). Dissolving, entrapping, or encapsulating the active material can be accomplished with nanoparticles as drug carriers (Singh and Lillard, 2009). Nanoparticles have been explored as drug carriers for a variety of illnesses, including cancer and tuberculosis (TB) (Sung et al., 2007; Yhee et al., 2016). They are also employed in cancer treatment to target tumour

* Corresponding author.
E-mail address: m.zhao@westernsydney.edu.au (M. Zhao).

https://doi.org/10.1016/j.ejps.2022.106279
Received 18 April 2022; Received in revised form 18 July 2022; Accepted 15 August 2022
Available online 17 August 2022

Nanoparticle transport and deposition in a heterogeneous human lung airway tree: An efficient one path model for CFD simulations

Md. M. Rahman [1, 2], Ming Zhao [1, *], Mohammad S. Islam [3], Kejun Dong [4], and Suvash C. Saha [3]

[1] School of *Engineering*, Design and Built Environment, Western Sydney University, Penrith, NSW 2751, Australia.

[2] Department of Mathematics, Faculty of Science, Islamic University, Kushtia-7003, Bangladesh.

[3] School of Mechanical and Mechatronic Engineering, University of Technology Sydney, Ultimo, NSW 2007, Australia.

[4] Center for Infrastructure Engineering, Western Sydney University, Penrith, NSW 2751, Australia.

***Correspondence:** m.zhao@westernsydney.edu.au

5.1 Abstract

Understanding nano-particle inhalation in human lung airways helps targeted drug delivery for treating lung diseases. A wide range of numerical models have been developed to analyse nano-particle transport and deposition (TD) in different parts of airways. However, a precise understanding of nano-particle TD in large-scale airways is still unavailable in the literature. This study developed an efficient one-path numerical model for simulating nano-particle TD in large-scale lung airway models. This first-ever one-path numerical approach simulates airflow and nano-particle TD in generations 0-11 of the human lung, accounting for 93% of the whole airway length. The one-path model enables the simulation of particle TD in many generations of airways with an affordable time. The particle TD of 5-nm, 10-nm and 20-nm particles is simulated at inhalation flow rates for two different physical activities: resting and moderate activity. It is found that particle deposition efficiency of 5-nm particles is 28.94% higher than 20-nm particles because of the higher dispersion capacity. It is further proved that the diffusion mechanism dominates the particle TD in generations 0-11. The deposition efficiency decreases with the increase of generation number irrespective of the flow rate and particle size. The effects

of the particle size and flow rate on the escaping rate of each generation are opposite to the corresponding effects on the deposition rate. The quantified deposition and escaping rates at generations 0-11 provide valuable guidelines for drug delivery in human lungs.

Keywords: Airflow Dynamics (AD), Heterogeneous vasculature tree, Particle transport and deposition (TD), Cutting/Truncated path model, Drug delivery, boundary condition.

5.2 Introduction

Nanoparticles have been successfully used as multipurpose carrier frameworks for the therapeutic delivery of drugs for treating respiratory illnesses such as lung cancer, cystic fibrosis, and asthma (Sung et al. 2007, Willis et al. 2012). Targeted distribution of drugs reduces the overall dose and the number of adverse effects associated with high levels of systemic drug treatment (Azarmi et al. 2008). As a result, the study of particle transportation and deposition (TD) in human pulmonary airways is essential to the effectiveness of drugs delivered by the aerosol inhalation (Nahar et al. 2013, Mangal et al. 2017, Koullapis et al. 2018, Valiulin et al. 2021).

For the treatment of respiratory illnesses, many nanomedicines and drug delivery systems have been developed. Intravenous injection and inhalational delivery are the most popular methods to deliver therapeutic or diagnostic materials to the lungs (Babu et al. 2013, Lee et al. 2015, Scherließ et al. 2022). Significant research has been done on nanoparticle transport during inhalational delivery (Azarmi et al. 2008, Ruge et al. 2013). However, little investigation has been done on nanoparticle transport in the pulmonary circulation (Sohrabi et al. 2017). Thus, developing an efficient technique for evaluating nanoparticle delivery in human lungs is essential. To achieve this, a detailed investigation of nanoparticle TD in a human lung model, taking into consideration as many as the lung airways as possible, is necessary.

Chapter 5 Nanoparticle Transport and Deposition in a Heterogeneous Human Lung Airway Tree: An Efficient One Path Model for CFD Simulations

The factors influencing drug carrier distribution in a heterogeneous vasculature tree include particle size, particle density, inhalation flow conditions, and lung geometry (Kim and Iglesias 1989). Nanoparticles are solid colloidal particles made up of macromolecular material with diameters ranging from 1 to 1000-nm (Kaur et al. 2008). Dissolving, entrapping, or encapsulating the active material can be accomplished with nanoparticles as drug carriers (Singh and Lillard Jr 2009). Nanoparticles have been explored as drug carriers for a variety of illnesses, including cancer and tuberculosis (TB) (Sung et al. 2007, Yhee et al. 2016). They are also employed in cancer treatment to target tumour cells, which play a significant role in inflammation and house germs that cause bacterial infections (Alexiou et al. 2006, Barani et al. 2021).

Nanoparticle TD in the extrathoracic area (nasal, oral and pharynx airways) and tracheobronchial lung airways have been investigated through Computational Fluid Dynamics (CFD) (Xi et al. 2012, Zhao et al. 2020). Yu et al. (1996) used a computer model to simulate the deposition of nanoparticles in a single bifurcation airway. They concluded that the inlet condition significantly impacts concentration and flow pattern. Comer et al. (1999) simulated airflow and particle TD in generations 3 to 5 (G3-G5) of a double bifurcation lung geometry based on Weibel's model (Weibel, 1963). Zhang and Kleinstreuer (2004) investigated airflow and nanoparticle ($1 \leq nm \leq 150$) deposition in G0 to G3 of a human upper airway model numerically and concluded that turbulence has negligible effects on nanoparticle deposition in the lung model. Islam et al. (2021) studied polydisperse aerosol particle deposition in the upper airways up to G5 through CFD. The results showed that the diameter of the lung airway reduction significantly affects the particle deposition in the upper lung airway. CFD has been proved a reliable and accurate methodology for estimating the efficiency of local particle deposition in the human lung airways (Ghalati et al. 2012, Rahimi-Gorji et al. 2016, Vachhani and Kleinstreuer 2021). Using simplified lung models in CFD studies can find fundamental

mechanisms of particle TD through reasonable computational time. However, all the studies mentioned above only investigate a limited number of generations. Rahman et al. (2021) developed an efficient numerical method to study the deposition of microscale aerosol particles in the symmetric lung model over 14 generations. In the model by Rahman et al. (2021), the G0 to G14 lung model was cut into a number of sections. The particle mass and flow rates satisfy continuity conditions at the interfaces between sections but not the fluid momentum. The results indicated that the microscale aerosol particle deposition also increased when particle size or flow rate increased.

Some researchers have studied particle TD in realistic lung models, which is more complicated than the symmetric lung model (Huang et al. 2021). Russo et al. (2018) conducted CFD simulations of magnetic nanoparticle drug delivery in a patient-specific realistic lung model of G0 to G3. They found that despite the produced magnetic field intensity, only a tiny percentage of the particles reached the respiratory airways. Through CFD simulations, Rahman, Zhao et al. (2021) found that 10% of 5-nm particles are deposited in the mouth to G3 airways, allowing over 90% to reach the deeper lung. Dong et al. (2021) recently investigated nanoparticle TD in realistic human airways generation up to G3. They found Brownian diffusion is a dominating particle deposition mechanism for particles below 10-nm. However, the deposition efficiency dropped substantially when the particle size was increased to 100-nm.

Sosnowski (2018) found that particle flow and deposition in the respiratory tract are influenced by particle coagulation, hygroscopic growth, and dry powder inhalation. Kadota et al. (2022) found that the particle deposition is influenced by airway geometry. They also found that small particles are deposited in the lower bronchial tree and large particles are deposited in the upper airways generations (G2-G6). Ahookhosh et al. (2021) studied the micron-sized particle transport and deposition in human lung airways based on various inhalation flow rates using pressurized metered-dose inhalers drug delivery devices. It was found that the particle

deposition rate in the right lung is greater than in the left lung. Ahookhosh et al. (2020) studied the airflow and micron-size particle deposition in realistic human tracheobronchial airways with varying inhalation flow rates. The results showed that more particles are deposited in the extra-thoracic region, and inertial impaction is the dominant deposition mechanism.

Longest and Holbrook (2012) conducted a review on aerosol transport in the respiratory tract. The review indicated that more accurate models need to be developed through contemporaneous experimental and CFD methods. Longest and Xi (2007) investigated nanoparticle deposition in the upper airways using three models: a straight tubular flow field, a 90° tubular bend, and an idealised human oral airway reproduction. The results show that the oral airway model, which combines a Lagrangian model with a user-defined Brownian motion model and a near-wall interpolation approach, is suitable for nanoparticle deposition in the respiratory tract with diameters ranging from 1 to 120 nanometers. Tian et al. (2011) developed an individual stochastic path (SIP) model that considers transient and steady-state conditions to predict aerosol dry powder inhalation from the mouth-throat to the tracheobronchial (TB) airways. The findings show that steady-state simulations produced an excellent view of the overall, regional, and local deposition. At the same time, the transient conditions had little effect on deposition in the TB region, starting with the fourth bifurcation. Tian et al. (2011) investigated an enhanced condensational growth strategy for aerosol particle delivery in a single path bifurcation model from the mouth to the tracheobronchial zone. The findings show that large aerosol droplets (aerodynamic diameters of 2.4–3.3 m) enhance the tracheobronchial B5 region under ECG delivery settings.

All numerical simulations for realistic geometry only consider limited generations to keep computing costs low (Sohrabi al. 2014). The complexity of realistic lungs make CFD simulation of whole airways completely impossible (Zhang et al. 2008, Sohrabi et al. 2017, Ahookhosh et al. 2020). Therefore, symmetric lung based on theoretic models have been

constructed to represent the lung trees to predict the particle deposition (Kolanjiyil and Kleinstreuer 2019).

Considering simulating airflow through the G0-G11 airway using CFD, the total number of bifurcations of only G11 is 2^{11}=2048. Detailed CFD simulation for such a significant number of airway bifurcations is impossible. This study aims to develop an efficient numerical model to simulate particle deposition in many generations of human lung airways. Instead of predicting all the bifurcations, only two representative bifurcations of each generation is simulated in the numerical model to predict the airflow and particle TD. The deposition efficiency of these two representative bifurcations of each generation is then converted to the deposition efficiency of all the bifurcations of this generation. The continuity of the airflow mass, airflow momentum and the particle numbers are ensured in the numerical model. The details of the numerical method will be presented in section 3. Using the newly developed numerical method, we investigated the effect of particle size and inhalation airflow rates on the distribution of deposited particles in G0 to G11 airways. The parameters used in the numerical simulations are summarized in Table 5.1.

Table 5.1. Numerical parameters and simulation conditions.

Parameters	Value
Fluid density (kg/m^3)	1.225
Viscosity of fluid (kg/m.s)	1.7894×10^{-5}
Inhalation flow rates (L/min)	15 and 30
Aerosol particle density (kg/m^3)	1100
Particle diameter (nm)	5, 10 and 20
Total number of injected particles	97200

5.3 Numerical Methods

5.3.1 Geometry of the Lung Model

The simplified (all called theoretical) geometry developed by Xu and Yu (1986) is used to create the three-dimensional (3D) lung model with symmetric and planner lung airways from generation G0 to G13. The bifurcation angle of lung airways is 70 . The rotation angle is considered because the lung airways are assumed to be symmetric and planar (Deng, Ou et al. 2018). The extra-thoracic airways are not considered because they are not available in the theoretical lung models (Poorbahrami and Oakes 2019). Considering the extra-thoracic airways will reduce the number of particles entering lung airways (Xi et al. 2012). Table 5.2 lists geometric parameters of the theoretical lung airways from G0 to G13. We implemented an efficient truncating method to construct an efficient theoretical lung model to explore the fundamental mechanisms of particle TD in a lung model with many generations. A whole human lung has G0 to G23 generations of airways. We simulated G0 to G13 using CFD and analysed the nanoparticle particle TD in G0 to G11 airways. The airway length from G0 to G11 is 93% of the whole lung from G0 to G23. In an airway tree, the number of airway branches of a generation increases with the increase of generation number exponentially. Because of this, G0 to G11 takes 93% of the airway route length but only about 20% of the whole airway volume.

Table 5. 2. Geometric parameters of lung airways were calculated using Xu and Yu (1986)

Generation (G)	Generation number, n (Z)	Diameter (cm)	Length (cm)
0	1	1.665	12.286
1	2	1.220	4.284
2	4	0.830	1.896
3	8	0.560	0.759
4	16	0.450	1.268
5	32	0.350	1.071
6	64	0.280	0.901
7	128	0.230	0.759
8	256	0.186	0.639
9	512	0.154	0.538
10	1024	0.130	0.460
11	2048	0.109	0.390
12	4096	0.095	0.330
13	8192	0.082	0.271

Figure 5.1. depicts the 3D heterogeneous pulmonary vascular symmetric lung tree of adults up to generation G11 used in this study. In the complete lung tree, n-th generation has 2^n bifurcations of the lung airways. Simulating the airflow of all generations from G0 to G11 using CFD without any simplification would be prohibitively unaffordable in terms of computing time. Therefore, we only choose two representative bifurcations for each generation to make it affordable to simulate G0 to G11 using CFD, as shown in Figure 5.1. The simplification results in a single path lung up to G11 but does not lose geometric features of the human lung.

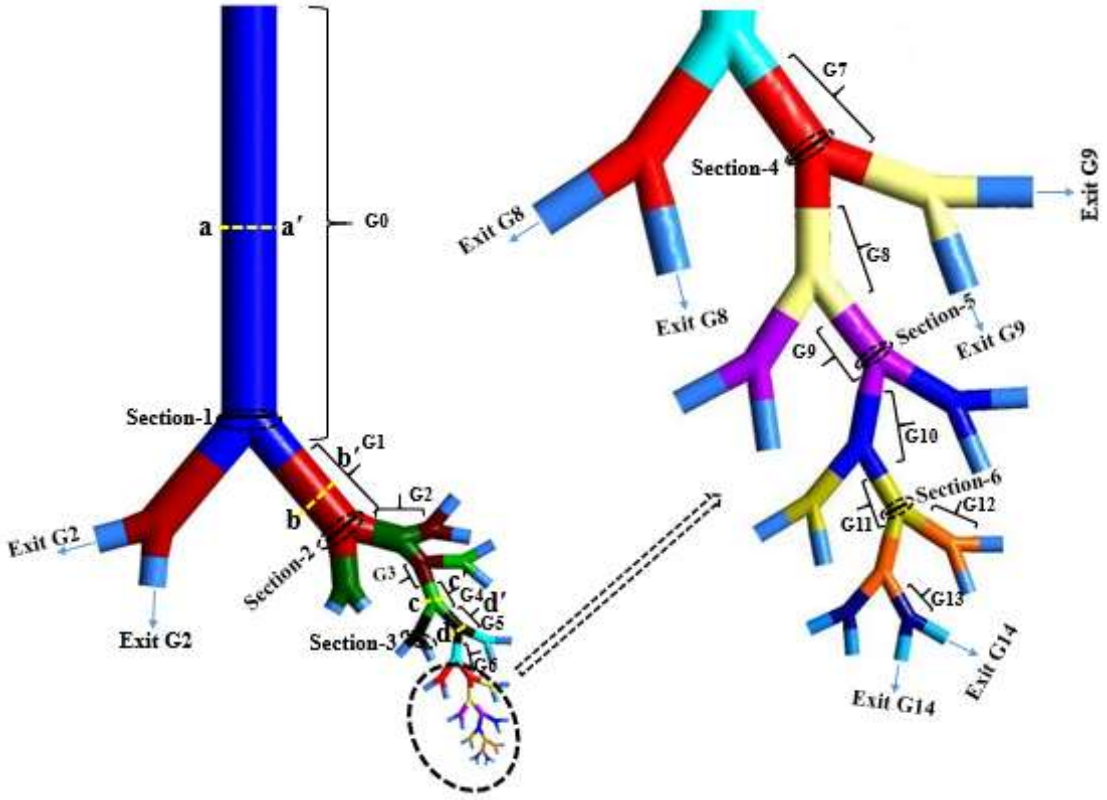

Figure 5.1. A model of the adult lung's tracheobronchial airways (G0-G13). When the results are given, the sections indicated in the Figure will be referred to.

5.3.2 Airflow Model

The airflow and particle TD in the lung airways are solved using the ANSYS FLUENT software. The Reynolds-averaged Navier-Stokes (RANS) equations are the governing equations for calculating the flow:

$$\frac{\partial \rho}{\partial t} + \frac{\partial}{\partial x_i}(\rho u_i) = 0 \tag{5.1}$$

$$\frac{\partial}{\partial t}(\rho u_i) + \frac{\partial}{\partial x_j}(\rho u_i u_j) = -\frac{\partial p}{\partial x_i} + \frac{\partial}{\partial x_j}\left[\mu\left(\frac{\partial u_i}{\partial x_j} + \frac{\partial u_j}{\partial x_i}\right)\right] + \frac{\partial}{\partial x_j}(-\rho\overline{u_i' u_j'}) \tag{5.2}$$

where t is time, x_i (i=1,2 and 3) are the Cartesian coordinates, ρ is the air density, u_i is the fluid velocity in the x_i-direction, p is the fluid pressure, μ is the molecular viscosity. On the right-hand side of equation (2), $\rho\overline{u_i' u_j'}$ represents the Reynolds stresses of turbulence.

The realisable k-ε turbulence model is used to simulate the turbulence and calculate the Reynolds stresses. Realisable k-ε turbulence performs better than the standard k-ε turbulence model, including boundary-free shear flows, channel and flat boundary layer flow with and without pressure gradients, rotating homogeneous shear flows, and backwards-facing step flow (Shih et al. 1995). In addition, the realisable k-ε model can correctly calculate the flow of complex lung geometries without the need for a near-wall correction (Tash et al. 2019, Fletcher, Chaugule et al. 2021, Massarotti et al. 2021, Rahman et al. 2021).

5.3.3 Boundary Conditions

The RANS equations are solved using the second-order upwind and pressure-velocity coupling schemes. In some investigations (Bahmanzadeh et al. 2016, Gu et al. 2019), the effects of an unsteady inhalation profile on particle TD were investigated. In the present one path model, only two bifurcations of each generation are retained. Out of these two bifurcations, one is followed by lower generations and one is truncated at the next generation. As a result, there are two exits each truncated bifurcation. In Figure 5.1, exit Gn is the cutting position where n-th generation and following generations are cut off. To ensure the conservation of airflow mass, the airflow rate is assumed to be evenly distributed among all the 2^n bifurcations of the n-th generation. As a result, the airflow rate of exit Gn is given as $Q_e^n = Q_{in}/2^n$, where Q_{in} is the inlet flow rate at G0. In the numerical simulations, the velocity on each exit is given as:

$$u_n = Q_e^n / A_n \tag{5.3}$$

where A_n is the cross-sectional area of exit Gn. A reference pressure is specified on the inlet of G0. The airway wall was assumed to be stationary, and the airway wall surfaces were regarded as no-slip surfaces (Rahimi-Gorji et al. 2016, Farghadan et al. 2020).

A trap condition is implemented on the Discrete Phase Model (DPM) airway walls for particle deposition (Inthavong et al. 2011, Rahman et al. 2022). In the trap condition, particles colliding with the inner surface of the lung airways are trapped. This trap condition is

appropriate as the airway walls contain very sticky mucus (Islam et al. 2021). The escape condition is used in the outlet section for DPM so that the particles can pass through the truncated boundary without being reflected.

5.3.4 Particle Transport Model

The current particle TD model is a one-way coupling model that takes into account particle movement driven by airflow but ignores particle impacts on the airflow (Lintermann and Schröder 2017, Chen et al. 2021). Agglomeration between the particle and water may occur due to external forces such as van der Waals, electrostatic, and capillary forces. The interaction of particles with water is also influenced by air humidity. In this study, agglomeration and air humidity are not considered. However, collision-free conditions can be utilised to simulate particle transport if the density of the particles is low (Tsuji 2007). Direct particle collision is ignored in this paper because the particles entering the tracheobronchial airway is sufficiently diluted (Feng and Kleinstreuer 2014, Kadota et al. 2022). Therefore, the dynamics of the particles, such as collision, growth, and aggregation during the particle transportation and deposition into the human lung, were not considered (Deng et al. 2019). The Lagrangian approach is used to describe particle TD in the lung airways. The equation of motion of each particle is expressed as (Inthavong et al. 2011, Rahman et al. 2021):

$$\frac{d\boldsymbol{u}_i^{\boldsymbol{p}}}{dt} = \boldsymbol{F}_{Di} + \boldsymbol{F}_{gi} + \boldsymbol{F}_{Bi} + \boldsymbol{F}_{Li} \tag{5.4}$$

where u_i^p is particle velocity in the x_i-direction, $\boldsymbol{F}_{\mathrm{Di}}$, $\mathbf{F}_{\mathrm{gi}}$, $\boldsymbol{F}_{\mathrm{Bi}}$ and $\boldsymbol{F}_{\mathrm{Li}}$ are the drag force, gravitational force, Brownian force, and Saffman's lift force per unit mass. The following formula determines the gravitational force:

$$\boldsymbol{F}_{gi} = \left(\frac{\rho_p - \rho}{\rho}\right)\boldsymbol{g} \tag{5.5}$$

where $\boldsymbol{g}$ denotes gravitational acceleration and $\rho_p$denotes particle density. The drag force is calculated using the following formula:

$$\boldsymbol{F}_{Di} = \frac{18\mu}{\rho_p d_p^2} C_D \frac{Re_p}{24} (\boldsymbol{u}_i - \boldsymbol{u}_i^p) \tag{5.6}$$

where $Re_p = \rho d_p |\boldsymbol{u}_i^p - \boldsymbol{u}_i| / \mu$ and the drag coefficient C_D for the spherical particles is calculated by

$C_D = a_1 + \frac{a_2}{Re_p} + \frac{a_3}{Re_p^2}$ for $0 < Re_p < 10$ (Morsi and Alexander 1972), where a_1, a_2, a_3 are functions of the Reynolds number Re_P given by:

$$\mathrm{a}_1, \mathrm{a}_2, \mathrm{a}_3 = \begin{cases} 0, \quad 24, \quad 0 & 0 < R_e < 0.1 \\ 3.690, \quad 22.73, \quad 0.0903 & 0.1 < R_e < 1 \\ 1.222, \quad 29.17, \quad 3.89 & 1 < R_e < 10 \\ 0.617, 46.50, -116.67 & 10 < R_e < 100 \\ 0.364, 98.33, -2778 & 100 < R_e < 1000 \\ 0.357, 148.62, -47500 & 1000 < R_e < 5000 \\ 0.46, -490.546, 578700 & 5000 < R_e < 10000 \\ 0.519, -1662.5, \quad 5416700 & R_e > 10000 \end{cases}$$

When particles interact with a fluid, Brownian motion describes particles' random, uncontrolled movement (Grassia et al. 1995). It is prominent when small size particles are in a fluid with small viscosity and high temperature (Jang and Choi, 2004). If the particle size is more than 1 μm, Brownian motion in the air is undetectable (Hou et al. 1990). The Brownian force is calculated by:

$$\boldsymbol{F}_{Bi} = \boldsymbol{G}_i \sqrt{\frac{\pi S_0}{\Delta t}} \tag{5.7}$$

where G_i is a Gaussian random number with unit variance and zero mean, Δt is the particle time step, and S_0 is the spectral intensity function associated with the diffusion coefficient by:

$$S_0 = \frac{216 \nu k_B T}{\pi^2 \rho_p d_p^2 \left(\frac{\rho_p}{\rho}\right)^2 C_c} \tag{5.8}$$

where, ν is the kinematic viscosity, $K_B = 1.380649 \times 10^{-23}$ J/K is the Boltzmann constant,$T = 300K$ is the absolute fluid temperature, and C_c is the Stokes-Cunningham slip correction coefficient as defined by:

$$C_c = 1 + \frac{2\lambda}{d_p}\left(1.257 + 0.4e^{-\left(\frac{1.1d_p}{2\lambda}\right)}\right) \tag{5.9}$$

where, the gas molecule mean free path (λ) is 65 nm (Xi, Berlinski et al. 2012). The lift force of Saffman is calculated using the following formula:

$$\boldsymbol{F}_{Li} = \frac{2K\nu^{\frac{1}{2}}\rho d_{ij}}{\rho_p d_p (d_{lk}d_{kl})^{\frac{1}{4}}}(\boldsymbol{u}_j - \boldsymbol{u}_j^p) \tag{5.10}$$

where, $K = 2.594$ is the constant coefficient of Saffman's lift force and $d_{ij} = (\partial u_i/\partial x_j - \partial u_j/\partial x_i)/2$ is the deformation tensor of the flow velocity.

5.3.5 Deposition Efficiency Calculation

The deposition efficiency of *n*-th generation is defined as the proportion of particles absorbed (trapped) in this generation of airways out of the particles released at the inlet boundary and is denoted by η_n where the subscript n stands for *n*-th generation.

$$\eta_n = \frac{2^n N_n}{N} \tag{5.11}$$

where N_n is the number of particles deposited at each bifurcation of n-th generation and N is the total number of particles released on the inlet of G0. In Figure 5.1, each generation has two bifurcations, and N_n is the averaged numbers of deposited particles deposited at these two bifurcations. The particle escaping rate at the n-th generation is defined as the percentage of particles that enter deeper lung at all the bifurcations of this generation, and it is calculated as:

$$e_n = 1 - \sum_{i=1}^{n} \eta_i \tag{5.12}$$

5.4 Grid Dependency Study and Model Validation

5.4.1 Grid Dependency Study

The computational mesh of the symmetric lung airways is shown in Figure 5.2. Ten-layer smooth inflation was implemented near the walls to ensure that the boundary layer flow

was correctly represented (Figure 5.2a). In addition, the denser mesh is used at carinal angles for the proper resolution of complicated flows.

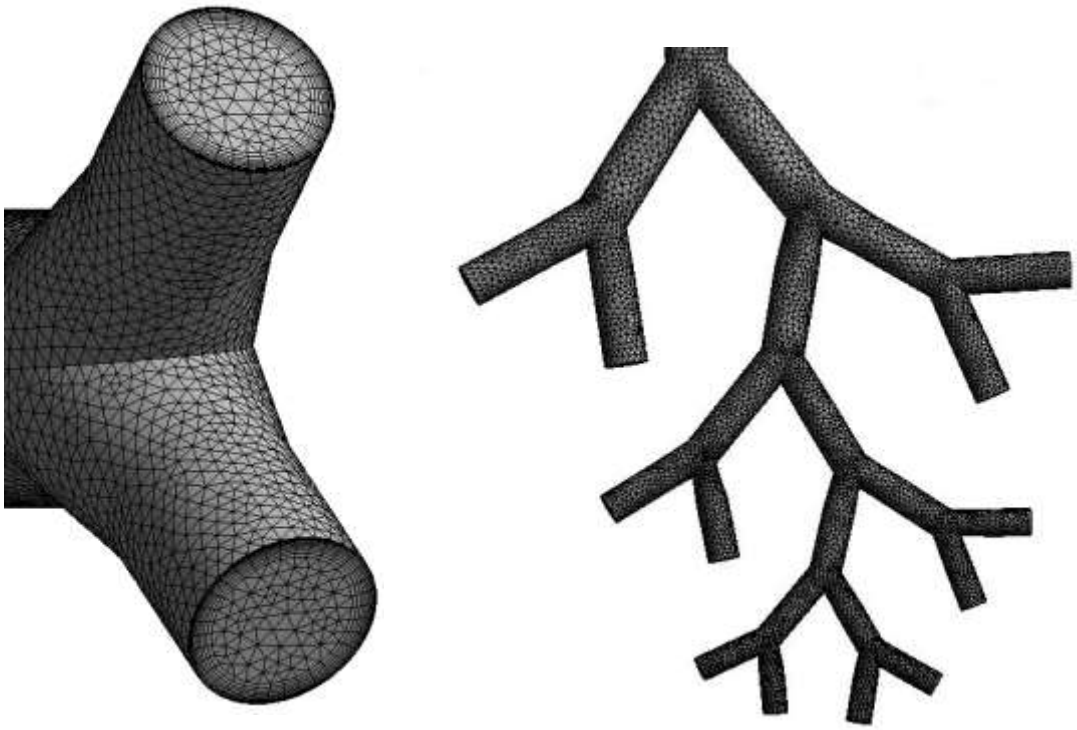

(a) (b)

Figure 5.2. Computational mesh; (a) Refined mesh near the airway wall; (b) Mesh resolution on the inner wall of G7 to G11 airways

The grid independence test is conducted by performing numerical simulations with six meshes, Mesh-1 to Mesh-6, whose element numbers range from 338349 to 1908633. While the mesh size is inversely proportional to the element number, the densest mesh has the smallest grid size of 0.11 mm. In that situation, asymmetric flow distributions appear when the flow passes in the truncated branch. To ensure the continuity of the airflow rate, we use the mass flow rate at each truncated outlet to guarantee that the velocity is distributed uniformly. The air is sucked in the lung through the inlet by the low pressure of the lung. As a result, the velocity follows a naturally developed velocity profile as shown in Figure 5.3 (b). It can be found that the velocity

profile at the inlet face is nearly parabolic, with an increase in the element number shown in Figure 5.3 (b). Line 1 and 2 in Figure 5.3 (a) are near the end of the flow path and chosen because the flow at these two lines is sensitive to any numerical errors along the air flow route. Therefore, velocities on section-7 and lines 1 and 2 indicated in Figure 5.3 (a) are evaluated. Figure 5.3 (e) show the average velocity at section 7, and Figure 5.3 (c) and (d) shows the velocity distribution along two lines 1 and 2, where *X* denotes the direction along the line. As shown, increasing the node number has a negligible effect on the velocity if the mesh density exceeds Mesh-4. The maximum velocity difference between Mesh-5 and Mesh-6 is 0.011 %. As a result, the velocity at Mesh-5 is used for all the simulations.

The non-dimensional wall unit (y^+) is defined inside the boundary layer as

$$y^+ = \frac{\rho U_\tau y}{\mu} \tag{5.13}$$

where $U_\tau \left(= \sqrt{\frac{\tau_w}{\rho}} \right)$ is the friction velocity, *y* is the distance the first layer of mesh to the wall, and τ_w is the shear stress on the wall, the value of *y* and y^+ for Mesh-5 are 0.117 mm and 1.48, respectively.

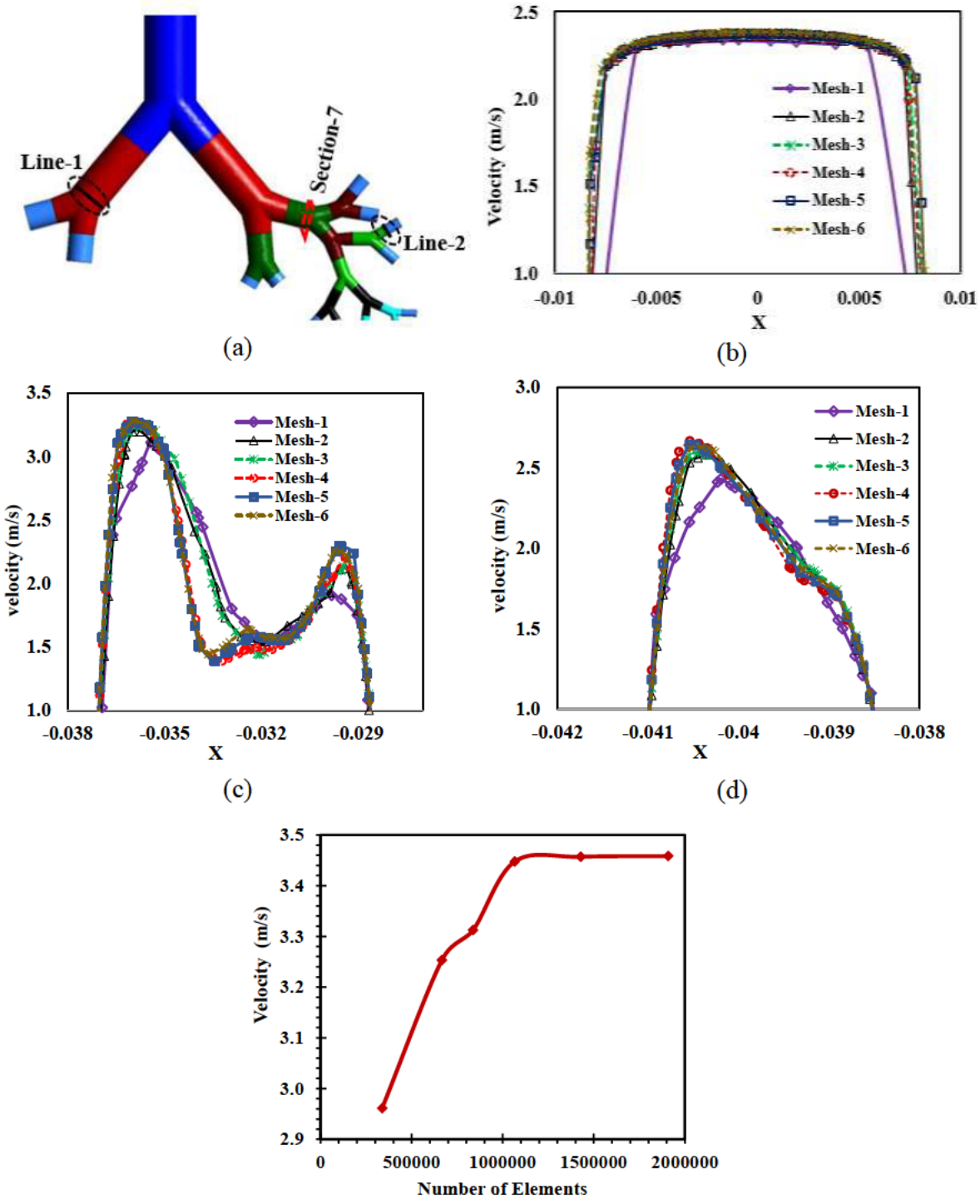

Figure 5.3. Grid independent test at flow rate 30 L/min in generations G0-G4. (a) Definition of sections and lines; (b) Velocity distribution at inlet face; (c) Velocity distribution at Line-1; (d) Velocity distribution at Line-2 (average velocity calculated at the selected line in Figure 5. 3a); (e) Average velocity as a function of grid number.

Figure 5.4 (a) depicts the effect of mesh element number on deposition efficiency. The deposition efficiency remains nearly unchanged after increasing the mesh density above Mesh-4 (1.07 million elements). All numerical simulations in this investigation employed Mesh-5, which has 1.43 million elements. To show that sufficiently large number of particles have been released, simulations are repeatedly conducted by releasing different numbers of particles on the inlet. Figure 5.4 (b) demonstrates how the G0-G11 lung model's deposition efficiency varies with the number of particles released at the inlet. If the number of particles released exceeds 64 000, the deposition efficiency is unaffected by the particle number. Figure 5.4 (b) proves that the particle number of 97,200 used in this paper is large enough to produce converged results.

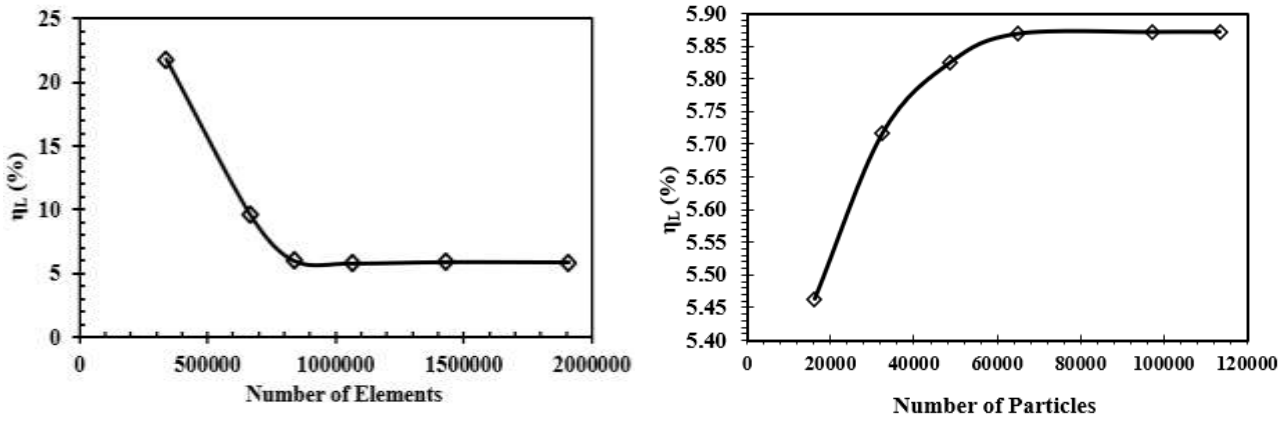

(a) (b)

Figure 5. 4. shows (a) Deposition efficiency as a function of grid number, (b) Deposition efficiency as a function of released particles number, at generations G0 to G11 at the flow rate of 30 L/min and aerosol particle diameter of 20-nm.

5.4.2 Model Validation

In our previous study (Rahman et al. 2021), we have already conducted the validation of particle TD of nanoparticles in human lung airways with the limited number of generations G3-

G5. To further validate the proposed one path model in the simulation of TD of nanoparticles, we simulated the flow and particle TD in G6 to G7 using the completed G6-G7 model in Figure 5.5 (a) and one path G6-G7 model in Figure 5.5 (b). Two bifurcations of G8 have been cut off in Figure 5.5 (b). The details of the deposition efficiencies for the whole G6-G7 model and one path G6-G7 model are compared with each other in Table 5.3. It can be found that the present CFD results of the one-path model are very similar to the whole model, with a maximum difference of 0.681% occurring at G7 and d_p=20-nm. Assuming this maximum error of 0.681% at each generation, simulating particle deposition with G0 to G11 will have a maximum error of about 0.681%×11=7.5%. With this maximum error, the proposed one-path model enables the simulation of particle TD in many generations to be performed.

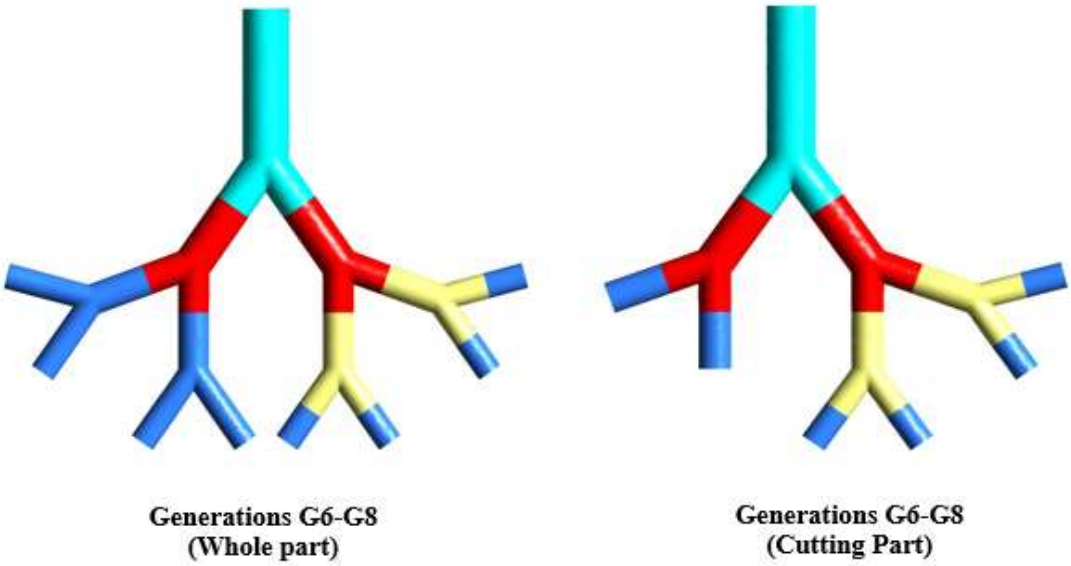

Figure 5.5. Comparison of the deposition efficiency results for the current simulation cutting method with the whole G6-G8 model.

Table 5.3. Local particle deposition efficiency comparison

Particle size	Local Particle Deposition Efficiency, η_L (%)								
	Whole part model (G6-G9)			Cutting part model (G6-G9)			Difference (%)		
	G6	G6	G6	G6	G6	G8	G6	G7	G8
5-nm	47.986	18.653	7.027	47.831	18.531	7.013	0.323	0.654	0.209
10-nm	33.153	10.639	4.806	33.047	10.584	4.798	0.320	0.514	0.168
20-nm	17.486	5.833	2.847	17.456	5.794	2.839	0.171	0.681	0.276

5.5 Results and Discussion

The airflow dynamics and particle deposition are analysed under two flow conditions: low-level breathing (Q_{in} =15 L/min) at rest and moderate activity breathing (Q_{in} =30 L/min) during walking (Zhang and Kleinstreuer 2003, Gorji et al. 2013). The sizes of medicine particles are generally in the range of 1 nm ≤d_p≤1000 μm (Singhal et al. 2016). Solid colloidal particles with a diameter between 1 and 1000 nm are the most typical definition of nanoparticles used for drug delivery (Kreuter 1991, Dailey et al. 2006, Sung et al. 2007, De Jong and Borm 2008). However, some researchers argued that nanoparticles in the 50 - 500 nm (Uchechi et al. 2014) and 1-200 nm (Mansour et al. 2009) are suitable for drug delivery. Moreover, most existing studies considered nanoparticles as a drug delivery range of 1nm ≤d_p≤100 nm (Bahrami et al. 2017, Kong et al. 2017, Sun et al. 2021). Therefore, nanoparticles TD of particles with diameters in the range of $5\ \text{nm} \leq d_p \leq 20\ \text{nm}$ are considered in this study.

5.5.1 Airflow Characteristics

Figure 5.6 depicts airflow velocity profiles on the symmetric plane within the lung generations up to G13. In the numerical simulations, the conservation of mass is ensured by specifying flow rates at all the exits. Figure 5.6 shows very uneven velocity distribution near each bifurcation. After air passes through each bifurcation, its velocity accelerates locally on

one side and reduces at another side of each airway. The distribution patterns of the velocity in the airways for the two flow rates are similar to each other in Figure 5.6. The distribution of the velocity near each bifurcation in Figure 5.6 is in a same pattern as that reported by Mutuku and Chen (2018). After each airway is split into two, air flow velocity is accelerated at the inner airway walls that face the incoming flow.

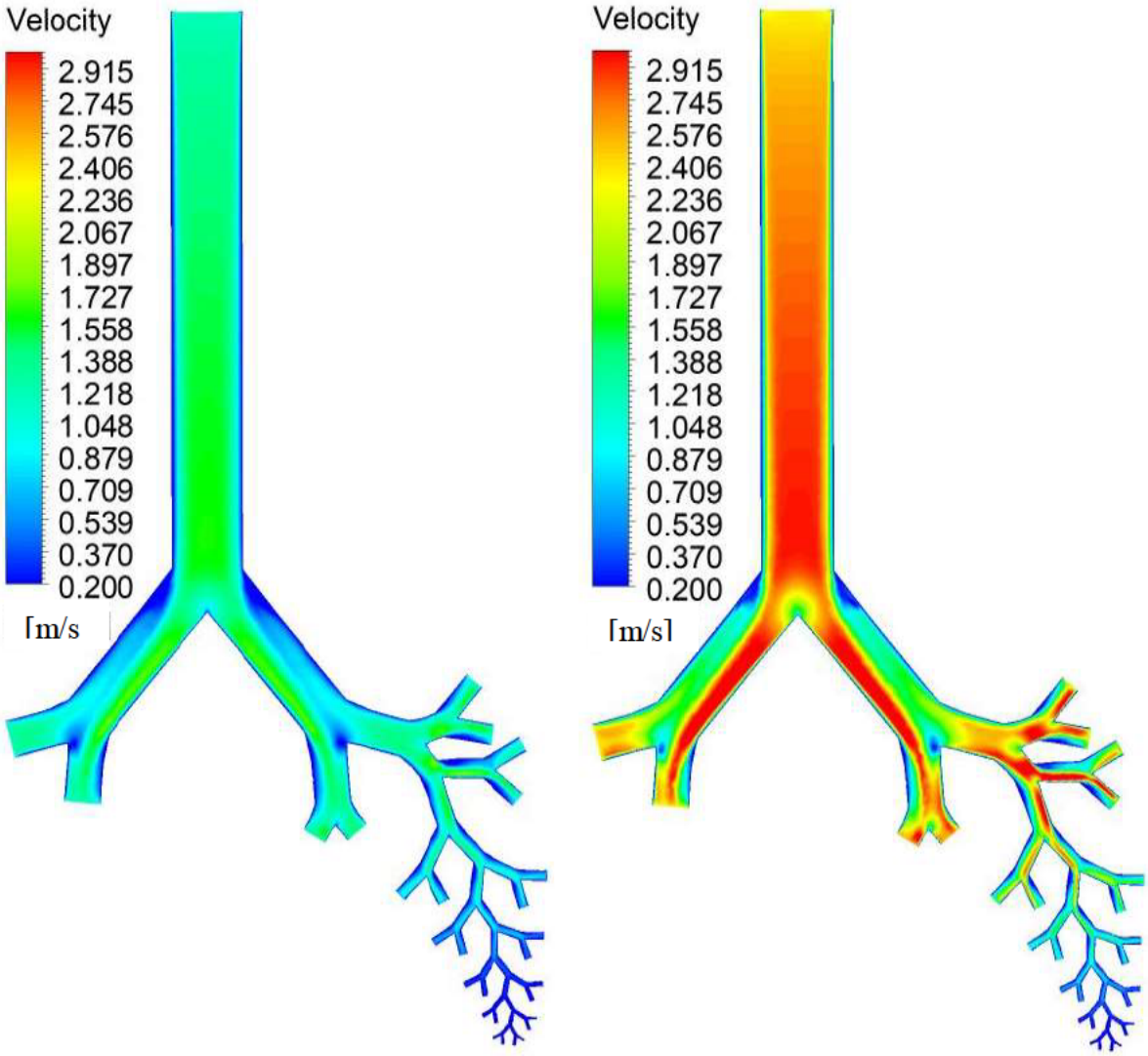

(a) Q_{in}=15 L/min (b) Q_{in}=30 L/min

Figure 5.6. Velocity contours for different flow rates at the lung airways generation (G0–G13); (a) Q_{in}=15 L/min; (b) Q_{in}=30 L/min

The airflow distribution in airways is further explored using velocity profiles at various sections in the upper airway regions in Figure 5.7. The averaged velocity at the inlet u_0 is used for non-dimensional velocity. Because of the difference in the Reynolds number, the non-dimensional velocity distributions along each line in Figure 5.7 of two flow rates follow a similar pattern but are not identical. The non-dimensional velocity profile on aa' line in the upper airway is symmetrical before the air enters the first bifurcation. After G1, however, velocities varied significantly because of the complexity of airway geometry. The velocity on one side of bb' is significantly higher than the other side. In addition, the velocity distribution in the lung airways of different generations are very different from each other. For example, the velocity of G1 (bb') are very different from that of G5 (cc'). The most unevenness of the velocity is found to be at section bb'.

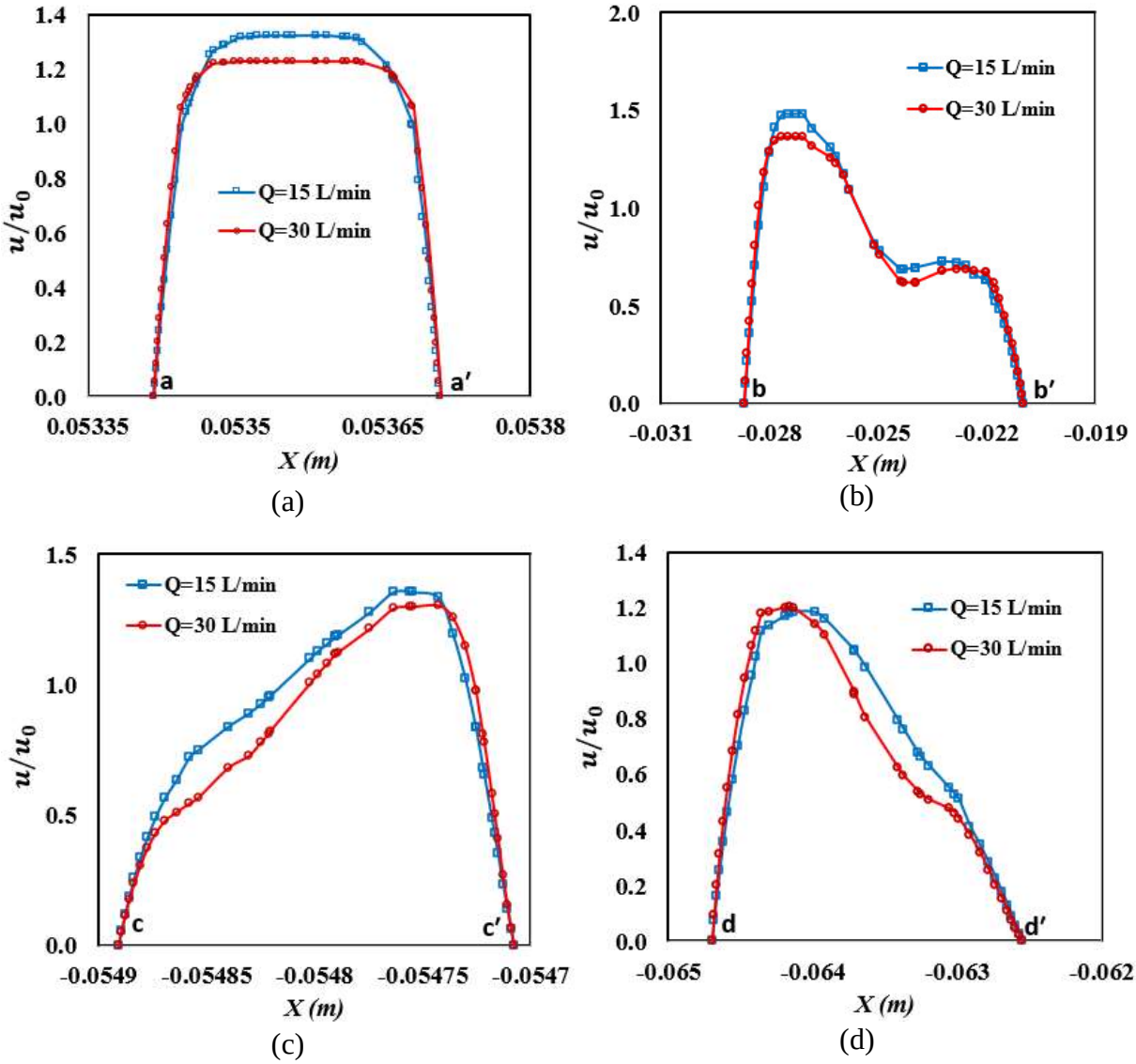

Figure 5.7. Velocity profiles at various flow rates, (a) Line aa′, (b) Line bb′, (c) Line cc′, and (d) Line dd′ (Figure 1 illustrates the locations of these lines).

5.5.2 Wall Shear Stress

It is understandable that the shear stress increase with the increase in flow rate. Because different flow rates have different Reynolds number, the shear stress will not be linearly proportional to the square of the velocity. The non-dimensional shear stress defined by $(\tau/(\rho u_0^2))$ can easily quantify the shear stress relative to the incoming flow velocity. Figure 5.8 shows the averaged non-dimensional shear stress $(\tau/(\rho u_0^2))$ at six sections indicated in Figure

5.1 along the airflow route, where wall shear stress τ on each section is averaged shear stress over the circumference of this section. The variations of the wall shear stress along the airflow route for the two flow rates follow a similar trend. However, the non-dimensional wall shear stress at Q_{in} =15 L/m is significantly greater than that at Q_{in} =30 L/min because the contribution of viscosity decreases with the increase of the Reynolds number.

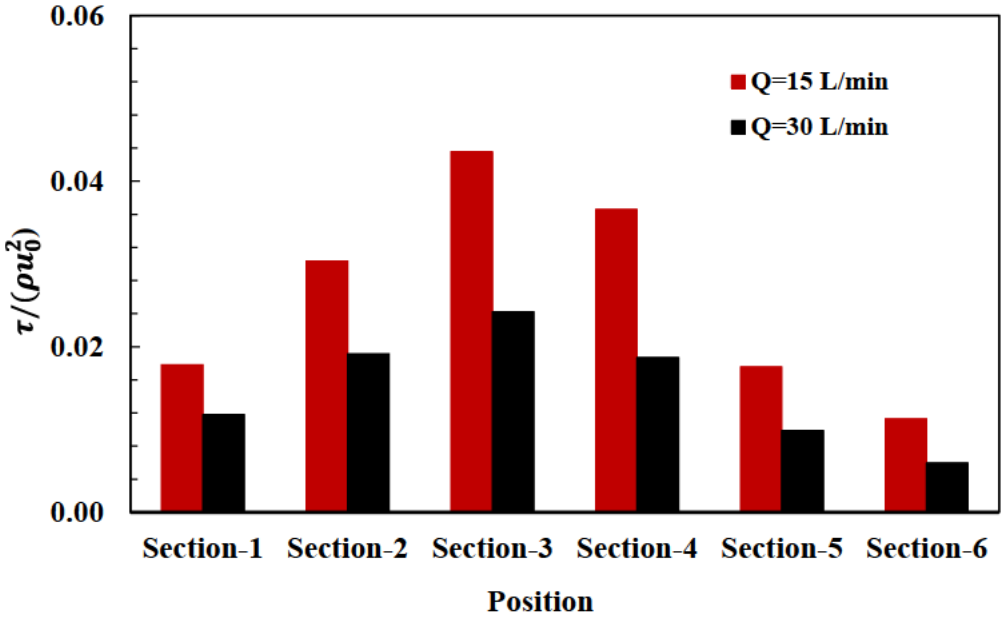

Figure 5.8. Averaged wall shear stress for a particular lung portion is indicated in Figure 5.1.

The non-dimensional pressure distribution along the lung airways at six different locations are shown in Figure 5.9, where the locations are indicated in Figure 5.1. The pressure decreases with the increase of distance from the inlet of G0, i.e. the deeper a location in the lung, the lower the pressure. Based on Bernoulli's theory and neglecting the potential energy, the velocity decreases as the air enters the deep lung, which is also demonstrated in Figure 5.6. The air pressure decreases as air goes into the deep lung mainly because the airflow overcomes much resistance from the friction caused by the viscosity of the flow.

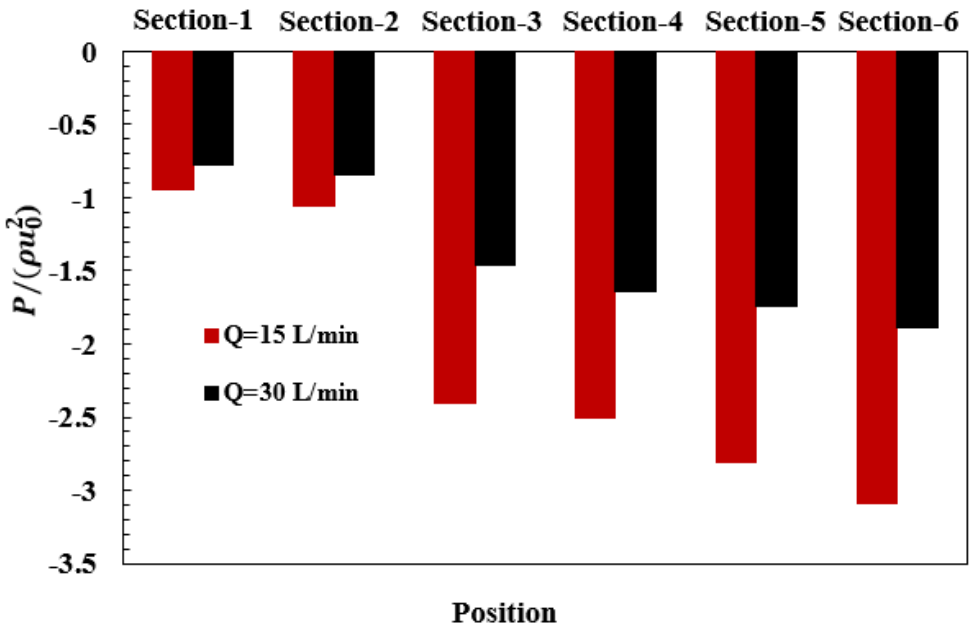

Figure 5.9. Pressure drop at two distinct flow rates in a different section of the lung model; the section numbers are shown in Figure 5.1.

5.5.3 Particle Deposition

The effects of flow rate and particle size on global particle deposition efficiency in lung airway generations G0-G11 are depicted in Figure 5.10. The deposition efficiencies of all three particle sizes decrease with increased flow rates at every generation in Figure 5.10 because the diffusion mechanism weakens. The deposition efficiency of 5-nm particles in each generation is significantly higher than those of 10-nm and 20-nm particles. At Q_{in}=15 L/min, 24.92%, 12.50% and 4.10% of 5-nm, 10-nm and 20-nm particles are deposited at G0, respectively, in Figure 5.10 (a). When the flow rate is increased to 30 L/min, the deposition efficiencies of 5-nm, 10-nm and 20-nm at generation G0 are reduced to 17.21%, 7.29% and 1.67%, respectively, compared with the flow rate of 15 L/min. Moreover, 9.58% of 5-nm, 4.93% of 10-nm and 2.09% of 20-nm particles are deposited at the generation G11 at flow rate Q_{in}=15 L/min, while

8.44% of 5-nm, 4.75% of 10-nm and 1.72% of 20-nm particles are deposited at the same generation at Q_{in}=30L/min.

It has been proved that the deposition of nanoparticles in human lungs are mainly dominated by the Brownian diffusion and Saffman lift force (Kleinstreuer et al. 2008, Inthavong et al. 2011). The combined Brownian diffusion and Saffman lift force are called diffusion mechanisms in this paper since they contribute to particle motion in the crossflow direction. The diffusion mechanism weakens with the increase of particle size and flow rate (Dong et al. 2019, Islam et al. 2021). The contribution of the impaction mechanism to the deposition of nanoparticles is weak because drag forces on particles are strong. Without diffusion mechanism strong drag forces make particles follow to the outlet and cause no deposition. Figure 5.10 indicates that a drop in flow rate increases the deposition efficiency of nanoparticles because reduced flow velocity provides particles a longer time to travel in the crossflow direction towards the wall (Darquenne 2020).

The difference between the deposition efficiencies at 30 L/min and 15 L/m decreases with increasing particle size. In Figure 5.10 (c), the ratio $\eta_{\mathrm{d,30\ L/min}}/\eta_{\mathrm{d,15\ L/min}}$ further illustrates the effect of the flow rate on the deposition rate. When the particle size is 20-nm, $\eta_{\mathrm{d,30\ L/min}}/\eta_{\mathrm{d,15\ L/min}}$ is 0.97, indicating that the flow rate has very weak effect on the deposition efficiency. The effects of flow rate decrease with decreasing particle size. The variation of the deposition efficiency with the generation number in Figure 5.10 follows similar trend that was reported by Sohrabi et al. (2017), who used a single route model to increase the efficiency of the numerical simulations.

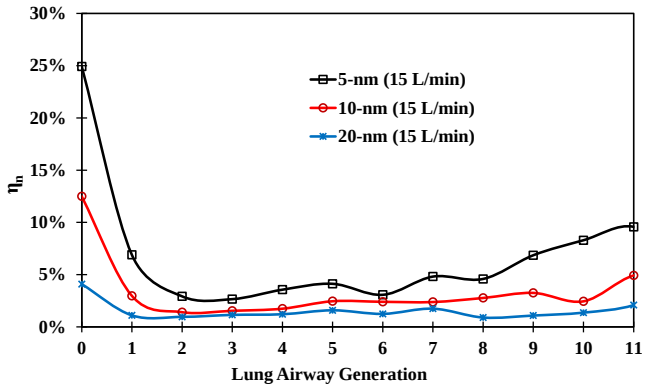

(a)

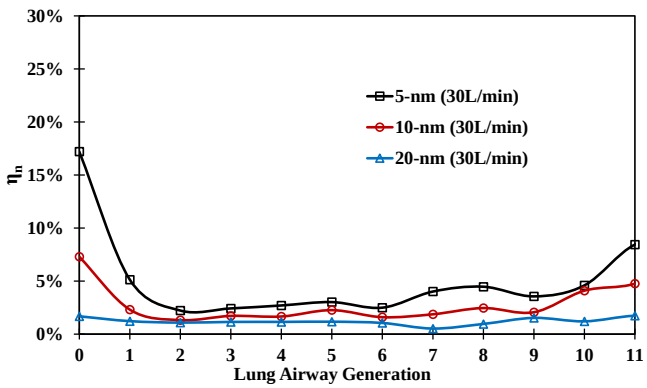

(b)

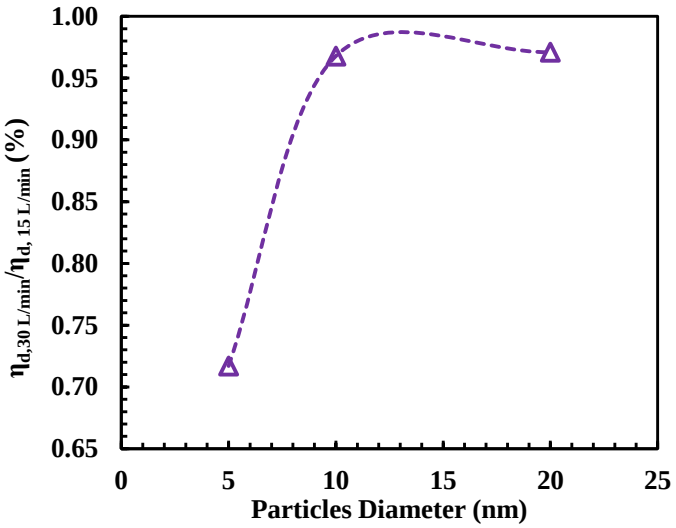

(c)

Figure 5.10. Particle deposition efficiency in airway lung generation: (a) Q_{in}=15 L/min; (b) Q_{in}=30 L/min; (c) Ratio of the deposition rates at the two flow rates

5.5.4 Visualisation of Particle Deposition

Figure 5.11 shows the visualisation of the local particle distribution of different sized particles at generation G0-G11 at the flow rate of 15 L/min. The calculated total deposition efficiency of G0 to G11 of 5-nm, 10-nm and-20 nm particles are 36.88%, 18.73% and 7.94%, respectively. Because of the higher dispersion capacity, the 5-nm particles have much higher deposition efficiency than 20-nm particles at Generation G0-G11. As a result, the deposited 5-nm particles are much more evenly distributed in all the airways than 20-nm particles, as shown

in Figures 5.11 (a) and 11 (b). In addition to stronger Brownian diffusion mechanism, smaller particles also receive a stronger lift force than bigger particles, which contributes to the particle motion in the crossflow direction. As a result, particles can move in the crossflow direction and reach the inner airway wall even if the airway is vertically straight at G0.

It has been proved that the diffusion of microscale particles is dominated by the impaction mechanism (Shi et al. 2007). Under the impaction mechanism, particles are deposited in the wall surface where the velocity is amplified (Rahman et al. 2021); as a result, the velocity distribution is significantly correlated to the deposited particle distribution along the lung airway wall. However, it can be seen that the distribution pattern in the airway in Figure 5.11 is not correlated to the velocity. For example, the area where the velocity is high in Figure 5.6 does not necessarily have large deposition in Figure 5.11. It appears that, the deposited particles are evenly distributed along the circumference on each section of an airway. This further prove that deposition of nanoparticles are dominated by diffusion instead of impaction.

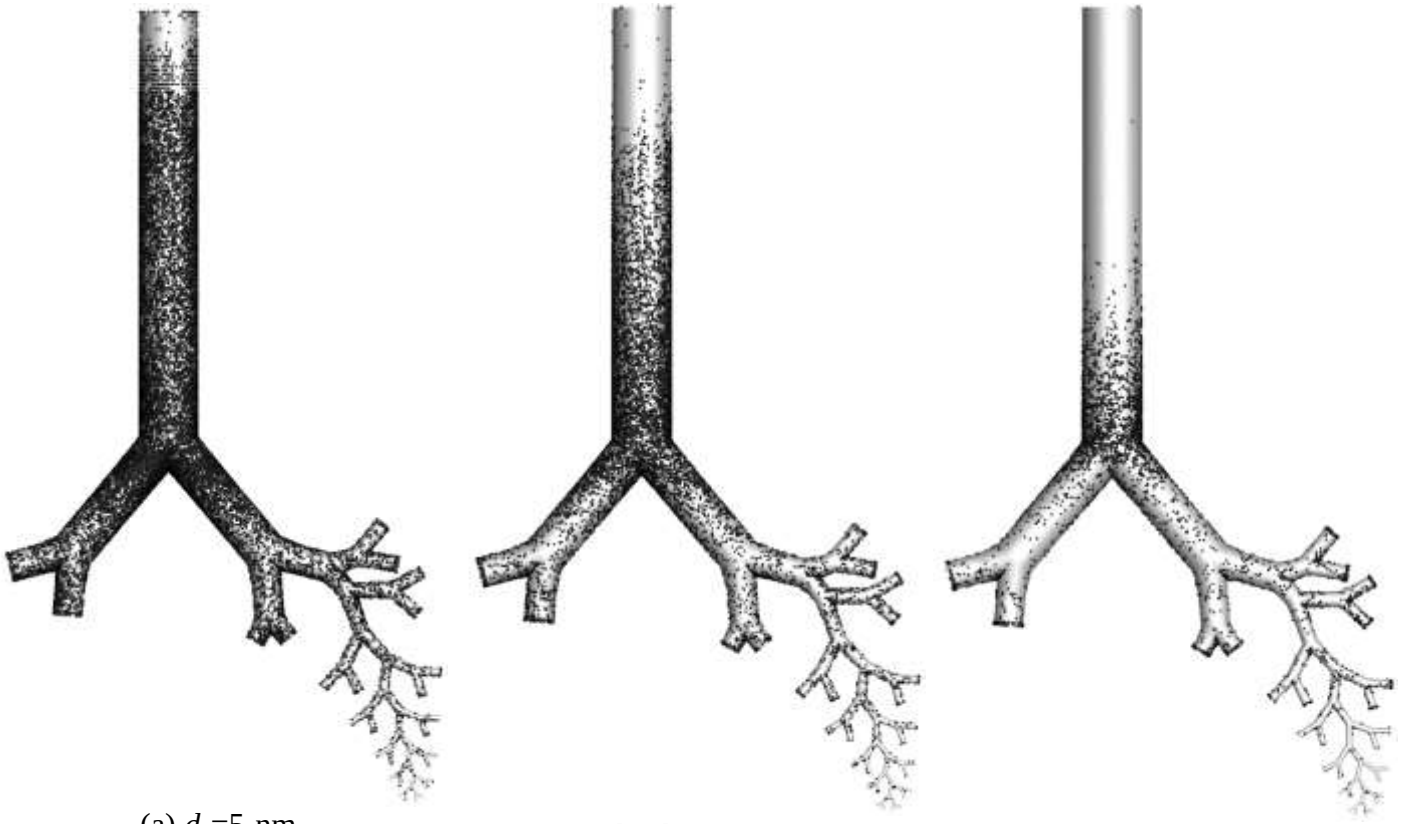

(a) d_p=5-nm (b) d_p=10-nm (c) d_p=20-nm

Figure 5.11. shows the distribution of deposited particles in human lung airways at flow rates of 15 L/min: (a) 5-nm particles, (b) 10-nm particles, and (c) 20-nm particles.

5.5.5 Particle Escaping Rate

The percentage of particles that escape from the outlets each generation and enter the deep lung is known as the escaping rate (defined as e_n). The rate of escape from all exits of a generation is equal to $1 - \eta_n$, where η_n represent the deposition efficiency of all bifurcation of this generation. The percentage of particles that can escape G11 and reach generations after G12 is known as the escape rate at G11. Particle size has the opposite impact on escape rate as it has on deposition rate. Figure 5.11 quantifies the escape rate at generations G0-G11 for two flow rates. The escape rate reduces as the generation increases because of particle deposition on the upper lungs. At both flow rates, the escape rate of 5-nm particles at every generation is much lower than that of 20-nm particles.17.68% and 39.77% of 5-nm particles can pass G11

and go into the deeper lung airways for flow rates 15 L/min and 30 L/min, respectively (Figure 5.12). At 15 L/min, the escaping rates of 10-nm and 20-nm particles at G11 are 59.15% and 81.42%, respectively. As the flow rate is increased to 30L/min, the escaping rates of 10-nm and 20-nm particles at generation are increased to 66.60% and 85.62%, respectively. Hence, the particle escape rate increases with the increase of the flow rate.

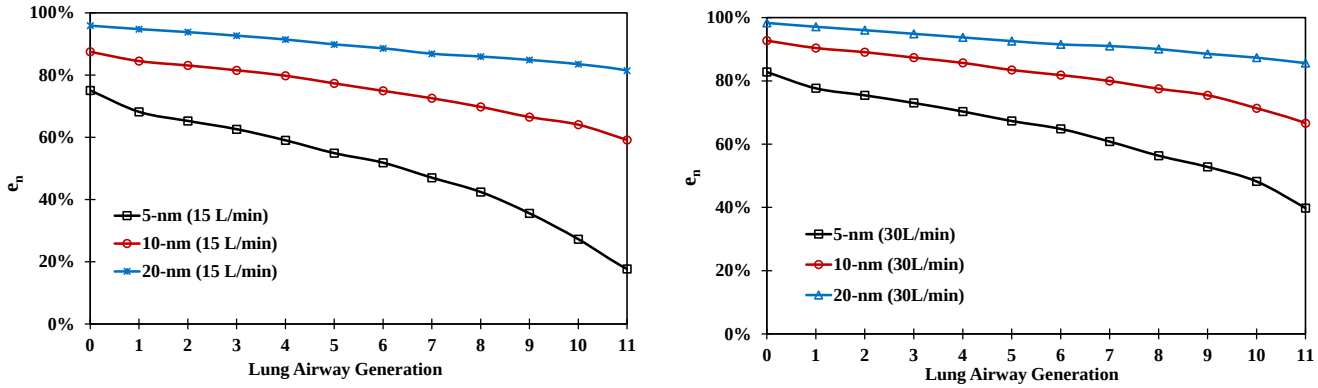

Figure 5.12. Escape rates (e_n) for 5 nm $\leq d_p \leq$ 20 nm particles at different flow rate: (a) Q_{in}=15 L/min; (b) Q_{in}=30 L/min

5.6 Conclusions

This paper presents a new one path numerical model for simulating particle deposition in human lungs with a reasonable computational effort and investigates the deposition in generations G0 to G11 using the method. We develop a correlation to convert local deposition efficiency to global deposition efficiency for all the generations. Furthermore, the effects of the particle size and the inhaled air flow rate on the deposition efficiency are studied. The key conclusions are summarized below.

- Non-dimensional velocity distributions in lung of the two flow rates follow a similar trend, but not the same because of the difference in the Reynolds number.

- More pressure drop is observed at the flow rate of 30 L/min compared to 15 L/min. It was observed that average pressure drops of 38.32% at a flow rate of 30 L/min compared to a flow rate of 15 L/min because the volume flow rate decreases.
- The particle size affects the distribution of the deposited particles in different generations of the lung. However, the majority of nanoparticles are deposited in the G0 generation.
- 5-nm particle is more evenly distributed than 20-nm particles (Figure 5.11) because the diffusion effect increases with the reduction in the particle size and is not affected by the geometry of the airways. Therefore, the diffusion is strong when the particle size is small.
- Particles with a small diameter and small flow rate are more deposited in the upper lung airways.
- The total particle deposition efficiency of 5-nm and 20-nm at flow rate Q_{in}=15 L/min is 36.88% and 7.94%, respectively. Therefore, the 5-nm particles have much higher deposition efficiency than 20-nm because of the higher dispersion capacity.
- The analysis of the escaping rates for nanoparticles shows that more particles enter the deep lung with a high flow rate. Therefore, the findings are crucial for treating lung diseases that affect the deep lung airways.

Conflicts of Interest

The authors state no conflict of interest.

Acknowledgments:

Mr Rahman acknowledges the support of the Australian Government Research Training Program's International Postgraduate Research Scholarship (IPRS). The authors also acknowledge that the WSU High-Performance computer provided the computational facilities.

References

Ahookhosh, K, Pourmehran, O, Aminfar, H, Mohammadpourfard, M, Sarafraz, MM & Hamishehkar, H 2020, 'Development of human respiratory airway models: A review', *European Journal of Pharmaceutical Sciences*, vol. 145, 105233.

Ahookhosh, K, Saidi, M, Aminfar, H, Mohammadpourfard, M, Hamishehkar, H & Yaqoubi, S 2020, 'Dry powder inhaler aerosol deposition in a model of tracheobronchial airways: validating CFD predictions with in vitro data', *International journal of pharmaceutics*, vol. 587, 119599.

Ahookhosh, K, Saidi, M, Mohammadpourfard, M, Aminfar, H, Hamishehkar, H, Farnoud, A et al. 2021, 'Flow structure and particle deposition analyses for optimization of a pressurized metered dose inhaler (pMDI) in a model of tracheobronchial airway', *European Journal of Pharmaceutical Sciences*, vol. 164, 105911.

Alexiou, C, Schmid, RJ, Jurgons, R, Kremer, M, Wanner, G, Bergemann, C et al. 2006, 'Targeting cancer cells: magnetic nanoparticles as drug carriers', *European biophysics journal*, vol. 35, no. 5, pp. 446-450.

Azarmi, S, Roa, WH & Löbenberg, R 2008, 'Targeted delivery of nanoparticles for the treatment of lung diseases', *Advanced Drug Delivery Reviews*, vol. 60, no. 8, pp. 863-875.

Babu, A, Templeton, AK, Munshi, A & Ramesh, R 2013, 'Nanoparticle-based drug delivery for therapy of lung cancer: progress and challenges', *Journal of Nanomaterials*, vol. 2013, 863951.

Bahmanzadeh, H, Abouali, O & Ahmadi, G 2016, 'Unsteady particle tracking of micro-particle deposition in the human nasal cavity under cyclic inspiratory flow', *Journal of Aerosol Science*, vol. 101, pp. 86-103.

Bahrami, B, Hojjat-Farsangi, M, Mohammadi, H, Anvari, E, Ghalamfarsa, G, Yousefi, M et al. 2017, 'Nanoparticles and targeted drug delivery in cancer therapy', *Immunology letters*, vol. 190, pp. 64-83.

Barani, M, Mukhtar, M, Rahdar, A, Sargazi, G, Thysiadou, A & Kyzas, GZ 2021, 'Progress in the Application of Nanoparticles and Graphene as Drug Carriers and on the Diagnosis of Brain Infections', *Molecules*, vol. 26, no. 1, 186.

Chen, W-H, Chang, C-M, Mutuku, JK, Lam, SS & Lee, W-J 2021, 'Analysis of microparticle deposition in the human lung by taguchi method and response surface methodology', *Environmental research*, vol. 197, 110975.

Comer, J, Kleinstreuer, C, Hyun, S & Kim, C 1999, 'Aerosol transport and deposition in sequentially bifurcating airways', *J. Biomech. Eng.*, vol. 122, no. 2, pp. 152-158.

Dailey, L, Jekel, N, Fink, L, Gessler, T, Schmehl, T, Wittmar, M et al. 2006, 'Investigation of the proinflammatory potential of biodegradable nanoparticle drug delivery systems in the lung', *Toxicology and applied pharmacology*, vol. 215, no. 1, pp. 100-108.

Darquenne, C 2020, 'Deposition mechanisms', *Journal of aerosol medicine and pulmonary drug delivery*, vol. 33, no. 4, pp. 181-185.

De Jong, WH & Borm, PJ 2008, 'Drug delivery and nanoparticles: applications and hazards', *International journal of nanomedicine*, vol. 3, no. 2, 133.

Deng, Q, Deng, L, Miao, Y, Guo, X & Li, Y 2019, 'Particle deposition in the human lung: Health implications of particulate matter from different sources', *Environmental research*, vol. 169, pp. 237-245.

Deng, Q, Ou, C, Chen, J & Xiang, Y 2018, 'Particle deposition in tracheobronchial airways of an infant, child and adult', *Science of the Total Environment*, vol. 612, pp. 339-346.

Dong, J, Li, J, Tian, L & Tu, J 2021, 'Transport and deposition of ultrafine particles in the upper tracheobronchial tree: a comparative study between approximate and realistic respiratory tract models', *Computer Methods in Biomechanics and Biomedical Engineering*, vol. 24, no. 10, pp. 1125-1135.

Dong, J, Shang, Y, Tian, L, Inthavong, K, Qiu, D & Tu, J 2019, 'Ultrafine particle deposition in a realistic human airway at multiple inhalation scenarios', *International journal for numerical methods in biomedical engineering*, vol. 35, no. 7, e3215.

Farghadan, A, Poorbahrami, K, Jalal, S, Oakes, JM, Coletti, F & Arzani, A 2020, 'Particle transport and deposition correlation with near-wall flow characteristic under inspiratory airflow in lung airways', *Computers in biology and medicine*, vol. 120, 103703.

Feng, Y & Kleinstreuer, C 2014, 'Micron-particle transport, interactions and deposition in triple lung-airway bifurcations using a novel modeling approach', *Journal of Aerosol Science*, vol. 71, pp. 1-15.

Fletcher, DF, Chaugule, V, Gomes dos Reis, L, Young, PM, Traini, D & Soria, J 2021, 'On the use of computational fluid dynamics (CFD) modelling to design improved dry powder inhalers', *Pharmaceutical Research*, vol. 38, no. 2, pp. 277-288.

Ghalati, PF, Keshavarzian, E, Abouali, O, Faramarzi, A, Tu, J & Shakibafard, A 2012, 'Numerical analysis of micro-and nano-particle deposition in a realistic human upper airway', *Computers in biology and medicine*, vol. 42, no. 1, pp. 39-49.

Gorji, TB, Fatouraee, N & Mozaffari, A 2013, 'Numerical simulation of transport and deposition of micro-particles in two-phase flow in a human upper airway model from CT images', *International Journal of Experimental and Computational Biomechanics*, vol. 2, no. 2, pp. 171-188.

Grassia, PS, Hinch, EJ & Nitsche, LC 1995, 'Computer simulations of Brownian motion of complex systems', *Journal of Fluid mechanics*, vol. 282, pp. 373-403.

Gu, X, Wen, J, Wang, M, Jian, G, Zheng, G & Wang, S 2019, 'Numerical investigation of unsteady particle deposition in a realistic human nasal cavity during inhalation', *Experimental and Computational Multiphase Flow*, vol. 1, no. 1, pp. 39-50.

Hou, L, Luby-Phelps, K & Lanni, F 1990, 'Brownian motion of inert tracer macromolecules in polymerized and spontaneously bundled mixtures of actin and filamin', *The Journal of cell biology*, vol. 110, no. 5, pp. 1645-1654.

Huang, F, Zhu, Q, Zhou, X, Gou, D, Yu, J, Li, R et al. 2021, 'Role of CFD based in silico modelling in establishing an in vitro-in vivo correlation of aerosol deposition in the respiratory tract', *Advanced Drug Delivery Reviews*, vol. 170, pp. 369-385.

Inthavong, K, Ge, Q, Se, CM, Yang, W & Tu, J 2011, 'Simulation of sprayed particle deposition in a human nasal cavity including a nasal spray device', *Journal of Aerosol Science*, vol. 42, no. 2, pp. 100-113.

Inthavong, K, Zhang, K & Tu, J 2011, 'Numerical modelling of nanoparticle deposition in the nasal cavity and the tracheobronchial airway', *Computer Methods in Biomechanics and Biomedical Engineering*, vol. 14, no. 7, pp. 633-643.

Islam, MS, Larpruenrudee, P, Hossain, SI, Rahimi-Gorji, M, Gu, Y, Saha, SC et al. 2021, 'Polydisperse aerosol transport and deposition in upper airways of age-specific lung', *International Journal of Environmental Research and Public Health*, vol. 18, no. 12, 6239.

Islam, MS, Larpruenrudee, P, Paul, AR, Paul, G, Gemci, T, Gu, Y et al. 2021, 'SARS CoV-2 aerosol: How far it can travel to the lower airways?', *Physics of Fluids*, vol. 33, no. 6, 061903.

Islam, MS, Larpruenrudee, P, Saha, SC, Pourmehran, O, Paul, AR, Gemci, T et al. 2021, 'How severe acute respiratory syndrome coronavirus-2 aerosol propagates through the age-specific upper airways', *Physics of Fluids*, vol. 33, no. 8, 081911.

Kadota, K, Matsumoto, K, Uchiyama, H, Tobita, S, Maeda, M, Maki, D et al. 2022, 'In silico evaluation of particle transport and deposition in the airways of individual patients with chronic obstructive pulmonary disease', *European Journal of Pharmaceutics and Biopharmaceutics*, vol. 174, pp. 10-19.

Kaur, IP, Bhandari, R, Bhandari, S & Kakkar, V 2008, 'Potential of solid lipid nanoparticles in brain targeting', *Journal of controlled release*, vol. 127, no. 2, pp. 97-109.

Kim, CS & Iglesias, AJ 1989, 'Deposition of inhaled particles in bifurcating airway models: I. Inspiratory deposition', *Journal of aerosol medicine*, vol. 2, no. 1, pp. 1-14.

Kleinstreuer, C, Zhang, Z & Donohue, J 2008, 'Targeted drug-aerosol delivery in the human respiratory system', *Annu. Rev. Biomed. Eng.*, vol. 10, pp. 195-220.

Kolanjiyil, AV & Kleinstreuer, C 2019, 'Modeling airflow and particle deposition in a human acinar region', *Computational and mathematical methods in medicine*, vol. 2019, 5952941.

Kong, F-Y, Zhang, J-W, Li, R-F, Wang, Z-X, Wang, W-J & Wang, W 2017, 'Unique roles of gold nanoparticles in drug delivery, targeting and imaging applications', *Molecules*, vol. 22, no. 9, 1445.

Koullapis, P, Kassinos, SC, Muela, J, Perez-Segarra, C, Rigola, J, Lehmkuhl, O et al. 2018, 'Regional aerosol deposition in the human airways: The SimInhale benchmark case and a critical assessment of in silico methods', *European Journal of Pharmaceutical Sciences*, vol. 113, pp. 77-94.

Kreuter, J 1991, 'Nanoparticle-based dmg delivery systems', *Journal of controlled release*, vol. 16, no. 1-2, pp. 169-176.

Lee, W-H, Loo, C-Y, Traini, D & Young, PM 2015, 'Inhalation of nanoparticle-based drug for lung cancer treatment: Advantages and challenges', *Asian journal of pharmaceutical sciences*, vol. 10, no. 6, pp. 481-489.

Lintermann, A & Schröder, W 2017, 'Simulation of aerosol particle deposition in the upper human tracheobronchial tract', *European Journal of Mechanics-B/Fluids*, vol. 63, pp. 73-89.

Longest, PW & Holbrook, LT 2012, 'In silico models of aerosol delivery to the respiratory tract—development and applications', *Advanced Drug Delivery Reviews*, vol. 64, no. 4, pp. 296-311.

Longest, PW & Xi, J 2007, 'Effectiveness of direct Lagrangian tracking models for simulating nanoparticle deposition in the upper airways', *Aerosol Science and Technology*, vol. 41, no. 4, pp. 380-397.

Mangal, S, Gao, W, Li, T & Zhou, QT 2017, 'Pulmonary delivery of nanoparticle chemotherapy for the treatment of lung cancers: challenges and opportunities', *Acta pharmacologica sinica*, vol. 38, no. 6, pp. 782-797.

Mansour, HM, Rhee, Y-S & Wu, X 2009, 'Nanomedicine in pulmonary delivery', *International journal of nanomedicine*, vol. 4, pp. 299-319.

Massarotti, N, Mauro, A, Mohamed, S & Romano, MR 2021, 'Air contamination inside an actual operating room due to ultrafine particles: An experimental-numerical thermo-fluid dynamic study', *Atmospheric environment*, vol. 249, 118155.

Morsi, S & Alexander, A 1972, 'An investigation of particle trajectories in two-phase flow systems', *Journal of Fluid mechanics*, vol. 55, no. 2, pp. 193-208.

Mutuku, JK & Chen, W-H 2018, 'Flow characterization in healthy airways and airways with chronic obstructive pulmonary disease (COPD) during different inhalation conditions', *Aerosol and Air Quality Research*, vol. 18, no. 10, pp. 2680-2694.

Nahar, K, Gupta, N, Gauvin, R, Absar, S, Patel, B, Gupta, V et al. 2013, 'In vitro, in vivo and ex vivo models for studying particle deposition and drug absorption of inhaled pharmaceuticals', *European Journal of Pharmaceutical Sciences*, vol. 49, no. 5, pp. 805-818.

Poorbahrami, K & Oakes, JM 2019, 'Regional flow and deposition variability in adult female lungs: A numerical simulation pilot study', *Clinical Biomechanics*, vol. 66, pp. 40-49.

Rahimi-Gorji, M, Gorji, TB & Gorji-Bandpy, M 2016, 'Details of regional particle deposition and airflow structures in a realistic model of human tracheobronchial airways: two-phase flow simulation', *Computers in biology and medicine*, vol. 74, pp. 1-17.

Rahman, M, Zhao, M, Islam, MS, Dong, K & Saha, SC 2022, 'Numerical study of nano and micro pollutant particle transport and deposition in realistic human lung airways', *Powder Technology*, vol. 402, 117364.

Rahman, MM, Zhao, M, Islam, MS, Dong, K & Saha, SC 2021a, 'Aerosol Particle Transport and Deposition in Upper and Lower Airways of Infant, Child and Adult Human Lungs', *Atmosphere*, vol. 12, no. 11, 1402.

Rahman, MM, Zhao, M, Islam, MS, Dong, K & Saha, SC 2021b, 'Aging effects on airflow distribution and micron-particle transport and deposition in a human lung using CFD-DPM approach', *Advanced Powder Technology*, vol. 32, pp. 3506-3516.

Rahman, MM, Zhao, M, Islam, MS, Dong, K & Saha, SC 2021c, 'Numerical study of nanoscale and microscale particle transport in realistic lung models with and without stenosis', *International Journal of Multiphase Flow*, vol. 145, 103842.

Ruge, CA, Kirch, J & Lehr, C-M 2013, 'Pulmonary drug delivery: from generating aerosols to overcoming biological barriers—therapeutic possibilities and technological challenges', *The lancet Respiratory medicine*, vol. 1, no. 5, pp. 402-413.

Russo, F, Boghi, A & Gori, F 2018, 'Numerical simulation of magnetic nano drug targeting in patient-specific lower respiratory tract', *Journal of Magnetism and Magnetic Materials*, vol. 451, pp. 554-564.

Scherließ, R, Bock, S, Bungert, N, Neustock, A & Valentin, L 2022, 'Particle engineering in dry powders for inhalation', *European Journal of Pharmaceutical Sciences*, 106158.

Shi, H, Kleinstreuer, C & Zhang, Z 2007, 'Modeling of inertial particle transport and deposition in human nasal cavities with wall roughness', *Journal of Aerosol Science*, vol. 38, no. 4, pp. 398-419.

Shih, TH, Liou, WW, Shabbir, A, Yang, Z & Zhu, J 1995, 'A new k-ϵ eddy viscosity model for high reynolds number turbulent flows', *Computers and Fluids*, vol. 24, no. 3, pp. 227-238.

Singh, R & Lillard Jr, JW 2009, 'Nanoparticle-based targeted drug delivery', *Experimental and molecular pathology*, vol. 86, no. 3, pp. 215-223.

Singhal, C, Malhotra, N, Chauhan, N, Narang, S, Pundir, C & Narang, J 2016, 'Hierarchical electrodeposition of methylene blue on ZnO nanocrystals thin films layered on SnO2/F electrode for in vitro sensing of anti-thalassemic drug', *Materials Science and Engineering: C*, vol. 62, pp. 596-604.

Sohrabi, S, Wang, S, Tan, J, Xu, J, Yang, J & Liu, Y 2017, 'Nanoparticle transport and delivery in a heterogeneous pulmonary vasculature', *Journal of biomechanics*, vol. 50, pp. 240-247,

Sohrabi, S, Zheng, J, Finol, EA & Liu, Y 2014, 'Numerical simulation of particle transport and deposition in the pulmonary vasculature', *Journal of biomechanical engineering*, vol. 136, no. 12, 121010.

Sosnowski, TR 2018, 'Powder particles and technologies for medicine delivery to the respiratory system: Challenges and opportunities', *KONA Powder and Particle Journal*, vol. 35, pp. 122-138.

Sun, T, Zhang, YS, Pang, B, Hyun, DC, Yang, M & Xia, Y 2021, 'Engineered nanoparticles for drug delivery in cancer therapy', *Nanomaterials and Neoplasms*, pp. 131-142.

Sung, JC, Pulliam, BL & Edwards, DA 2007, 'Nanoparticles for drug delivery to the lungs', *Trends in biotechnology*, vol. 25, no. 12, pp. 563-570.

Tash, MA, Tavakol, MM, Abouali, O & Ahmadi, G 2019, 'Deposition of Ellipsoidal Fibers in Nasal Cavity: Influence of Non-Creeping Flow Conditions', *Proceedings of the American Society of Mechanical Engineers*, vol. 5, V005T05A53, July 28–August 1, San Francisco, California, USA.

Tian, G, Longest, PW, Su, G & Hindle, M 2011, 'Characterization of respiratory drug delivery with enhanced condensational growth using an individual path model of the entire tracheobronchial airways', *Annals of Biomedical Engineering*, vol. 39, no. 3, pp. 1136-1153.

Tian, G, Longest, PW, Su, G, Walenga, RL & Hindle, M 2011, 'Development of a stochastic individual path (SIP) model for predicting the tracheobronchial deposition of pharmaceutical aerosols: Effects of transient inhalation and sampling the airways', *Journal of Aerosol Science*, vol. 42, no. 11, pp. 781-799.

Tsuji, Y 2007, 'Multi-scale modeling of dense phase gas–particle flow', *Chemical engineering science*, vol. 62, no. 13, pp. 3410-3418.

Uchechi, O, Ogbonna, JD & Attama, AA 2014, 'Nanoparticles for dermal and transdermal drug delivery', *Application of nanotechnology in drug delivery*, vol. 4, pp. 193-227.

Vachhani, S & Kleinstreuer, C 2021, 'Comparison of micron-and nano-particle transport in the human nasal cavity with a focus on the olfactory region', *Computers in biology and medicine*, vol. 128, 104103.

Valiulin, SV, Onischuk, AA, Dubtsov, SN, Baklanov, AM, An'kov, SV, Plokhotnichenko, ME et al. 2021, 'Aerosol Inhalation Delivery of Triazavirin in Mice: Outlooks for Advanced Therapy Against Novel Viral Infections', *Journal of Pharmaceutical Sciences*, vol. 110, no. 3, pp. 1316-1322.

Willis, L, Hayes, D & Mansour, HM 2012, 'Therapeutic liposomal dry powder inhalation aerosols for targeted lung delivery', *Lung*, vol. 190, no. 3, pp. 251-262.

Xi, J, Berlinski, A, Zhou, Y, Greenberg, B & Ou, X 2012, 'Breathing resistance and ultrafine particle deposition in nasal–laryngeal airways of a newborn, an infant, a child, and an adult', *Annals of Biomedical Engineering*, vol. 40, no. 12, pp. 2579-2595.

Xu, G & Yu, C 1986, 'Effects of age on deposition of inhaled aerosols in the human lung', *Aerosol science and technology*, vol. 5, no. 3, pp. 349-357.

Yhee, JY, Im, J & Nho, RS 2016, 'Advanced therapeutic strategies for chronic lung disease using nanoparticle-based drug delivery', *Journal of clinical medicine*, vol. 5, no. 9, 82.

Yu, G, Zhang, Z & Lessmann, R 1996, 'Computer simulation of the flow field and particle deposition by diffusion in a 3-D human airway bifurcation', *Aerosol Science and Technology*, vol. 25, no. 3, pp. 338-352.

Zhang, Z & Kleinstreuer, C 2003, 'Computational thermodynamics analysis of vaporizing fuel droplets in the human upper airways', *JSME International Journal Series B Fluids and Thermal Engineering*, vol. 46, no. 4, pp. 563-571.

Zhang, Z & Kleinstreuer, C 2004, 'Airflow structures and nano-particle deposition in a human upper airway model', *Journal of computational physics*, vol. 198, no. 1, pp. 178-210.

Zhang, Z, Kleinstreuer, C & Kim, CS 2008, 'Airflow and nanoparticle deposition in a 16-generation tracheobronchial airway model', *Annals of Biomedical Engineering*, vol. 36, no. 12, pp. 2095-2110.

Zhao, J, Feng, Y & Fromen, CA 2020, 'Glottis motion effects on the particle transport and deposition in a subject-specific mouth-to-trachea model: A CFPD study', *Computers in biology and medicine*, vol. 116, 103532.

Chapter 6: Numerical Study of Nanoscale and Microscale Particle Transport in Realistic Lung Models With and Without Stenosis

This chapter presents a final accepted version paper published in 2021, International Journal of Multiphase Flow, 145, 103842. The first page of the published paper was shown at the beginning of the chapter, followed by the accepted version.

Chapter 6 Numerical Study of Nanoscale and Microscale Particle Transport in Realistic Lung Models With and Without Stenosis

International Journal of Multiphase Flow 145 (2021) 103842

Contents lists available at ScienceDirect

International Journal of Multiphase Flow

journal homepage: www.elsevier.com/locate/ijmulflow

Numerical study of nanoscale and microscale particle transport in realistic lung models with and without stenosis

Md. M Rahman [a,b], Ming Zhao [a,*], Mohammad S. Islam [c], Kejun Dong [d], Suvash C Saha [c]

[a] School of Engineering, Design and Built Environment, Western Sydney University, Penrith, NSW 2751, Australia
[b] Department of Mathematics, Faculty of Science, Islamic University, Kushtia-7300, Bangladesh
[c] School of Mechanical and Mechatronic Engineering, University of Technology Sydney, Ultimo, NSW 2007, Australia
[d] Center for Infrastructure Engineering, Western Sydney University, Penrith, NSW 2751, Australia

ARTICLE INFO

Keywords:
Airflow dynamics (AD)
Stenosis airway
Aerosol particle transport and deposition (TD)
Inhalation
Drug delivery

ABSTRACT

The transport and deposition (TD) of inhaled aerosol particles in airways of human lungs are important for therapeutically targeted drug delivery in respiratory tracts. The airflow and particle TD depend on various aspects, including breathing pattern, geometry of lungs, particle properties and deposition mechanisms. In this paper, a computational fluid dynamics (CFD) study is conducted to understand the flow behaviour and PD of both nanoparticles and microparticles (particle diameter = 5 nm, 100 nm, 500 nm, 1 μm, 5 μm and 10 μm) in airways of mouth–throat and tracheobronchial of a human lung under the effect of stenosis. The contribution of impaction and diffusion mechanisms to the TD of particles with different diameters in human lung models with and without stenosis are investigated through numerical simulations using ANSYS FLUENT solver. The study was conducted under two flow rates of 15 L/min and 60 L/min. The stenosis at the right primary bronchi reduces the airway sectional by 75%. It is found that the pressure drop of the stenosis model increases by 83% compared to the healthy model. Over 75% of 10 μm particles are deposited in the mouth–throat and tracheobronchial airways. As the particle size is decreased to 5 nm, less than 10% of the particles are deposited in the airways, allowing over 90% particles to enter deeper part of the lung. The results suggest that the particle deposition efficiency in airways of mouth–throat and tracheobronchial increases with increasing the flow rate as well as the particle diameter because of the inertia impaction mechanism. The contribution of the diffusion mechanism is significantly decreased with the increase of either particle size or flow rate. The predicted particle deposition patterns in the airway with stenosis model would be useful to optimise a patient's treatment for drug delivery in the stenosis airway.

1. Introduction

Airflow dynamics and particle TD in lung airways are attracting increasing attention of researchers in biomedical engineering because of its practical application in real life. However, numerical modelling of the human lung through CFD simulations is still a challenge because of the complexity of lung geometry. To treat lung diseases in the respiratory tract, aerosol particle inhalation as drug delivery is cost-effective and has smaller side effects compared to aggressive drugs (Kuzmov and Minko (2015). The delivery of the aerosol particles through the mouth-throat, nasal and pulmonary region has been developed as non-invasive alternative routes (Karakosta et al., 2015; Longest et al., 2011). The key target of aerosol drug delivery is to maximize the particle deposition inside human lungs. To ensure the effectiveness of aerosol particle inhalation and delivery of drugs into the targeted area of respiratory airways, understanding the mechanisms of particle TD in 3D realistic anatomical lung models is essential. CFD simulations are efficient methods to ensure inhaled aerosol particles to be deposited in targeted areas of human lungs.

Studying particle inhalation and TD into human lungs is also useful to detect the cause of lung diseases like asthma, lung cancer and chronic obstructive pulmonary disease (COPD) caused by particulate matter (PM) air pollution. PM comes from different sources, e.g. industrial pollutants, burning fuels of vehicles, coal combustion and pesticide (Davidson et al., 2005; Kampa and Castanas, 2008) and is often hazardous to public health. Moreover, some particles absorbed by the

* Corresponding author.
E-mail address: M.Zhao@westernsydney.edu.au (M. Zhao).

https://doi.org/10.1016/j.ijmultiphaseflow.2021.103842
Received 24 June 2021; Received in revised form 31 August 2021; Accepted 27 September 2021
Available online 29 September 2021

Numerical study of nanoscale and microscale particle transport in realistic lung models with and without stenosis

Md. M. Rahman [1, 2], Ming Zhao [1, *], Mohammad S. Islam [3], Kejun Dong [4], and Suvash C. Saha [3]

[1] School of *Engineering*, Design and Built Environment, Western Sydney University, Penrith, NSW 2751, Australia.

[2] Department of Mathematics, Faculty of Science, Islamic University, Kushtia-7003, Bangladesh.

[3] School of Mechanical and Mechatronic Engineering, University of Technology Sydney, Ultimo, NSW 2007, Australia.

[4] Center for Infrastructure Engineering, Western Sydney University, Penrith, NSW 2751, Australia.

***Correspondence author:** M.Zhao@westernsydney.edu.au

6.1 Abstract

The transport and deposition (TD) of inhaled aerosol particles in airways of human lungs are important for therapeutically targeted drug delivery in respiratory tracts. The airflow and particle TD depend on various aspects, including breathing pattern, geometry of lungs, particle properties and deposition mechanisms. In this paper, a computational fluid dynamics (CFD) study is conducted to understand the flow behaviour and PD of both nanoparticles and microparticles (particle diameter = 5 nm, 100 nm, 500 nm, 1 μm, 5 μm and 10 μm) in airways of mouth–throat and tracheobronchial of a human lung under the effect of stenosis. The contribution of impaction and diffusion mechanisms to the TD of particles with different diameters in human lung models with and without stenosis are investigated through numerical simulations using ANSYS FLUENT solver. The study was conducted under two flow rates of 15 L/min and 60 L/min. The stenosis at the right primary bronchi reduces the airway sectional by 75%. It is found that the pressure drop of the stenosis model increases by 83% compared to the healthy model. Over 75% of 10 μm particles are deposited in the mouth–throat and tracheobronchial airways. As the particle size is decreased to 5 nm, less than 10% of the particles are deposited in the airways, allowing over 90% particles to enter deeper part of the

lung. The results suggest that the particle deposition efficiency in airways of mouth–throat and tracheobronchial increases with increasing the flow rate as well as the particle diameter because of the inertia impaction mechanism. The contribution of the diffusion mechanism is significantly decreased with the increase of either particle size or flow rate. The predicted particle deposition patterns in the airway with stenosis model would be useful to optimise a patient's treatment for drug delivery in the stenosis airway.

Keywords: Airflow Dynamics (AD), Stenosis Airway, Aerosol particle transport and deposition (TD), Inhalation, Drug delivery.

6.2 Introduction

Airflow dynamics and particle TD in lung airways are attracting increasing attention of researchers in biomedical engineering because of its practical application in real life. However, numerical modelling of the human lung through CFD simulations is still a challenge because of the complexity of lung geometry. To treat lung diseases in the respiratory tract, aerosol particle inhalation as drug delivery is cost-effective and has smaller side effects compared to aggressive drugs (Kuzmov and Minko 2015). The delivery of the aerosol particles through the mouth-throat, nasal and pulmonary region has been developed as non-invasive alternative routes (Longest et al. 2011, Karakosta et al. 2015). The key target of aerosol drug delivery is to maximize the particle deposition inside human lungs. To ensure the effectiveness of aerosol particle inhalation and delivery of drugs into the targeted area of respiratory airways, understanding the mechanisms of particle TD in 3D realistic anatomical lung models is essential. CFD simulations are efficient methods to ensure inhaled aerosol particles to be deposited in targeted areas of human lungs.

Studying particle inhalation and TD into human lungs is also useful to detect the cause of lung diseases like asthma, lung cancer and chronic obstructive pulmonary disease (COPD) caused by particulate matter (PM) air pollution. PM comes from different sources, e.g. industrial pollutants, burning fuels of vehicles, coal combustion and pesticide (Davidson et al. 2005, Kampa and Castanas 2008) and is often hazardous to public health. Moreover, some particles absorbed by the epithelium cells may cause respiratory diseases (Hussain, Laumbach et al. 2012), and some carcinoma and toxic particles may cause different levels of health damages depending on their residence time in the lung.

Therefore, the realistic in-vivo lung models reconstructed from computed tomography (CT)-scan data (Xiong et al. 2012, Koullapis et al. 2018, Asgari et al. 2019, Hosseini and Golshahi 2019), non-realistic in-silico lung models (Zhang et al. 2002, Rahimi-Gorji et al. 2016, Chen et al. 2018, Feng et al. 2018), and experimental (Ahookhosh et al. 2019, Farkas et al. 2019) models have been used to examine aerosol particle TD in human respiratory airways. The experimental data is normally used for validating numerical models to ensure they can be reliably used to investigating fundamental mechanisms of aerodynamics and particle TD in lungs. Many researchers have developed different types of non-realistic lung geometries, either symmetric or asymmetric, to analyze the airflow pattern (Kim and Fisher 1999, Kleinstreuer et al. 2008, Russo et al. 2008). Kleinstreuer et al. (2008) simulated airflow in a 16 generation (the number of division of trachea is called cell generation) triple bifurcation non-realistic lung model using the LRN k–ω model to investigate laminar to turbulent flow behavior in the lung. Islam et al. (2017) developed a realistic lung model with 17 generations using CT-scan data. Many studies have described the airflow dynamic and particles deposition in the deep lung airways and a few studies have investigated radioactive aerosol particles TD in the mouth-throat airway (Stahlhofen et al. 1980, Jayaraju et al. 2008, Inthavong et al. 2011, Ma et al. 2020, Zhao et al. 2020).

Chapter 6 Numerical Study of Nanoscale and Microscale Particle Transport in Realistic Lung Models With and Without Stenosis

The tracheobronchial stenosis happens when the lung airways don't grow properly during fetal development. For patients who suffer from airway stenosis, the inhalation ability of air into deep lung reduces (Noppen 2004). Stenosis in airways can be diagnosed by bronchoscope techniques such as the laser and electrocautery (Bolliger et al. 2006). Tracheal stenosis causes not only breathing difficulty but also trachea injury. Serious stenosis can cause life threating diseases like pneumonia and collagen diseases (Cebral and Summers 2004). Tsuboi et al. (2019) studied the effects of airway obstruction of the trachea wall caused by stenosis on the flow velocity and pressure losses. The result shows that the pressure changes dramatically in the stenosis section. Recently, Malvè et al. (2020) studied the healthy and stented tracheobronchial airways model based on the non-realistic (Weibel symmetric model) and realistic (CT-based) lung model to determine the particle deposition. Rajaraman et al. (2020) studied the hygroscopic particles transport and deposition with and without airway narrowing. The results show that the deposition fractions in constricted airways with narrowing are increased compared to the airways without narrowing.

Because breathing air is correlated into the pressure in human lungs, it is crucial to accurately predict the change of local pressure drop of the airways caused by stenosis, and CFD has been proved an effective and efficient method. Limited studies have been conducted to analyse airflow in tracheal stenosis airways based on non-realistic airway models (Brouns et al. 2007, Luo et al. 2007). However, CT-scan-based realistic lung models are necessary to fully understand particle TD in the mouth and tracheal branches. The airflow and particle TD in the upper part of lung airways especially mouth–throat and tracheobronchial airways has a crucial effect on particles entering deep lung airways. This study is aimed to understand the flow characteristics, pressure drop and particle deposition efficiency in CT-scanned, realistic mouth–throat and tracheobronchial airways through CFD simulations. The effect of stenosis in the right trachea branch of the lung was quantified. The contribution of diffusion and impaction

mechanisms on the particle deposition efficiency of both nanoparticles and microparticles are discussed systematically.

6.3 Numerical Method

6.3.1 Reconstructed Anatomical Model

A 3D anatomical model of the mouth-throat part and the tracheobronchial lung airways as shown in Figure 6.1 is generated based on digital CT-images of a 50-year-old person, which were provided by the Prince Charles Hospital, Brisbane, Australia. The SolidWorks software is used to reconstruct the lung airways. To study the effects of stenosis on particle TD and airflow dynamics, artificial stenosis is created at section 5 of the right lung indicated in Figure 6.1. For the convenience of discussion, the whole model is divided into parts A-J.

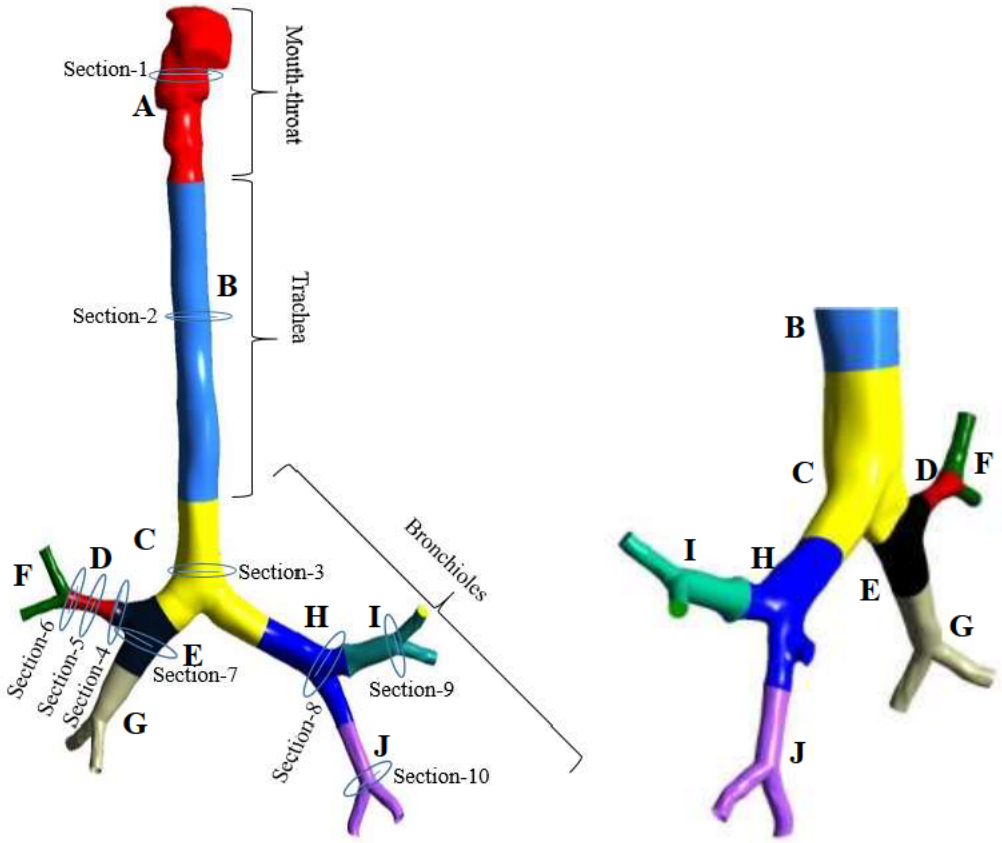

Figure 6.1. Reconstructed realistic mouth–throat and tracheobronchial airways with a stenosis on section-5. The two pictures are the same but in different views. The sections indicated in the Figure 6.1 will be referred when the results are discussed.

6.3.2 Airflow Model

The air flow in the airways of the above-mentioned lung model is solved using the software ANSYS FLUENT. The fluid flow is simulated by solving the Reynolds-averaged Navier-Stokes (RANS) equations:

$$\frac{\partial \rho}{\partial t} + \frac{\partial}{\partial x_i}(\rho u_i) = 0 \tag{6.1}$$

$$\frac{\partial}{\partial t}(\rho u_i) + \frac{\partial}{\partial x_j}(\rho u_i u_j) = -\frac{\partial p}{\partial x_i} + \frac{\partial}{\partial x_j}\left[\mu\left(\frac{\partial u_i}{\partial x_j} + \frac{\partial u_j}{\partial x_i}\right)\right] + \frac{\partial}{\partial x_j}(-\rho\overline{u_i' u_j'}) \tag{6.2}$$

where t is time, x_i (i=1,2 and 3) are the Cartesian coordinates, u_i is the fluid velocity in the x_i-direction, μ is the molecular viscosity, ρ is the air density, p is the static fluid pressure. The term $\rho\overline{u_i' u_j'}$ on the right-hand side of the equation (6.2) is the Reynolds stresses of turbulence.

In the present study, we have adopted the realisable k-ε turbulence model, which was proved to perform better than the standard k-ε model in various flow conditions including: rotating homogeneous shear flows; boundary-free shear flows; channel and flat boundary layer flows with and without pressure gradients; and backward facing step flows (Shih et al. 1995). To overcome the overprediction of turbulent energy near the wall by the k-ω turbulent model, a damping function can be used to modify the turbulence kinetic energy for the near-wall cells (Chen et al. 2016)**.** The realisable k-ε model was proved to be able to accurately predict the mean flow rate of complex lung geometries without near-wall modification near (Tian et al. 2007, Ball et al. 2008, Isa et al. 2014, Abolhassantash et al. 2020, Rahman et al. 2021).

The second-order upwind and the pressure-velocity coupling scheme are used to solve the RANS equations. A uniform distributed velocity is specified at the inlet and zero gauged pressure condition is considered for all the outlets of the lung model. The airway wall was considered stationary, and the wall surface was recognised as 'no-slip' (Islam et al. 2020).

6.3.3 Particle Transport and Deposition Model

The Lagrangian approach is applied to simulate the particle transport in human lung airways. The force balance equation of each particle motion can be represented as (Inthavong et al. 2011):

$$\frac{du_i^p}{dt} = F_{Di} + F_{gi} + F_{Bi} + F_{Li} \tag{6.3}$$

where u_i^p is particle velocity in the x_i-direction, F_{Di}, F_{gi}, F_{Bi} and F_{Li} are the drag force, gravitational force, Brownian force and Saffman's lift force, respectively. The gravitational force is calculated by

$$F_{gi} = \left(\frac{\rho_p - \rho}{\rho}\right) g_i \tag{6.4}$$

where g_i is the gravitational acceleration and ρ_p is the density of particles. The drag force is calculated by

$$F_{Di} = \frac{18\mu}{\rho_p d_p^2} C_D \frac{Re_P}{24} (u_i - u_i^p) \tag{6.5}$$

where $Re_p = \rho d_p \left|u_i^p - u_i\right| / \mu$ and the drag coefficient C_D for the spherical particles is calculated by:

$C_D = a_1 + \frac{a_2}{Re_P} + \frac{a_3}{{Re_P}^2}$ for $0 < Re_p < 10$. The Brownian force due to Brownian motion of the fluid is defined as

$$F_{Bi} = G_i \sqrt{\frac{\pi S_0}{\Delta t}} \tag{6.6}$$

where, G_i is zero mean, unit-variance independent Gaussian random number, Δt is the particle time step, and S_0 is the spectral intensity function which is related to the diffusion coefficient by:

$$S_0 = \frac{216 \nu k_B T}{\pi^2 \rho_p d_p^2 \left(\frac{\rho_p}{\rho}\right)^2 C_c} \tag{6.7}$$

where, $T = 300K$ is the absolute fluid temperature, $K_B = 1.380649 \times 10^{-23}$ J/K is the Boltzmann constant, ν is the kinematic viscosity and the Stokes-Cunningham slip correction coefficient C_c is defined as

$$C_c = 1 + \frac{2\lambda}{d_p}\left(1.257 + 0.4e^{-\left(\frac{1.1d_p}{2\lambda}\right)}\right) \tag{6.8}$$

where, $\lambda = 65$ nm is the mean free path of the gas molecules. The Saffman's lift force is calculated by:

$$F_{Li} = \frac{2K\nu^{\frac{1}{2}}\rho d_{ij}}{\rho_p d_p (d_{lk}d_{kl})^{\frac{1}{4}}}(u_j - u_j^p) \tag{6.9}$$

where, $K = 2.594$ is the constant coefficient of Saffman's lift force and $d_{ij} = (u_{i,j} - u_{j,i})/2$ is the deformation tensor.

In the simulations, 81480 spherical particles with a uniform diameter were injected randomly from the inlet boundary at one time. The particles density is 1100 kg/m^3 (Islam et al. 2020). A 'trap' condition is implemented on the airway walls for particles deposition and an escape condition is implemented at the outlets (Deng et al. 2018, Islam et al. 2018, Ghosh et al. 2020). The escape condition allows the particles go through the outlet boundary without any reflection. More specifically, the particles are trapped and stay on the surface when they touch the lung airways inner surface, instead of bouncing back.

The deposition efficiency (η_d) is defined as the percentages of the particles absorbed (trapped) on the inner surfaces of the human lung airways. It is calculated by:

$$\eta_{\mathrm{d}} = \frac{\text{Number of deposited particles in a specific region}}{\text{Number of particles entering the lung through mouth}}$$

6.4 Grid Dependency Study and Model Validation

6.4.1 Grid Dependency Study

Figure 6.2 shows the computational mesh near the asymmetric mouth-throat region, tracheobronchial region and the stenosis part of the lung airways. Ten-layer smooth inflation

was used near the wall to ensure the boundary layer flow is simulated properly. Dense mesh elements are used at the carinal angle for better resolution of near the airways wall.

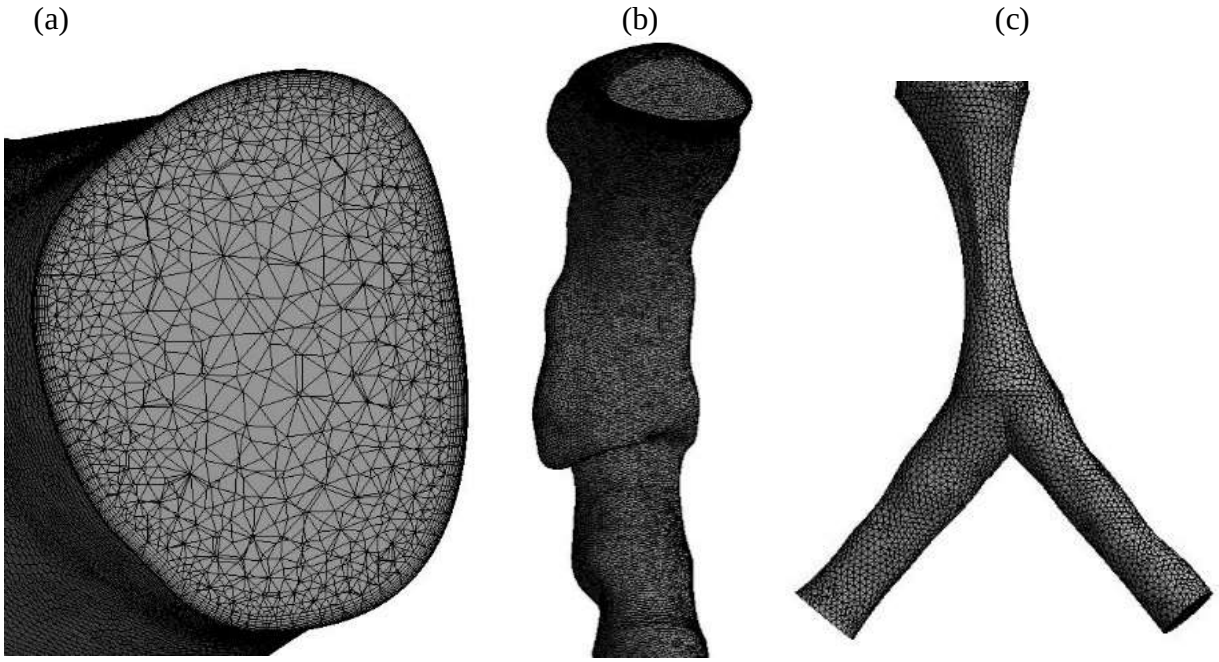

Figure 6.2. An overview mesh generation for realistic lung model, (a) Inflation layer in an airway, (b) the mouth–throat part, and (c) the mesh near the stenosis.

The grid independency test is conducted by conducting numerical simulations using 6 meshes whose cell numbers are 2056464 (Mesh-1), 2569134 (Mesh-2), 3006447 (Mesh-3), 3270843 (Mesh-4), 3809718 (Mesh-5) and 4511589 (Mesh-6), respectively. The smallest grid size of the densest mesh is 0.143mm next to the wall, and the mesh size is inversely proportional the number of elements. The results of the average velocity magnitude and the pressure on the position indicated by a circle in Figure 6.3 (a) are shown in Figure 6.3 (b) and (c), respectively, where *Y* is the direction along the diameter of the section. It can be seen that after mesh is denser than Mesh-3, an increase in the grid number makes little change on the velocity. Specifically, the velocity difference between mesh-5 and mesh-6 is about 0.01%. The velocity and total pressure converge at Mesh-5 with 3.81 million elements. Therefore, we used Mesh-5 to do all

the numerical simulations. The non-dimensional wall unit (y^+) inside the boundary layer is defined as

$$y^+ = \frac{\rho U_\tau y}{\mu} \tag{6.10}$$

where $U_\tau \left(= \sqrt{\frac{\tau_w}{\rho}}\right)$ is the friction velocity, τ_w is the wall shear stress, y (=0.143 mm) is the distance of the first layer of mesh point from the boundary. Pan et al. (2019) showed that when the y^+ value was 3.5, their solution of the RANS and LES methods for structured and unstructured meshes agreed with the experimental data. The maximum y^+ of Mesh-5 in our simulation is about 3.4 and the mesh dependency shows the solution converges at study this value of y^+.

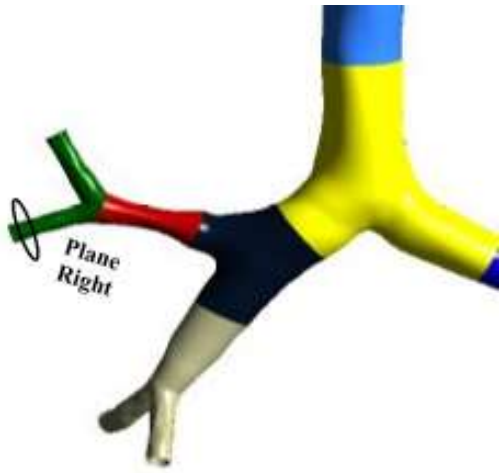

(a)

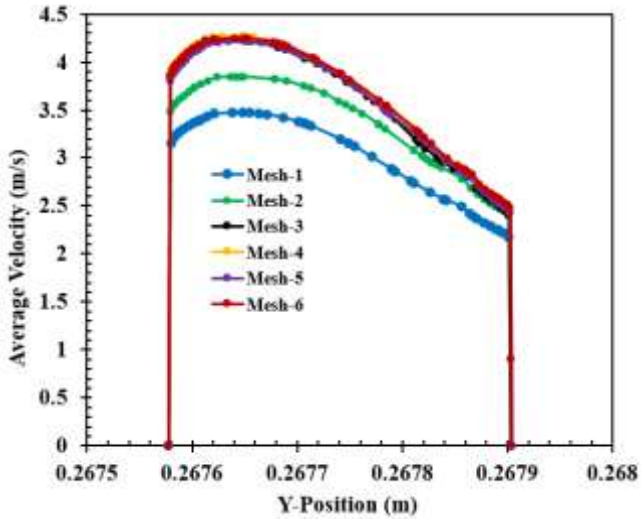

(b)

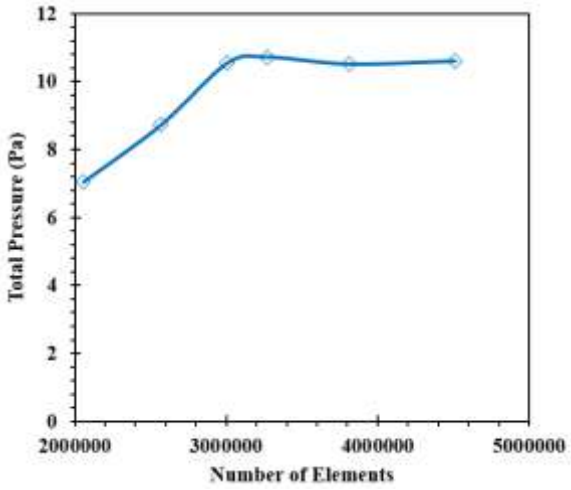

(c)

Figure 6.3. (b) Grid refinement/mesh-independent test for velocity distribution as functions of grid number α= 75% model (average velocity calculated at the selected plane in Figure 6.3 (a) of the right-side stenosis section), (c) total pressure as functions of grid number at the flow rate 60 L/min.

To demonstrate the number of particles is sufficiently large that it does not affect the deposition efficiency. Figure 6.4 shows the variation of efficiency of deposition of the whole lung model with the number of particles released at the inlet. The released particle number does

not affect the efficiency if it is above 60000. Figure 6.3 demonstrates that the particle number used in this paper (81480) is sufficiently large for converged results.

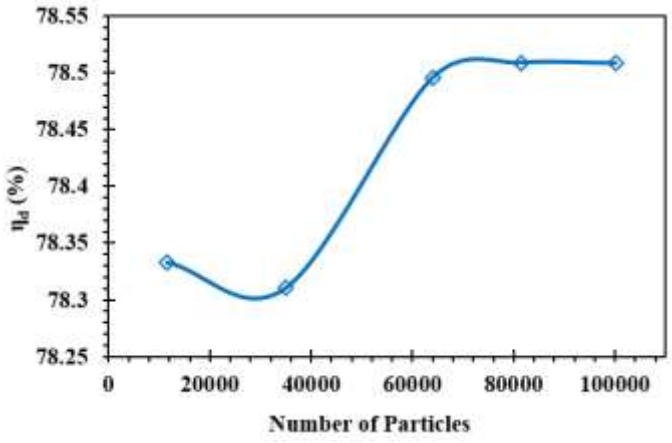

Figure 6.4. Deposition efficiency of the whole model as a function of released particles number at the flow rate of 60 L/min. The diameter of particles is 10 μm.

6.4.2 Model Validation

The present CFD method is validated against the published experimental and numerical data of particle deposition only in the mouth-throat part of a lung system, since no data are available inside realistic lung models. The calculated deposition efficiency versus particle diameter for nanoparticle simulation is shown in Figure 6.5 (b). Moreover, the particle deposition efficiency as a function of impaction parameter, $d_p^2 Q_{in}$ (μm^2·L/min) for microparticles is presented in Figure 6.5 (c), where Q_{in} is the volume flow rate, are compared with the theoretical results (Emmett et al. 1982), the experimental data (Chan and Lippmann 1980, Stahlhofen et al. 1980, Stahlhofen et al. 1983, Cheng et al. 1993, Cheng et al. 1997, Cheng et al. 1999) and the numerical results (Kleinstreuer et al. 2008, Xi and Longest 2008). It is interesting that the deposition efficiency of the nanoparticles decreases with the particle size, while that of the microparticles increases. In Figure 6.5 (c), the increasing trend of the deposition efficiency of the microparticle with the impaction parameter are in good agreement of with those in other studies, but the data from different studies are scattered. Figure 6.5 (b)

and (c) demonstrates that the present model can accurately calculate the particle TD in a realistic 3D mouth-throat and the tracheobronchial airways of a lung for both micro and nano particles.

(a) Mouth-throat part of the lung

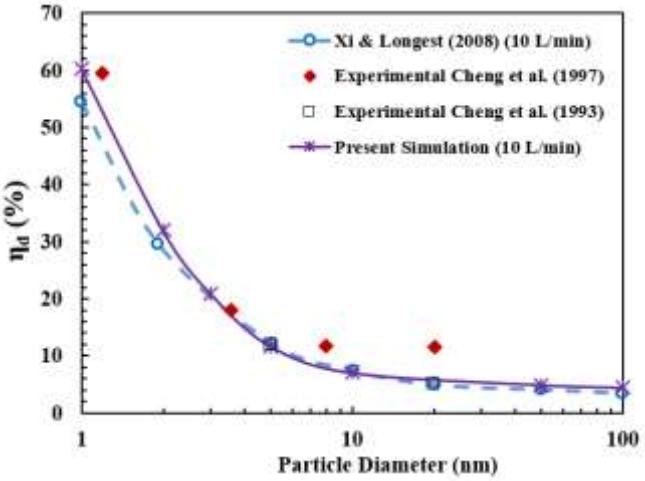

(b) Nanoparticles

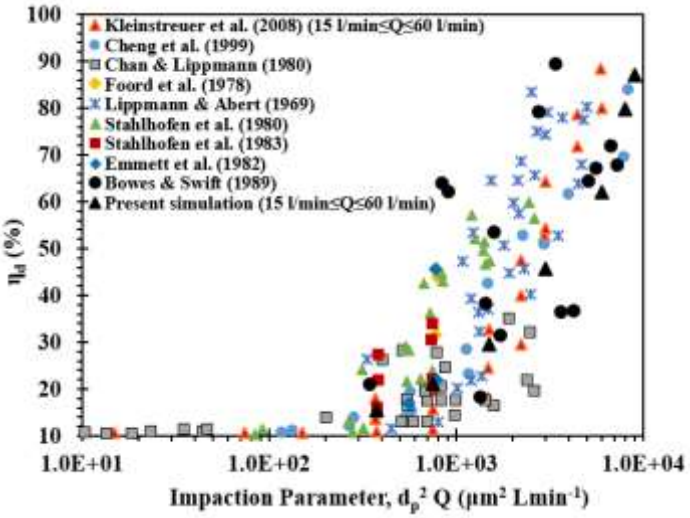

(c) Microparticles (1 μm ≤ d_p ≤ 13 μm)

Figure 6.5. Comparison between present simulations of the deposition of nanoparticles and microparticles in the mouth-throat part and results from literature (Lippmann and Albert 1969, Foord et al. 1978, Chan and Lippmann 1980, Stahlhofen et al. 1980, Emmett et al. 1982, Stahlhofen et al. 1983, Bowes III and Swift 1989, Cheng et al. 1999, Kleinstreuer et al. 2008, Xi and Longest 2008).

6.5 Results and Discussion

In the present study, the airflow dynamics and particles deposition is considered under three different flow conditions: low-level breathing (Q_{in}=15 L/min) under rest condition, light activity breathing (Q_{in}=30 L/min) under walk condition, intense breathing (Q_{in}=60 L/min) during excise (Kleinstreuer and Zhang 2003, Zhou and Cheng 2005).

6.5.1 Airflow Characteristics

Figure 6.6 (a) shows the velocity streamlines and the contours of velocity magnitude in the right lung with stenosis. The streamlines are found to be very irregular in the bifurcation areas because of the complex geometry of the airways. In addition, the streamline contraction in the stenosis area amplifies the velocity significantly in Figure 6.6 (a). The blockage effect of the air flow by the stenosis causes the velocity in narrowed down airway to increase by 72%. After the air flows through the stenosis area, the strong variation of the pressure causes some rotational streamlines in Figure 6.6 (a). Weak streamline contractions are also observed near the bifurcation areas, where one airway is divided into two. It is found later that the velocity near bifurcation areas are increased because of the streamline contraction.

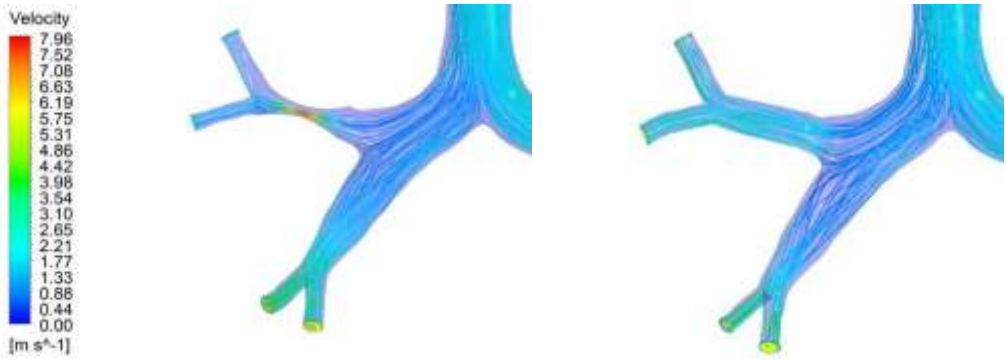

Figure 6.6. Velocity streamline at the stenosis section of 10 μm particles at flow rate 60 L/min: (a) Stenosis model, and (b) Healthy lung model.

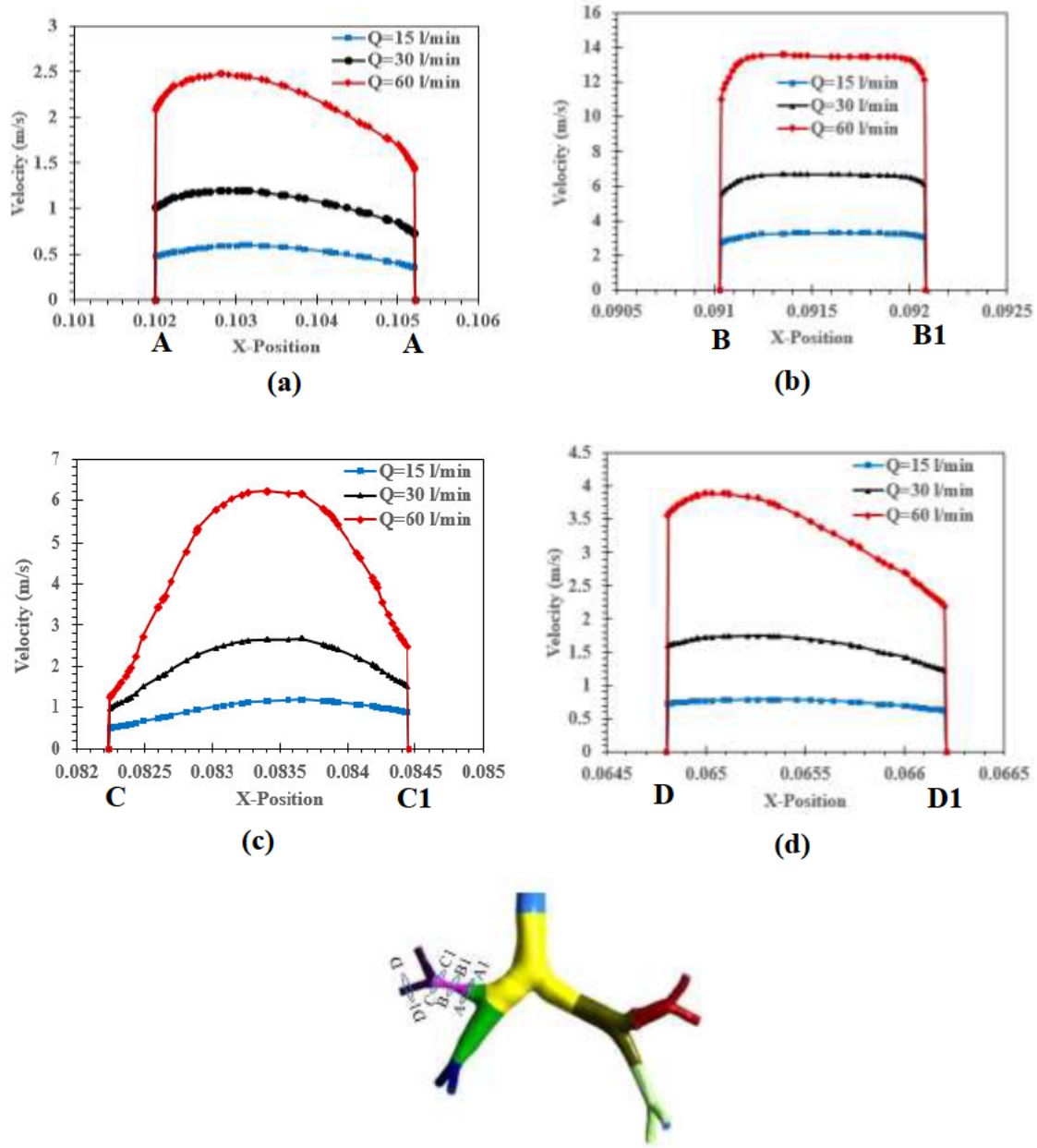

Figure 6.7. Velocity profiles at stenosis model under different flow rates, at (a) Line AA1, (b) Line BB1, (c) Line CC1, and (d) Line DD1. The lines are defined at the bottom of the Figure 6.7.

Figure 6.7 shows the velocity distribution near the stenosis along the diameter direction (X-direction) of four sections (indicated at the bottom of the Figure 6.7) in the airways at three flow rates. The velocity is increased significantly along the middle section BB1 of the stenosis (Figure 6.7 (b)). Due to the contraction, the velocity profiles in the stenosis section for different

flow rates are nearly uniform at the central part. After flow goes through the contracted area, it becomes turbulent because of sudden expansion. However, the velocity profile is an asymmetric parabolic profile, shown in Figure 6.7 (c). It can be seen in Figure 6.7 (d) that the velocity distribution in each branch becomes very non-uniform after the air goes through a bifurcation, especially at a high flow rate.

The pressures at different locations in the airways are quantified in Figure 6.8. The pressure generally decreases when air goes into the deep lune because of the energy loss, except at the stenosis section. The pressure at Section 3 is increased compared with that at section 2 mainly because of the increase of the airway diameter. Based on the Bernoulli's principle, a reduction of velocity (due to the increase of airway diameter) will cause an increase in the pressure without considering energy loss. A significant drop of pressure in the stenosis area is correlated to a big increase in the flow velocity. The pressure decreases significantly as air flows from section 1 to section 2 because the airway surface complicity between these two sections causes significant wall shear and energy loss. In the stenosis area, the pressure reduction for the stenosis model is 83% more than that of the healthy model. In addition, the pressure at all the sections (except section 5) are increased by the stenosis. Therefore, breathing air into a lung with stenosis is more difficult than a healthy lung.

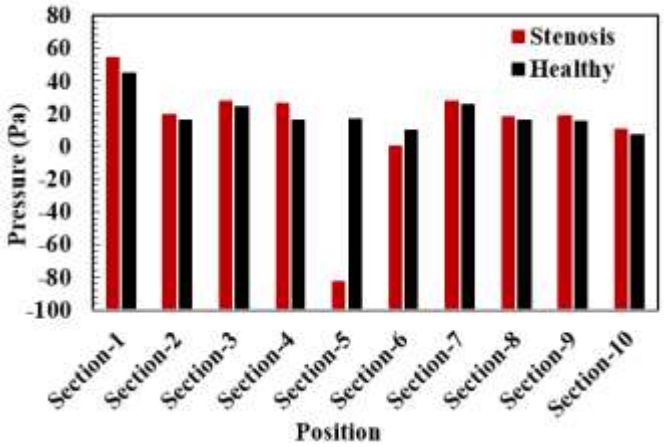

Figure 6.8. Pressure drop at different section of the two models at a flow rate 60 L/min; see Figure 6.1 for section numbers.

6.5.2 Particle Deposition

Deposition mechanisms of inhaled particles of human lungs is complicated because of the complex lung structure (Kumar et al. 2009, Islam et al. 2017, Islam, Saha et al. 2017). Particle deposition in human lung airways is mainly affected by the breathing pattern as well as particle size (Hofmann 2011). In case of slow breathing (sleeping or resting activity), the main deposition mechanism is sedimentation for large particles in micro-scale and Brownian diffusion and Saffman's lift force for nanoscale particles. It has been reported that the contribution of Saffman's lift force and Brownian diffusion is insignificant when the particle size is in the microscale (Schlesinger 1985, Darquenne 2020). As a result, some studies of microparticle TD in human lungs only consider impaction mechanism (Dehbi 2008, Naseri et al. 2017). The impaction deposition mechanism weakens if the breathing becomes slow or the particle size reduces as shown in Figure 6.5.

This study quantifies the contribution of impaction, Brownian diffusion and Saffman's lift force by conducting numerical simulations in two scenarios: (1) only impaction term is included in the particle motion equation and (2) all the impaction, diffusion and Saffman's terms are considered. Because both Brownian diffusion and Saffman's lift consider particle transport in the crossflow directions, the sum of them are referred to as diffusion term. As a result, scenarios (1) and (2) are referred to as impaction only and impaction+diffusion, respectively, in the following discussion. To find out the contribution of each mechanism under various particle sizes, both nano and micron-scale particles in the range of $5\ \text{nm} \leq d_p \leq 10\ \mu\text{m}$ are used in the simulations.

The particle deposition efficiency in the lung model and stenosis part of the lung at the flow rate of $Q_{in} = 15\ \text{L/min}$, and $60\ \text{L/min}$ are shown in Figure 6.9. The total deposition efficiency is defined as the percentage of the particles that are deposited in the whole lung

model. The total deposition efficiency (η_d) in Figure 6.9 (a) and (b) are significantly affected by both the particle diameter and the flow rate.

When the flow rate is 15 L/min and at d_p=5 nm, the particle deposition efficiency of stenosis and healthy lung models are 15.71% and 15.67%, respectively. The deposition efficiency decreases with the increase of d_p to its minimum value at d_p=500 nm. In the micro-scale (d_p>1μm), the deposition efficiency increases with the increase of particle diameter. At Q_{in}=15 L/min and d_p=10 μm, the deposition efficiency for stenosis and healthy lung models are 29.35% and 28.26%, respectively (Figure 6.9a). The particle deposition efficiency is low when the particle size is between 5nm and 500nm because both diffusion and impaction mechanisms are weak. The variation of the deposition efficiency with the particle size in Figure 6.9 is consistent with that in the validation case shown in Figure 6.5. The impaction and diffusion mechanisms are significantly affected by the combination nano-size particles and low flow rate (Zhang and Kleinstreuer 2004). If the particles are in nanoscale, the strong drag force makes them follow the streamlines and it is difficult for them to reach the airway wall. However, the Brownian and Saffman's lift forces increases with the decrease of the particle diameter and these forces could be in the crossflow direction and make the particle travel towards the airway wall. As a result, the deposition rate increases with the decrease of particle size in the nanoscale. Comparing Figure 6.9 (b) with (a), one can see that an increase in the flow rate reduces η_d in the nanoscale because diffusion becomes weaker and increases η_d in the micro-scale because impaction becomes stronger.

The deposition efficiencies of the particles with d_p=5 nm and 100 nm at Q_{in}=60 L/min is significantly decreased compared with those at Q_{in}=15 L/min because strong airflow velocity forces small particles to follow the flow direction and weakens the diffusion effect (Lu Phuong et al. 2018). Without strong crossflow diffusion, the deposition efficiency is reduced. However, the deposition efficiency of large particles (5 μm and 10 μm) at Q_{in}=60 L/min is increased

significantly compared to those at Q_{in}=15 L/min, because strong inertia effect. At locations where large-velocity streamlines changes their directions, strong inertial effect makes large particles remain its original tracks and hit the airway wall, instead of following the streamlines. This mechanism of deposition is the typical impaction mechanism. The variation trend of total deposition efficiency with particle diameter in Figure 6.9 (b) is in good agreement with that found in the literature (Darquenne et al. 1997, Koullapis et al. 2016, Ou et al. 2017).

To quantify the contribution of diffusion and impaction mechanisms to the particle TD, the ratio of the deposition efficiency calculated by considering impaction only in Eq. (6.3), which is defined as $\eta_{\mathrm{d,I}}$ to the total diffusion efficiency (η_{d} when both impaction and diffusion are considered) is shown in Figure 6.9 (c). The ratio $\eta_{\mathrm{d,I}}/\eta_{\mathrm{d}}$ is above 0.9 when d_p is greater than 1000 nm, indicating strong impaction mechanism and weak influence from diffusion. At d_{p}=5 nm and 100 nm, the contribution of the impaction was reduced to less than 60% and 70%, respectively.

How the stenosis affects deposition rates at different parts of the lung can be examined by the bar charts of deposition rates in parts A – J shown in Figure 6.10. The locations of different parts are defined in Figure 6.1. Most of the particles are deposited in mouth-throat part A. The effect of the stenosis on the deposition of microparticles with d_p=10 μm is found to be much stronger than that on the nanoparticles with d_p=5 nm in many the parts of the lung model, especially when both the particle size and flow rates are small (Figure 6.10 d). Particles are mainly deposited before and after at D-region (stenosis area) of the stenosis model due to diffusion+ impaction and impaction only mechanism (Taherian et al. 2018). The deposition rates of both sides of the lung with stenosis is increased compared with the health lung because the narrow airway's diameter increases the flow velocities. At $Q = 60$ L/min, the deposition efficiency for the stenosis and healthy lung models is very similar for nanoscale particles (5nm $\leq d_{\mathrm{p}} \leq$ 500nm) with the effect of the diffusion+ impaction and impaction only mechanism

because the small particles follow the fluid flow streamline (Figure 6.10). For the stenosis model, the flow velocity is high throughout airway D. Therefore, it has the capacity to convey particles to F, and as a result, more particles are deposited at F and E region at stenosis model. However, the flow velocity is distributed uniformly at the D region in the Healthy lung model; therefore, some particles are deposited at D-region. Hence the total deposition efficiency at the right side (C+D+E+F) stenosis region is increased with increasing particle size.

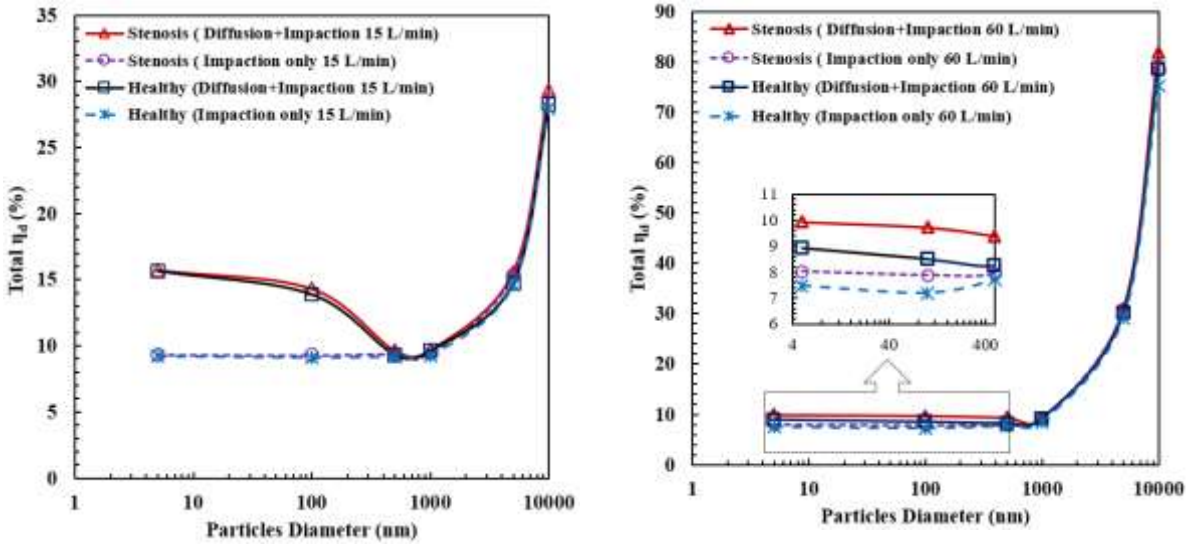

(a) (b)

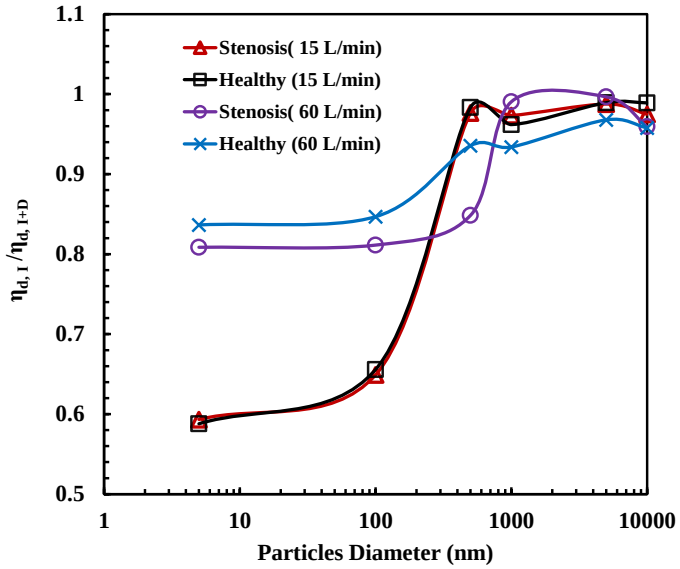

(c)

Figure 6.9. Particle deposition efficiency in the lung model. (a) Total deposition at flow rate 15 L/min; (b) Total deposition at a flow rate 60 L/min (c) Ratio of impaction only to impaction+diffusion.

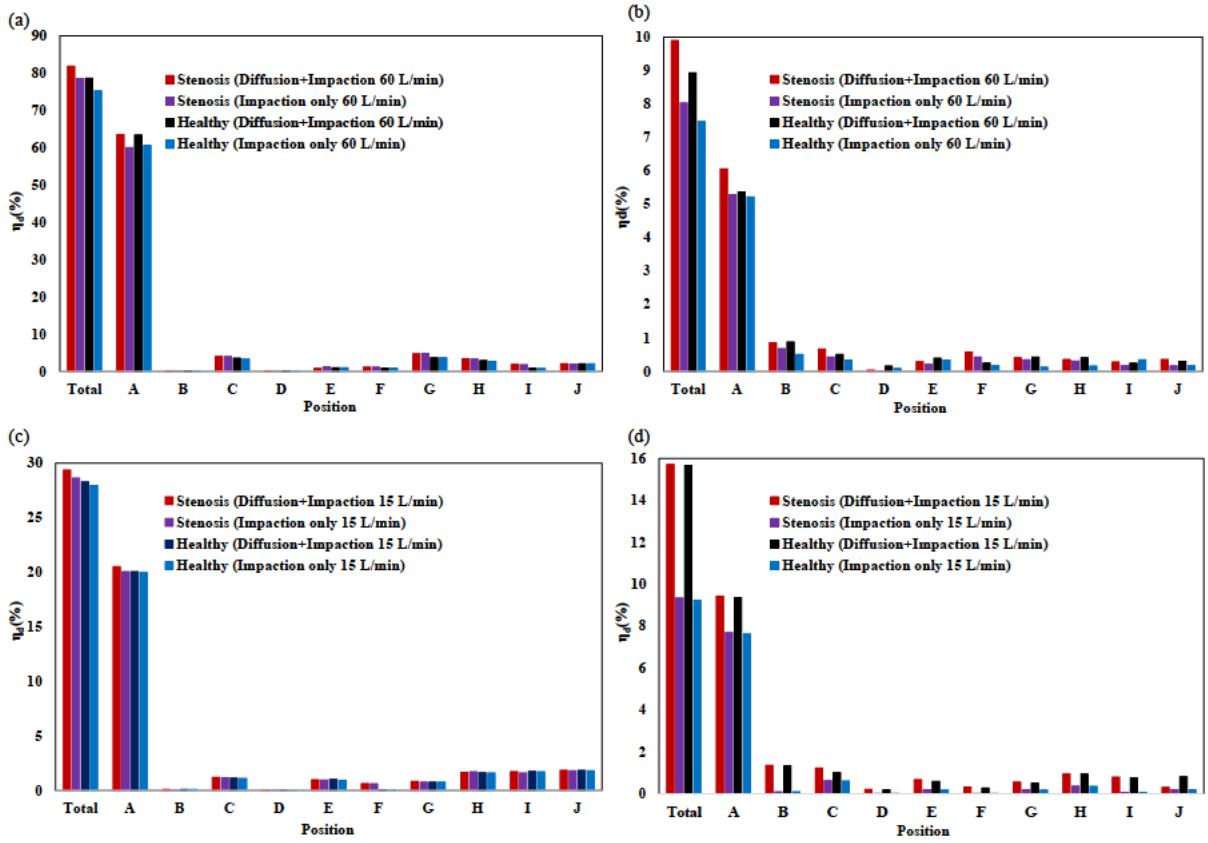

Figure 6.10. Particle deposition efficiencies at different parts of the lung defined in Figure 6.1. (a) d_p=10 µm, Flow rate=60 L/min; (b) d_p=5 nm, Flow rate=60 L/min; (c) d_p=10 µm, Flow rate=15 L/min; (d) d_p=5 nm, Flow rate=15 L/min.

Figure 6.11 (a) – (d) show the distribution of particles after they are deposited in the human lung with only the effect of impaction at the flow rate of 60 L/min, and Figure 6.11 (e) and (f) show trajectories of particles for the same flow rate. To see the particles and trajectories clearly, only 400 particles are released at the inlet for producing Figure 6.11 (e, f). The results show that 10 µm particles have higher deposition efficiency than 5 nm particles. More 10 µm particles (Figure 6.11 (a, c)) are deposited in the mouth-throat region compared to the 1 nm particles (Figure 6.11 (b, d)) due to structure of irregular complex shape lung geometry. This further proves the theory that impaction mechanism become strong as particle diameter increases. Around 9% of 5 nm size particles and approximately 79% of 10 µm size particles are deposited in the whole lung model. Small quantity of 5 nm particles are deposited in

tracheobronchial walls than 10 μm particle, because the sedimentation effect of 5 nm particles is weaker. However, the reversal flow may be happening in the stenosis area during the inhalation that would be effective for particles deposition pattern. The finding that different sized particles are deposited in the different stenosis models would help develop a targeted aerosol drug delivery method. Because very weak impaction mechanisms due to inertia effect, small particles tend to follow the curved streamlines when flow changes its direction. That is the reason why the trajectories of 5 nm particles in Figure 6.11 (e) are more curved than those of 10 μm particles in Figure 6.11 (f). A reduction in particle size increases the ability of particles to follow curved streamlines where an airway bends, bifurcates or changes its geometry, instead of hitting the inner wall of airway due to inertia mechanism. This cause reduces the change of particles depositing on the inner airway wall.

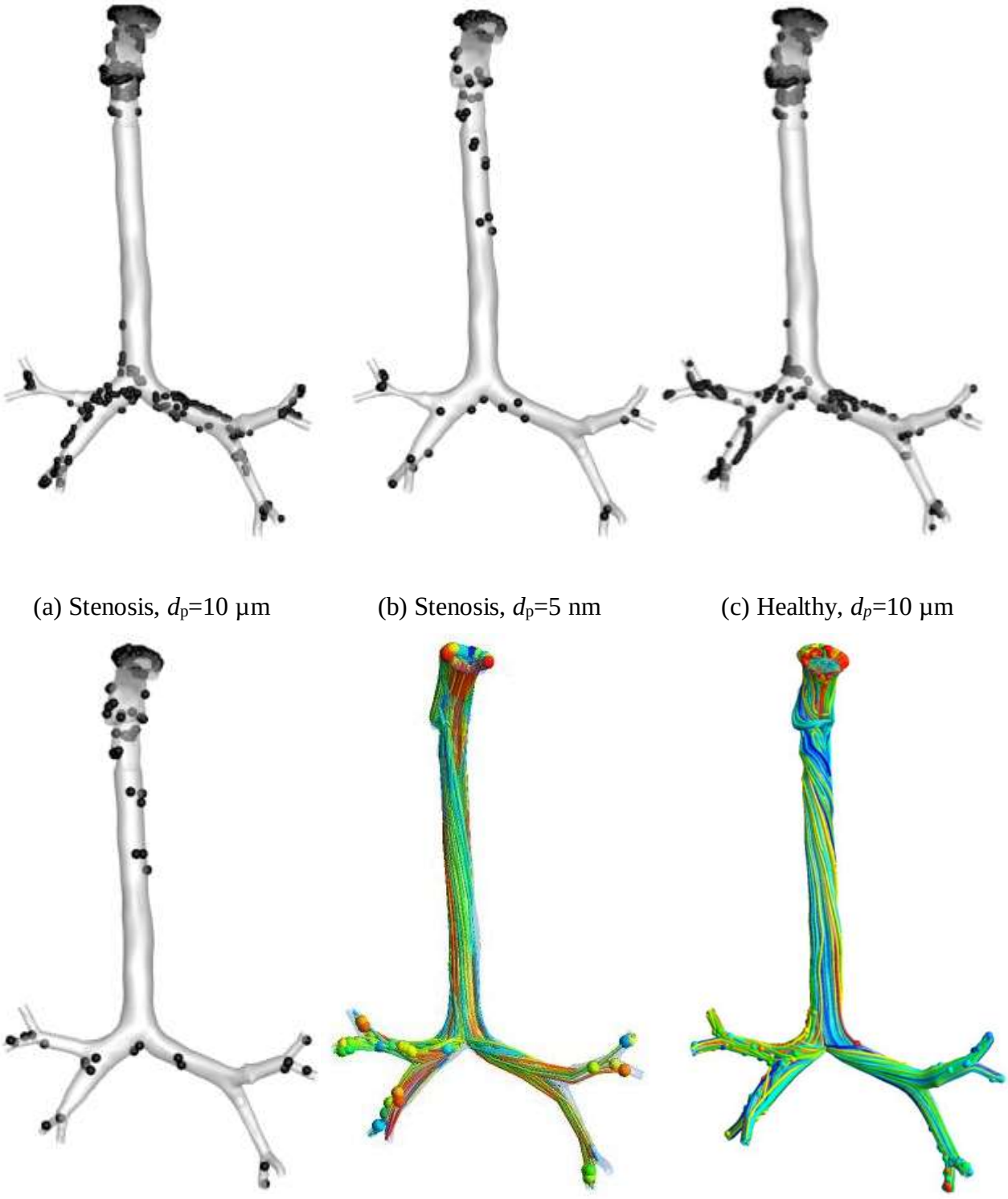

(a) Stenosis, d_p=10 µm (b) Stenosis, d_p=5 nm (c) Healthy, d_p=10 µm

(d) Healthy, d_p=5 nm (e) Healthy, d_p=10 µm (f) Healthy, d_p=5 nm

Figure 6.11. (a) – (d), Particles deposition of 10 µm particles and 5 nm particles for healthy and Stenosis lungs. (e) and (f) the trajectories of 10 µm particles and 5 nm particles for the health lung. The flow rate is 60 L/min.

The percentage of particles that escape from the outlet of the model and enters the deep lung is defined as escaping rate (defined as ηe), and it is important for the treatment of lung diseases, which usually happen in the deep lung airways. The escaping rates from the four exiting regions (each region has two outlets as indicated in Figure 6.1) are represented in Figure 6.12. In Figure 6.12 (d), the escaping rates of the small exit in region H (shown in the right picture of Figure 6.1) and region J are combined. Due to the stenosis the escaping rate at exiting region F is reduced to one-third of that of a healthy lung. The escaping rate for the stenosis model are significantly different from that for the healthy lung model in Figure 6.12 (a). The contraction of stenosis makes the flow rate towards F-region reduces and the flow rates towards G, I and H+J regions increases. As a result, the effect of stenosis on the escaping rate of exit G, I and J is opposite to that of exist F. This is because that it is difficult for the particles to go through the contraction. At nanoscale ($d_p \leq 1000$ nm), the effect of the stenosis on the escaping rate is smaller in region I but higher in region H+J. The stenosis affects the escaping rate in region I differently from in region H+J because the significant difference between the geometries of these two regions. From Figure 6.12 it can been seen that to increase the number of escaping particles that go into deep lung, the particle size needs to be reduced.

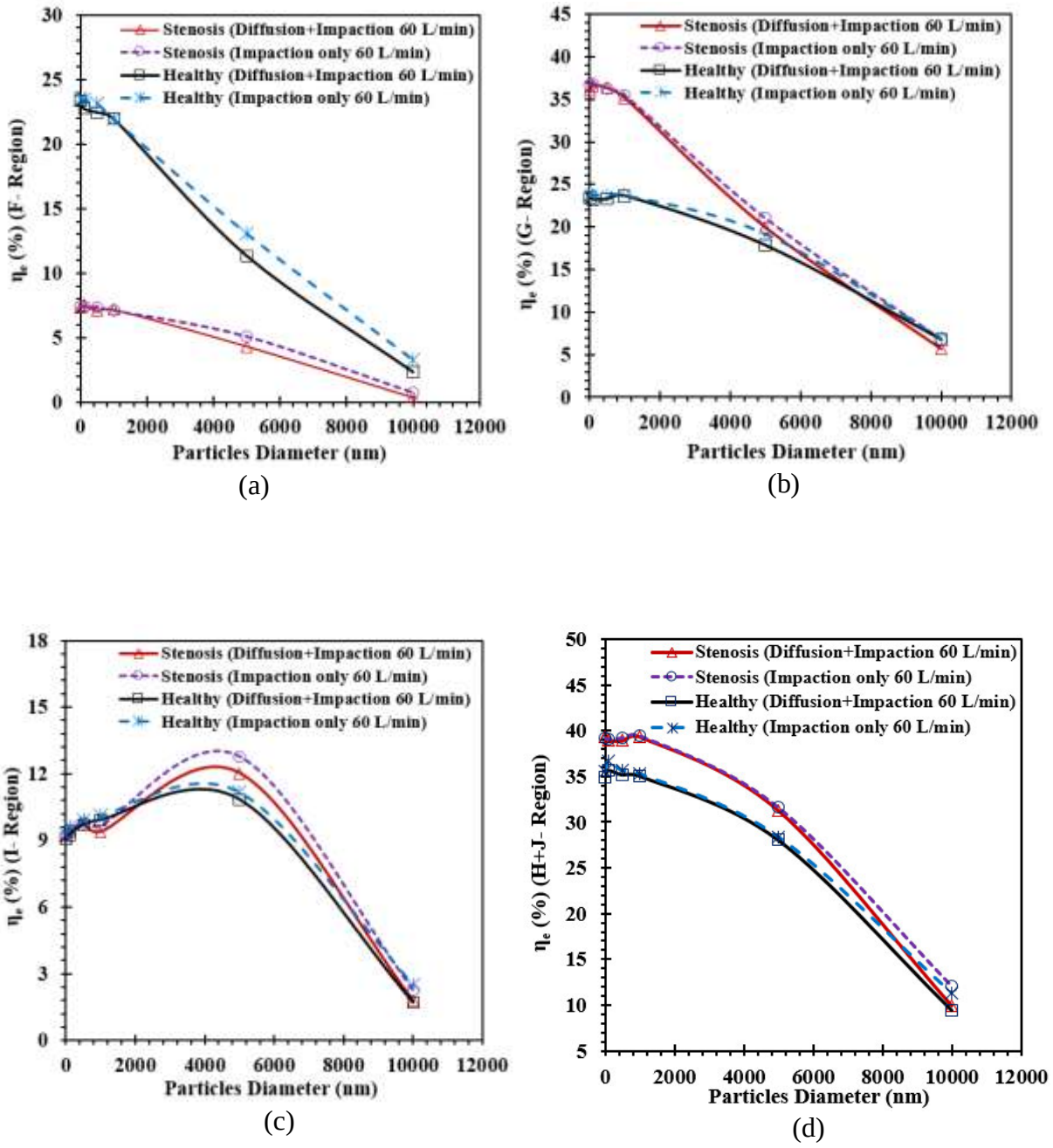

Figure 6.12. Escape rate (η_e) for 5nm ≤ d_p ≤ 10 μm particles at a flow rate 60 L/min: (a) F region, (b) G region, (c) I region, and (d) H+J region (see the region definition in Figure 6.1).

6.6 Conclusions

We investigated nano-and micro-particle TD in the mouth-throat and the tracheobronchial airways through numerical simulations. The effects of stenosis on the deposition efficiency of different particle diameters in the range of 5nm ≤ d_p ≤ 10 μm are

examined. We have considered CT scan based on two different realistic lung models. The contribution of the impaction and diffusion mechanisms is quantified by simulating the deposition considering impaction only and considering both impaction and diffusion. The knowledge of the particle TD in airways with stenosis obtained in this paper will be useful for targeted drug delivery in the clinical process. The conclusions of the study are summarized as follows.

- The streamline contraction in the stenosis area considerably amplifies the velocity in the stenosis airway increases by 72%, which is significant for assessing respiratory health risk. It is found that the pressure drop of the stenosis model increases by 83% compared to the healthy model.
- With the increase of the particle diameter, the particle deposition efficiency in the lung model increases for microparticles and decreases for the nanoparticles. When the flow rate is low (15 L/min), ultrafine particles smaller than 500nm can be significantly affected by the diffusion mechanism which has positive effect on deposition.
- At d_p=10 μm, very large percentage of the particles (over 75%) are deposited in the mouth–throat and tracheobronchial airways, resulting in a very small escaping rate. As the particle size is decreased to 5 nm, less than 10% of the particles are deposited in the airway, allowing over 90% particles to enter deeper part of the lung. The increase of the deposition rate with the increase of particle diameter in the upper lung indicates that particles must have small diameter if they are used to treat diseases in deep lung.
- The contribution of the diffusion mechanism increases with the decrease of either particle size or flow rate. The contribution of the diffusion mechanism is less than 10% as d_p=1 μm and 10 μm and Q_{in}=15 and 60 L/min. However, when the particle size is 5 nm and Q_{in}=15 L/min, the diffusion mechanism for both stenosis and healthy lung models contributes more than 60% of the total deposition.

- At Q_{in}=60 L/min, stenosis affects the deposition efficiency of different size particles differently. It reduces the deposition efficiency of nano particles and increase the deposition efficiency of microparticles. The effect of the stenosis on the total deposition efficiency is very small when the flow rate is 15 L/min.

Conflicts of Interest

The authors state no conflict of interest.

Acknowledgement

The authors would like to acknowledge the computing HPC facility and realistic lung model at UTS is gratefully acknowledged.

References

Abolhassantash, M, Tavakol, M, Abouali, O, Yaghoubi, M & Ahmadi, G 2020, 'Deposition fraction of ellipsoidal fibers in the human nasal cavity-Influence of non-creeping formulation of hydrodynamic forces and torques', *International Journal of Multiphase Flow*, vol. 126, 103238.

Ahookhosh, K, Yaqoubi, S, Mohammadpourfard, M, Hamishehkar, H & Aminfar, H 2019, 'Experimental investigation of aerosol deposition through a realistic respiratory airway replica: An evaluation for MDI and DPI performance', *International journal of pharmaceutics*, vol. 566, pp. 157-172.

Asgari, M, Lucci, F, Bialek, J, Dunan, B, Andreatta, G, Smajda, R et al. 2019, 'Development of a realistic human respiratory tract cast representing physiological thermal conditions', *Aerosol science and technology*, vol. 53, no. 8, pp. 860-870.

Ball, C, Uddin, M & Pollard, A 2008, 'High resolution turbulence modelling of airflow in an idealised human extra-thoracic airway', *Computers & Fluids*, vol. 37, no. 8, pp. 943-964.

Bolliger, C, Sutedja, T, Strausz, J & Freitag, L 2006, 'Therapeutic bronchoscopy with immediate effect: laser, electrocautery, argon plasma coagulation and stents', *European Respiratory Journal*, vol. 27, no. 6, pp. 1258-1271.

Bowes III, SM & Swift, DL 1989, 'Deposition of inhaled particles in the oral airway during oronasal breathing', *Aerosol Science and Technology*, vol. 11, no. 2, pp. 157-67.

Brouns, M, Jayaraju, ST, Lacor, C, De Mey, J, Noppen, M, Vincken, W et al. 2007, 'Tracheal stenosis: a flow dynamics study', *Journal of Applied Physiology*, vol. 102, no. 3, pp. 1178-1184.

Cebral, JR & Summers, RM 2004, 'Tracheal and central bronchial aerodynamics using virtual bronchoscopy and computational fluid dynamics', *IEEE transactions on medical imaging*, vol. 23, no. 8, pp. 1021-1033.

Chan, TL & Lippmann, M 1980, 'Experimental measurements and empirical modelling of the regional deposition of inhaled particles in humans', *Am Ind Hyg Assoc J*, vol. 41, no. 6, pp. 399-409.

Chen, C, Lin, C-H, Wei, D & Chen, Q 2016, 'Modeling particle deposition on the surfaces around a multi-slot diffuser', *Building and Environment*, vol. 107, pp. 79-89.

Chen, X, Feng, Y, Zhong, W, Sun, B & Tao, F 2018, 'Numerical investigation of particle deposition in a triple bifurcation airway due to gravitational sedimentation and inertial impaction', *Powder technology*, vol. 323, pp. 284-293.

Cheng, K-H, Cheng, Y-S, Yeh, H-C & Swift, DL 1997, 'An experimental method for measuring aerosol deposition efficiency in the human oral airway', *American Industrial Hygiene Association Journal*, vol. 58, no. 3, pp. 207-213.

Cheng, Y-S, Su, Y-F, Yeh, H-C & Swift, DL 1993, 'Deposition of thoron progeny in human head airways', *Aerosol Science and Technology*, vol. 18, no. 4, pp. 359-375.

Cheng, Y-S, Zhou, Y & Chen, BT 1999, 'Particle deposition in a cast of human oral airways', *Aerosol Science & Technology*, vol. 31, no. 4, pp. 286-300.

Darquenne, C 2020, 'Deposition mechanisms', *Journal of aerosol medicine and pulmonary drug delivery*, vol. 33, no. 4, pp. 181-185.

Darquenne, C, Paiva, M, West, JB & Prisk, GK 1997, 'Effect of microgravity and hypergravity on deposition of 0.5-to 3-μm-diameter aerosol in the human lung', *Journal of Applied Physiology*, vol. 83, no. 6, pp. 2029-2036.

Davidson, CI, Phalen, RF & Solomon, PA 2005, 'Airborne particulate matter and human health: a review', *Aerosol Science and Technology*, vol. 39, no. 8, pp. 737-749.

Dehbi, A 2008, 'Turbulent particle dispersion in arbitrary wall-bounded geometries: A coupled CFD-Langevin-equation based approach', *International Journal of Multiphase Flow*, vol. 34, no. 9, pp. 819-828.

Deng, Q, Ou, C, Chen, J & Xiang, Y 2018, 'Particle deposition in tracheobronchial airways of an infant, child and adult', *Science of the Total Environment*, vol. 612, pp. 339-346.

Emmett, P, Aitken, R & Hannan, W 1982, 'Measurements of the total and regional deposition of inhaled particles in the human respiratory tract', *Journal of Aerosol Science*, vol. 13, no. 6, pp. 549-560.

Farkas, Á, Lizal, F, Elcner, J, Jedelsky, J & Jicha, M 2019, 'Numerical simulation of fibre deposition in oral and large bronchial airways in comparison with experiments', *Journal of aerosol science*, vol. 136, pp. 1-14.

Feng, Y, Zhao, J, Kleinstreuer, C, Wang, Q, Wang, J, Wu, DH et al. 2018, 'An in silico inter-subject variability study of extra-thoracic morphology effects on inhaled particle transport and deposition', *Journal of aerosol science*, vol. 123, pp. 185-207.

Foord, N, Black, A & Walsh, M 1978, 'Regional deposition of 2.5–7.5 μm diameter inhaled particles in healthy male non-smokers', *Journal of Aerosol Science*, vol. 9, no. 4, pp. 343-357.

Ghosh, A, Islam, MS & Saha, SC 2020, 'Targeted drug delivery of magnetic nano-particle in the specific lung region', *Computation*, vol. 8, no. 1, 10.

Hofmann, W 2011, 'Modelling inhaled particle deposition in the human lung—A review', *Journal of Aerosol Science*, vol. 42, no. 10, pp. 693-724.

Hosseini, S & Golshahi, L 2019, 'An in vitro evaluation of importance of airway anatomy in sub-regional nasal and paranasal drug delivery with nebulizers using three different anatomical nasal airway replicas of 2-, 5-and 50-year old human subjects', *International journal of pharmaceutics*, vol. 563, pp. 426-436.

Hussain, S, Laumbach, R, Coleman, J, Youseff, H, Kelly-McNeil, K, Ohman-Strickland, P et al. 2012, 'Controlled exposure to diesel exhaust causes increased nitrite in exhaled breath condensate among subjects with asthma', *Journal of occupational and environmental medicine/American College of Occupational and Environmental Medicine*, vol. 54, no. 10, 1186.

Inthavong, K, Zhang, K & Tu, J 2011, 'Numerical modelling of nanoparticle deposition in the nasal cavity and the tracheobronchial airway', *Computer Methods in Biomechanics and Biomedical Engineering*, vol. 14, no. 7, pp. 633-643.

Isa, NM, Ahmad Fara, ANK & Asmuin, NZ 2014, 'Investigation on the Turbulence Models Effect of a Coal Classifier by Using Computational Fluids Dynamics', *Trans Tech Publ*, vol. 465, pp. 617-621.

Islam, MS, Gu, Y, Farkas, A, Paul, G & Saha, SC 2020, 'Helium–Oxygen Mixture Model for Particle Transport in CT-Based Upper Airways', *International Journal of Environmental Research and Public Health*, vol. 17, no. 10, 3574.

Islam, MS, Paul, G, Ong, HX, Young, PM, Gu, Y & Saha, SC 2020, 'A Review of Respiratory Anatomical Development, Air Flow Characterization and Particle Deposition', *International Journal of Environmental Research and Public Health*, vol. 17, no. 2, 380.

Islam, MS, Saha, SC, Gemci, T, Yang, IA, Sauret, E & Gu, Y 2018, 'Polydisperse microparticle transport and deposition to the terminal bronchioles in a heterogeneous vasculature tree', *Scientific reports*, vol. 8, no. 1, pp. 1-9.

Islam, MS, Saha, SC, Sauret, E, Gemci, T & Gu, Y 2017, 'Pulmonary aerosol transport and deposition analysis in upper 17 generations of the human respiratory tract', *Journal of Aerosol Science*, vol. 108, pp. 29-43.

Islam, MS, Saha, SC, Sauret, E, Gemci, T, Yang, IA & Gu, Y 2017, 'Ultrafine particle transport and deposition in a large scale 17-generation lung model', *Journal of biomechanics*, vol. 64, pp. 16-25.

Jayaraju, S, Brouns, M, Lacor, C, Belkassem, B & Verbanck, S 2008, 'Large eddy and detached eddy simulations of fluid flow and particle deposition in a human mouth–throat', *Journal of Aerosol Science*, vol. 39, no. 10, pp. 862-875.

Kampa, M & Castanas, E 2008, 'Human health effects of air pollution', *Environmental pollution*, vol. 151, no. 2, pp. 362-367.

Karakosta, P, Alexopoulos, AH & Kiparissides, C 2015, 'Computational model of particle deposition in the nasal cavity under steady and dynamic flow', *Computer Methods in Biomechanics and Biomedical Engineering*, vol. 18, no. 5, pp. 514-526.

Kim, CS & Fisher, DM 1999, 'Deposition characteristics of aerosol particles in sequentially bifurcating airway models', *Aerosol Science & Technology*, vol. 31, no. 2-3, pp. 198-220.

Kleinstreuer, C & Zhang, Z 2003, 'Laminar-to-turbulent fluid-particle flows in a human airway model', *International Journal of Multiphase Flow*, vol. 29, no. 2, pp. 271-289.

Kleinstreuer, C, Zhang, Z & Li, Z 2008, 'Modeling airflow and particle transport/deposition in pulmonary airways', *Respiratory physiology & neurobiology*, vol. 163, no. 1-3, pp. 128-138.

Kleinstreuer, C, Zhang, Z, Li, Z, Roberts, WL & Rojas, C 2008, 'A new methodology for targeting drug-aerosols in the human respiratory system', *International Journal of Heat and Mass Transfer*, vol. 51, no. 23-24, pp. 5578-5589.

Koullapis, P, Kassinos, SC, Bivolarova, MP & Melikov, AK 2016, 'Particle deposition in a realistic geometry of the human conducting airways: Effects of inlet velocity profile, inhalation flowrate and electrostatic charge', *Journal of biomechanics*, vol. 49, no. 11, pp. 2201-2212.

Koullapis, P, Kassinos, SC, Muela, J, Perez-Segarra, C, Rigola, J, Lehmkuhl, O et al. 2018, 'Regional aerosol deposition in the human airways: The SimInhale benchmark case and a critical assessment of in silico methods', *European Journal of Pharmaceutical Sciences*, vol. 113, pp. 77-94.

Kumar, H, Tawhai, MH, Hoffman, EA & Lin, C-L 2009, 'The effects of geometry on airflow in the acinar region of the human lung', *Journal of biomechanics*, vol. 42, no. 11, pp. 1635-1642.

Kuzmov, A & Minko, T 2015, 'Nanotechnology approaches for inhalation treatment of lung diseases', *Journal of controlled release*, vol. 219, pp. 500-518.

Lippmann, M & Albert, RE 1969, 'The effect of particle size on the regional deposition of inhaled aerosols in the human respiratory tract', *American Industrial Hygiene Association Journal*, vol. 30, no. 3, pp. 257-275.

Longest, PW, Tian, G & Hindle, M 2011, 'Improving the lung delivery of nasally administered aerosols during noninvasive ventilation—an application of enhanced condensational

growth (ECG)', *Journal of aerosol medicine and pulmonary drug delivery*, vol. 24, no. 2, pp. 103-118.

Lu Phuong, N, Dang Khoa, N, Inthavong, K & Ito, K 2018, 'Particle and inhalation exposure in human and monkey computational airway models', *Inhalation toxicology*, vol. 30, no. 11-12, pp. 416-428.

Luo, H, Liu, Y & Yang, X 2007, 'Particle deposition in obstructed airways', *Journal of biomechanics*, vol. 40, no. 14, pp. 3096-3104.

Ma, B, Kourmatzis, A, Zhao, Y, Yang, R, Chan, H-K, Salehi, F et al. 2020, 'Potential effects of lingual fats on airway flow dynamics and particle deposition', *Aerosol science and technology*, vol. 54, no. 3, pp. 321-331.

Malvè, M, Sánchez-Matás, C & López-Villalobos, JL 2020, 'Modelling Particle Transport and Deposition in the Human Healthy and Stented Tracheobronchial Airways', *Annals of Biomedical Engineering*, pp. 1-16.

Naseri, A, Shaghaghian, S, Abouali, O & Ahmadi, G 2017, 'Numerical investigation of transient transport and deposition of microparticles under unsteady inspiratory flow in human upper airways', *Respiratory physiology & neurobiology*, vol. 244, pp. 56-72.

Noppen, M 2004, 'Airway injury and sequelae: conservative view', *Eur Respir Mon*, vol. 29, pp. 234-245.

Ou, C, Li, Y, Wei, J, Yen, H-L & Deng, Q 2017, 'Numerical modeling of particle deposition in ferret airways: A comparison with humans', *Aerosol science and technology*, vol. 51, no. 4, pp. 477-487.

Pan, Y, Lin, C-H, Wei, D & Chen, C 2019, 'Experimental measurements and large eddy simulation of particle deposition distribution around a multi-slot diffuser', *Building and Environment*, vol. 150, pp. 156-163.

Rahimi-Gorji, M, Gorji, TB & Gorji-Bandpy, M 2016, 'Details of regional particle deposition and airflow structures in a realistic model of human tracheobronchial airways: two-phase flow simulation', *Computers in biology and medicine*, vol. 74, pp. 1-17.

Rahman, MM, Zhao, M, Islam, MS, Dong, K & Saha, SC 2021, 'Aging effects on airflow distribution and micron-particle transport and deposition in a human lung using CFD-DPM approach', *Advanced Powder Technology*, vol. 32, no. 10, pp. 3506-3516.

Rajaraman, PK, Choi, J, Hoffman, EA, O'Shaughnessy, PT, Choi, S, Delvadia, R et al. 2020, 'Transport and deposition of hygroscopic particles in asthmatic subjects with and without airway narrowing', *Journal of aerosol science*, vol. 146, 105581.

Russo, J, Robinson, R & Oldham, MJ 2008, 'Effects of cartilage rings on airflow and particle deposition in the trachea and main bronchi', *Medical engineering & physics*, vol. 30, no. 5, pp. 581-589.

Schlesinger, RB 1985, 'Comparative deposition of inhaled aerosols in experimental animals and humans: a review', *Journal of Toxicology and Environmental Health, Part A Current Issues*, vol. 15, no. 2, pp. 197-214.

Shih, TH, Liou, WW, Shabbir, A, Yang, Z & Zhu, J 1995, 'A new k-ϵ eddy viscosity model for high reynolds number turbulent flows', *Computers and Fluids*, vol. 24, no. 3, pp. 227-238.

Stahlhofen, W, Gebhart, J & Heyder, J 1980, 'Experimental determination of the regional deposition of aerosol particles in the human respiratory tract', *American Industrial Hygiene Association Journal*, vol. 41, no. 6, pp. 385-398.

Stahlhofen, W, Gebhart, J, Heyder, J & Scheuch, G 1983, 'New regional deposition data of the human respiratory tract', *Journal of Aerosol Science*, vol. 14, no. 3, pp. 186-188.

Taherian, S, Rahai, H, Bonifacio, J, Gomez, B & Waddington, T 2018, 'Particulate deposition in a patient with tracheal stenosis', *Journal of Engineering and Science in Medical Diagnostics and Therapy*, vol. 1, no. 1, 011005.

Tian, Z, Tu, J & Yeoh, G 2007, 'CFD studies of indoor airflow and contaminant particle transportation', *Particulate Science and Technology*, vol. 25, no. 6, pp. 555-570.

Tsuboi, N, Matsumoto, S, Nishimura, N, Nakagawa, S & Kobayashi, H 2019, 'Fluid dynamics approach to airway obstruction', *Medical hypotheses*, vol. 132, 109341.

Xi, J & Longest, P 2008, 'Effects of oral airway geometry characteristics on the diffusional deposition of inhaled nanoparticles', *Journal of biomechanical engineering*, vol. 130, no. 1, 011008.

Xiong, T, Ilmi, H, Hoarau, Y, Choquet, P, Goetz, C, Fouras, A et al. 2012, 'Flow and particles deposition in anatomically realistic airways', *Computer Methods in Biomechanics and Biomedical Engineering*, vol. 15, no. sup1, pp. 56-58.

Zhang, Z & Kleinstreuer, C 2004, 'Airflow structures and nano-particle deposition in a human upper airway model', *Journal of computational physics*, vol. 198, no. 1, pp. 178-210.

Zhang, Z, Kleinstreuer, C & Kim, C 2002, 'Computational analysis of micron-particle deposition in a human triple bifurcation airway model', *Computer Methods in Biomechanics & Biomedical Engineering*, vol. 5, no. 2, pp. 135-147.

Zhao, Y, Raco, J, Kourmatzis, A, Diasinos, S, Chan, H-K, Yang, R et al. 2020, 'The effects of upper airway tissue motion on airflow dynamics', *Journal of biomechanics*, vol. 99, 109506.

Zhou, Y & Cheng, Y-S 2005, 'Particle deposition in a cast of human tracheobronchial airways',

Aerosol science and technology, vol. 39, no. 6, pp. 492-500.

Chapter 7: Numerical Study of Nano and Micro Pollutant Particle Transport and Deposition in Realistic Human Lung Airways

This chapter presents a final accepted version paper published in 2022, Powder Technology, 402, 117364. The first page of the published paper was shown at the beginning of the chapter, followed by the accepted version.

Chapter 7 Numerical Study of Nano and Micro Pollutant Particle Transport and Deposition in Realistic Human Lung Airways

Powder Technology 402 (2022) 117364

Contents lists available at ScienceDirect

Powder Technology

journal homepage: www.elsevier.com/locate/powtec

Numerical study of nano and micro pollutant particle transport and deposition in realistic human lung airways

M. Rahman [a,b], Ming Zhao [a,*], Mohammad S. Islam [c], Kejun Dong [d], Suvash C. Saha [c]

[a] School of Engineering, Design and Built Environment, Western Sydney University, Penrith, NSW 2751, Australia
[b] Department of Mathematics, Faculty of Science, Islamic University, Kushtia 7003, Bangladesh
[c] School of Mechanical and Mechatronic Engineering, University of Technology Sydney, Ultimo, NSW 2007, Australia
[d] Center for Infrastructure Engineering, Western Sydney University, Penrith, NSW 2751, Australia

ARTICLE INFO

Article history:
Received 22 January 2022
Received in revised form 14 March 2022
Accepted 3 April 2022
Available online 07 April 2022

Keywords:
Airflow
Traffic particle
Smoke particle
Dust particle
Human lungs
Drug delivery
Physical activity
Deposition mechanism

ABSTRACT

For respiratory health risk assessment, it is essential to evaluate the transportation and deposition (TD) of pollutant particles in human lung airways, which are responsible for lung diseases. Studies to date improved the knowledge of the particle TD in airways. However, the understanding of the TD of different pollutant particles in realistic airways has not been fully understood. This study investigates TD of three types of pollutant particles: traffic, smoke and dust, with various sizes ranging from nano- to micro-scales in the mouth–throat and tracheobronchial lung airways of a human lung using computational fluid dynamics (CFD). Three different physical activities are considered: sleeping, resting, and intense breathing, corresponding to inhalation flow rates of Q_{in} = 15, 30 and 60 L/min, respectively. Nearly 99.8% of 10-μm traffic particles are deposited in the upper lung airways considered here. However, the TD efficiency of 10-μm dust particles is reduced to 64.28% due to the reduction in particle density. Nanoparticles have a much smaller deposition efficiency than microparticles because impaction effect of microparticles is stronger. Only less than 10% of 5-nm traffic particles are deposited in the airways for all three flow rates, allowing over 90% of particles to reach the deep lung. An important finding is that the effects of density on the particle TD of nanoparticles are much weaker than that of microparticles. At 15 L/min flow rate, the difference between the deposition efficiencies of the heaviest traffic particles and the lightest dust particles is only 3.5%. The effects of particle density on the deposition efficiencies of nano- and micro-particles are different from each other because impaction and diffusion dominate the TD of nano- and micro-particles, respectively. Density only affects impaction significantly but has little effect on diffusion.

1. Introduction

Pollutant particles or Particulate matter (PM) of varying sizes, coming from diverse sources, inhaled into human lungs, affect respiratory health globally [1,2]. PM is a complex mixture of solid and liquid particles suspended in the air that can be carried far distances by the wind. Hazardous PM damages human health after it is inhaled into the human lungs and further enters the blood circulation system [3,4]. Some of the particles absorbed by epithelial cells can induce respiratory diseases such as asthma, lung cancer, and chronic obstructive pulmonary disease [5,6]. According to the global burden of disease, air pollution is responsible for 3.1 million premature deaths and 3.2% of worldwide disability-adjusted life each year [7,8]. Since 1990, ambient PM has been placed 6th among 79 risk factors in the worldwide burden of human diseases [9].

Because of its huge hazard to human health, pollutant-related particle emission has been a significant source of worry in recent years [10]. The risk is dependent on the size of pollutant particles. Fine particles may pose a significant threat to people because of their potential to penetrate deep into the lungs and lung cell membranes [11,12], and affect the entire organ system, including the brain [13,14]. Fine particles have been demonstrated to be more hazardous than larger particles [11,15].

Large/coarse pollutant particles (2.5–10 μm) produced by crustal material may cause morbidity and mortality [16,17]. However, they have not been shown to have any substantial negative health impacts in several epidemiological research [18,19]. However, other studies have discovered that the damage of large pollutant particles on health is much more serious than or at least as powerful as fine pollutants [20,21].

Diesel and compressed natural gas (CNG) engines create the most ultrafine traffic particles [22]. Most diesel particles are in the 1 nm to 1 μm range [23]. The large surface area of diesel particles allows them to absorb a wide range of hazardous, genetic, and carcinogenic substances [24]. Diesel particle exposure can lead to coughs, itchy or burning eyes, and

* Corresponding author.
E-mail address: m.zhao@westernsydney.edu.au (M. Zhao).

https://doi.org/10.1016/j.powtec.2022.117364
0032-5910/

Numerical study of nano and micro pollutant particle transport and deposition in realistic human lung airways

Md. M. Rahman [1, 2], Ming Zhao [1, *], Mohammad S. Islam [3], Kejun Dong [4], and Suvash C. Saha [3]

[1] School of *Engineering*, Design and Built Environment, Western Sydney University, Penrith, NSW 2751, Australia.

[2] Department of Mathematics, Faculty of Science, Islamic University, Kushtia-7003, Bangladesh.

[3] School of Mechanical and Mechatronic Engineering, University of Technology Sydney, Ultimo, NSW 2007, Australia.

[4] Center for Infrastructure Engineering, Western Sydney University, Penrith, NSW 2751, Australia.

***Correspondence author:** M.Zhao@westernsydney.edu.au

7.1 Abstract

For respiratory health risk assessment, it is essential to evaluate the transportation and deposition (TD) of pollutant particles in human lung airways, which are responsible for lung diseases. Studies to date improved the knowledge of the particle TD in airways. However, the understanding of the TD of different pollutant particles in realistic airways has not been fully understood. This study investigates TD of three types of pollutant particles: traffic, smoke and dust, with various sizes ranging from nano- to micro-scales in the mouth–throat and tracheobronchial lung airways of a human lung using computational fluid dynamics (CFD). Three different physical activities are considered: sleeping, resting, and intense breathing, corresponding to inhalation flow rates of Q_{in}= 15, 30 and 60 L/min, respectively. Nearly 99.8% of 10-µm traffic particles are deposited in the upper lung airways considered here. However, the TD efficiency of 10-µm dust particles is reduced to 64.28% due to the reduction in particle density. Nanoparticles have a much smaller deposition efficiency than microparticles because impaction effect of microparticles is stronger. Only less than 10% of 5-nm traffic particles are deposited in the airways for all three flow rates, allowing over 90% of particles to reach the deep lung. An important finding is that the effects of density on the particle TD of nanoparticles

are much weaker than that of microparticles. At 15 L/min flow rate, the difference between the deposition efficiencies of the heaviest traffic particles and the lightest dust particles is only 3.5%. The effects of particle density on the deposition efficiencies of nano- and micro-particles are different from each other because impaction and diffusion dominate the TD of nano- and micro-particles, respectively. Density only affects impaction significantly but has little effect on diffusion.

Keywords: Airflow, Traffic particle, Smoke particle, Dust particle, Human Lungs, Drug delivery, Physical activity, Deposition mechanism

7.2 Introduction

Pollutant particles or Particulate matter (PM) of varying sizes, coming from diverse sources, inhaled into human lungs, affect respiratory health globally (Pražnikar and Pražnikar 2012, Kim et al. 2015). PM is a complex mixture of solid and liquid particles suspended in the air that can be carried far distances by the wind. Hazardous PM damages human health after it is inhaled into the human lungs and further enters the blood circulation system (Anderson et al. 2012, Patra et al. 2016). Some of the particles absorbed by epithelial cells can induce respiratory diseases such as asthma, lung cancer, and chronic obstructive pulmonary disease (Borghardt et al. 2018, Tahery et al. 2021). According to the global burden of disease, air pollution is responsible for 3.1 million premature deaths and 3.2 % of worldwide disability-adjusted life each year (Olaniyan et al. 2015, Collaborators and Ärnlöv 2020). Since 1990, ambient PM has been placed 6th among 79 risk factors in the worldwide burden of human diseases (Cohen et al. 2017).

Because of its huge hazard to human health, pollutant-related particle emission has been a significant source of worry in recent years (Manisalidis et al. 2020). The risk is dependent on

the size of pollutant particles. Fine particles may pose a significant threat to people because of their potential to penetrate deep into the lungs and lung cell membranes (Albrecht et al. 2006, Schraufnagel 2020), and affect the entire organ system, including the brain (Donaldson, Li et al. 1998, Gao and Sang 2020). Fine particles have been demonstrated to be more hazardous than larger particles (Oberdörster 2000, Schraufnagel 2020).

Large/coarse pollutant particles (2.5-10 μm) produced by crustal material may cause morbidity and mortality (Peng et al. 2008, Diao, Holloway et al. 2019). However, they have not been shown to have any substantial negative health impacts in several epidemiological research (Donaldson et al. 2001, Englert 2004). However, other studies have discovered that the damage of large pollutant particles on health is much more serious than or at least as powerful as fine pollutants (Brunekreef and Forsberg 2005, Charron and Harrison 2005).

Diesel and compressed natural gas (CNG) engines create the most ultrafine traffic particles (Hammond et al. 2007). Most diesel particles are in the 1 nm to 1 μm range (de Sarabia et al. 2003). The large surface area of diesel particles allows them to absorb a wide range of hazardous, genetic, and carcinogenic substances (Zhao and Castranova 2011). Diesel particle exposure can lead to coughs, itchy or burning eyes, and neuropsychiatric symptoms such as headache, vomiting, nausea, complicated breathing, chest tightness, and wheezing. (Ritchie et al. 2003). On the other hand, biomass burning due to bushfire smoke and smoke from planned burns releases a large amount of PM that is very hazardous to human health (Johnston et al. 2019). These microscopic particles can spread throughout the distal lung areas, causing illnesses at chronic cardio pulmonary. Long-term exposure to such fine particles has been associated with higher mortality risk. In addition, human lungs are severely harmed by cigarette smoke particles (CSP) (Ravindra et al. 2001). Usage of Tobacco emits 5.2 million tonnes of methane and 2.6 million tonnes of CO_2 into the environment (Buchanan and Honey 1994). Around 7000 compounds have been found in cigarettes and other tobacco products, 250 of which are harmful

to people and 70 of which are carcinogenic to humans (Drummond and Upson 2014). This is because of inducing epithelial cell mutagenesis and so biologically caused cancers. Smoking is still a significant cause of mortality and disability worldwide (Ferrucci et al. 1999).

Coarse dust particles (>10 μm) usually lodge in the upper respiratory tract after being inhaled. Toxic dust particles pose a health risk regardless of where they lodge in the respiratory system. The dust particle (<10 μm) may stay suspended in the environment for weeks, and they can penetrate the deep lung airways (Derbyshire 2007). The finer (≤4 μm) dust particles are inhaled and eventually deposit in the pulmonary alveoli, causing chronic lung disease. Particles appear to be rapidly absorbed and deposited in the lung alveolar region (Bakand et al. 2012). The deposition of inhaled particles in human lungs is influenced by several parameters, including exposure concentration and particle parameters such as size, density, shape, and individual breathing conditions (Stuart 1984). Particle deposition in the lungs is usually governed by inertial impaction, gravity sedimentation, and diffusion mechanism (Choi and Kim 2007). In addition, particle size grows, and hygroscopic growth influences particle deposition, causing particles to deposit in the respiratory tract (Asgharian 2004).

Inhalation of aerosol particles is an efficient medicine delivery system in the treatment of lung illnesses (Azarmi et al. 2008, Nassimi et al. 2010). As a result, the dynamics of particle deposition in human lung airways are essential for human health to assess the efficacy of inhaled medicine therapy and the health implications of air pollution (Deng et al. 2018). Therefore, many researchers have attempted to characterise particle deposition in the human lung, from total to local depositions (Balásházy et al. 2003, Chen et al. 2012) and with findings ranging from empirical to numerical models (Hofmann 2011, Chen et al. 2018, Bui et al. 2020). Particles coming from various sources have a variety of sizes and chemical compositions (Leoni et al. 2018). Several studies on the impact of particle size on deposition have found that finer particles

are more likely to be deposited in the deep lung airways (Asgharian and Price 2007, Moller et al. 2008). However, few studies have considered pollutant particles with different densities.

This study aims to quantify the deposition of particles with various densities and various sizes in human lungs under different breath conditions so that health risks related to particle exposure from various sources may be assessed. Airflow and particle deposition in a human lung are simulated numerically by CFD. We investigated the effects of both size and density of particles for calculating the deposition efficiency (DE) in a realistic human lung airway. Especially, we analyse three typical forms of pollutant particles: traffic, smoke, and dust, and analyse which particles are deposited in which part of lung airways. We also separated the contributions of inertial impaction and Brownian diffusion from each other to find out the fundamental mechanisms of particle deposition. The outcomes of this study will provide quantitative knowledge of how pollutant particle TD in the human lung airways is affected by particle size, density, and physical activity.

Nomenclatures

p	Fluid pressure	ρ	Air density
T	Fluid temperature	ρ_p	Particle density
D	Hydraulic diameter	μ	Molecular viscosity
$\mathrm{S_t}$	Stokes number	Δt	Particle time step
Q_{in}	Flow rate	G_i	Gaussian random number
$\mathrm{u_i^p}$	Particle velocity	S_0	Spectral intensity function
d_{p}	Particle diameter	ν	kinematic viscosity
u_i	Fluid velocity	K_B	Boltzmann constant
Re_P	Particle Reynolds number	C_c	Stokes-Cunningham
F_{Di}	Drag force	λ	Gas molecules' mean free path
$\mathrm{F_{gi}}$	Gravitational force	d_{ij}	Deformation tensor
F_{Bi}	Brownian force	η_{d}	Deposition efficiency
F_{Li}	Saffman's lift force	U_τ	Friction velocity
$\mathrm{C_D}$	Drag coefficient	τ_w	Wall shear stress
u_0	Fluid inlet velocity	η_{e}	Escaping rate

7.3 Numerical Method

The breathing pattern, particle shape, and particle size are the key factors that influence particle deposition in human lung airways (Yousefi et al. 2017, Ou et al. 2020, Xu et al. 2020). Diffusion and sedimentation are the primary deposition mechanisms for nanoscale particles during slow breathing (resting activity). When the particle size is in the nanoscale, the contribution of Saffman's lift force and Brownian diffusion has been observed to be significant (Dang Khoa et al. 2020, Rahman et al. 2021). In the study by Rahman et al. (2021), Saffman's lift force and Brownian diffusion's combined mechanism is defined as diffusion. At intense breathing (exercise mode), the inertial impaction mechanism for microscale particle deposition contributes to particle TD more than diffusion. As a result, several investigations on microparticle TD in human lungs focus only on impaction mechanisms (Chen et al. 2018, Huang et al. 2021). However, when the particle size is in between nano- and micro-scales, both impaction and diffusion should be considered if their contributions to particle TD do not differ from each other. In this study, a numerical model that considers all the particle TD mechanisms including diffusion, sedimentation, impaction and Saffman's lift forces are used to simulate TD of a variety of particles.

7.3.1 Reconstructed Anatomical Model

The three-dimensional (3D) anatomical model, including the mouth-throat area and the tracheobronchial upper lung airways shown in Figure 7.1, was generated using digitised CT scans of a 50-year-old person. For the convenience of discussion of Particle TD in different areas, the lung model is divided into Parts A-I as seen in Figure 7.1.

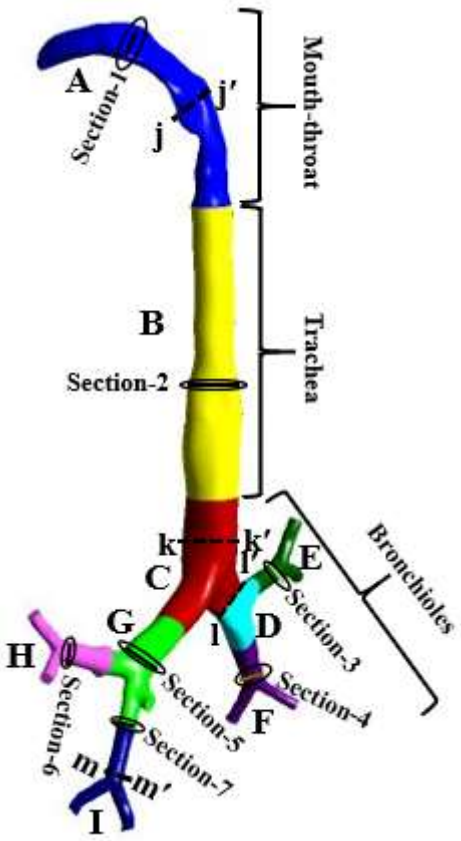

Figure 7.1. Reconstruction of realistic mouth–throat and tracheobronchial lung airways. The portions shown in the Figure 7.1 will be referred to when the findings are presented.

7.3.2 Airflow Model

ANSYS FLUENT (version 19.2) software is used to solve the airflow and particle TD in the lung airways. The governing equations for simulating the flow are the Reynolds-averaged Navier-Stokes (RANS) equations:

$$\frac{\partial \rho}{\partial t} + \frac{\partial}{\partial x_i}(\rho u_i) = 0 \tag{7.1}$$

$$\frac{\partial}{\partial t}(\rho u_i) + \frac{\partial}{\partial x_j}(\rho u_i u_j) = -\frac{\partial p}{\partial x_i} + \frac{\partial}{\partial x_j}\left[\mu\left(\frac{\partial u_i}{\partial x_j} + \frac{\partial u_j}{\partial x_i}\right)\right] + \frac{\partial}{\partial x_j}(-\rho\overline{u_i' u_j'}) \tag{7.2}$$

where t is time, x_i (i=1,2 and 3) are the Cartesian coordinates, u_i is the fluid velocity in the x_i-direction, p is the fluid pressure, ρ is the air density, μ is the molecular viscosity. The Reynolds stresses of turbulence are represented by $\rho\overline{u_i' u_j'}$ on the right-hand side of equation (7.2).

In this study, the realisable k-ε turbulence model is used for simulating the governing equations. It performs better than the standard k-ε turbulence model in a variety of complex flow conditions, including rotating homogeneous shear flows, boundary-free shear flows, channel and flat boundary layer flow with and without pressure gradients, and backwards-facing step flow (Shih et al. 1995). It has been demonstrated that the realisable k-ε model can accurately predict the flow of complicated lung geometries without the requirement for near-wall adjustment (Isa et al. 2014, Abolhassantash et al. 2020, Rahman et al. 2021).

The RANS equations are solved using the second-order upwind and pressure-velocity coupling schemes in FLUENT. The inlet of the lung model has a uniformly distributed velocity, and all its exits have zero gauged pressure. The boundary conditions at the outlets strongly influence the airflow partitions. As a result, Luo and Liu (2008) have tested zero pressure at the outlet and outflow boundary conditions (i.e., a zero normal gradient for all flow variables except pressure). As a result, they observed that the airflow rate is identical to each outlet given the outflow boundary condition. Therefore, they conclude that zero pressure's outlet boundary condition is more acceptable than the outflow boundary condition. The airway wall was considered stationary and smooth with a non-slip boundary condition (Singh et al. 2020, Islam et al. 2021, Rahman et al. 2021).

7.3.3 Particle Transport Model

The current particle TD model is a one-way coupling model that considers particle movement due to airflow but ignores particle effects on airflow (Inthavong et al. 2011, Lintermann and Schröder 2017). When the particle volume concentration is larger than 15%, two-way models that account for particle–particle interaction are needed. However, in all drug delivery applications, the volume concentration is less than 15% (Islam et al. 2019). Therefore, collision-free conditions can be used to simulate the transport of dilute, suspended particles in the human lung, or particle-particle interaction can be eliminated (Tsuji 2007). Because direct

particle-particle interactions may be neglected if the particle suspension entering the tracheobronchial airway is dilute (Islam et al. 2019, Chen et al. 2021). As a result, most of the published studies did not include particle-particle interactions (Feng and Kleinstreuer 2014). Particle TD in lung airways is modelled using the Lagrangian approach. The equation of motion of each individual particle is expressed as (Inthavong et al. 2011, Rahman et al. 2021):

$$\frac{d\boldsymbol{u}_i^p}{dt} = \boldsymbol{F}_{Di} + \boldsymbol{F}_{gi} + \boldsymbol{F}_{Bi} + \boldsymbol{F}_{Li} \tag{7.3}$$

where u_i^p is particle velocity in the x_i-direction, $\boldsymbol{F}_{\mathrm{Di}}$, $\boldsymbol{F}_{\mathrm{gi}}$, $\boldsymbol{F}_{\mathrm{Bi}}$ and $\boldsymbol{F}_{\mathrm{Li}}$ are, respectively, the drag force, gravitational force, Brownian force, and Saffman's lift force per unit mass. The following formula determines the gravitational force:

$$\boldsymbol{F}_{gi} = \left(\frac{\rho_p - \rho}{\rho}\right)\boldsymbol{g} \tag{7.4}$$

where $\boldsymbol{g}$ denotes gravitational acceleration and $\rho_p$denotes particle density. The drag force is calculated using the following formula:

$$\boldsymbol{F}_{Di} = \frac{18\mu}{\rho_p d_p^2} C_D \frac{Re_p}{24}(\boldsymbol{u}_i - \boldsymbol{u}_i^p) \tag{7.5}$$

where $Re_p = \rho d_p \left|\boldsymbol{u}_i^p - \boldsymbol{u}_i\right|/\mu$ and the drag coefficient C_D for the spherical particles is calculated by (Morsi and Alexander 1972):

$C_D = a_1 + \frac{a_2}{Re_p} + \frac{a_3}{Re_p^2}$ for $0 < Re_p < 10$.

where a_1, a_2, a_3 are functions of the Reynolds number Re_P given by:

$$\mathrm{a}_1, \mathrm{a}_2, \mathrm{a}_3 = \begin{cases} 0, \quad 24, \quad 0 & 0 < Re_p < 0.1 \\ 3.690, \quad 22.73, \quad 0.0903 & 0.1 < Re_p < 1 \\ 1.222, \quad 29.17, \quad 3.89 & 1 < Re_p < 10 \\ 0.617, 46.50, -116.67 & 10 < Re_p < 100 \\ 0.364, 98.33, -2778 & 100 < Re_p < 1000 \\ 0.357, 148.62, -47500 & 1000 < Re_p < 5000 \\ 0.46, -490.546, 578700 & 5000 < Re_p < 10000 \\ 0.519, -1662.5, \quad 5416700 & Re_p > 10000 \end{cases}$$

Brownian motion describes the random, uncontrollable movement of particles in a fluid when molecules interact with each other (Torrens and Castellano 2018). It is strong in a less viscous fluid at a higher temperature with smaller particles (Jang and Choi 2004). Brownian motion in the air is unnoticeable if the particle size is bigger than 1 μm (Franosch et al. 2011). Brownian force that causes Brownian motion is defined as:

$$\boldsymbol{F}_{Bi} = \boldsymbol{G}_i \sqrt{\frac{\pi S_0}{\Delta t}} \tag{7.6}$$

where G_i is a Gaussian random number with unit variance and zero mean, Δt is the particle time step, and S_0 is the spectral intensity function associated with the diffusion coefficient by:

$$S_0 = \frac{216 \nu k_B T}{\pi^2 \rho_p d_p^2 \left(\frac{\rho_p}{\rho}\right)^2 C_c} \tag{7.7}$$

where, ν is the kinematic viscosity, $K_B = 1.380649 \times 10^{-23}$ J/K is the Boltzmann constant,$T = 300K$ is the absolute fluid temperature, and C_c is the Stokes-Cunningham slip correction coefficient as

$$C_c = 1 + \frac{2\lambda}{d_p}\left(1.257 + 0.4e^{-\left(\frac{1.1 d_p}{2\lambda}\right)}\right) \tag{7.8}$$

where, the gas molecules' mean free path (λ) is 65 nm (Xi, Berlinski et al. 2012). The lift force of Saffman is calculated using the following formula:

$$\boldsymbol{F}_{Li} = \frac{2K\nu^{\frac{1}{2}}\rho d_{ij}}{\rho_p d_p (d_{lk} d_{kl})^{\frac{1}{4}}}(\boldsymbol{u}_j - \boldsymbol{u}_j^p) \tag{7.9}$$

where, $K = 2.594$ is the constant coefficient of Saffman's lift force and $d_{ij} = (\partial u_i/\partial x_j - \partial u_j/\partial x_i)/2$ is the deformation tensor of the flow velocity.

In the simulations, 81000 spherical particles were released randomly at one time from the inlet boundary. A 'trap' condition is implemented on the airway walls for particle deposition, and an 'escape' condition is implemented at the outlets (Gu et al. 2019, Islam et al. 2021, Wu et al. 2022). In the escape condition, the particles can pass through the output

boundary without being reflected back. In the trap condition, particles colliding with the inner surface of the lung airways are trapped. This "trap" condition seems appropriate as the airway walls contain mucus which is very sticky (Islam et al. 2018, Ghosh et al. 2020).

7.3.4 Particle Deposition Efficiency Calculation

The percentages of particles absorbed (trapped) on the inner surfaces of the human lung airways are referred to as deposition efficiency (η_d) and it is calculated by:

$$\eta_d(\%)=\frac{\text{The number of particles deposited in a given area}}{\text{Total number of particles inhaled through the mouth}}\times 100$$

7.4 Grid Dependency Study and Model Validation

7.4.1 Grid Dependency Study

Figure 7.2 (a) to (c) show the computational mesh near the asymmetric mouth-throat area, bronchioles section, and part of the lung airways, respectively. Near the walls, ten-layer smooth inflation was used to guarantee that the boundary layer flow was accurately simulated (Figure 7.2c). At carinal angles, denser mesh is used for accurate resolution of complex flows.

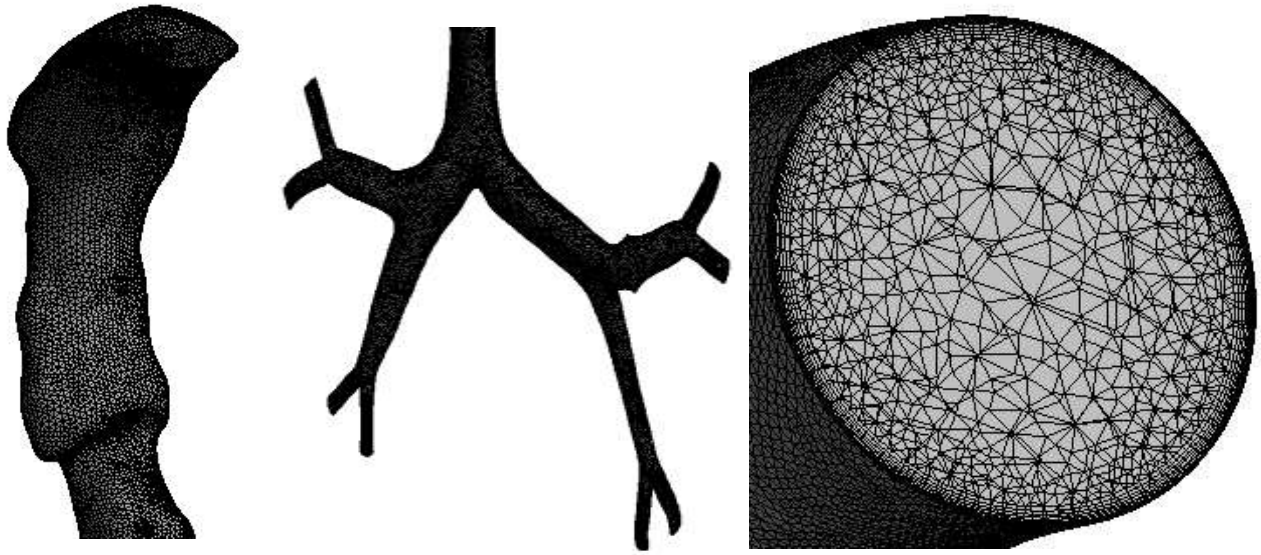

(a) (b) (c)

Figure 7.2. Mesh generation for (a) the mouth–throat portion, (b) the bronchioles portion, and (c) the inflation layer in an airway in a realistic lung model.

The grid independence test is performed using six mesh sizes with cell numbers of 632006 (Mesh-1), 1300952 (Mesh-2), 2557333 (Mesh-3), 3053482 (Mesh-4), 3870593 (Mesh-5) and 4568314 (Mesh-6), respectively. The densest mesh has a grid size of 0.1 mm near the wall, and the mesh size is inversely proportional to the number of elements. The pressure and average velocity magnitude are shown in Figure 7.3 (b), (c), and (d) for the three sections indicated in Figure 7.3 (a), where *X* is the direction along the section diameter. Increasing the grid number does not influence pressure and velocity if the mesh density exceeds Mesh-4 as can be demonstrated. The maximum difference between the velocities from Mesh-5 and mesh-6 is about 0.01%. The velocity and pressure converge at Mesh-5 also. The non-dimensional wall unit (y^+) is defined inside the boundary layer as

$$y^+ = \frac{\rho U_\tau y}{\mu} \tag{7.10}$$

where $U_\tau \left(= \sqrt{\frac{\tau_w}{\rho}} \right)$ is the friction velocity, *y* (=0.143 mm for Mesh-5) is the distance between the first layer of mesh points and the boundary, and τ_w is the wall shear stress. The maximum y^+ of Mesh-5 in our simulation is 3.2. Pan et al. (2019) found RANS and LES solutions for structured and unstructured meshes agreed with experimental data when the y^+ value was 3.5.

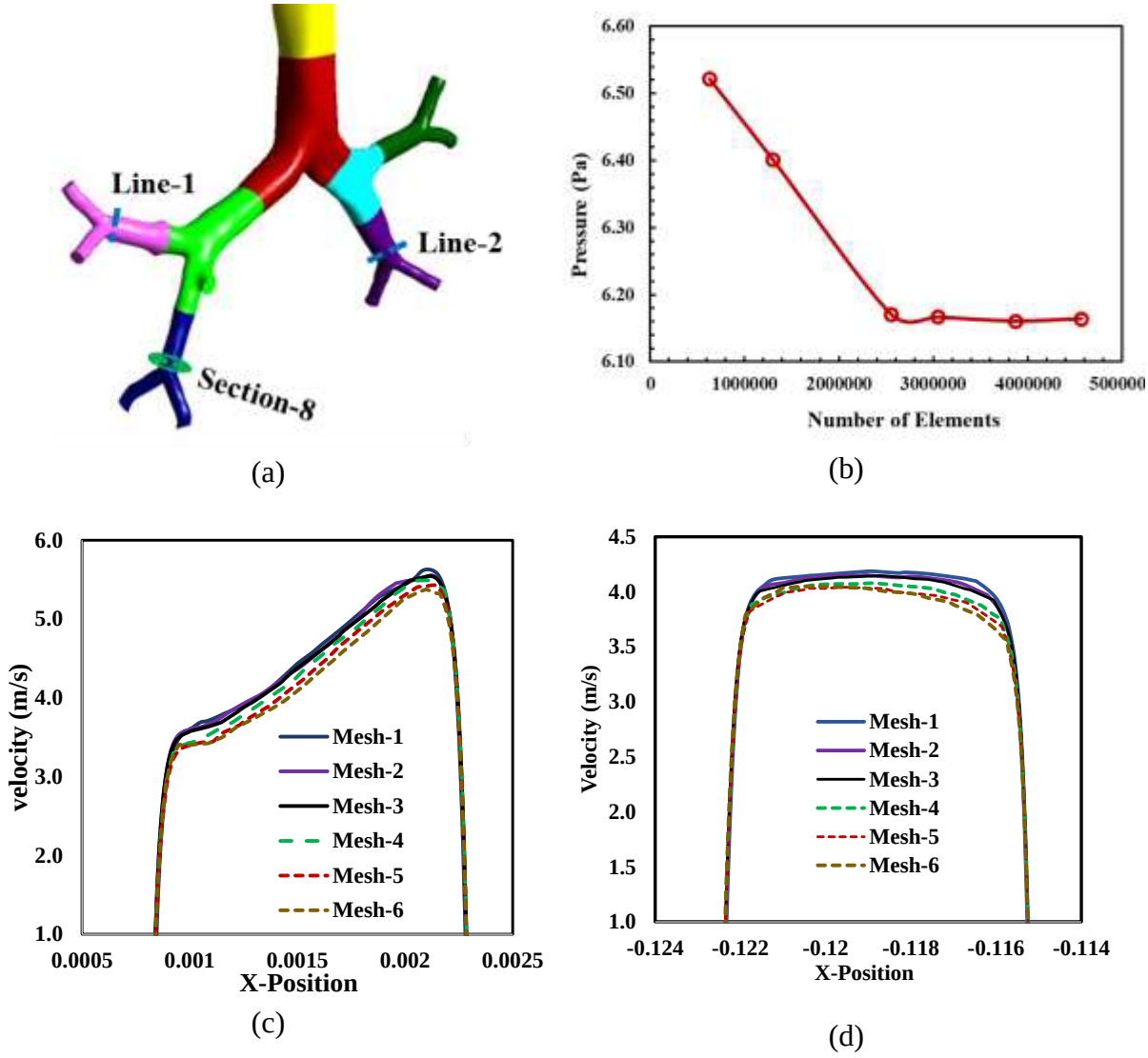

Figure 7.3. Grid refinement/mesh-independent test at the flow rate 60 L/min for realistic lung model, (b) average pressure as functions of grid number (average pressure calculated at the selected section-8 in Figure 7.3a); (c) velocity distribution at the Line-1; (d) velocity distribution at the Line-2 (average velocity calculated at the selected line in Figure 7.3a).

Figure 7.4 shows the variation of the calculated deposition efficiency with a mesh element number. The deposition efficiency remains virtually unchanged after the mesh density is higher than Mesh-4 with 3.05 million elements. The Mesh-5 with 3.87 million elements was used in all the numerical simulations in this study.

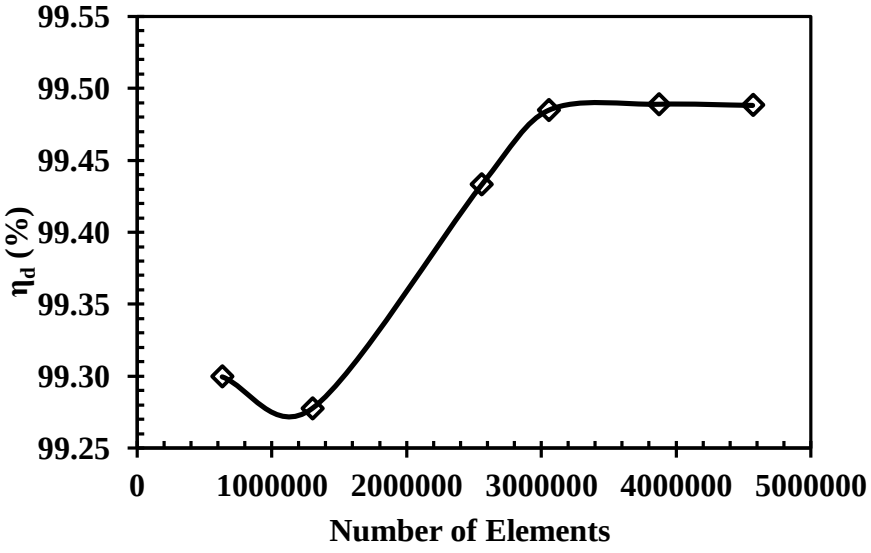

Figure 7.4. Deposition efficiency as a function of the grid number at the flow rate of 60 L/min. The diameter of traffic particles is 10 μm.

7.4.2 Model Validation

The validation of micro and nano-particles has already been conducted in our previous studies (Rahman et al. 2021a, Rahman et al. 2021b). To further validate the numerical method for nanoparticles, the present CFD results are compared to experimental data (Cheng et al. 1993, Cheng et al. 1999) and numerical predictions (Kleinstreuer et al. 2008, Xi and Longest 2008) of particle deposition in the mouth-throat area of a realistic lung. For a nanoparticle simulation, Figure 7. 5 (a) shows the predicted deposition efficiency as a function of particle diameter for a constant of flow rate of 4 L/min. In addition, Figure 7.5 (b) shows the particle deposition efficiency as a function of Stokes number defined as $\mathrm{S_t} = \rho_p d_p^2 u_0 / 18\mu \mathrm{D}$ for microparticles simulation, where u_0 denotes the inlet velocity at the boundary, and D (=0.0124 m) denotes the hydraulic diameter. In Figure 7.5 (a) the deposition efficiency of nanoparticles decreases with the increase of particle size. According to the linear relationship between particle size and Stokes number, it can be further deduced that the deposition efficiency of nanoparticles decreases with the increase of the Stokes number. However, the deposition efficiency of microparticles

increases as the Stokes number increases. The relationship between deposition efficiency and Stokes number and particle diameter is well predicted by numerical models in Figure 7.5. Figure 7.5 (a) and (b) show that the current model can accurately calculate particle TD of micro-and nanoparticles in a realistic 3D mouth-throat and tracheobronchial airway of a lung.

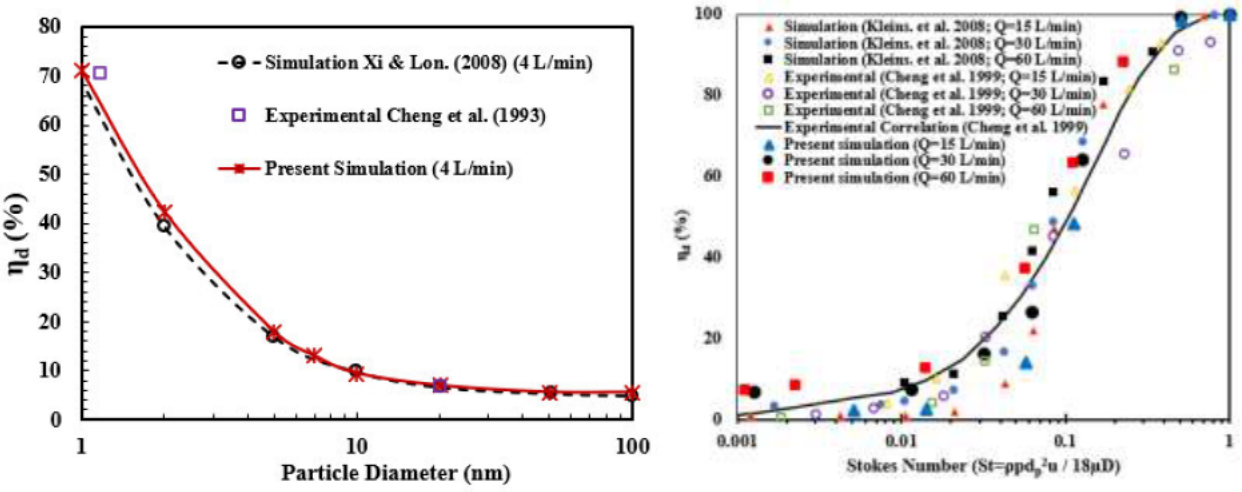

(a) Nanoparticles (1 nm $\leq d_p \leq$ 100 nm) (b) Microparticles (0.7 μm $\leq d_p \leq$ 42 μm)

Figure 7.5. Comparison of current nanoparticle and microparticle deposition simulations in the mouth-throat region with data from the literature (Cheng et al. 1999, Kleinstreuer et al. 2008, Xi and Longest 2008).

7.5 Results and Discussion

The airflow dynamics and particle deposition are investigated in this study under three flow conditions: low-level breathing (Q_{in}=15 L/min) at rest, moderate activity breathing (Q_{in} =30 L/min) at the walk, and intense breathing (Q_{in} =60 L/min) during excise (Deng et al. 2019, Islam et al. 2021).

7.5.1 Airflow Characteristics

Velocity profiles at various locations in the mouth-throat, trachea, and bronchioles regions are compared with each other to investigate airflow patterns in lung airways. The velocity profiles for the three flow rates along the diameter direction (X-direction) of four

selected cross-sections (indicated in Figure 7.1) are shown in Figure 7.6. The velocity is nondimensionalised by the inlet velocity of the whole lung model u_0. Non-dimensional velocity distributions of different flow rates follow a similar trend, but they are not the same because of the difference in the Reynolds number. The velocity on each section is very asymmetric because of the complexity of the lung geometry. The mouth-throat area (jj') had the maximum non-dimensional velocity in all selected regions, whereas the bronchioles (ll') had the lowest velocity. Velocities changed largely at the mouth-throat region with complex airway structure. The velocity is reduced at kk' because of the increase in the cross-sectional area. In addition to the effect of airway geometry complexity, the velocity distribution in each branch becomes very non-uniform once the air passes through a bifurcation. However, as illustrated in Figure 7.6 (d), the velocity profile (mm' section) is symmetrical parabolic in the lower airway. The difference velocity distributions of different flow rates are found to be the maximum at the lowest section mm'.

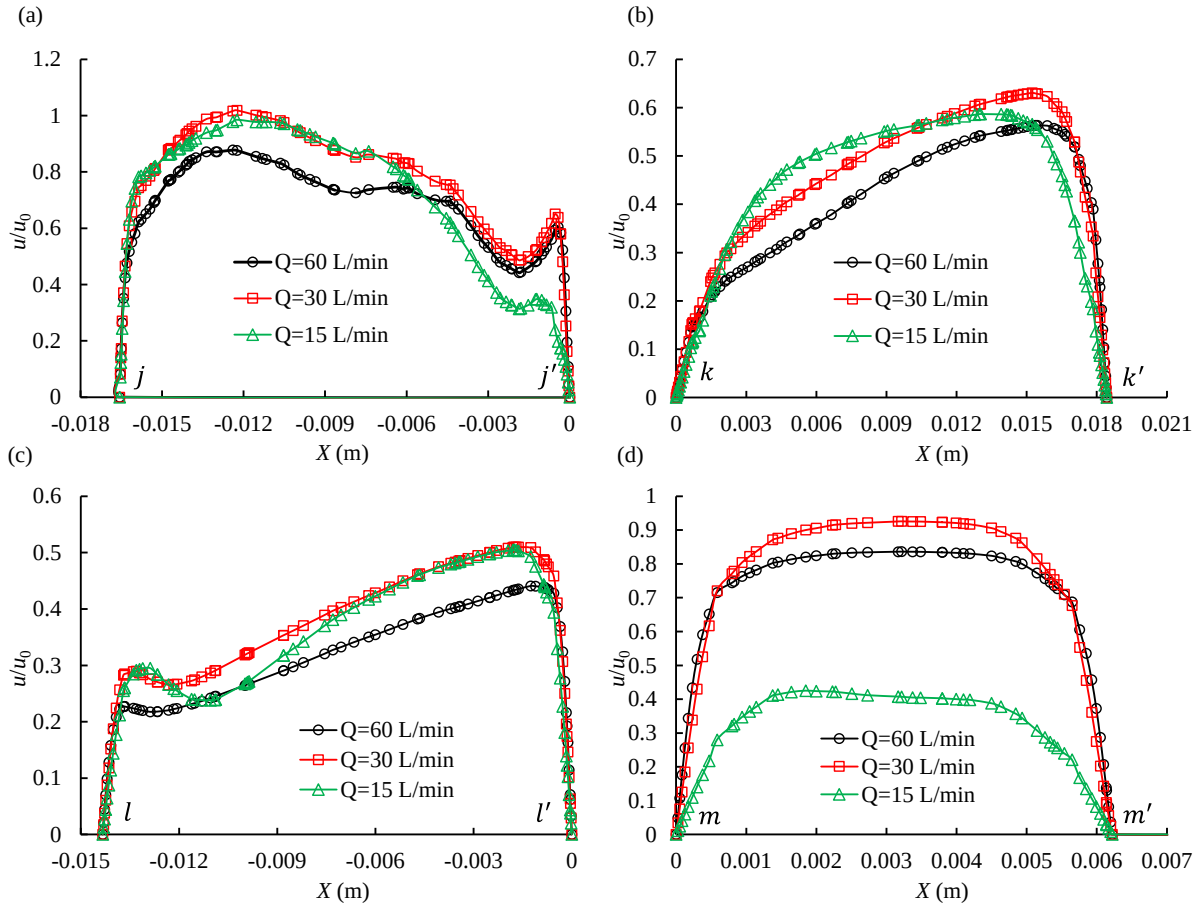

Figure 7.6. Velocity profiles under different flow rates, (a) Line jj′, (b) Line kk′, (c) Line ll′, and (d) Line mm′ (Figure 7.1 illustrates the lines).

7.5.2 Wall Shear Stress

Figure 7.7 quantitatively depicts the averaged non-dimensional shear stress ($\tau/(\rho u_0^2)$) along the inner wall of the lung as a function of flow rate in the upper lung airway model on seven sections defined in Figure 7.1, where wall shear stress τ is defined as the tangential force per unit area exerted by the flowing fluid on the wall surface. The wall shear stress distributions in the seven sections for different flow rates follow a similar trend but not the same. The wall shear stress varies considerably with each section at the lung airway because of the flow rate variation caused by complicated lung geometry.

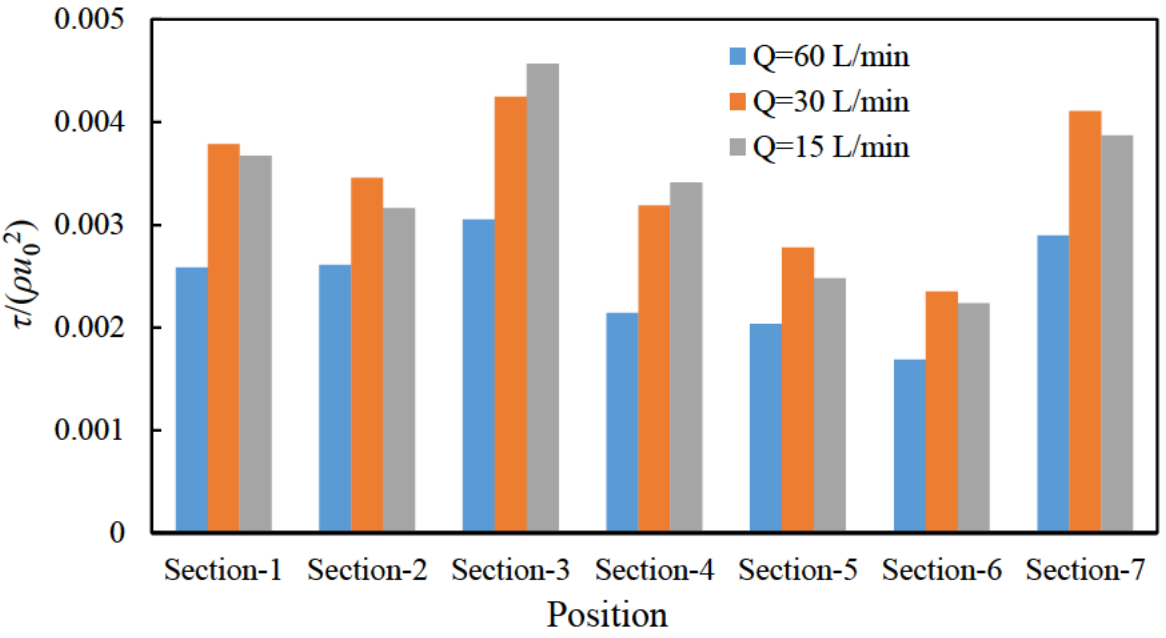

Figure 7.7. Averaged wall shear stress for a particular lung portion is indicated in Figure 7.1. The traffic particle diameter is 10-μm.

Figure 7. 8 illustrate the pressure distribution along the lung airways at several positions, from the mouth to the bronchioles. As air enters the deep lung, the pressure drops because of the energy loss. The biggest drop happens when air flows through a long airway between sections 1 and 2. The cross-section areas of sections 1 and 2 are 0.00024 m^2 and 0.00021 m^2, respectively. Due to the higher cross-section area, the pressure in Section 1 is higher than in the remaining sections (sections 2–7). According to Bernoulli's principle, a decrease in velocity causes an increase in pressure even if no energy is lost. A significant pressure drop is observed at a low flow rate of 15 L/min. It was observed that the pressure decrease for a low flow rate of 15 L/min is 53% more than that for a high flow rate of 60 L/min. Because the volume flow rate decreases, the pressure drops dramatically from section 1 to section 7. As a result, the pressure in all sections decreases as the flow rate decreases. As a result, breathing air into a low-flow lung is more complex than breathing air into a high-flow lung.

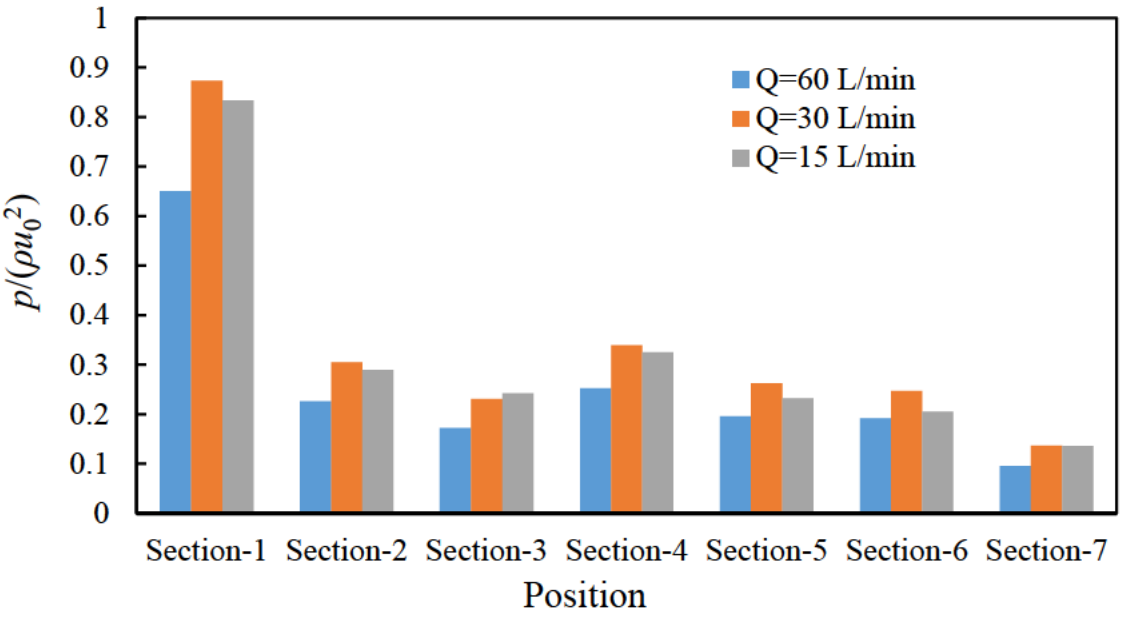

Figure 7.8. Pressure drop at three distinct flow rates in a different section of the realistic lung model, d_p=10 μm (traffic particle); the section numbers are shown in Figure 7.1.

7.5.3 Particle Deposition

We looked at three different forms of pollutant particles: traffic, smoke, and dust particles. Pollutant particles come from various sources, depending on the environmental factors, ranging in size and chemical composition, such as nitrogen oxides (NO and NO_2), carbon monoxide (CO), and sulphur dioxide (SO_2) (Sophonsiri and Morgenroth 2004, D'amato and Cecchi 2008, Leoni et al. 2018, Bălă et al. 2021). However, whereas particle size has generally been noted as a factor in the deposition in human lungs, the impact of particle chemical composition has been neglected in the current study. Therefore, the impact of particle chemical composition for the current study was demonstrated using the bulk density. Bulk density was used to express the difference in chemical composition between particles (Zhang et al. 2012). Therefore, we assumed that the density of traffic, smoke and dust particles are 2000 kg/m^3, 1120 kg/m^3 and 400 kg/m^3, respectively (Deng et al. 2019, Paul et al. 2021). The diameter of these pollutant particles in the range of 5nm $\leq d_p \leq$ 10 μm are examined.

To quantify the contributions of impaction ($\boldsymbol{F}_{\mathrm{Di}}$ and $\boldsymbol{F}_{\mathrm{gi}}$), Brownian diffusion ($\boldsymbol{F}_{Bi}$), and Saffman's lift force ($\boldsymbol{F}_{Li}$) using numerical simulations in two scenarios: (1) only the impaction term is included in the particle motion equation, and (2) all impaction, Brownian diffusion, and Saffman's terms are taken into consideration. Because both Brownian diffusion and Saffman's lift contribute to the motion of particles in crossflow directions, they are combined together and referred to as diffusion in this study (Rahman et al. 2021). As a result, situations (1) and (2) are referred to as impaction only and impaction+diffusion, respectively, in the discussion. The simulations of nano- to micron-scale particles in the range of $5\ \mathrm{nm} \leq d_p \leq 10\ \mu\mathrm{m}$ and the particle densities of 2000 kg/m^3, 1120 kg/m^3 and 400 kg/m^3 are performed to determine the contribution of each mechanism at various particle sizes and densities. In the discussion, the particles with densities of 2000 kg/m^3, 1120 kg/m^3 and 400 kg/m^3 are referred to as traffic, smoke and dust, respectively.

Figure 7.9 (a), (b) and (c) depict the variation of particle deposition efficiency in the whole lung model with particle diameter for three types of pollutants and three flow rates Q_{in}=15 L/min, 30 L/min, and 60 L/min. Simulations with impaction only (diffusion terms switched off in the equations) are also conducted, and the results with impaction only are denoted by $\eta_{\mathrm{d,I}}$, as presented in Figure 7.10. Table 7.1 lists the particle deposition rates at the largest and smallest particle diameters d_{p}=10 μm, and 5 nm. It can be found that the same size particle, d_{p}=10 μm but different density pollutant particles have significant different deposition efficiencies. The largest flow rate Q_{in}=60 L/min and largest particle diameter d_{p}=10 μm have the maximum total particle deposition efficiencies for traffic, smoke, and dust particle in Figure 7.9 (a) and Table 7.1. The deposition rate at d_{p}=10 μm decreases with the decrease of flow rate.

Table 7.1. Particle deposition rates at the largest and smallest particle diameters

Particle size	Particle type	ρ_d (kg/m^3)	η_d (%)			$\eta_{d,I}/\eta_d$		
			60 L/min	30 L/min	15 L/min	60 L/min	30 L/min	15 L/min
10 μm	Traffic	2000	99.82	80.19	40.41	0.996	0.987	0.995
	Smoke	1120	79.01	46.94	30.31	0.975	0.979	0.976
	Dust	400	35.72	24.98	17.92	0.970	0.964	0.965
5 nm	Traffic	2000	8.88	11.63	15.92	0.892	0.785	0.562
	Smoke	1120	9.01	11.68	15.94	0.900	0.787	0.579
	Dust	400	9.09	11.76	16.04	0.901	0.814	0.581

The effects of the particle density and flow rate on the deposition of 5-nm particles are different from that of 10-μm particles in the following aspect. First, the density has a very weak effect on the deposition rate of 5-nm particles, while an increase of the density from 400 kg/m^3 to 2000 kg/m^3 causes a significant increase of the deposition rate of 10-μm particles, for example by around three times for all the flow rates. Second, the particle deposition rate of 5 nm particles increases but that of 10 μm decreases with the flow rate increase. The increase of the deposition rate with the increase in density of 10-μm particles affects the distribution particles in the present lung model. The smallest deposition rate of 10-μm dust indicates the largest amount of 10-μm dust goes into the deeper lung (Deng et al. 2019).

Nanoscale particles follow streamlines due to the strong drag force, making it difficult for them to reach the airway wall only from the impaction mechanism (Zhang and Kleinstreuer 2004, Rahman et al. 2021). However, the Brownian and Saffman lift forces on nanoparticles increase with the decrease of the particle size. These forces in the crossflow direction enable particles to move towards the airway wall. As a result, the deposition rate rises in the nanoscale as particle size decreases. However, the deposition rate of the smallest nanoparticles caused by the diffusion effect is much smaller than that of the largest microparticles by impaction in Figure 7.9. Figure 7.9 also shows that an decrease in the flow rate increases η_d of nanoparticles because

smaller flow velocity gives particles more time to move in the crossflow direction towards the wall due to diffusion (Islam et al. 2019, Darquenne 2020). It can be seen in Table 7.1 that the deposition efficiencies of 5-nm particles at Q_{in}=60 L/min is nearly half of that at Q_{in}=15 L/min. The deposition efficiencies of 5-nm to 500-nm particles are small because both diffusion and impaction mechanisms are weak.

The reason why the deposition rate of microparticles increases with increasing particle size or flow rate can be explained by the inertial effect. When flow goes through curved airways, flow velocity follows the curved airway, but large particles tend to stay on their original tracks due to the initial mechanism and hit the airway wall. This type of deposition mechanism is known as impaction (Chen et al. 2012, Islam et al. 2019, Farghadan et al. 2020, Huang et al. 2021).

To quantify the contribution of impaction and diffusion to the particle deposition rate, the ratio of the deposition efficiency calculated using only impaction in Eq. (7.3), which is defined as $\eta_{\mathrm{d,I}}$ to the total diffusion efficiency η_{d}, when both impaction and diffusion are considered, for flow rates of 60 L/min, 30 L/min, and 15 L/min are presented in Figure 7.10 (a), (b) and (c), respectively.

The ratio $\eta_{\mathrm{d,I}}/\eta_{\mathrm{d}}$ of particles larger than 1000 nm is greater than 0.9 for all the three flow rates, suggesting a predominant contribution of impaction and negligible contribution from diffusion. In addition, the contribution of the impaction appears to be nearly independent on the particle size if the latter is greater than 1000 nm. The value of $\eta_{\mathrm{d,I}}/\eta_{\mathrm{d}}$ is found to be greater than 50% at the smallest particle size of 5 nm, indicating the effect of impaction is still comparable to the diffusion at this particle size. When the flow rate decreases from 60 L/min to 15 L/min, the impaction contribution of 5-nm particles is reduced from 88% to 57%.

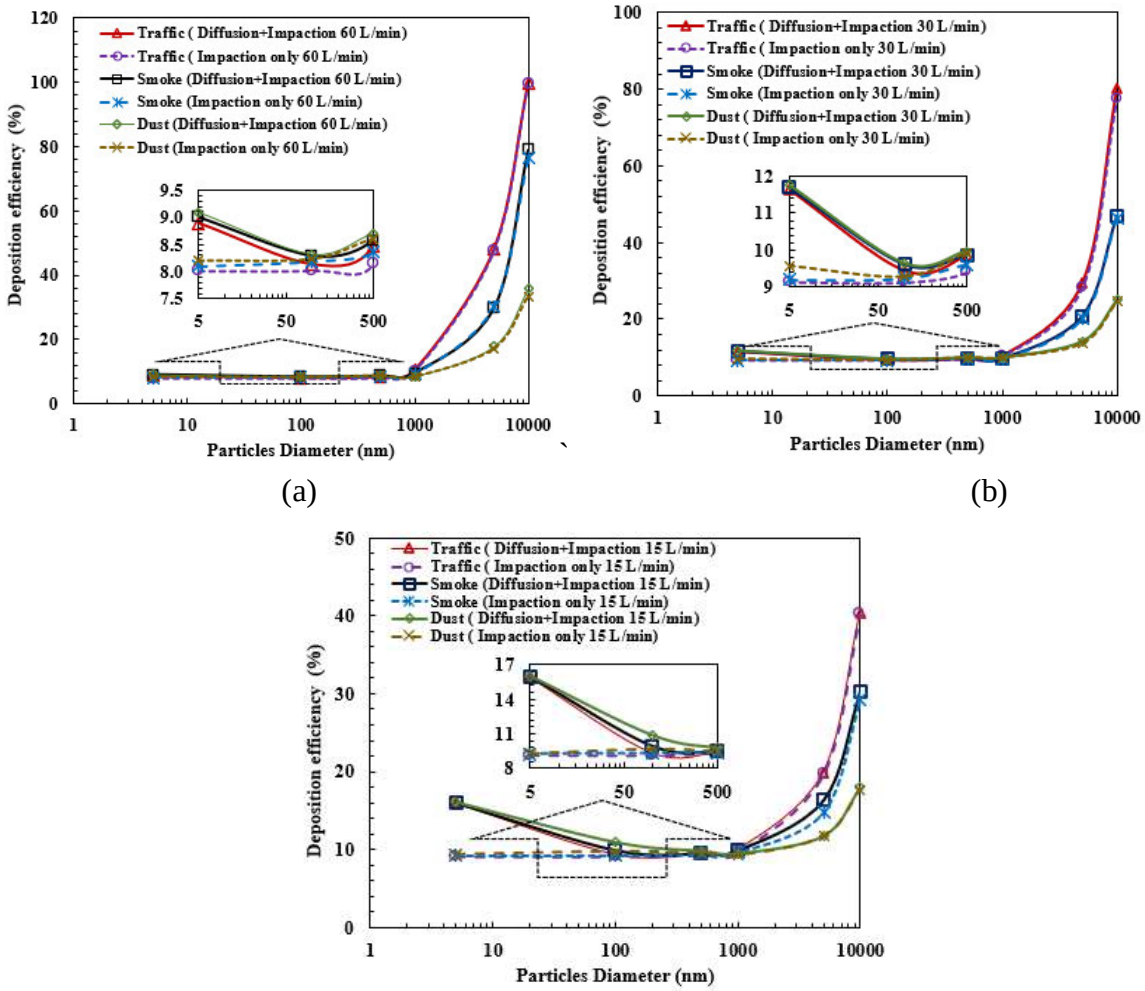

Figure 7.9. Particle deposition efficiency in the lung model for (a) Q_{in}=60 L/min; (b) Q_{in}=30 L/min and (c) Q_{in}=15 L/min.

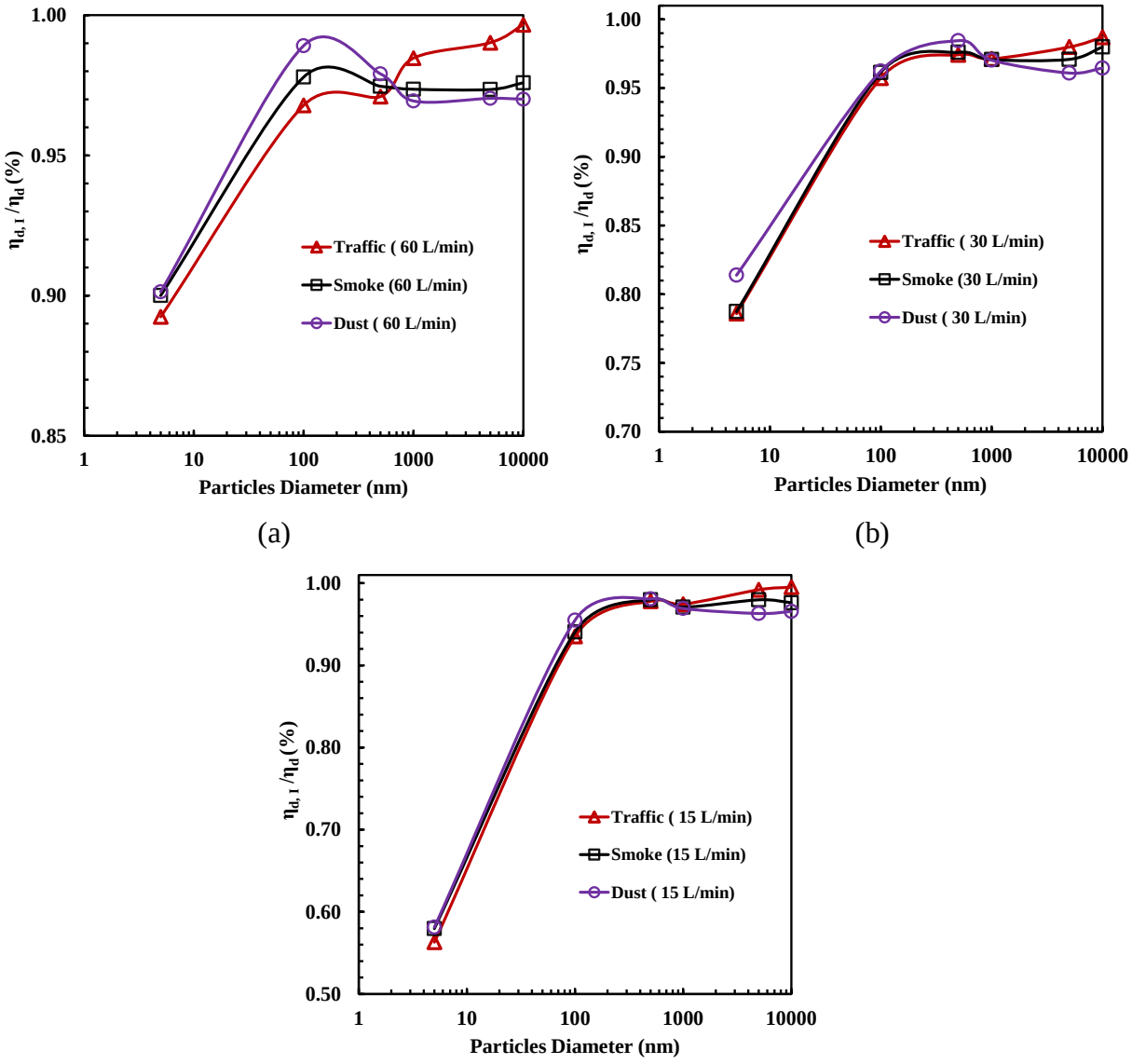

Figure 7.10. Contribution of the impaction mechanism on the deposition efficiency in the lung model for (a) Q_{in}=60 L/min; (b) Q_{in}=30 L/min and (c) Q_{in}=15 L/min.

The lung model is divided into parts A to I in Figure 7.1 and the distribution of the 10-µm particles among different parts is demonstrated by the bar charts in Figure 7.11. The type of the 10-µm particles significantly affects the deposition efficiency. At 60 L/min, the deposition efficiency in the mouth-throat part A is 98.7% for 10-µm heaviest traffic particles and it decreases to 22.0% for 10-µm lightest dust. For a specific particle type with d_p=10 µm, the highest flow rate of 60 L/min has the largest deposition efficiency because of its strongest

impact mechanism. At the smallest flow rate of 15 L/min, 28.71% of traffic, 21.51% of smoke, and 14.73% of dust particles are deposited at region A. Because 10-μm traffic particles are mostly deposited (98.7%) at part A at 60 L/min, the deposition efficiencies at parts B to I are much smaller than those of smoke and dust as seen in Figure 7.11 (d). The deposition efficiency due to impaction increases with the increase of particle density. When the flow rate is reduced from 60L/min to 15 L/min, the number of 10-μm traffic particles passing through Part A increases, so the deposition efficiency of traffic particles is higher than those of smoke and dust particles as seen in Figure 7.11 (f). Impaction mechanism causes deposition where an airway bends, contracts, or bifurcates. Some deposition efficiencies are zero at part B in Figure 7.11 because part B is a vertical straight airway without bending or bifurcation.

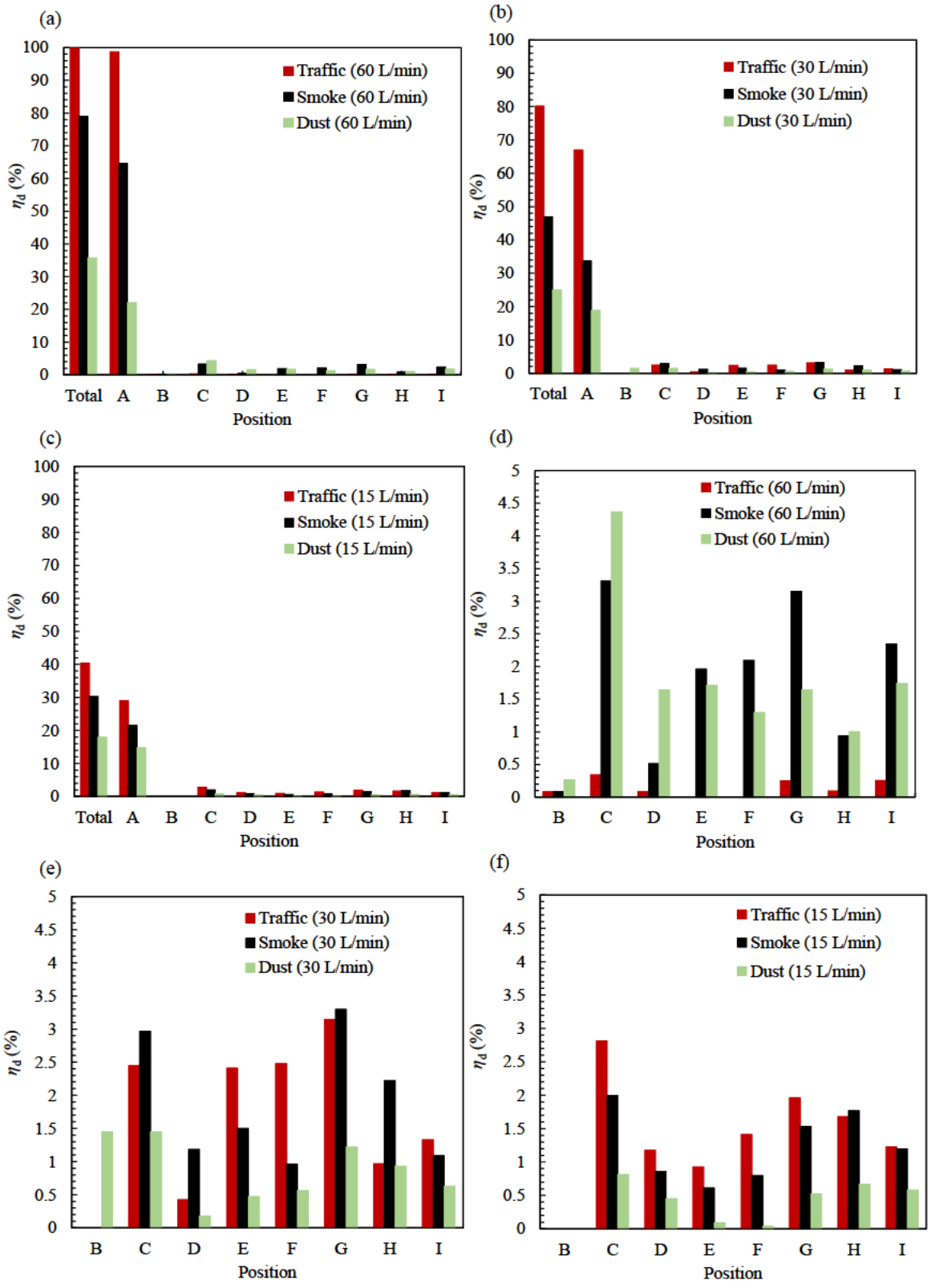

Figure 7.11. Deposition efficiencies of 10-μm particles at various parts of the lung indicated in Figure 7. 1. (a) Q_{in}=60 L/min; (b) Q_{in}=30 L/min; (c) Q_{in}=15 L/min; (d) to (f) are the same as (a) to (c), respectively, except with smaller vertical axis scale for precise observation of deposition efficiencies at B to I.

Figure 7.12 shows the deposition efficiencies of 5-nm particles at parts A to I for three flow rates. The effect of the flow rate on the deposition efficiency of 5-nm particles is opposite to that of 10-μm particles. The deposition efficiencies of 5-nm particles at all the parts in Figure 7.12 increase as the flow rate decreases. However, the density of particles has a very small effect on the deposition efficiency of 5-nm particles. Take the flow rate of 15 L/min in Figure 7.12 (c) as an example, the deposition efficiency in Part A only increases from 9.40% to 9.51% as the particle type changes from the heaviest traffic to the lightest dust.

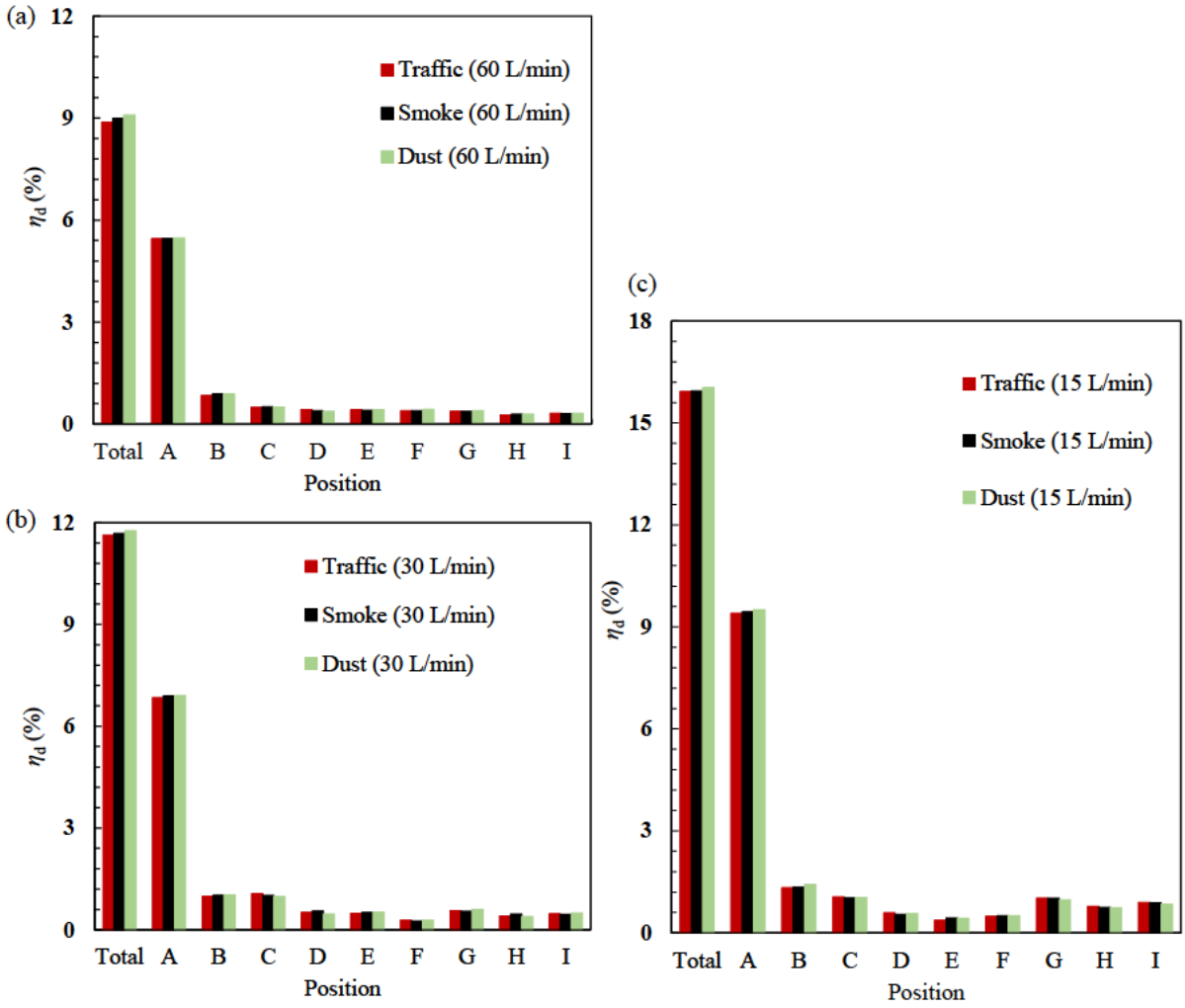

Figure 7.12. Deposition efficiencies of 5-nm particles at various parts of the lung indicated in Figure 7. 1. (a) Q_{in}=60 L/min; (b) Q_{in}=30 L/min; (c) Q_{in}=15 L/min.

The effect of particle density on other parts and other flow rates are also similarly weak. At Part A, the deposition efficiency of 5-nm particles is significantly smaller than that of the deposition efficiency of 10-μm particles.

7.5.4 Visualisation of Particle Deposition

Figure 7.13 depicts the distribution of deposited particles in the human lung at a flow rate of 60 L/min. The deposition efficiencies of microparticles are much higher than those of nanoparticles but seemly more nanoparticles are deposited in the airways than microparticles in Figure 7.13. Under impaction mechanisms, particles are only deposited in the area where the airway bends, bifurcates or changes its diameter. A large number of 10-μm particles are found to be repeatedly deposited in the mouth-throat area where the airway is curved and rough and the bifurcation area. Repetitive deposition of many particles in the same areas makes the number of 10-μm particles look smaller than that of 5-nm particles in Figure 7.13 but not. Very small 10-μm particles are deposited in the long vertical straight airway (Part B) because impaction is weak in straight airways. About 98.72% of 10-μm traffic particles are deposited in the mouth-throat area (Part A), leaving nearly no particles passing this area. The reduced deposition efficiency of 10-μm dust particles in the mouth-throat area allows rest particles to either be deposited in the bifurcation areas or escape and enter the deep lung.

The deposited 5-nm particles are found to be much more evenly distributed in all the airways than 10-μm particles as shown in Figure 7.13 (d) -(f). Under the diffusion mechanism, the particles move in the crossflow direction, regardless of the shape of the airway. Even along the straight vertical airway (Part B), particles can also move in the crossflow direction through diffusion and reach the inner airway wall. The diffusion is strong only when the particle size is in the nanoscale. However, the diffusion does not make 10-μm particles move in the crossflow direction because it is negligibly weaker than the impaction mechanism.

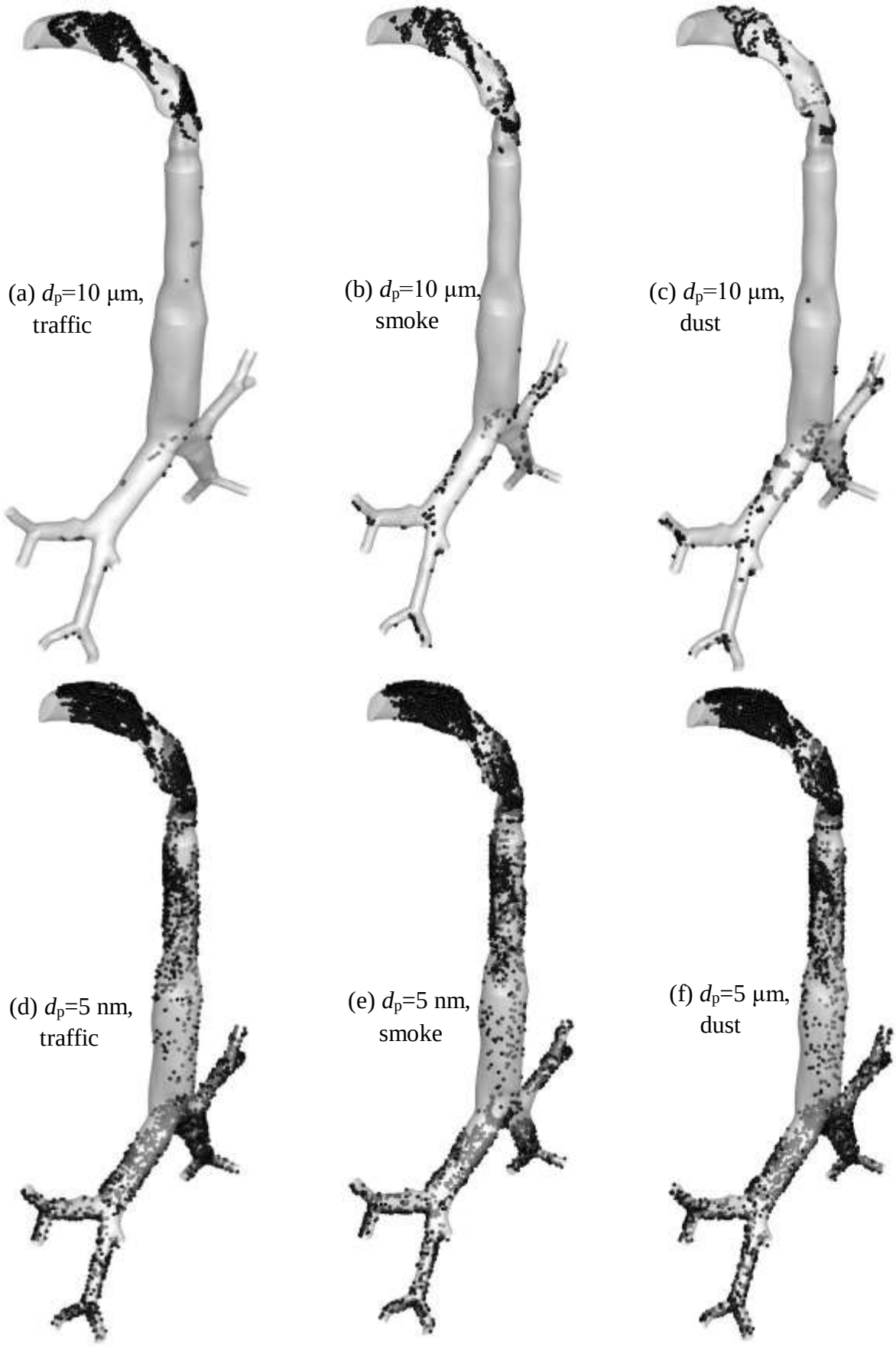

Figure 7.13. Distribution of deposited 10-μm and 5-nm particles in the human lung model at a flow rate of 60 L/min.

7.5.5 Particle Escaping Rate

The escaping rate (defined as η_e) is defined as the percentage of particles that escape from the model's outlet and enter the deep lung. The escaping rate from all the exits equals to $1 - \eta_d$. To understand the distribution of the escaped particles among different exits, the escape rates from the four exit regions for Q_{in}=60 L/min are represented in Figure 7.14. Each region has two exits, as shown in Figure 7.1, except region G+I where there are three exits. The escaping rate of the traffic particle in the regions E, F, H and I+G is nearly zero because most of the 10-μm traffic particles are deposited in the upper part at 60 L/min. The escape rate of 10-μm particles increases as the particles changes from traffic to dust. The escaping rate of 10-μm dust particles that escape from the right side (regions E & F) and left side (regions H and I+G) are 28.76% and 37.79%, respectively. Therefore, more dust particles escape from the four exit regions compared to smoke and traffic particles.

The escaping rate of Region H is smaller than other regions because of the complex lung structure. The small dust particle can follow the fluid streamline and pass through the exit quickly because of the low inertial impaction effect. As a result, low-density dust particles sharply escape than high-density particles (Figure 7.14c) because the small exit in the lung model is present before H-region.

The significant effects of the density on the escaping rates of the three pollutant particles can be seen in Figure 7.14. The escaping rate of impaction only mechanism is a little bit higher than the rate of diffusion+ impaction mechanism because of the diffusion effect weakness. In every region (E, F, H, I+G-region), the influence of a high flow rate on the escape rate is greater than that of a micron-sized particle at the nanoscale ($d_p \leq 1000$ nm). As a result, particle size must be reduced to enhance the number of escaping particles that reach the deep lung.

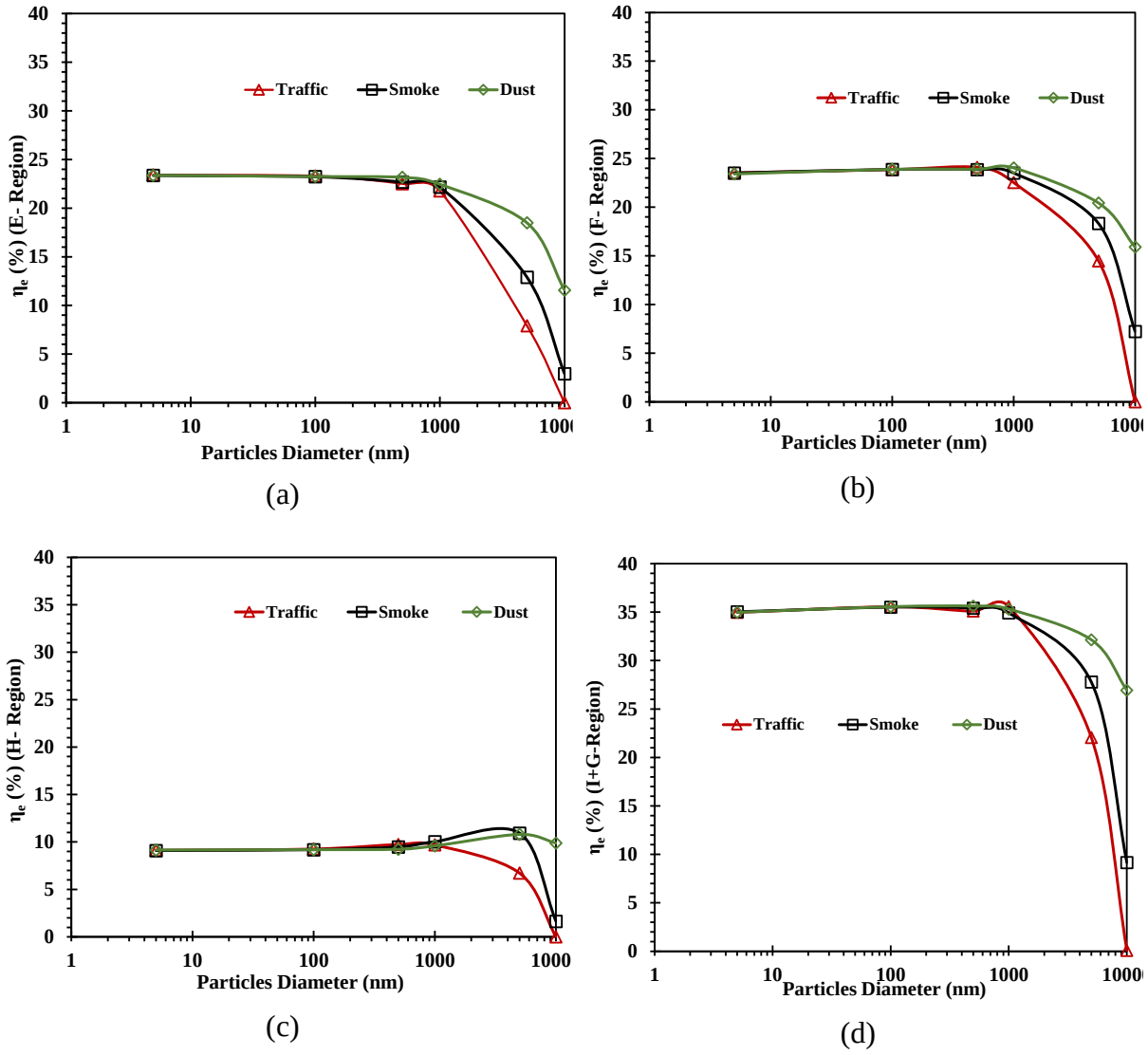

Figure 7.14. Escape rate (η_e) for 5 nm $\leq d_p \leq$ 10 μm particles at a flow rate 60 L/min: (a) E region, (b) F region, (c) H region, and (d) I+G region (Figure 7.1 shows the description of a region).

7.6 Conclusions

Numerical simulations were used to analyse TD of nano- and micro-sized pollutant particles in the mouth-throat and tracheobronchial lung airways of a human lung. The effects of particle density, particle size and flow rate on deposition efficiency were investigated. The simulations include three particle densities, three flow rates and five particle sizes in micro and

nanoscales. The contributions of the impaction and diffusion mechanisms were evaluated. The key findings of the numerical study are listed below;

- The strong impaction mechanism makes most of the 10-μm particles deposited in the human lung airway model, leaving an extremely small number of particles entering the deep lung. The contribution of impaction on the deposition efficiencies of 500-nm to 10-μm particles is over 97.6% when the flow rate is between 15 L/min to 60 L/min. The contribution of impaction on the deposition of the smallest 5-nm particles and the lowest flow rate of 15 L/min is reduced to about 57.4%.
- The deposition efficiencies of nanoparticles with d_p=5 nm on all the parts of the lung model is only affected by the flow rate and is nearly independent of the particle density (Figure 7.12). However, the deposition efficiency of 10-μm particles in the human lung is significantly affected by particle density. It increases with the increase of particle density.
- The deposited nanoparticles are found to be more evenly distributed in airways than the deposited microparticles (Figure 7.12). This is because the airway geometry affects the impaction mechanism, but the diffusion mechanism is not. As proved in Figure 7.13 (a) and (b), impaction induced deposition only happens wherever the airway bends, bifurcates or change diameter, while diffusion occurs everywhere if it is strong.
- The analysis of the escaping rates shows that more particles enter the left side than the right side of the lung, regardless of particle size, particle density or flow rate. This uneven distribution of escaping rate is mainly due to the asymmetry of the geometry of the lung.
- It can be concluded that particles with large diameter, large density and large flow rate deposit at the upper lung, while particles with small diameter, small density and small

flow rate enter the deep lung. If the particle diameter is extremely small (i.e. 5 nm), the density does not have a sensible influence on the particle deposition.

- It was found that not only small particles enter into the deep lungs, large (10 μm) dust particles with low density (400 kg/m^3) can also be able enter the deep airways. It is estimated that 64.28% of the particles can go into the deep lung.

Pollutant particles and their possible health consequences are a major concern because they cause pulmonary diseases. Through this study, it was found that different mechanisms make different particles deposited in different area of human lungs. This conclusion help design strategies of protecting human lungs from different kinds of pollutant. If particles are electrically charged, a improved model need to be developed in the future to consider the interparticle interaction, which enhances with the increase of electrical charge.

Conflicts of Interest

The authors state no conflict of interest.

Acknowledgments

Mr Rahman acknowledges the support of the Australian Government Research Training Program's International Postgraduate Research Scholarship (IPRS). The authors also acknowledge that the WSU High-Performance VM machine provided the computational facilities.

References

Abolhassantash, M, Tavakol, M, Abouali, O, Yaghoubi, M & Ahmadi, G 2020, 'Deposition fraction of ellipsoidal fibers in the human nasal cavity-Influence of non-creeping formulation of hydrodynamic forces and torques', International Journal of Multiphase Flow, vol. 126, 103238.

Albrecht, MA, Evans, CW & Raston, CL 2006, 'Green chemistry and the health implications of nanoparticles', Green chemistry, vol. 8, no. 5, pp. 417-432.

Anderson, JO, Thundiyil, JG & Stolbach, A 2012, 'Clearing the air: a review of the effects of particulate matter air pollution on human health', Journal of medical toxicology, vol. 8, no. 2, pp. 166-175.

Asgharian, B 2004, 'A model of deposition of hygroscopic particles in the human lung', Aerosol Science and Technology, vol. 38, no. 9, pp. 938-947.

Asgharian, B & Price, OT 2007, 'Deposition of ultrafine (nano) particles in the human lung', Inhalation Toxicology, vol. 19, no. 13, pp. 1045-1054.

Azarmi, S, Roa, WH & Löbenberg, R 2008, 'Targeted delivery of nanoparticles for the treatment of lung diseases', Advanced Drug Delivery Reviews, vol. 60, no. 8, pp. 863-875.

Bakand, S, Hayes, A & Dechsakulthorn, F 2012, 'Nanoparticles: a review of particle toxicology following inhalation exposure', Inhalation Toxicology, vol. 24, no. 2, pp. 125-135.

Bălă, G-P, Râjnoveanu, R-M, Tudorache, E, Motișan, R & Oancea, C 2021, 'Air pollution exposure—the (in) visible risk factor for respiratory diseases', Environmental Science and Pollution Research, vol. 28, no. 16, pp. 19615-19628.

Balásházy, I, Hofmann, W & Heistracher, T 2003, 'Local particle deposition patterns may play a key role in the development of lung cancer', Journal of Applied Physiology, vol. 94, no. 5, pp. 1719-1725.

Borghardt, JM, Kloft, C & Sharma, A 2018, 'Inhaled therapy in respiratory disease: the complex interplay of pulmonary kinetic processes', Canadian respiratory journal, vol. 2018, 2732017.

Brunekreef, B & Forsberg, B 2005, 'Epidemiological evidence of effects of coarse airborne particles on health', European Respiratory Journal, vol. 26, no. 2, pp. 309-318.

Buchanan, AH & Honey, BG 1994, 'Energy and carbon dioxide implications of building construction', Energy and Buildings, vol. 20, no. 3, pp. 205-217.

Bui, VKH, Moon, J-Y, Chae, M, Park, D & Lee, Y-C 2020, 'Prediction of aerosol deposition in the human respiratory tract via computational models: A review with recent updates', Atmosphere, vol. 11, no. 2, 137.

Charron, A & Harrison, RM 2005, 'Fine (PM2. 5) and coarse (PM2. 5-10) particulate matter on a heavily trafficked London highway: sources and processes', Environmental science & technology, vol. 39, no. 20, pp. 7768-7776.

Chen, W-H, Chang, C-M, Mutuku, JK, Lam, SS & Lee, W-J 2021, 'Analysis of microparticle deposition in the human lung by taguchi method and response surface methodology', Environmental research, vol. 197, 110975.

Chen, X, Feng, Y, Zhong, W, Sun, B & Tao, F 2018, 'Numerical investigation of particle deposition in a triple bifurcation airway due to gravitational sedimentation and inertial impaction', Powder Technology, vol. 323, pp. 284-293.

Chen, X, Zhong, W, Zhou, X, Jin, B & Sun, B 2012, 'CFD–DEM simulation of particle transport and deposition in pulmonary airway', Powder Technology, vol. 228, pp. 309-318.

Cheng, Y-S, Su, Y-F, Yeh, H-C & Swift, DL 1993, 'Deposition of thoron progeny in human head airways', Aerosol Science and Technology, vol. 18, no. 4, pp. 359-375.

Cheng, Y-S, Zhou, Y & Chen, BT 1999, 'Particle deposition in a cast of human oral airways', Aerosol Science & Technology, vol. 31, no. 4, pp. 286-300.

Choi, J-I & Kim, CS 2007, 'Mathematical analysis of particle deposition in human lungs: an improved single path transport model', Inhalation Toxicology, vol. 19, no. 11, pp. 925-939.

Cohen, AJ, Brauer, M, Burnett, R, Anderson, HR, Frostad, J, Estep, K et al. 2017, 'Estimates and 25-year trends of the global burden of disease attributable to ambient air pollution:

an analysis of data from the Global Burden of Diseases Study 2015', The lancet, vol. 389, no. 10082, pp. 1907-1918.

Collaborators, G & Ärnlöv, J 2020, 'Global burden of 87 risk factors in 204 countries and territories, 1990–2019: a systematic analysis for the Global Burden of Disease Study 2019', The lancet, vol. 396, no. 10258, pp. 1223-1249.

D'amato, G & Cecchi, L 2008, 'Effects of climate change on environmental factors in respiratory allergic diseases', Clinical & Experimental Allergy, vol. 38, no. 8, pp. 1264-1274.

Dang Khoa, N, Phuong, NL & Ito, K 2020, 'Numerical modeling of nanoparticle deposition in realistic monkey airway and human airway models: a comparative study', Inhalation Toxicology, vol. 32, no. 7, pp. 311-325.

Darquenne, C 2020, 'Deposition mechanisms', Journal of aerosol medicine and pulmonary drug delivery, vol. 33, no. 4, pp. 181-185.

de Sarabia, ER-F, Elvira-Segura, L, Gonzalez-Gomez, I, Rodrıguez-Maroto, J, Munoz-Bueno, R & Dorronsoro-Areal, J 2003, 'Investigation of the influence of humidity on the ultrasonic agglomeration of submicron particles in diesel exhausts', Ultrasonics, vol. 41, no. 4, pp. 277-281.

Deng, Q, Deng, L, Miao, Y, Guo, X & Li, Y 2019, 'Particle deposition in the human lung: Health implications of particulate matter from different sources', Environmental research, vol. 169, pp. 237-245.

Deng, Q, Ou, C, Chen, J & Xiang, Y 2018, 'Particle deposition in tracheobronchial airways of an infant, child and adult', Science of the Total Environment, vol. 612, pp. 339-346.

Deng, Q, Ou, C, Shen, Y-M, Xiang, Y, Miao, Y & Li, Y 2019, 'Health effects of physical activity as predicted by particle deposition in the human respiratory tract', Science of the Total Environment, vol. 657, pp. 819-826.

Derbyshire, E 2007, 'Natural minerogenic dust and human health', AMBIO: A Journal of the Human Environment, vol. 36, no. 1, pp. 73-77.

Diao, M, Holloway, T, Choi, S, O'Neill, SM, Al-Hamdan, MZ, Van Donkelaar, A et al. 2019, 'Methods, availability, and applications of PM2. 5 exposure estimates derived from ground measurements, satellite, and atmospheric models', Journal of the Air & Waste Management Association, vol. 69, no. 12, pp. 1391-1414.

Donaldson, K, Li, X & MacNee, W 1998, 'Ultrafine (nanometre) particle mediated lung injury', Journal of Aerosol Science, vol. 29, no. 5-6, pp. 553-560.

Donaldson, K, Stone, V, Seaton, A & MacNee, W 2001, 'Ambient particle inhalation and the cardiovascular system: potential mechanisms', Environmental health perspectives, vol. 109, no. suppl 4, pp. 523-527.

Drummond, MB & Upson, D 2014, 'Electronic cigarettes. Potential harms and benefits', Annals of the American Thoracic Society, vol. 11, no. 2, pp. 236-342.

Englert, N 2004, 'Fine particles and human health—a review of epidemiological studies', Toxicology letters, vol. 149, no. 1-3, pp. 235-242.

Farghadan, A, Poorbahrami, K, Jalal, S, Oakes, JM, Coletti, F & Arzani, A 2020, 'Particle transport and deposition correlation with near-wall flow characteristic under inspiratory airflow in lung airways', Computers in biology and medicine, vol. 120, 103703.

Feng, Y & Kleinstreuer, C 2014, 'Micron-particle transport, interactions and deposition in triple lung-airway bifurcations using a novel modeling approach', Journal of Aerosol Science, vol. 71, pp. 1-15.

Ferrucci, L, Izmirlian, G, Leveille, S, Phillips, CL, Corti, M-C, Brock, DB et al. 1999, 'Smoking, physical activity, and active life expectancy', American journal of epidemiology, vol. 149, no. 7, pp. 645-653.

Franosch, T, Grimm, M, Belushkin, M, Mor, FM, Foffi, G, Forró, L et al. 2011, 'Resonances arising from hydrodynamic memory in Brownian motion', Nature, vol. 478, no. 7367, pp. 85-88.

Gao, R & Sang, N 2020, 'Quasi-ultrafine particles promote cell metastasis via HMGB1-mediated cancer cell adhesion', Environmental pollution, vol. 256, 113390.

Ghosh, A, Islam, MS & Saha, SC 2020, 'Targeted drug delivery of magnetic nano-particle in the specific lung region', Computation, vol. 8, no. 1, 10.

Gu, Q, Qi, S, Yue, Y, Shen, J, Zhang, B, Sun, W et al. 2019, 'Structural and functional alterations of the tracheobronchial tree after left upper pulmonary lobectomy for lung cancer', Biomedical engineering online, vol. 18, no. 1, pp. 1-18.

Hammond, D, Jones, S & Lalor, M 2007, 'In-vehicle measurement of ultrafine particles on compressed natural gas, conventional diesel, and oxidation-catalyst diesel heavy-duty transit buses', Environmental monitoring and assessment, vol. 125, no. 1, pp. 239-246.

Hofmann, W 2011, 'Modelling inhaled particle deposition in the human lung—A review', Journal of Aerosol Science, vol. 42, no. 10, pp. 693-724.

Huang, F, Zhang, Y, Tong, Z, Chen, X, Yang, R & Yu, A 2021, 'Numerical investigation of deposition mechanism in three mouth–throat models', Powder Technology, vol. 378, pp. 724-735.

Inthavong, K, Zhang, K & Tu, J 2011, 'Numerical modelling of nanoparticle deposition in the nasal cavity and the tracheobronchial airway', Computer Methods in Biomechanics and Biomedical Engineering, vol. 14, no. 7, pp. 633-643.

Isa, NM, Ahmad Fara, ANK & Asmuin, NZ 2014, 'Investigation on the Turbulence Models Effect of a Coal Classifier by Using Computational Fluids Dynamics', Trans Tech Publ, vol. 465, pp. 617-621.

Islam, MS, Larpruenrudee, P, Hossain, SI, Rahimi-Gorji, M, Gu, Y, Saha, SC et al. 2021, 'Polydisperse Aerosol Transport and Deposition in Upper Airways of Age-Specific Lung', International Journal of Environmental Research and Public Health, vol. 18, no. 12, 6239.

Islam, MS, Larpruenrudee, P, Paul, AR, Paul, G, Gemci, T, Gu, Y et al. 2021, 'SARS CoV-2 aerosol: How far it can travel to the lower airways?', Physics of Fluids, vol. 33, no. 6, 061903.

Islam, MS, Larpruenrudee, P, Saha, SC, Pourmehran, O, Paul, AR, Gemci, T et al. 2021, 'How severe acute respiratory syndrome coronavirus-2 aerosol propagates through the age-specific upper airways', Physics of Fluids, vol. 33, no. 8, 081911.

Islam, MS, Saha, SC, Gemci, T, Yang, IA, Sauret, E & Gu, Y 2018, 'Polydisperse microparticle transport and deposition to the terminal bronchioles in a heterogeneous vasculature tree', Scientific Reports, vol. 8, no. 1, pp. 1-9.

Islam, MS, Saha, SC, Gemci, T, Yang, IA, Sauret, E, Ristovski, Z et al. 2019, 'Euler-Lagrange prediction of diesel-exhaust polydisperse particle transport and deposition in lung: Anatomy and turbulence effects', Scientific Reports, vol. 9, no. 1, pp. 1-16.

Islam, MS, Saha, SC, Sauret, E, Ong, H, Young, P & Gu, Y 2019, 'Euler–Lagrange approach to investigate respiratory anatomical shape effects on aerosol particle transport and deposition', Toxicology Research and Application, vol. 3, 2397847319894675.

Jang, SP & Choi, SU 2004, 'Role of Brownian motion in the enhanced thermal conductivity of nanofluids', Applied physics letters, vol. 84, no. 21, pp. 4316-4318.

Johnston, HJ, Mueller, W, Steinle, S, Vardoulakis, S, Tantrakarnapa, K, Loh, M et al. 2019, 'How harmful is particulate matter emitted from biomass burning? A Thailand perspective', Current Pollution Reports, vol. 5, no. 4, pp. 353-377.

Kim, K-H, Kabir, E & Kabir, S 2015, 'A review on the human health impact of airborne particulate matter', Environment international, vol. 74, pp. 136-143.

Kleinstreuer, C, Zhang, Z, Li, Z, Roberts, WL & Rojas, C 2008, 'A new methodology for targeting drug-aerosols in the human respiratory system', International Journal of Heat and Mass Transfer, vol. 51, no. 23-24, pp. 5578-5589.

Leoni, C, Pokorná, P, Hovorka, J, Masiol, M, Topinka, J, Zhao, Y et al. 2018, 'Source apportionment of aerosol particles at a European air pollution hot spot using particle number size distributions and chemical composition', Environmental pollution, vol. 234, pp. 145-154.

Lintermann, A & Schröder, W 2017, 'Simulation of aerosol particle deposition in the upper human tracheobronchial tract', European Journal of Mechanics-B/Fluids, vol. 63, pp. 73-89.

Luo, H & Liu, Y 2008, 'Modeling the bifurcating flow in a CT-scanned human lung airway', Journal of biomechanics, vol. 41, no. 12, pp. 2681-2688.

Manisalidis, I, Stavropoulou, E, Stavropoulos, A & Bezirtzoglou, E 2020, 'Environmental and health impacts of air pollution: a review', Frontiers in public health, vol. 8, 14.

Moller, W, Felten, K, Sommerer, K, Scheuch, G, Meyer, G, Meyer, P et al. 2008, 'Deposition, retention, and translocation of ultrafine particles from the central airways and lung periphery', American journal of respiratory and critical care medicine, vol. 177, no. 4, pp. 426-432.

Morsi, S & Alexander, A 1972, 'An investigation of particle trajectories in two-phase flow systems', Journal of Fluid mechanics, vol. 55, no. 2, pp. 193-208.

Nassimi, M, Schleh, C, Lauenstein, HD, Hussein, R, Hoymann, H-G, Koch, W et al. 2010, 'A toxicological evaluation of inhaled solid lipid nanoparticles used as a potential drug

delivery system for the lung', European Journal of Pharmaceutics and Biopharmaceutics, vol. 75, no. 2, pp. 107-116.

Oberdörster, G 2000, 'Pulmonary effects of inhaled ultrafine particles', International archives of occupational and environmental health, vol. 74, no. 1, pp. 1-8.

Olaniyan, T, Dalvie, M & Jeebhay, M 2015, 'Ambient air pollution and childhood asthma: a review of South African epidemiological studies: allergies in the workplace', Current Allergy & Clinical Immunology, vol. 28, no. 2, pp. 122-127.

Ou, C, Jian, H & Deng, Q 2020, 'Particle Deposition in Human Lung Airways: Effects of Airflow, Particle Size, and Mechanisms', Aerosol and Air Quality Research, vol. 20, no. 12, pp. 2846-2858.

Pan, Y, Lin, C-H, Wei, D & Chen, C 2019, 'Experimental measurements and large eddy simulation of particle deposition distribution around a multi-slot diffuser', Building and Environment, vol. 150, pp. 156-163.

Patra, AK, Gautam, S & Kumar, P 2016, 'Emissions and human health impact of particulate matter from surface mining operation—A review', Environmental Technology & Innovation, vol. 5, pp. 233-249.

Paul, AR, Khan, F, Jain, A & Saha, SC 2021, 'Deposition of smoke particles in human airways with realistic waveform', Atmosphere, vol. 12, no. 7, 912.

Peng, RD, Chang, HH, Bell, ML, McDermott, A, Zeger, SL, Samet, JM et al. 2008, 'Coarse particulate matter air pollution and hospital admissions for cardiovascular and respiratory diseases among Medicare patients', Jama, vol. 299, no. 18, pp. 2172-2179.

Pražnikar, Z & Pražnikar, J 2012, 'The effects of particulate matter air pollution on respiratory health and on the cardiovascular system', Slovenian Journal of Public Health, vol. 51, no. 3, pp. 190-199.

Rahman, MM, Zhao, M, Islam, MS, Dong, K & Saha, SC 2021a, 'Aerosol Particle Transport and Deposition in Upper and Lower Airways of Infant, Child and Adult Human Lungs', Atmosphere, vol. 12, no. 11, 1402.

Rahman, MM, Zhao, M, Islam, MS, Dong, K & Saha, SC 2021b, 'Aging effects on airflow distribution and micron-particle transport and deposition in a human lung using CFD-DPM approach', Advanced Powder Technology, vol. 32, pp. 3506-3516.

Rahman, MM, Zhao, M, Islam, MS, Dong, K & Saha, SC 2021c, 'Numerical study of nanoscale and microscale particle transport in realistic lung models with and without stenosis', International Journal of Multiphase Flow, vol. 145, 103842.

Ravindra, K, Mittal, AK & Van Grieken, R 2001, 'Health risk assessment of urban suspended particulate matter with special reference to polycyclic aromatic hydrocarbons: a review', Reviews on environmental health, vol. 16, pp. 169-189.

Ritchie, G, Still, K, Rossi Iii, J, Bekkedal, M, Bobb, A & Arfsten, D 2003, 'Biological and health effects of exposure to kerosene-based jet fuels and performance additives', Journal of Toxicology and Environmental Health, Part B, vol. 6, no. 4, pp. 357-451.

Schraufnagel, DE 2020, 'The health effects of ultrafine particles', Experimental & molecular medicine, vol. 52, no. 3, pp. 311-317.

Shih, TH, Liou, WW, Shabbir, A, Yang, Z & Zhu, J 1995, 'A new k-ϵ eddy viscosity model for high reynolds number turbulent flows', Computers and Fluids, vol. 24, no. 3, pp. 227-238.

Singh, P, Raghav, V, Padhmashali, V, Paul, G, Islam, MS & Saha, SC 2020, 'Airflow and particle transport prediction through stenosis airways', International Journal of Environmental Research and Public Health, vol. 17, no. 3, 1119.

Sophonsiri, C & Morgenroth, E 2004, 'Chemical composition associated with different particle size fractions in municipal, industrial, and agricultural wastewaters', Chemosphere, vol. 55, no. 5, pp. 691-703.

Stuart, BO 1984, 'Deposition and clearance of inhaled particles', Environmental health perspectives, vol. 55, pp. 369-390.

Tahery, N, Zarea, K, Cheraghi, M, Hatamzadeh, N, Farhadi, M, Dobaradarn, S et al. 2021, 'Chronic Obstructive Pulmonary Disease (COPD) and Air Pollution: A Review', Jundishapur Journal of Chronic Disease Care, vol. 10, no. 1, 110273.

Torrens, F & Castellano, G 2018, 'Brownian Motion, Random Trajectory, Diffusion, Fractals, Theory of Chaos, and Dialectics', in Modern Physical Chemistry: Engineering Models, Materials, and Methods with Applications, Apple Academic Press, pp. 27-36.

Tsuji, Y 2007, 'Multi-scale modeling of dense phase gas–particle flow', Chemical engineering science, vol. 62, no. 13, pp. 3410-3418.

Wu, C, Yan, W, Chen, R, Liu, Y & Li, G 2022, 'Numerical study on targeted delivery of magnetic drug particles in realistic human lung', Powder Technology, vol. 397, 116984.

Xi, J, Berlinski, A, Zhou, Y, Greenberg, B & Ou, X 2012, 'Breathing resistance and ultrafine particle deposition in nasal–laryngeal airways of a newborn, an infant, a child, and an adult', Annals of Biomedical Engineering, vol. 40, no. 12, pp. 2579-2595.

Xi, J & Longest, P 2008, 'Effects of oral airway geometry characteristics on the diffusional deposition of inhaled nanoparticles', Journal of biomechanical engineering, vol. 130, no. 1, 011008.

Xu, C, Zheng, X & Shen, S 2020, 'A numerical study of the effect of breathing mode and exposure conditions on the particle inhalation and deposition', Inhalation Toxicology, vol. 32, no. 13-14, pp. 456-467.

Yousefi, M, Pourmehran, O, Gorji-Bandpy, M, Inthavong, K, Yeo, L & Tu, J 2017, 'CFD simulation of aerosol delivery to a human lung via surface acoustic wave nebulization', Biomechanics and modeling in mechanobiology, vol. 16, no. 6, pp. 2035-2050.

Zhang, Z & Kleinstreuer, C 2004, 'Airflow structures and nano-particle deposition in a human upper airway model', Journal of computational physics, vol. 198, no. 1, pp. 178-210.

Zhang, Z, Song, H, Peng, Z, Luo, Q, Ming, J & Zhao, G 2012, 'Characterization of stipe and cap powders of mushroom (Lentinus edodes) prepared by different grinding methods', Journal of Food Engineering, vol. 109, no. 3, pp. 406-413.

Zhao, J & Castranova, V 2011, 'Toxicology of nanomaterials used in nanomedicine', Journal of Toxicology and Environmental Health, Part B, vol. 14, no. 8, pp. 593-632.

Chapter 8: Conclusions and Future Work

Airflow dynamics and particle TD in the human lung were studied extensively in this research through CFD simulations. The outcomes have been published in four highly prestigious journals, and one additional journal article is currently in review for publication. The thesis includes these papers as Chapters 3–7.

8.1 Conclusions

In Chapter 3, the effects of age on particle TD in human lungs are analysed systematically. Human lung airway diameter and breathing capacity increases with age up to 30 years. However, after the age of 50 years, lung airway diameters reduce by around 10% every decade. Therefore, TD of nanoparticles and microparticles in the upper and lower lung airways of infants (9 months), children (6 years), adults (30 years) and the elderly (50–70 years) were examined in this thesis to understand the effect of airflow dynamic and particle deposition in human lung airways.

A comprehensive analysis of nanoparticle TD in the upper (G0–G3) and lower (G12–G15) airways is performed on infants to adults. Particle deposition is predicted for various airway geometry and breathing airflow rates. The decrease in lung airway diameters due to aging significantly affects particle deposition. When comparing lower to upper generation airways, more particles are deposited in the 30-year-old lung than the 9-month-old lung. In addition, a large percentage (>95%) of nanoparticles (5 nm) can enter G12, yet only 3% of particles enter G12 when particle size increases to 500 nm.

In Chapter 4, a novel numerical cutting method is developed and applied in the first-ever approach to the study of particle deposition in a symmetric lung model. A wide range of microparticle TD in tracheobronchial lung airway generations up to G14 are extensively

investigated for elderly people. Numerical results show that airflow velocity in the airways increases with age. Wall shear stress may also be observed at each bifurcation of the lung airway because flow resistance occurs there. With increasing age, a particle's ability to escape each generation decreases. Findings from the developed numerical model of particle TD will help improve the therapeutic efficiency of targeted drug delivery for elderly people.

In Chapter 5, the first-ever one-path numerical model to simulate airflow and nanoparticle TD in human lung G0–G11 airways is established. Compared with the cutting method in Chapter 4, this one-path model ensures the conservation of momentum throughout the airflow path. Because there are 2^{11}=2,048 bifurcations between G0 and G11, a full CFD simulation by generation for many airway generations is infeasible. With reasonable computational effort, the current research examines particle TD in the human lung up to generation G11. Because of the difference in the Reynolds number, non-dimensional velocity distributions of different flow rates—depending on the degree of physical activity—follow a similar trend, but are not identical. The examination of nanoparticle escape rates indicates that more particles enter the deep lung when the flow rate is high. Thus, the findings are critical in the treatment of lung diseases affecting deep lung airways.

In Chapters 4 and 5, simplified airway models are used because realistic models for many generations are not available. In Chapter 6, nano- and microparticle TD in the first three generations of a realistic lung model are analysed, and the effects of stenosis on particle TD are examined. Velocity in a stenosis airway increases by 72% due to streamlined contraction in the stenosis zone, which is important for determining respiratory health risk. It is also found that the pressure drop of the stenosis model is 83% higher than in the healthy model. Further, the role of impaction and diffusion processes in particle TD in stenosis lung models is investigated. The research shows that the contribution of the diffusion mechanism increases with a decrease in either particle size or flow rate.

Chapter 8: Conclusions and Future Work

Studying particle TD is important not only in drug delivery but also in evaluating the negative effects of pollutant particles on health. Different types of pollutant particles have different densities and particle sizes. In Chapter 7, TD for different types of pollutant particle in a CT scan based on realistic lung airways is studied. The pollutant particles cover traffic, smoke and dust and their sizes range from nano- to microscales. The contribution of impaction to deposition efficiencies for 500-nm to 10-μm particles is over 97.6% when the flow rate is 15–60 L/min. The contribution of impaction to deposition of the smallest (5-nm) particles, with the lowest flow rate of 15 L/min declines to approximately 57.4%. Nanoparticles are observed to be more uniformly dispersed than are microparticles in airways. This is because the impaction process is influenced by airway geometry, whereas the diffusion mechanism is not.

Particulate pollution and its potential health consequences are a major issue as they promote pulmonary disease. This study finds that different mechanisms cause different particles to be deposited in different areas of the human lung. It was observed that microscopic particles and large (10 μm) dust particles with low density (400 kg/m^3) might reach the deep lungs. Almost two-thirds (64.3%) are estimated to enter the deep lung. This result will assist in development of strategies to protect human lungs from various types of pollution.

To summarise, a human airway model is used in this thesis to conduct a complete nanoscale and microscale particle TD investigation. The numerical model developed for particle TD research shows that different diameter particles are deposited in different sections of the lung airways. This research on new boundary condition development is important in proving that aerosol nanoparticles are deposited in the terminal lung airways. The finding of nanoparticles in the deep lung has implications for pharmaceutical aerosol manufacturing and drug delivery. Further, these extensive nanoparticle TD studies will enable researchers to better understand how drug aerosols are delivered to treat obstructive lung diseases like asthma and COPD.

8.2 Limitations and Future Study

This study has some limitations that should be addressed in future studies.

- The study exclusively examined one-way inhalation to predict particle TD in pulmonary airways. Two-way inhalation and exhalation effects may enhance particle TD comprehension. This study considered no breath-hold effects on deposition for different flow rates.
- This study used symmetric and planner lung airways models because of the lack of high-resolution CT images for age-specific realistic lung geometry. However, CT images based on realistic lung geometry up to the third generation were considered. More branches of realistic lung airway models are required to better estimate particle TD in human lung airways.
- The current study did not include any hygroscopic particles to estimate particle TD. Some particles may absorb water and expand somewhat in size.
- A static airway model was used to estimate particle TD in this study. For the purposes of this investigation, no airway deformation was considered.
- In reality, the airway branching pattern is different regardless of age and sex. Therefore, reconstructing an age-specific realistic lung model is necessary for future studies.